

University of Nottingham
UK | CHINA | MALAYSIA

The Effect of Fretting Conditions on the Lifetime of Aero-engine Dry Film Lubricant Systems

Emmanuel Laolu-Balogun, MSc.

Thesis submitted to The University of Nottingham for the degree of Doctor of Philosophy

January 2023

Abstract

This study was initiated to address existing fretting failure modes of the aero engine fan blade root components which are protected through the application of a bonded MoS_2-based dry film lubricant (DFL), with a focus upon understanding the wear of the DFL system as a route to its lifetime extension. Fretting wear tests have been conducted over a wide range of testing conditions on Ti-6Al-4V specimens which are coated with a DFL system to understand the driving wear and damage mechanisms and reveal pathways to which the extension of fretting lifetimes could be achieved.

Investigations of how humidity and oxygen influence the fretting wear behaviour and performance of the MoS_2-based DFL coating demonstrated that, in low humidity conditions (0.5 – 3 % RH), sustained low friction and low wear capabilities were observed with or without the presence of oxygen in the environment which led to significant extension of fretting wear lifetimes. The presence of oxygen in the low-humidity environment is however shown to alter the wear interface with the formation of a cracked layer composed of molybdenum oxide. As humidity levels were increased, rapid wear of the MoS_2 DFL occurred along with an increased coefficient of friction which shortened the lifetime of the system. A transition occurred from low friction adhesive wear in low humidity environments where limited damage on the MoS_2 DFL coating was incurred to high friction abrasive wear after air with increased humidity was introduced to the system which resumed the progression of fretting wear damage. A graphite modified MoS_2 DFL (where ~ 5 % graphite powder was added to the MoS_2 paint matrix) was shown to provide an order of magnitude increase in the coating lifetime in atmospheric (25 – 40 % RH) and high humidity (60 – 75 % RH) conditions.

Examining the substrate surface conditions upon which the polymer-bonded MoS_2 DFL is deposited on illuminated the effects of interfacial topography and substrate material type. The addition of a thermally sprayed Cu-Ni-In under-layer prior to the application of the DFL resulted in an extension of fretting lifetime and durability to the fretting system. Increased surface roughness provided a mechanical key for the retention of the DFL which prevents delamination and delivers a stable low friction interface through the generation of a metal-mixed layer for additional durability and increased lifetimes.

By incorporating additional fretting testing capabilities into the experiment program, an expansion of the testing conditions which included increased loading and alternate (flat-on-flat) contact configuration could be tested to gauge the performance limits of the both the MoS_2 and graphite modified MoS_2 DFL coatings. Two distinct fretting wear behaviours were identified; (i) a steady low friction wear which is characterised by maintenance of low friction for the testing duration and providing an extension of fretting lifetime; (ii) tests which are characterised as having an initial low friction plateau followed by a rapid increase of friction consequently followed by coating film failure.

A threshold limit was proposed using a PV concept to determine the fretting wear behaviours of the DFL coatings. Below the proposed PV limit, a steady state low friction is observed whilst high above the limit, high friction tests to early failure are observed. Under more aggressive loading conditions, the graphite modified MoS_2 DFL was found to offer increased fretting lifetimes along with a rise of the threshold limit between these two regimes in both cylinder-on-flat and flat-on-flat tests but much more moderate enhancement in performance were observed when tested in flat-on-flat tests under equivalent conditions; the reasons for the difference in behaviour between the test types is not clear.

Alongside the laboratory testing, post-service fan blades were made available so that an investigation of the DFL degradation modes in service could be undertaken. As a result of this work, test programmes looking at coating durability where attritive wear is the dominant mechanism of failure (such as the cylinder-on-flat and flat-on-flat tests reported in this thesis) need to be reviewed, and more appropriate and representative tests designed and evaluated.

This work has provided unique insights into the damage mechanisms and fretting wear behaviours of bonded DFL coating systems by investigating the individual operational factors of environment conditions, substrate surface conditions and fretting loading conditions. Distinct fretting conditions that generate sustained low friction and low wear behaviours have been identified and the mechanisms that drive this behaviour dissected. This has provided a better understanding of how the extension of DFL fretting lifetimes could be potentially achieved and how the performance of the DFL system can be further increased with additives.

Publications

E. Laolu-Balogun, S. P. Owen, S. Read, G. Pattinson, P. H. Shipway, and K. T. Voisey, “Effects of Ti-6Al-4V Surface Condition on the Performance of DFL Lifetimes,” in Proceedings of the 8th International Conference on Fracture, Fatigue and Wear, 2021, pp. 657–672.

E. Laolu-Balogun, S. P. Owen, S. Read, G. Pattinson, P. H. Shipway, and K. T. Voisey, “Lifetime of MoS_2-based DFL systems in fretting with and without a Cu-Ni-In under-layer: the dependence on the topography of the surface onto which the DFL is deposited,” (In preparation) – to be submitted to Wear or Tribology International

Acknowledgement

I would first like to thank my supervisors Dr Katy Voisey and Professor Philip Shipway, they have made the completion of this research possible through their guidance, support, and patience. Their incredible insights, knowledge and advice has shaped my learning and growth as a researcher and most of all, the kindness they have shown will always remain with me, I am very grateful to have had an opportunity to work with them. My sincere thanks and appreciation to Dr Tom Buss who has been a tremendous help with experimental testing and sharing his technical expertise. I would also like to acknowledge all the technicians who have helped me over the years for all their contributions. I would like to express my gratitude to Rolls-Royce plc for their support of the research and to Sam Owen of Rolls-Royce plc for his assistance throughout this work. My utmost thanks and warmest gratitude to my mum Helen Akachili, my sister Theresa, my brothers Winston, Fred and Richard and to my love Soojin who have given their unwavering support and encouragement through my studies.

Table of Contents

Chapter 1. Introduction 1

1.1 Background 1

1.2 Research aims and scope 2

1.3 Objectives 3

1.4 Thesis overview 4

Chapter 2. Literature Review 5

2.1 Fan blade root 5

2.1.1 Ti-6Al-4V alloy 7

2.2 Fretting 8

2.2.1 Fretting damage 9

2.2.2 Fretting wear mechanism 9

2.2.3 Fretting wear mechanism of titanium alloy 10

2.2.4 Quantifying fretting and wear 12

2.2.4.1 Fretting maps/regimes 12

2.2.4.2 Description of fretting loops 13

2.2.4.3 Wear rate 15

2.3 Parameters affecting fretting 16

2.3.1 Contact geometry 16

2.3.2 Fretting loading conditions 17

2.3.3 Environmental conditions 20

2.4 Mitigation of fretting damage on the fan blade root system 21

2.4.1 Change of design 21

2.4.2 Surface engineering methods employed on fan blade root 21

2.4.3 Lubricants 24

2.5 Solid lubricants 25

2.5.1 MoS_2 solid lubricant 28

2.5.1.1 Effect of humidity and oxygen on the performance of MoS_2 31

2.5.2 Graphite solid lubricant 36
2.6 Fretting wear behaviour of polymers.....40
2.6.1 PV limit.....44
2.6.2 Transfer film mechanism.....46
2.6.3 Fretting wear behaviour of polymer-bonded MoS_2-based dry film lubricant..... 48
2.6.4 Effect of surface condition on polymer-bonded MoS_2-based dry film lubricant 52
2.7 Summary 55
2.7.1 Basis for current work 56
Chapter 3. Experimental Methodology.....58
3.1 Specimen preparation.....58
3.2 Substrate surface preparation.....60
3.2.1 Cylindrical specimen 60
3.2.2 Flat specimens.....62
3.3 DFL spray deposition process 65
3.4 Fretting wear test.....67
3.4.1 Environmental chamber 72
3.5 Flat-on-flat (Scitek) Fretting wear test rig.....73
3.6 Fretting wear scar assessment.....76
3.6.1 Sample preparation for characterisation 76
3.6.2 Surface topography and profilometry 76
3.6.3 Scanning electron microscopy and energy dispersive x-ray (EDX) analysis.....77
Chapter 4. Effects of humidity and oxygen on the performance of polymer-bonded MoS_2-based; graphite-based; and graphite-modified MoS_2-based DFL coatings.. 78
4.1 Background – Initial results of the polymer-bonded MoS_2-based DFL (Mo-DFL) and graphite-modified MoS_2 DFL (Gr-Mo-DFL).....78

4.2 Polymer-bonded MoS_2-based DFL (Mo-DFL) performance in low-humidity environments 82

4.3 Polymer-bonded MoS_2-based DFL (Mo-DFL) in high-humidity environments 91

4.4 Graphite-based DFL (Gr-DFL) and graphite-modified MoS_2-based DFL (Gr-Mo-DFL) in high humidity environments 96

4.5 Discussion 101

4.5.1 Effect of humidity on polymer-bonded MoS_2-based DFL (Mo-DFL) in air and argon environments 101

4.5.2 Effect of ambient and high-humidity on graphite-based DFL (Gr-DFL) and graphite-modified MoS_2-based DFL (Gr-Mo-DFL) in air and argon environments....104

4.6 Conclusion....106

Chapter 5. Lifetime of MoS_2-based DFL systems in fretting with and without a Cu-Ni-In under-layer: the dependence on the topography of the surface onto which the DFL is deposited 107

5.1 Background 107

5.2 Effect of Cu-Ni-In interface roughness on system failure....109

5.3 Effect of Cu-Ni-In interlayer material and Ti-6Al-4V substrate surface on systems failure....117

5.4 Discussion 122

5.4.1 Effect of roughness of Cu-Ni-In layer 122

5.4.2 Comparison between Cu-Ni-In interlayer and Ti-6Al-4V substrate with similar roughnesses 124

5.5 Conclusion....126

Chapter 6. Examining the performance of polymer-bonded MoS_2-based DFL and graphite-modified MoS_2-based DFL on different fretting contact configurations and loading conditions 128

6.1 Background 128

6.2 Performance of the Mo-DFL and Gr-Mo-DFL coatings on a cylinder-on-flat contact configuration....129

6.3 Comparison of performance of Mo-DFL and Gr-Mo-DFL coatings when tested with a flat-on-flat contact configuration.....138
6.4 Discussion 150
6.4.1 Cylinder-on-flat and flat-on-flat fretting wear behaviour.....150
6.5 Conclusion.....154
Chapter 7. Case Study: Aero-engine fan blade root component wear analysis.....155
7.1 Discussion 163
7.2 Conclusion.....164
Chapter 8. Summary and Conclusion 165
Chapter 9. Future Work 169
References.....171
Appendices.....188
Appendix A: Specimen drawing and shot peening Conditions.....188
Appendix B: Technical data sheet for PL237-R2 (as-received MoS2-based DFL).....190
Appendix C: Technical data sheet for IP9136-R1 (graphite-based DFL).....191
Appendix D: Material safety data sheet for graphite powder 192
Appendix E: Material safety data sheet for compressed air cylinder 194
Appendix F: Material safety data sheet for compressed argon cylinder.....196
Appendix G: Material safety data sheet for thinner (IP9151) 199
Appendix H: Mechanics of the contact.....202

List of Figures

Figure 2.1 Illustration of fretting wear process at aero-engine fan blade/disc interface…… 6

Figure 2.2 SEM images of the microstructure of α + β phases of the Ti-6Al-4V alloy…….. 7

Figure 2.3 Creation and evolution of the third body through the contact interface [64]…….....11

Figure 2.4 Illustration of the dependence of wear coefficient with displacement amplitude in fretting with reference to the slip regime. Cited by [67] and recreated from [39]…….. 12

Figure 2.5 Schematic diagram of an idealised fretting loop [72]. 14

Figure 2.6 Energy analysis of the wear volume as a function of accumulated dissipated energy for fretting of TiN/alumina [75]. 16

Figure 2.7 Schematic drawing of shot-peening treatment and surface state of fan blade root [107] 23

Figure 2.8 Crystal structure of molybdenum disulfide [141]. 29

Figure 2.9 Friction coefficients of MoS_2 films deposited by various techniques [150]…….....30

Figure 2.10 Friction of conditioned sputtered MoS_2 coatings in dry nitrogen, dry air, humid nitrogen and humid air as a function of temperature. Water increases friction at low temperatures with or without oxygen. Oxygen increases friction at high temperature with or without water [168].....34

Figure 2.11 Crystal structure of graphite [141] 37

Figure 2.12 Simplified approach to classification of the wear of polymers [200]…….....42

Figure 2.13 Two-term model of friction and wear process. Total friction is the sum of the forces required for interfacial and cohesive energy dissipations. Likewise, the distinction between interfacial and cohesive wear processes arises from the extent of deformation in the softer material (usually polymer) by rigid asperity of the counter-face. For interfacial wear, the friction is dissipated mainly

by adhesive interactions while for the cohesive wear, the energy is dissipated by adhesive and abrasive (sub-surface) interactions [200]. 42

Figure 2.14 Comparison of the time-related wear depth wear rate if epoxy composites filled with and without nano-TiO_2 as a function of PV factor. [204] [217]…….....46

Figure 2.15 Evolution of the ratio of the maximum tangential force (Q_{max}) to normal force (P) at various imposed displacements. Q_{max}/P corresponds to friction coefficient in a gross slip regime. Labels denote imposed displacement magnitudes [11]…… 50

Figure 2.16 Wear depth as a function of exposure to fretting wear for a nominally 50 µm thick DFL deposited onto a grit-blasted Ti-6Al-4V substrate [225]. 53

Figure 3.1 Cylinder-on-flat specimen configuration used in fretting tests where P is the applied normal load is, and Δ is the applied displacement. 59

Figure 3.2 Topographic 3D profile of the shot-peened Ti-6Al-4V substrate surface prior to DFL coating application. 62

Figure 3.3 Topographic 3D profiles of the flat Cu-Ni-In layer and Ti-6Al-4V substrate surfaces prior to DFL coating application. (a) As-sprayed Cu-Ni-In, (b) Grit-blasted Cu-Ni-In, (c) Ground Cu-Ni-In, (d) Grit-blasted Ti-6Al-4V, (e) Ground Ti-6Al-4V……. 64

Figure 3.4 SE SEM images of (a) plasma sprayed Cu-Ni-In coating (b) grit-blasted Ti-6Al-4V.....65

Figure 3.5 Image of the DFL coating process in progress 67

Figure 3.6 Electro servo hydraulic fretting rig operating schematics and environmental set up (1) Ti-6Al-4V flat specimen with contact length w = 10 mm (2) Ti-6Al-4V cylindrical specimen with radius R = 15 mm (3) Fixed position hydraulic cylinder for applied normal load P = 575 N (4) Vertical controlled actuator for applied displacement amplitude Δ* = 0.3 mm (5) Load cell (6) LVDT (7) Mounting block (8) Dry air or argon cylinder (9) Flow meter (10) Water bubbler (11) Humidity sensor (12) Environment chamber. 68

Figure 3.7 Annotated schematic diagram of fretting loop.....71

Figure 3.8 Scitek Flat-on-Flat fretting wear test rig 73

Figure 3.9 (a) Schematic of Scitek fretting wear testing sample configuration, (b) photographic images of the flat-on-flat fretting wear testing samples showing the wear specimen which represent the fan blade root and the pad specimen which represent the disc after a test. 75

Figure 4.1 (a) Evolution of friction coefficient against number of cycles for polymer-bonded MoS_2-based DFL (Mo-DFL) on grit-blasted self-mated Ti-6Al-4V samples conducted in atmospheric conditions from previous work [225], (b) Repeat of the Mo-DFL test conducted on self-mated grit-blasted Ti-6Al-4V samples at a load of 575 N, 0. 3mm applied displacement and 2.5 Hz frequency at atmospheric conditions (25 – 40 % RH) to verify previous results on a new testing rig which compares the lifetime. 79

Figure 4.2 (a) Evolution of friction coefficient against number of cycles for graphite modified polymer-bonded MoS_2-based DFL (Gr-Mo-DFL) on grit-blasted self-mated Ti-6Al-4V samples conducted in atmospheric conditions from previous work [234] interrupted at 658 k cycles, (b) Plan-view BSE SEM images of the Gr-Mo-DFL testing sample which was stopped at 658 k cycles from previous work [234]…… 81

Figure 4.3 Repeat of the original MoS_2 DFL (Mo-DFL) and graphite modified (Gr-Mo-DFL) equivalent tests conducted on self-mated grit-blasted Ti-6Al-4V samples at a load of 575 N, 0.3mm applied displacement and 2.5 Hz frequency at atmospheric conditions (25 – 40 % RH) to verify previous results on a new testing rig which compares the lifetime. 82

Figure 4.4 Performance of the as-received MoS_2 bonded DFL coating (Mo-DFL) in tested ambient (~ 30% RH) air and in low humidity air and argon. (a) ECoF evolution against test exposure of self-mated grit-blasted Mo-DFL coating system in different atmospheric conditions (b) The maximum depths of the averaged wear profiles taken from the wear surface upon failure for the Mo-DFL upon failure at 65 k cycles in atmospheric air and at 600 k cycles upon test interruption in different atmospheric conditions..... 84

Figure 4.5 Plan-view BSE SEM images of the flat specimen of the Mo-DFL coating in low-humidity air conditions which was interrupted at 600 k cycles (a) Low magnification image (b) High magnification image with EDX point analysis..... 85

Figure 4.6 Plan-view BSE SEM images of the flat specimen of the Mo-DFL coating in low humidity argon conditions which was interrupted at 600 k cycles (a)

Low magnification image (b) High magnification image with EDX point analysis…….....85

Figure 4.7 Performance of the as-received MoS_2 bonded DFL coating (Mo-DFL) which were interrupted and failure had not occurred at test duration intervals of 300 k cycles, 600 k cycles in low-humidity air and at 815 k cycles at low humidity to atmospheric air transition. (a) Friction evolution against cycles of fretting tests of self-mated grit-blasted Mo-DFL coating system in low-humidity air at 300 k cycles, 600 k cycles and 815 k cycles (in low-humidity to atmospheric transition) (b) The maximum depths of the averaged wear profiles taken from the wear surface upon interruption at 300 k cycles, 600 k cycles in low-humidity air and at 815 k cycles in low humidity to atmospheric humidity transition 88

Figure 4.8 Plan-view BSE SEM images of flat specimen of Mo-DFL low-humidity air tests interrupted at various test duration intervals. (a) 300 k cycles (b) 600 k cycles (c) 815 k cycles which was terminated after a period of continuously increasing humidity had been imposed 89

Figure 4.9 Friction evolution against cycles showing fretting tests of self-mated grit-blasted Mo-DFL coating tests in atmospheric air conditions and a test initially conducted in low-humidity air and transitioned to atmospheric air condition. 90

Figure 4.10 Friction evolution against cycles showing fretting tests of self-mated grit-blasted Mo-DFL coating in atmospheric air, high-humidity air and high-humidity argon conditions.....92

Figure 4.11 (a) Interrupted friction evolution against cycles of fretting tests of self-mated grit-blasted Mo-DFL coating in atmospheric air which was stopped at 23 k cycles and high-humidity argon environment stopped at 27 k cycles before the point (b) Wear depths of corresponding interrupted tests.....93

Figure 4.12 Plan-view BSE SEM images of flat specimen of interrupted Mo-DFL tests. (a) Low magnification of interrupted atmospheric air test (b) high magnification and EDX point analysis of interrupted atmospheric air test stopped at 23 k cycles. (c) Low magnification of interrupted high-humidity argon test (d) High magnification and EDX point analysis on interrupted high-humidity argon test stopped at 27 k cycles.....95

Figure 4.13 Performance of the MoS_2 bonded DFL coating (Mo-DFL), graphite bonded DFL coating (Gr-DFL) and graphite modified MoS_2 bonded DFL coating (Gr-Mo-DFL) which was interrupted at 600 k cycles in atmospheric air environment

(a) Friction evolution against cycles of fretting tests (b) Wear depths of the corresponding tests. 97

Figure 4.14 Plan-view BSE SEM images of the flat specimen of the Gr-Mo-DFL coating atmospheric air condition which was interrupted at 600 k cycles (a) Low magnification image (b) High magnification image with EDX point analysis. 98

Figure 4.15 Performance of the MoS_2 bonded DFL coating (Mo-DFL), graphite bonded DFL coating (Gr-DFL) and graphite modified MoS_2 bonded DFL coating (Gr-Mo-DFL) which was interrupted at 600 k cycles in high-humidity air environment (a) Friction evolution against cycles of fretting tests (b) Wear depths of the corresponding tests. 100

Figure 5.1 Cross sectional BSE images of flat specimens with a layer of MoS_2 DFL coating before fretting test with the thickness measurements of layers as indicated. DFL deposited onto the following surface types: a) as-sprayed Cu-Ni-In layer, b) ground Cu-Ni-In layer, c) grit-blasted Cu-Ni-In layer, d) grit-blasted Ti-6Al-4V……..109

Figure 5.2 a) Evolution of ECoF with number of cycles for fretting tests where flat samples had the DFL applied to the Cu-Ni-In layer with different surface preparations as indicated and the round counterpart was shot peened and DFL coated, b) Maximum depths of the averaged wear profiles at failure of the Cu-Ni-In coated flat samples and the shot peened Ti-6Al-4V round samples following tests to failure. 111

Figure 5.3 Cross sectional BSE SEM fretting wear scar images of flat samples. (a) test with DFL which had been deposited onto ground Cu-Ni-In following completed test to failure at 69 kilocycles, (b) test with DFL which had been deposited onto grit-blasted Cu-Ni-In following completed test to failure at 229 kilocycles, (c) test with DFL which had been deposited onto as-sprayed Cu-Ni-In following completed test to failure at 615 kilocycles. 112

Figure 5.4 a) Evolution of ECoF with number of cycles for as-sprayed Cu-Ni-In fretting wear test which were interrupted and run to failure; b) Maximum depths of averaged wear profiles of as-sprayed flat Cu-Ni-In sample and the shot peened cylindrical Ti-6Al-4V samples of tests that were (i) interrupted at 200 k cycles and (ii) run to failure at 615 k cycles. 114

Figure 5.5 Cross sectional BSE SEM fretting wear scar images of flat samples. (a) test with DFL which had been deposited onto as-sprayed Cu-Ni-In following a

test that was interrupted at 200 k cycles, (b) test with DFL which had been deposited onto as-sprayed Cu-Ni-In following completed test to failure at 615 k cycles…….....115

Figure 5.6 BSE SEM images of fretting wear scars of a test where the DFL was deposited on an as-sprayed Cu-Ni-In flat sample that was interrupted at 200 k cycles a) plan view high magnified area, b) cross-section high magnified area…….....116

Figure 5.7 a) Evolution of ECoF with number of cycles for fretting tests to failure where the DFL was deposited onto either Ti-6Al-4V or Cu-Ni-In, both with a ground or grit-blast surface condition, b) Maximum depths of the averaged wear profiles of the flat ground Ti-6Al-4V and Cu-Ni-In and the flat grit-blasted Ti-6Al-4V and Cu-Ni-In samples as well as their round shot peened Ti-6Al-4V counterparts upon failure……. 119

Figure 5.8 Cross sectional BSE SEM fretting wear scar images of flat samples. (a) test with DFL which had been deposited onto grit-blasted Ti-6Al-4V following completed test to failure at 45 k cycles, (b) test with DFL which had been deposited onto grit-blasted Cu-Ni-In following completed test to failure at 229 k cycles…120

Figure 5.9 High magnification cross sectional BSE SEM images of flat samples from fretting wear scars, along with EDX analysis: a) test with DFL which had been deposited onto grit -blasted Ti-6Al-4V substrate upon failure at 45 k cycles, b) test with DFL which had been deposited onto grit-blasted Cu-Ni-In layer upon failure at 229 k cycles. 121

Figure 6.1 Fretting performance of the as-received MoS_2 bonded DFL coating (Mo-DFL) and the modified (Gr-Mo-DFL) version using relative fan blade root surface architecture. (a) Friction evolution against cycles of Mo-DFL and Gr-Mo-DFL deposited on top of a thermally sprayed Cu-Ni-In under-layer (b) The maximum depth of the averaged wear profile taken from the wear surface upon failure for Mo-DFL at 615 k cycles and at 1570 k cycles for modified Gr-Mo-DFL which was stopped before failure occurred. 130

Figure 6.2 BSE SEM images of the flat specimen of the Mo-DFL system upon failure at 615 k cycles (a) plan-view image (b) cross-sectional BSE SEM fretting wear scar images of flat samples. 131

Figure 6.3 BSE SEM images of the flat specimen of the Gr-Mo-DFL system stopped at 1570 k cycles (a) plan-view image with EDX analysis (b) Cross-

sectional BSE SEM fretting wear scar images of flat samples (c) High magnification of the top surface (d) Increased magnification. 134

Figure 6.4 ECoF evolution against cycles of (a) Mo-DFL deposited on top of a Cu-Ni-In under-layer and (b) Gr-Mo-DFL deposited on top of a Cu-Ni-In under-layer, at different fretting loading conditions. 136

Figure 6.5 Plotted graph of the fretting wear test cycles and the corresponding PV values of Mo-DFL and Gr-Mo-DFL on a cylinder-on-flat contact. Failure was defined to have occurred when $\mu \geq 0.7$ and tests to failure (i.e., to completion) were automatically terminated when that condition was first satisfied as the critical wear depth of the DFL coating had occurred. 138

Figure 6.6 Evolution of CoF against number of cycles for fretting tests conducted on flat-on-flat contact configuration where Mo-DFL was deposited on top of a Cu-Ni-In under-layer (a) contact pressures of 500 MPa, 350 MPa and 300 MPa are imposed with an applied displacement amplitude of 0.4 mm; (b) applied displacement amplitudes of 0.4 mm and 0.25 mm are imposed. A frequency of 2.5 Hz is maintained in all tests. 140

Figure 6.7 Evolution of CoF against number of cycles for fretting tests conducted on flat-on-flat contact configuration for Mo-DFL and Gr-Mo-DFL which were deposited on top of a Cu-Ni-In under-layer. Performance is compared under two different fretting loading conditions. 141

Figure 6.8 (a) Cycles to failure as a function of the PV value for tests conducted on flat-on-flat contact configuration for both Mo-DFL and Gr-Mo-DFL (b) Map of failure mode for tests as a function of sliding speed and contact pressure for tests with Mo-DFL conducted with the flat-on-flat test setup. The line where PV = 0.65 MPa m s^{-1} is superimposed and is seen to provide a clear boundary between regimes……. 143

Figure 6.9 BSE SEM images of the wear specimen of the Mo-DFL system tested on flat-on- flat contact undergoing a steady state low friction wear behaviour which was stopped at 50 k cycles (a) plan-view BSE image of the wear sample surface (b) EDX mapping highlighting Mo and Cu contents on the wear sample surface (c) Cross sectional BSE SEM fretting wear scar images of flat samples. 145

Figure 6.10 BSE SEM images of the wear specimen of the Mo-DFL system tested on flat-on- flat contact undergoing a high friction test to failure wear behaviour (a) plan-view BSE image of the wear sample surface (b) EDX mapping

highlighting Mo, Cu, Ti contents on the wear sample surface (c) Cross sectional BSE SEM fretting wear scar images of flat samples, (d) Averaged wear profiles of the steady state low friction wear and high friction test to failure wear. 147

Figure 6.11 An example of the thermal image captured prior to when a steady state low friction wear test was stopped at 50 k cycles. The image captures a side on view of the fretting wear interface and temperatures at the edge of the contacting surface and not the direct contact interface are recorded. 148

Figure 6.12 Evolution of CoF against number of cycles for fretting tests with the Mo-DFL system deposited on top of a Cu-Ni-In under-layer and conducted on the flat-on-flat contact configuration showing the recorded temperature near the contact interface by a thermal camera at intervening stages of fretting wear lifetimes at different PV values of (a) 0.6, (b) 0.7, (c) 0.81, and (d) 1. 149

Figure 7.1 Wear surface analysis of the fan blade root section I which features, (a) Image of section I (b) Topographical analysis with a sectioned line profile (c) Corresponding line profile result. 156

Figure 7.2 BSE SEM images of section I of the fan blade root (a) low magnification plan-view image of the section wear surface (b) high magnification area with EDX point analysis of the wear surface (c) cross-sectional BSE SEM image of fan blade root section I. 157

Figure 7.3 Wear surface analysis of the fan blade root section II which features, (a) Image of section II (b) topographical analysis with a sectioned line profile (c) corresponding line profile result. 159

Figure 7.4 BSE SEM images of section II of the fan blade root (a) low magnification plan-view image of the section wear surface (b) high magnification area with EDX point analysis of the wear surface (c) cross-sectional BSE SEM image of fan blade root section II. 161

Figure 7.5 High magnification cross-sectional SE SEM images of crack regions on the Mo- DFL coating on fan blade root section II. 162

List of Tables

Table 2.1 Nominal chemical composition of Ti6Al4V alloy in (wt.%) [31].....7

Table 2.2 Classification of tribological coatings, depending on the nature of the constituting material [134]. 27

Table 2.3 Friction coefficient of selected polymers when slid against a steel disk counter-face (surface roughness, R_a = 1.34 µm) with the corresponding specific wear rates and Pressure *(P)* × Velocity (*V*) conditions [201].....43

Table 3.1 Raw material specification 60

Table 3.2 Surface processing and surface characteristics of the various forms of the cylinder fretting specimens onto which the DFL was applied which were employed in the experimental programme 61

Table 3.3 Surface processing and surface characteristics of the various forms of the flat fretting specimens onto which the DFL was applied which were employed in the experimental programme.....63

Table 3.4 Fretting test conditions employed 69

Table 3.5 Environment fretting test conditions.....72

Chapter 1. Introduction

1.1 Background

Fretting is the small amplitude reciprocating motion that occurs between contacting surfaces which can lead to material degradation and damage within a system [1]. Fretting is a concern in many items of industrial machinery and in the aerospace sector, splines, joints and couplings (including dovetails and firtrees), and bearings are commonly affected resulting in localised damage and (of particular concern) significantly reducing the fatigue strength of the material [2]. One particular component where the suppression of fretting damage remains an active pursuit through the application of surface engineering and dry film lubricant coatings in the dovetail joint of an aero-engine fan blade which is particularly affected by wear and degradation [3].The dovetail joint experiences sustained fretting damage due to the inherent mode of operation of the system based upon the mechanical interlocking structure where a highly loaded Ti-6Al-4V fan blade root (due to centripetal forces upon engine rotation) moves within the Ti-6Al-4V disc dovetail and produces a small relative slip displacement. Ti-6Al-4V is well known to have poor tribological properties, and the damage associated with relative movement under load results in a significant deficit for the structural integrity of the system.

The study and investigation of fretting damage and associated palliative methods has been a focus of scientific research and industrial action for decades with the aim of understanding the complex mechanisms and failure modes which are associated with the evolution of fretting damage and testing and developing various methods of palliative resistance to combat these effects. With as many as fifty parameters which are reported to have an influence on fretting (including mechanical variables such as the normal load, displacement amplitudes, frequency along with additional variables such as environmental conditions, material composition, chemical interactions and the geometry and topography that make up the fretting contacts [4]), the complexity involved in understanding mechanisms and tackling the effects caused by fretting damage is an ongoing problem.

Current industrial practices to resist and reduce the effects of fretting wear on the aero-engine dovetail joint includes the use of a polymer-bonded MoS_2-based dry film lubricant (DFL) coatings which are often deposited onto a thermally sprayed

Cu-Ni-In under-layer which has already been deposited onto the fan blade root whilst the disc counterpart is shot-peened and DFL coated [5]. Dry film lubricants (DFLs) are applied on the contacting surfaces as a sacrificial layer to supress the effects of fretting. However, current DFLs typically have an inadequate lifetime and in order to avoid metal-metal contact within the joint associated with their total failure, often require re-application at intervals shorter than the normal engine maintenance schedule [6].

As such, further developments are required to increase the performance and durability of the coating system for extended operating lifetimes for the aero-engine fan blade root system, with a lifetime longer than the normal engine maintenance interval being the first target. Through initial small-scale laboratory tests that employ various contact geometries, fretting loading conditions and environments, the understanding and development of aero-engine DFL systems can be investigated and coatings with potentially enhanced performance developed and evaluated.

1.2 Research aims and scope

An experimental testing programme was initiated to further illuminate the effects of fretting conditions on the lifetime of aero-engine dry film lubricant system. The individual operational factors of environment conditions, substrate surface conditions and fretting loading conditions were explored to understand how they impact and influence damage mechanisms and fretting wear behaviours of the polymer-bonded MoS_2-based DFL coating system and how an extension of fretting lifetimes could potentially be achieved.

Conducted in partnership with Rolls-Royce plc, this research project also aims to expand and further probe initial findings of the extended fretting lifetimes and system durability delivered by the modification of a commercially available polymer-bonded MoS_2-based DFL (termed Mo-DFL) via a graphite additive.

A previous PhD programme conducted at the University of Nottingham highlighted the possible use of implementing a range of additives into the currently used Mo-DFL to extend the overall fretting lifetimes and augment the fretting wear stability associated with the current fan blade root system. Initial results found significant extension of fretting lifetime by mixing 4.76% of graphite powder to the as-received polymer-bonded MoS_2-based DFL system. Further investigation of the

performance limits of the graphite modified DFL coating system (termed Gr-Mo-DFL) were not fully explored and this shortcoming will be addressed in this current work to uncover the suitability of the graphite modified DFL coating system across a range of fretting conditions.

1.3 Objectives

- Investigate how humidity and oxygen influence the wear mechanism and performance of the polymer-bonded MoS_2-based DFL coating and uncover if the graphite modified DFL (Gr-Mo-DFL) is able to maintain extended fretting wear lifetimes across the range of humidity.
- Explore the effects on DFL lifetime of the surface profile and type of substrate upon which the polymer-bonded DFL is deposited. In particular, this work will seek to understand the mechanisms associated with the extension of fretting lifetimes when the DFL is deposited on top of a Cu-Ni-In interlayer (current industrial practice).
- Expand the experimental programme to a wider range of fretting loading conditions to understand the fretting wear behaviours and the limitations of the polymer-bonded MoS_2-based coating system (Mo-DFL) and the graphite modified DFL (Gr-Mo-DFL) and gauge the limits of performance under different loading conditions.
- Investigate the damage mechanisms associated with post-service fan blade roots to provide further insights into the failure modes that can occur in operation service, and to compare these with those observed in laboratory testing (thus validating – or otherwise – the appropriateness of the currently deployed laboratory test programmes).

1.4 Thesis overview

In Chapter 2, a critical review of published literature is presented which covers a breadth of topics that are actively related to the work presented in the thesis. A focus on the fretting wear mechanisms of MoS_2 and graphite solid lubricants and specifically, polymer-bonded DFLs is presented as well as a review of the effects of fretting loading conditions, environmental conditions and substrate surface conditions on wear performance and lifetimes.

Chapter 3 details the experimental methods used during this work and provides a description of the materials, substrate surface treatments, the methods used for coatings samples and experimental designs of the fretting tests. Techniques used for characterising the substrate surface and the wear samples are also explained.

Chapter 4 presents results and discussion relating to the effects of humidity and oxygen on the performance polymer-bonded MoS_2-based DFL (Mo-DFL) and the graphite modified MoS_2 DFL (Gr-Mo-DFL).

Chapter 5 presents results and discussion relating to the effects of interfacial geometry and material type upon which the MoS_2 DFL coating is deposited and how these influence the wear mechanisms and stability of the DFL coated fretting system.

Chapter 6 presents results and discussion relating to fretting tests conducted on both a cylinder-on-flat and a flat-on-flat contact configuration for both the polymer-bonded MoS_2-based dry film lubricant (Mo-DFL) and the graphite modified equivalent (Gr-Mo-DFL). This chapter explores fretting wear behaviours occurring on the DFL coated systems under a wide range of fretting loading conditions.

In Chapter 7, a case study into the operative damage mechanisms of an aero-engine fan blade root component in-service is undertaking. Presented results are compared to the behaviour observed on specimens from the laboratory experimental test programmes.

Chapter 8 presents the conclusions of the thesis which provides an overall discussion and summarises the key work reported in Chapters 4, 5, 6 and 7. Suggestions for future work are given in Chapter 9.

Chapter 2. Literature Review

2.1 Fan blade root

Aero-engine titanium fan blades and discs are brought together at the dovetail joint [7], [8]. The blade dovetail is somewhat loosely fitted into the disc and as the rotor spins, centrifugal forces push the fan blade root firmly and radially upward against the dovetail slot in the disc [9]. This design aids the ease of insertion and removal of fan blades (required, for example, if a single blade is damaged in service) [9] but also results in the potential for contact damage due to the highly loaded interaction on the blade-disc interface as the blade is subjected to radial and circumferential oscillation under a centrifugal force leading to fretting damage at the blade/disc interface during in-service operation [10], [11] as illustrated in Figure 2.1.

During engine start-up, the blade comes into contact with the disc socket by a centrifugal force, inducing a simultaneous rise in normal force and displacement along the radial direction. During flight operation, small vibrations and movements can also occur on the loaded contact. When the engine stops, the blade falls to the bottom of the socket, and the contact is then nearly unloaded [12], [13]. The occurrence of small oscillatory movements [14] which can vary in frequency, amplitude and load [15] between the two contacting bodies causes fretting damage on the surfaces of the blade and disc [8], [16] which can go on to cause initial removal of material, premature crack initiation and propagation and consequent blade rotor failure [9], [17]–[20]. The blade/disc contact interface involves a typical geometry defined by an inner flat/flat interface surrounded by symmetrical rounded edge corners. This confers a typical pressure profile with a central contact low pressure domain bordered by two lateral pressure peaks [21].

Further studies of the contact stresses of the dovetail joint through FEM analysis [10] have showed that the stress values are very high near the contact edges where the stress singularity is shown to occur along the contact length of the fan blade dovetail joint. The contact stress is maximum in the lower edge of the contact region due to the contribution of the bending stresses. Hence, the dovetail attachment is weak in the edges of the contact region.

Similar results have been reported by Shi et al. [22] on the investigation of fretting fatigue in a circular arc dovetail joint with FEM analysis found that peak stresses are located near the edge of the contact where an abrupt change of stress distribution takes place. Complication variations of contact state exists near the edge of the contact zone due to the mutual interactions of pressing and sliding between the contact surfaces which leads to high stress gradients near the edges of the contact zone.

In the study of the variation of contact state near the contact boundary in dovetail attachment under different loads, Wei et al. [8] also found that the high gradient stress near the edge of contact zone of blade/disk dovetail attachment is a dominant factor for fretting fatigue life which can be analogical to the singular stress at the crack tip which is usually several or more than ten times of the mean contact stress in the contact zone. By implementing a 2D fluid flow analysis to estimate the aerodynamic forces exerted on the blade along with a 2D finite element analysis which evaluated the stress analysis Kermanpur et al. [23] also determined stress concentrations acting on the dovetail joint to occur the edges of the dovetail contact regions.

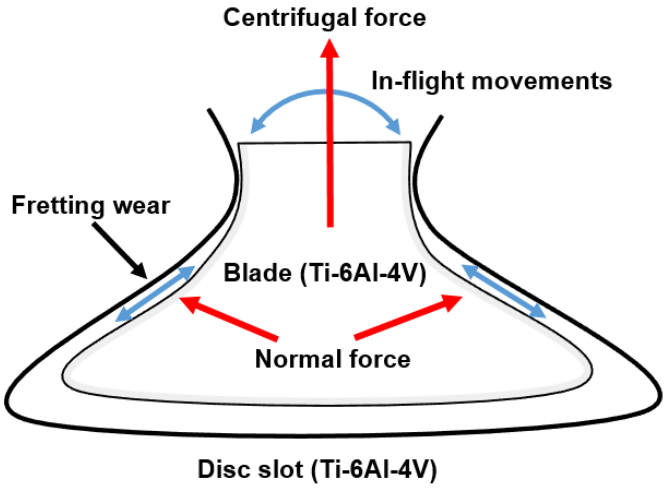


Figure 2.1 Illustration of fretting wear process at aero-engine fan blade/disc interface

2.1.1 Ti-6Al-4V alloy

The use of titanium alloys within the aerospace industry spans decades because of the unique set of properties of the material that include high specific strength, low density, excellent corrosion resistance and good high temperature performance which have been applied to both the structural and engine components in aircrafts [24]–[27]. Titanium based alloys are placed into three different categories; alpha titanium alloys, beta titanium alloys and alpha-beta titanium alloys [25], [28], [29].

Ti-6Al-4V is a two phase alpha-beta alloy (Figure 2.2) containing ~ 6 wt. % aluminium and ~ 4 wt. % vanadium (Table 2.1) [30], [31] which has the combination of strength, fracture toughness and ductile properties making it one of the most widely used titanium alloys in aerospace [26], [28]. Ti-6AL-4V is mainly utilised in the cold section part of the gas turbine engine, most notably for the fan blades and discs [32]. Titanium alloys exhibit poor tribological behaviour [24] which is a concern facing the aero-engine industry because of the susceptibility to fretting and severe adhesive wear in contact interfaces [33].

Table 2.1 Nominal chemical composition of Ti6Al4V alloy in (wt.%) [31]

Al	V	Fe	N	O	C	H	Ti
6.2	3.96	<0.20	<0.01	<0.03	<0.04	<0.003	Balance

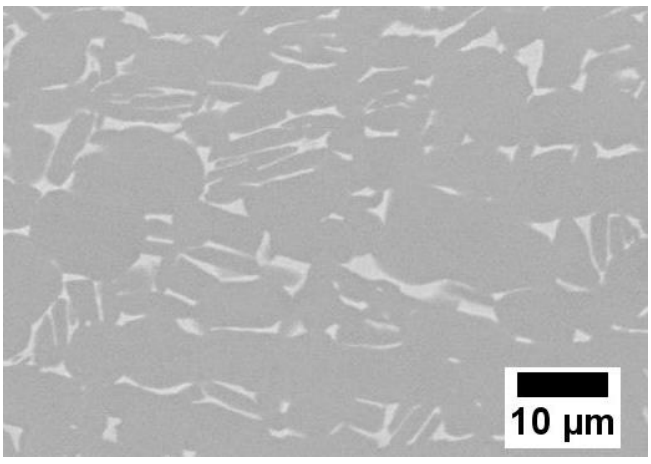


Figure 2.2 SEM images of the microstructure of α + β phases of the Ti-6Al-4V alloy.

2.2 Fretting

Fretting is the small amplitude oscillatory movement that may occur between contacting surfaces [15]. A comprehensive study on fretting was first conducted by Tomlinson [1] who characterised the occurrence of fretting as a small amplitude oscillatory motion between contacting surfaces when subjected to a load through a series of experiments that involved a plane and a spherical surface in relative motion under a load; the cause of the wear was cited as “molecular attrition”, noting the importance of the small relative displacement motion between the contacting surfaces. Prior to this, Eden et al. [34] had attributed the wear observed between the specimen and holder to alternating stresses.

Extensive work has since been carried out to further understand fretting behaviour of various materials and conditions. Fretting of metals is often identified by the production of oxide debris [35] in which Tomlinson et al. [36] further went on to examine, coining the term *fretting corrosion* from the red oxide observed. This oxide production was later understood to be the result of mechanical and environmental factors [37] rather than corrosion as some characteristics of the phenomenon can be ascribed to wear (formation of indentation and scars) and other characteristics are similar to corrosion (oxide formation). Fretting is difficult to predict due the large numbers of parameters affecting it and the complex interactions between them [38].

Fretting is said to be distinguished from reciprocating sliding wear by the displacement amplitude with the suggestion of 300 μm being the upper limit of fretting before the transition to reciprocating sliding wear [39]. Fouvry et al. [40] however defined the occurrence of fretting as when a fraction of the contact remains intact with the contact (unexposed) during the displacement cycle. A contact condition that limits environmental exposure to the centre of the contact promoting an oxygen depleted area [41] and the entrapment of loose wear particles within the scar adds to the complexity and tribo-chemical aspect of fretting. The initiation of fretting as noted by Godfrey et al. [42] is recognised by the increasing concentration of loose oxide debris found in and around the contact area and metal transfer between the surfaces in contact. Such relative oscillatory movements between contacting surfaces is usually the result of external vibration or the presence of cyclic stress which can affect many items of industrial machinery as well as mechanical and bolted or riveted joints [15]; in the aerospace sector,

turbomachinery splines, bearings and couplings are affected resulting in localised damage and drastically reducing the fatigue life of the material [43]–[45].

2.2.1 Fretting damage

Fretting damage is characterised into two broad categories, namely fretting wear and fretting fatigue [46], [47]. The former, wear, relates to the removal of material from the surfaces while the latter, fatigue, is linked to the nucleation and propagation of cracks [18]. Both are driven by the rate of formation of third-bodies between the initial contact surfaces [48]. Fretting wear in metals is induced by debris formation [35] from any one of the basic wear mechanisms (adhesive, oxidative, abrasive and surface fatigue) [49] with two or more mechanisms often occurring simultaneously depending on the operating parameter [50] and under varying wear modes (mostly tangential but also including torsional, radial and rotational modes [51]) and is usually the result of external vibration [52].

Fretting fatigue combines surface and bulk fatigue [49], [53] and is the consequence of one of the members of the contacts being subjected to cyclic fatigue loading [47]. Fretting fatigue failure is characterised by the nucleation and propagation of small cracks, often towards the edge of the contact patch [16].

This work centres on a palliative for fretting wear and the interactions that occur both mechanically and chemically between contacting surfaces to the point where the consequence fretting results in damage to the Ti-6Al-4V bodies due to wear.

2.2.2 Fretting wear mechanism

As previously mentioned, fretting of metals can include many of the basic wear processes. At initial stages when metal to metal contact is realised, both the mechanical and chemical aspects are present with a mechanical mechanism resulting in local welding, roughening of the surface, high friction and low contact resistance [15]. Metallic debris particles are formed which then oxidise to form an oxide debris [39]. Oxides protect the surface from damage while they remain adhered and at this stage, the oxide beds separate the fretting surfaces, reducing the metal-metal contact, adhesion and the coefficient of friction; however, depending on the hardness, the oxide can cause abrasive wear when they become loose [49], [54], [55]. The oxide layer is prominent in the intermediate stage as beds

of oxide debris begin to form. The oxides that form on a surface may be removed to form the debris as new oxide grows on the metal surface [15]. The final stage of fretting wear is referred to as steady state, where friction remains constant and the contact resistance is generally high. The previously formed oxide beds remain dynamically stable as debris continues to be formed and ejected [15].

The friction contact between similar and dissimilar metals has also been discussed in terms of mutual solubility. Mutually soluble pairs exhibit strong adhesive bonding and hence high friction, while insoluble pairs show weak adhesive bonding and hence low friction [56]. According to Rabinowicz [57], adhesion and friction should decrease as one progresses from couples of the same material and those that from solid solutions to insoluble couples and to metal non-metal pairs. However this approach should be regarded as a general guideline and not as an ultimate design rule for the selection of materials involving moving contacts [56].

2.2.3 Fretting wear mechanism of titanium alloy

The peculiar susceptibility of titanium alloys to fretting wear is an issue in the dovetail sections of the fan and compressor in turbine engines [58]. The vulnerability of titanium alloys to fretting can be attributed to the low resistance to plastic shearing and low protection exerted by surface oxide [10,11].

When subjected to fretting, there is a disruption of the thin oxide layer which can create hard oxide debris particles that become abrasive [61] and score the surface interface [62]. Other studies have suggested that the size of the particles in the contacts rather than the hardness is what causes the debris particle to become abrasive [63]. Further studies were undertaken by Sauger et al. [64] who argued that the initial debris generated on Ti-6Al-4V contacting surfaces comes from "*Tribologically Transformed Structures (TTS)*" also termed the "*Mechanically Mixed Layer (MML)"* by Rigney et al. [65]. The study by Sauger et al. [64] proposed that a nano-crystalline like structure is formed at the initial layer, although chemical analysis showed that the chemical composition of the TTS remains similar to that of the bulk material (Figure 2.3). The TTS layer formed on Ti-6Al-4V was three times harder than the bulk material.

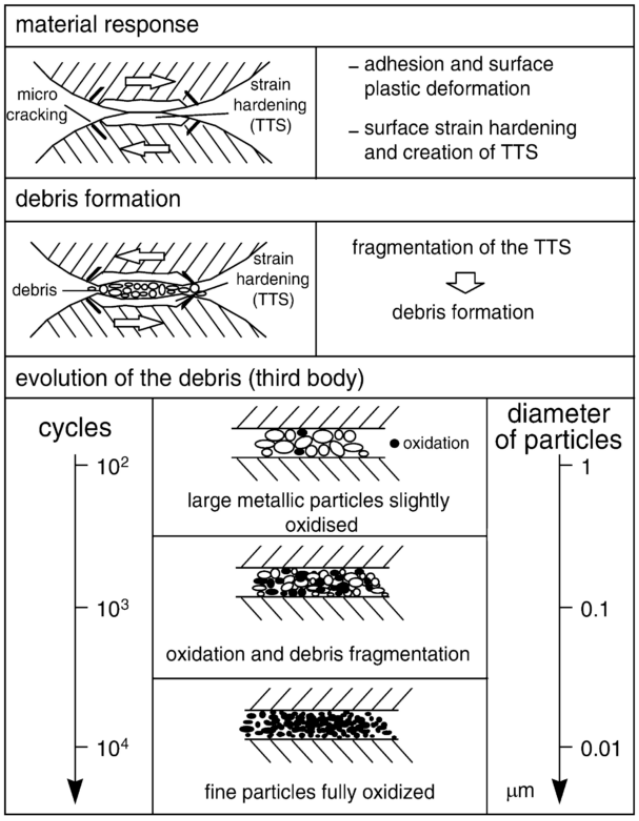


Figure 2.3 Creation and evolution of the third body through the contact interface [64]

Rigney et al. [65] argued that plastic deformation under the surface caused by the local contact results in the accumulation of strain which further aids shear instabilities in the near-surface encouraging the transfer and a complex mixing process to take place at the interface leading to the formation of a "*Metallic Mixed Layer (MML)*". The contested mechanism of the formation of this layer remains disputed. However, the influence of the two contacting parts along with the environmentally active components such as oxygen or nitrogen were said to be a key part on the formation of the MML which encourages the complex, intimate transfer and mixing process taking place at the interface from which debris particles are generated. In dry titanium alloy contacts, the reduction or low concentration of contact oxygenation can lead to a nitriding process in the centre of the fretting interface [12], [66].

2.2.4 Quantifying fretting and wear

2.2.4.1 Fretting maps/regimes

Vingsbo and Soderberg [39] introduced the concept of fretting maps which altered the way that fretting was reported. Through the recording and comparison of force-displacement loops (fretting loops), three distinct fretting regimes were identified[39], [67];

- Stick: Characteristic of very low displacement amplitudes (Figure 2.4). The wear scar shows no visible damage beyond limited plastic shearing of individual asperities with no indication of material damage in between.
- Stick-slip (partial-slip): At higher displacement amplitudes, a central stick area with a surrounding the slip-annulus was seen. There was evidence of plastic shearing of asperities in the central stick region similar to the stick regime; however, considerable damage has been inflicted on the contacting surface.
- Gross-sliding: The entire wear scar shows extensive plastic shear and visible sliding marks. Across the gross-slip fretting regime, the wear coefficient is thought to increase between one and two orders of magnitude as the fretting displacement amplitude increased.

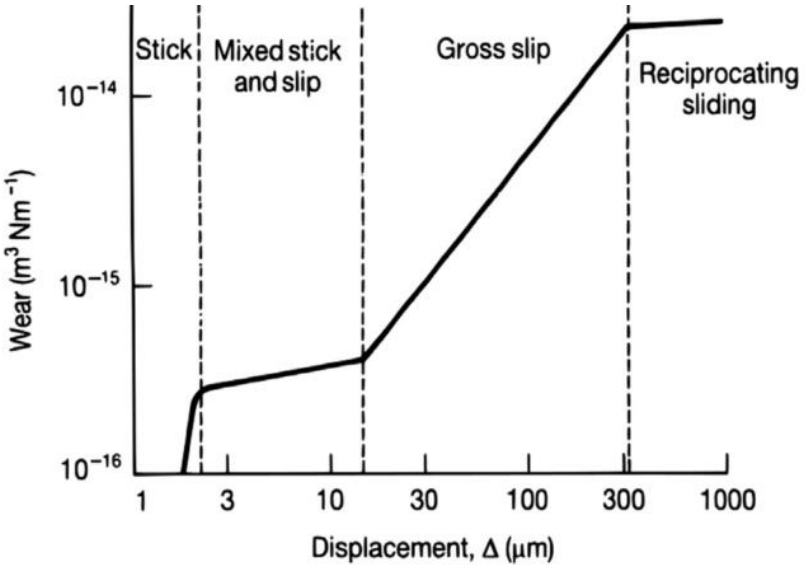


Figure 2.4 Illustration of the dependence of wear coefficient with displacement amplitude in fretting with reference to the slip regime. Cited by [67] and recreated from [39].

The wear mechanics operating within the fretting contact described by Mindlin [68] stated that when a normally loaded, non-conforming contact experiences a tangential load, there will be an inner region of the contact which is stuck and an outer region which experiences slip (making up partial slip conditions). The stuck zone will decrease in size until the tangential force is equal to the product of the coefficient of friction and the normal load. If slip occurs over the whole contacting region, the contact is said to enter the gross sliding regime [69].

Originally, the concepts proposed by Vingsbo and Soderberg derived from Mindlin's [68] fretting contact model had been assumed to be stable, i.e., not a function of slid distance. However, Zhou et al. [70] later introduced new regimes called the mixed fretting regime (MFR) which strongly depends on the normal load, imposed amplitude and material properties such as elongation. This regime is characterised by unstable fretting loops with periods encompassing elliptical fretting loads and periods of open fretting loops.

2.2.4.2 Description of fretting loops

Force-displacement plots, referred to as fretting loop are an essential tool in quantifying and defining fretting damage. A schematic diagram of a fretting loop is displayed in Figure 2.5. The applied displacement amplitude between the bodies is represented by the symbol Δ^*, and the corresponding maximum tractional force is Q^*. It should be noted that Δ^* is measured remotely from the contact and is distinct from the slip amplitude in the contact which is abbreviated as δ^*. The slip amplitude (δ^*) is always smaller than the applied displacement amplitude (Δ^*) and can be derived from the fretting loop as the displacement amplitude at zero tractional load [71], [72].

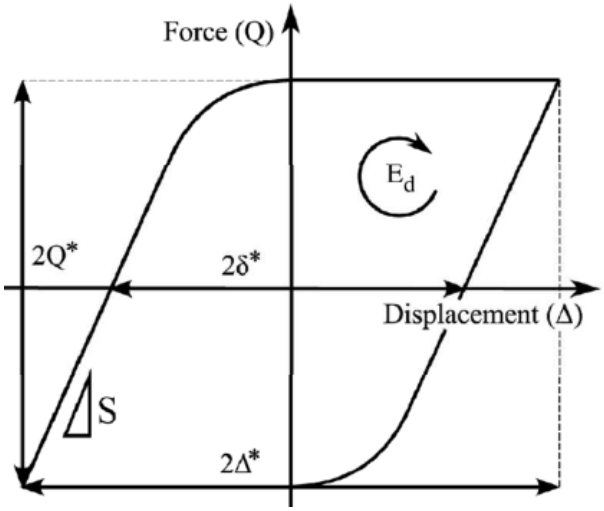


Figure 2.5 Schematic diagram of an idealised fretting loop [72].

There is a compliance in the system associated with elastic deformation of the specimens, the fixture and the test rig which physically separates the contact from the point of measurement. This is represented as the system stiffness, S, indicated as the slope at the side of the fretting loop. The displacement amplitude (Δ*) is often the controlled parameter in a fretting test. The slip amplitude (δ*) is dependent upon the tractional force in the cycle and the stiffness associated with the fretting rig as seen in the following equation:

$$\delta^* = \Delta^* - \frac{Q^*}{S}$$

Equation 2.1

where Q^* is the tractional force and S is the system stiffness.

The coefficient of friction is described by the following equation;

$$\mu = \frac{Q^*}{P}$$

Equation 2.2

In response to the ploughing effects associated with the traditional calculative method of coefficient of friction which can overestimate the global friction behaviour, Fouvry et al. [73] proposed the concept of energy coefficient of friction (ECoF) with the aim of producing a better representation of fretting contact through the energy dissipated over a fretting loop (E_d).

The dissipated energy per cycle, (E_d), is visualised by the area enclosed within the fretting loop (Figure 2.5) which relates to the friction work dissipated per fretting cycle due to micro-slip and gross sliding of the contact [74]. The area enclosed within the fretting loop can be estimated as 4*Q*δ* [67]. The accumulated dissipated energy is the sum of all dissipated energy magnitudes occurred during an entire fretting test.

The energy coefficient of friction is as follows;

$$\mu_E = \frac{E_d}{4\ P\ \delta^*}$$

Equation 2.3

The dissipated energy approach integrates the friction coefficient through its formulation and so allows more stable quantification of wear response for the tribosystem [75].

2.2.4.3 Wear rate

The Archard model [76] is the most common wear model proposed in tribology. The Archard equation relates the wear volume to the product of sliding distance and the normal force. From the model, a wear coefficient is obtained from the following equation;

$$k = \frac{V}{PS}$$

Equation 2.4

where *k*, is the wear coefficient, *V* is the wear volume, *S* is the sliding distance and *P* is the normal force. This quantitative analysis of wear takes a sliding wear perspective with an assumption that the real area of contact is proportional to the normal load with asperity contact being plastic in nature. The wear coefficient, *k*, measured in mm^3 / N m represents the volume of the material removed per unit sliding distance per unit normal load. The use of this model is a fundamental tool for comparing the wear performance of different materials and surface engineering methods of reducing wear. This was later transformed into an effective energy-based wear coefficient by Fouvry et al. [75] who developed and examined wear volume as a function of dissipated energy (Figure 2.6) and added an energy dissipated dimension to the wear coefficient. The energy wear coefficient (k_E)

considers a different form of wear coefficient defined as the volume of material lost per unit of energy dissipated in sliding (units of $m^3\ J^{-1}$). With this method, plain materials and coatings can be quantitatively compared [40].

$$k_E = \frac{volume\ (m^3)}{energy\ (J)}$$

Equation 2.5

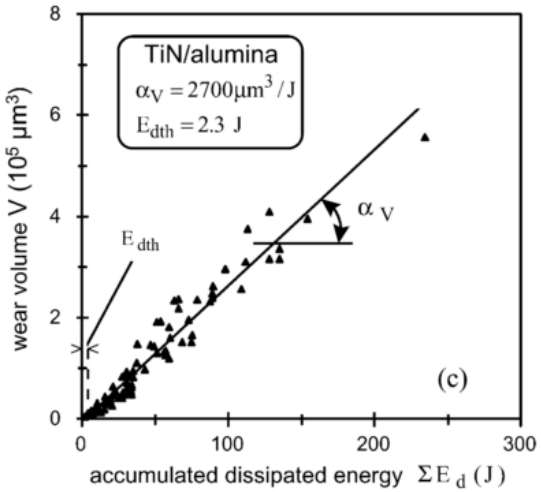


Figure 2.6 Energy analysis of the wear volume as a function of accumulated dissipated energy for fretting of TiN/alumina [75].

2.3 Parameters affecting fretting

2.3.1 Contact geometry

The type of contact geometry used dictates the degree of retention or ejection of wear debris in the contact and alters the contact pressure and distribution; this parameter is central to the fretting mechanism and can dictating the level of surface damage sustained on the material [77], [78].

Fouvry et al. [79] conducted studies aiming to uncover the impact that contact configuration has on fretting mechanism. The coefficient of friction and wear rates displayed an asymptotic decrease as the contact size increased until a steady state was reached. Fretted scar analysis suggested that an increase of the contact area accentuates the influence of the third body in the interface response. The friction and wear are reduced when debris are trapped within the interface, creating a

thicker third body layer and easy shear interfacial accommodation. Contact size has a critical impact on the wear rate. The larger the contact size, the smaller the wear rate. Compared to the size of the contact area, the contact morphology was found to not be a dominating factor which implied that a plain cylinder/plane contact configuration can be used to describe complex flat and rounded geometry assuming an equivalent contact size [21]. Similarly, Warmuth et al. [80] argued that the dependence of wear rates and mechanism for a high strength steel was associated with the influence of contact geometry on debris flow out of the fretting contact but also on the effectiveness of oxygen being able to diffuse into the centre of the fretting contact to promote oxide formation.

Flat-on-flat contact geometries can provide better description of the real blade/disc interface allowing a quasi-contact contact area and therefore constant pressure [81]. One of the drawbacks of flat-on-flat contact configuration is the stress concentration existing at the border of the contact which leads to a discontinuous pressure distribution at the interface. Numerical simulations of an original flat-on-flat experiment reveal a homogenous flat mean pressure profile after a fast honing of the contact borders induced by the fretting wear process. Except for the edges, iso-pressure conditions are achieved in less than 500 cycles resulting in uniform elastic pressure distribution [82].

Merhej et al. [83] utilised a non-conforming ball on flat configuration and found that wear was significantly lower for a larger contact with wear dropping asymptotically with increasing contact size and arguing that an increase in the contact area generates a third body layer at the interface and debris ejection is made more difficult as the contact size increases. Small contact sizes facilitate oxygen access to the contact favouring abrasive wear and high wear rates. On the other hand, larger contact sizes causes effective oxygen exclusion at the centre of the contact resulting in severe adhesive wear in the middle of the scar; this explains the preferential abrasive wear at the edges of the contact which are oxygen-rich, and the favoured adhesive wear toward the centre [84].

2.3.2 Fretting loading conditions

Mechanical loading variables in fretting include the normal load, displacement amplitude and frequency [85]. Studies on the effects of fretting loading conditions have generally shown that fretting wear is directly proportional to applied normal loading and sliding distance [76], [86].

The applied load and induced displacements ultimately control the sliding regime and intrinsically, the damage mechanism. An increasing normal load leads to a greater fraction of an applied displacement being accommodated by elastic compliance of the system [87]. For a given displacement amplitude, a change in applied load will result in a change in the slip amplitude due to system compliance, and that ultimately, this may result in a change in fretting regime (potentially from one of gross sliding to the stick regime) [15].

At non-conforming contacts, Tobi et al. [88] found that high loads will induce more plastic deformation and subsequently high wear rates in the early fretting cycles, but lower wear rates later in the test compared to low load cases.

In contrast to reciprocating sliding, the severity of fretting wear has been linked with increasing displacement magnitude [11] because of the abrasive wear produced by the entrapment of particles between the interfaces and the increased energy input observed in fretting [89], [90]. The displacement amplitude dictates the imposed relative movement of a constant stroke to and from the contacting point which is essential for fretting to occur as demonstrated by Tomlinson et al. [36]. This dependence upon displacement amplitude has spawned various studies with the purpose of uncovering the specific role of displacement amplitude within the fretting process.

Fretting wear of an Inconel 600 alloy was explored at different displacement amplitudes in the work by Li et al. [91] with the effects of displacement amplitude on the ratio of tangential force to normal load and wear volume being analysed. A strong effect of displacement amplitude was demonstrated with the authors finding a correlation between the increase of displacement amplitude, the ratio of tangential and normal applied load and wear volume, with these gradually increasing due to a transformation of the fretting mode from partial slip to gross sliding. Fan et al. [92] came to the same conclusion, observing an increase of Q/P ratio as displacement amplitude increased owing to the transformation of the fretting regime from partial slip regime to gross slip when the displacement amplitude was > 70 μm.

Two wear mechanisms have been proposed to explain how the increase in wear rate and friction coefficient relates to the increase of sliding amplitude; this includes the theory that the larger the sliding amplitude, more oxide debris is generated during the fretting tests and the easier the debris ejection becomes, and consequently the higher the energy wear rate [21], [91], [93]. The second hypothesis looks at how an increase in the sliding amplitude changes the exposure

of the contact to oxygen; it enlarges the zone exposed to the oxygen-rich environment and influences the fretting wear mechanism [40]. At low displacements, a decrease of oxygen access to the fretting contact interface can enhance contact adhesion [94] and at higher displacement, greater oxygen concentration can lead to a combination of adhesive, abrasive and oxidation wear mechanisms [92]. Baydoun et al. [81] studied how the two hypothesis of contact oxygenation and third body ejection can influence the evolution of wear rate of a steel contact in a dry flat-on-flat contact configuration by varying several parameters including test duration, contact pressure, sliding amplitude, and frequency. In this study, abrasive morphologies with the increase of sliding amplitude were found which is thought to be linked with both (i) the contact oxygenation which promotes an abrasive wear process and in turn increases wear rates and (ii) the third body mechanisms which favour the process of detachment and ejection of debris particles and in turn, increase wear rates, making the two fundamental concepts highly connected in terms of wear mechanism.

Easy contact oxygenation is promoted by low contact pressure, low frequency and small contact size and varying normal force which favours a U-shape fretting scar morphology and high abrasive wear rates. By contrast, increasing contact pressure, frequency and contact size reduces the contact oxygenation in the centre of the contact which promotes adhesive metal/metal interactions, transfers and TTS structures which induces a W-shape fretting scar and lower wear rates [12].

The role frequency has on fretting wear has been explored by Soderberg, Bryggmann and McCullough [95]. This study investigated the fretting wear behaviour of low carbon steel (AISI 1018) and stainless steel (AISI 304) under a series of vibrating frequencies ranging from 10 to 20,000 Hz. The temperature and strain rate generated in the interfacial material will both increase with increasing frequency. The contact conditions and the rate of surface damage being affected as frequency was increased.

Additional conditions have been considered alongside frequency. Warmuth et al. [96] who proposed that frequency and contact conformity fundamentally control the wear behaviour through influence of both the debris type and the retention or ejection of that debris from the contact. Debris retention within the contact is promoted by higher fretting frequencies which was associated with higher temperatures promoting debris agglomeration and sintering in the contacts.

A study by Peteghem et al. [13] reflected on the effects of variable normal force and frequency on fretting wear on Ti-6Al-4V contacts and found that increasing the loading frequency reduces the wear rate. When the frequency is increased by a factor of 45, the wear rate is reduced by a factor of 5. The loading frequency and, potentially, the sliding speed significantly affects the fretting wear kinetics. The reason why low frequencies (i.e. slow sliding speeds) induces higher wear rate remains unclear as it has been commonly observed that increasing the sliding speed leads to higher friction energy flow within the contact interface, resulting in high contact temperatures. Higher temperatures are supposed to accelerate the tribo-oxidation process and consequently the wear rate.

Jin et al. [97] investigated the role temperature and frequency plays in stainless steel contacts under fretting wear and expressed the complexities of the mechanism and rates of fretting under the influence of the two parameters (temperature and fretting frequency). At low temperatures, the author noticed that the ejection of formed oxide debris from the contact as wear proceeded was evident and as the temperature increased, retention of oxide debris that was formed developed into a protective oxide bed reducing the wear rates observed, however it was the frequency that dictated at which temperature the transition takes place.

2.3.3 Environmental conditions

The variations in environment factors such as the temperature, humidity and atmospheric gas content as well as the different materials in fretting contacts can have influence on the fretting damage observed due to their being a strong dependence of the tribo-chemical reaction on environment and operating conditions [98]. Wharton et al. [99] suggested that the formation and composition of corrosion products depended on the nature of the environment in which the contact is operating. Earlier studies on the effect different environmental conditions on fretting wear include works by Feng and Uhlig et al. [100] who found that fretting wear of mild steel decreases monotonically with increasing humidity indicating that moisture decreases abrasive wear associated with the oxide debris or decreases the rate of the chemical reaction of oxygen with iron.

Other studies focusing on iron, nickel and titanium fretted under varied humidity found differing results as each metal had their maximum fretting wear at a particular relative humidity with the iron and titanium exhibiting maximum fretting

wear rates at ~ 10 and 30 % relative humidity (RH) respectively whilst nickel exhibited a minimum fretting wear rate at ~ 10 % RH and increased as humidity also increased [101].

2.4 Mitigation of fretting damage on the fan blade root system

The familiar occurrence of fretting damage in industrial machinery has prompted initiatives to curb or reduce the rate of the degradation process imposed by the mechanical and chemical interactions. Such preventative efforts have usually employed three basic methods; change of design, surface engineering and the use of lubricants [102].

2.4.1 Change of design

Geometrical modifications that alter the contacting surface to supress the effects of fretting such as the blisk have been considered by Gordelier et al [103]. The blisk is an acronym derived from “blade and disc” and is one such design that aims to eradicate the blade/disc interface in cases where operating lifetimes are limited by fretting in gas turbine engines [104]. The blisk is a single engine component consisting of a rotor disc and blades which may be integrally cast, machined from a solid piece of material or fabricated by welding individual blades to the rotor disc.

Disadvantages of this design is the laborious and costly manufacturing process along with the quality control required to enable optimum performance [104]. Another setback of this design is the overhaul process. With a dovetail attachment, individual blades needing repair can be easily removed and replaced. The blisk on the other hand will require the entire blade/disc component to be overhauled or entirely replaced by a new one even if only one aerofoil of a blisk is damaged [105].

2.4.2 Surface engineering methods employed on fan blade root

Since fretting is related to wear, corrosion and fatigue [35], [46], readily available and well-established industrially deployed surface treatment techniques to combat the effects of fretting span several decades. Fu et al. [102] highlighted the mechanisms by which surface treatments are thought to increase fretting

resistance. These included (i) inducing a residual compressive stress; (ii) increasing the surface hardness; (iii) altering the surface chemistry and (iv) increasing the surface roughness. The intrinsic properties of the coatings, such as their density and mechanical and chemical properties as well as their adhesion to the substrate have been said to also significantly affect the performance of the coating under fretting conditions [102], [106].

To actively prolong the lifetimes of aero-engine fan blades, the current practices to curb the effects of fretting include the application of different surface engineering methods. Shot-peening in combination with a plasma sprayed copper-nickel-indium alloy coating followed by application of a polymer-bonded MoS_2-based dry film lubricant coating on the fan blade [107]–[113] is reported to be an effective process currently used. Whilst shot peening and the deposition of dry film lubricants can be applied to both the blade root and disc surfaces, geometric restrictions typically prevent the deposition of a thermally sprayed Cu-Ni-In under-layer on the disc interface leaving just the blade root to be thermally sprayed [114], [115].

Shot peening is among one of the more widely used techniques to enhance the material's resistance to fretting by the mechanism of inducing residual compressive stress on the surface [107]. The shot peening technique introduces compressive residual stress into the metal surface by way of propelling small beads (made from various materials including steel, cast iron, glass or ceramic) varying from 0.1 to 0.3 mm in diameter at high speeds onto the part to be treated [116]. This is reported to improve the fatigue strength on the surfaces of the component by delaying crack initiation and propagation [117]. Shot peening alters the properties of a material which include the introduction of a compressive residual, altering the surface roughness of the material and stimulating work hardening of the material near the surface [118].

The relative low cost and practicality of the method makes it one of the most widely used surface treatment techniques for Ti-6Al-4V titanium alloy components in gas turbine engines [119].

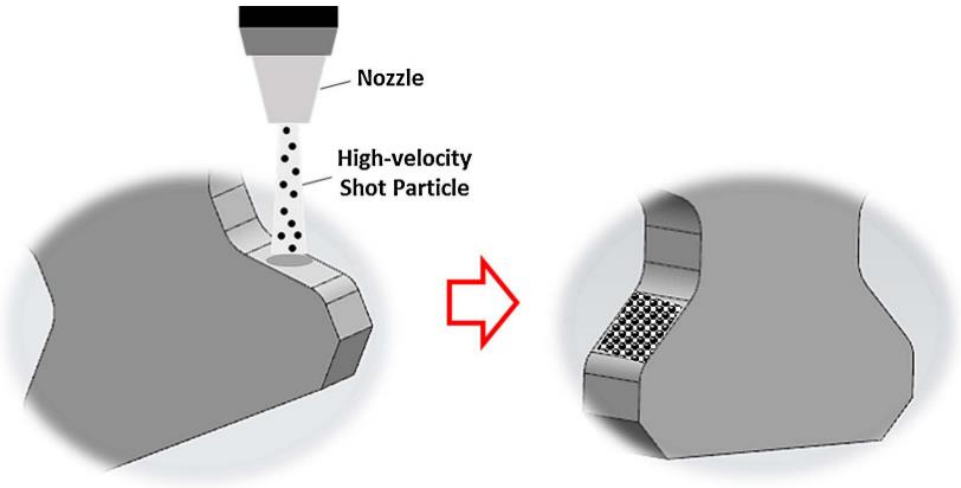


Figure 2.7 Schematic drawing of shot-peening treatment and surface state of fan blade root [107]

Thermal spraying covers a wide range of techniques in which coating materials are heated rapidly in a hot gaseous jet and thus projected at high temperature and high velocity onto a surface to produce a coating [102].

Thermally sprayed coatings are usually used at the blade/disc interfaces of aero-engines in order to increase fretting fatigue and wear life and consist of a metallic interlayer (e.g., containing elements of 59 wt. % Cu, 36 wt. % Ni, and 5 wt. % In) [11]. It has been argued that thermally sprayed Cu-Ni-In coatings for application in turbine engine blade attachments provide a soft layer to accommodate relative slip between components [120]. Additionally, the Cu-Ni-In layer performs as a mechanical retainer for any solid lubricant films which are subsequently deposited because of their high surface roughness [121], [122]. The presence of the Cu-Ni-In layer in the surface engineered system architecture is thought to alter the fretting contact configuration as it is less stiff and less resistant to plastic deformation than the fan blade material, with an elastic modulus of 60 GPa and a Vickers hardness of 170 HV compared to 119 GPa and 360 HV respectively for the Ti-6Al-4V blade [121].

By conducting fretting wear tests on unlubricated self-mating Ti-6Al-4V surfaces with a hardness of 284 HV, an elastic modulus of 143 GPa and a roughness (Ra) of 0.1 µm and then on Ti-6Al-4V mated against Cu-Ni-In which had a lower hardness and elastic modulus of 138 HV and 90 GPa respectively and a higher surface roughness (Ra) of around 9 µm, Hager et al. [58] observed comparable

coefficients of friction within the two systems that ranged between 0.68 – 0.85, however, less short-term variation in the friction coefficient (and hence, greater stability) was observed for the system where one of the components had the Cu-Ni-In coating.

This has also been observed in by Fridrici et al. [122] who conducted experimental tests to simulate the blade/disc interface (without the application of additional solid lubricant coatings) to determine the fretting wear behaviour of the Cu-Ni-In plasma coating and found that the friction coefficient (CoF = 0.9) to be the same with and without the CuNiIn coating. Due to the low hardness of the coating, the presence of the CuNiIn coating reduces the length of the cracks observed on the counter-body in Ti-6Al-4V and increases the contact area between the components.

Limited influence on the friction coefficient has been observed with or without the Cu-Ni-In coating but a reduction of wear has been reported [123]. This was credited to the delamination wear of the CuNiIn layer which generates soft and large flake debris that could be easily retained in the contact area to form a third body whilst under fretting [124]; the effective load carrying capacity of the debris effectively inhibited the damage of the Cu-Ni-In coated specimen.

2.4.3 Lubricants

Lubricants prevent fretting wear by lowering the coefficient of friction and can be categorised into three different physical states; liquid, semi-solid and solid lubricants [125]. Their overall effect, has however been subject to particular scepticism because of their low durability [126]. Targeted coating selection considers the fretting failure modes and properties of the lubricant coating including their physical, mechanical and chemical properties and adhesion with the substrate, which are all factors which are related to the performance of the coating [127], [128].

Liquid lubricants are generally oil based and restrict access of oxygen to the surface and provide a reduction of friction and adherence of the wearing surfaces and so has been implemented to combat fretting and corrosion [129] with the effects being most notable in the early stages of fretting [129]. Grease as a form of thickened oil is one of the most important semi-solid lubricant used in tribo-systems and acts to inhibiting oxygen access to the fretting contact as well as lowering the coefficient of friction [126]. Grease life is determined by the sustainability of the

lubricating and physical properties of grease which can be changed by mechanical and chemical degradation which primarily involves oxidation and evaporation [130].

A solid lubricant is defined as any solid material which reduces friction and/or wear of contacting surfaces in relative motion [131]. Whitehouse [132], defined solid lubricants as materials in the solid phase which leads to an improvement in sliding conditions when interposed between two sliding surfaces. Solid lubricants have been applied to fretting surfaces where liquid lubricants are deemed to be inadequate in controlling friction and wear under the appropriate service conditions including environments at high vacuum or high temperatures, or with highly loaded contacts and at high speeds [102]. Dry lubrication with solid lubricants is also required in nuclear reactors, in aggressive environment, and in applications where contamination by lubricating oils or greases cannot be tolerated [131].

The variables affecting the effectiveness of solid lubricants can include substrate metallurgy, stress levels, environment and adhesion between coating and substrate [133]–[135]. The implementation of solid lubricants can deliver a significant decrease in friction and wear under certain conditions; however, their durability under extended use has been called to question by the limited lifetime they possess since their replenishment into the contact is much more difficult to achieve than it is with liquid lubricants [135], [136]. The four main factors influencing tribological behaviour of coatings according to Mathews et al. [137] are i) hardness of the coating and substrate, ii) thickness of the coating, iii) roughness of the coating surface and iv) size and hardness of the debris in the contact.

2.5 Solid lubricants

The limitations associated with the physical states of liquid and semi-solid lubricants has led to the adoption and widespread use of solid lubricants which were originally developed for aerospace applications [138]. The desirable environmental and durability capabilities attributed to solid lubricants in controlling wear and reducing coefficient of friction in different applications has generated an increasing use of solid lubricants to replace liquid lubricants [56]. The ideal scenario for achieving low friction according to the Bowden and Tabor ([139]) concept is to have an elastically stiff and hard substrate to support the normal load and keep the contact area small, while the surface coating provides shear

accommodation and reduces junction strength, until the substrate begins to yield and plastically deform [56].

Based on their physical, chemical, structural and mechanical properties, solid lubricants can be categorised in two broad categories; soft solid lubricants with a hardness $\leq$ 10 GPa and hard solid lubricants exhibiting a hardness $\geq$ 10 GPa [134]. This distinction can be seen in Table 2.2. Hard coatings include oxides, carbides, nitrides, borides and some carbon-based compositions such as diamond-like carbon (DLC) coatings. Soft coatings include polymers, soft metals, and lamellar solids [127].

The focus within this work lies within the use of lamellar structured solid lubricant coatings. Among the best known examples of lamellar or layered solid lubricants are molybdenum disulfide (MoS_2), graphite and hexagonal boron nitride (h-BN) which are natural minerals [140], [141] Other lamellar solids, such as WS_2 and fluorinated graphite, are synthetic and are used at much smaller scales than graphite, h-BN and MoS_2 [140]. Lamellar based solid lubricants owe their lubricity to their unique layered structure [131]. The crystal structure of these solids are such that while the atoms lying on the same layer are closely packed and strongly bonded to each other [133], [134], the layers themselves are relatively far apart and the Van der Waals forces that bond them are weak. When such materials are present between sliding surfaces, these layers can align themselves parallel to the direction of relative motion and slide over one another with relative ease, thus providing shear accommodation and low friction [140], [141]. In addition, the strong interatomic bonding and packing within each layer is thought to help reduce wear damage [56], [140].

Table 2.2 Classification of tribological coatings, depending on the nature of the constituting material [134].

Hard coatings **Hardness higher than ≈ 10 GPa**	**Soft coatings** **Hardness lower than ≈ 10 GPa**
Nitrides TiN, CrN, ZrN, BN, $BaSO_4$ **Carbides** TiC, WC, CrC **Oxides** Al_2O_3, Cr_2O_3, TiO_2, ZnO, CdO, Cs_2O, PbO, Re_2O_7 **Borides** TiB_2 **DLC & Diamond** a-C, ta-C, a-C:H, ta-C:H, CN_x a-C:X(:H), (nc-)diamond	**Soft metals** Ag, Pb, Au, In, Sn, Cr, Ni, Cu **Lamellar solids** MoS_2, WS_2, Graphite H_3BO_3, HBN, GaS, GaSe **Halides sulfates, sulfur** CaF_2, BaF_2, PbS, $CaSO_4$, $BaSO_4$ **Polymers** PTFE, PE, Polyimide Polymerlike DLC

DLC = diamondlike carbon
a= amorphous
ta = tetrahedral amorphous
X = a metal
nc = nanocrystalline
PTFE = polytetrafluorethylene
PE = polyethylene

Solid lubricants exhibit some short comings as they have finite lives and their replenishment into the contact is more difficult than that of liquid lubricants; oxidation and related degradation may occur over time and present some problems; exposure to high temperatures or oxidative environments can cause degradation and they may undergo irreversible structural-chemistry changes that in turn lead to loss of lubricity and the generation of some abrasive, non-lubricious products [135], [140]. Solid lubricants are dependent on the testing environment and contact conditions which can significantly influence the friction coefficient exhibited and, because the lubrication mechanisms are not exactly the same from one lamellar solid to another, the nature of such changes are not easy to predict [142]. Environmental species such as water vapour and oxygen may also play significant roles in the development of lubricity within to contact [134], [140].

Depending on the test environment, temperature and sliding conditions, the performance and durability of solid lubricants vary a great deal [135]. Solid lubricants are degraded during sliding and thus the lifetime of most solid lubricants

are limited because of the finite lubricant film thickness. To increase their durability, a mechanism of self-replenishment (or resupply) is needed but very difficult to achieve [140].

Solid lubricants can be applied to a tribological surface in a variety of forms. The oldest and simplest method is to sprinkle, rub, or burnish the fine powders of solid lubricant on the surface to be lubricated. They are also typically deposited on surfaces by advanced vacuum deposition processes (e.g., sputtering, ion plating, and ion-beam assisted deposition) to achieve a strongly bonded, dense micro-structure with uniform thickness; mixing of layers during the deposition process can also be used to enhance the durability of the solid lubricants coatings [140]. Polymer-bonded solid film lubricants are also readily applied to surfaces and have been reported to have excellent low-friction and wear-resistance performance and are cited as having a higher load-carrying capacity of up to ten times higher than that of oil lubricants [112].

2.5.1 MoS_2 solid lubricant

Among solid lubricants currently in use, molybdenum disulfide (MoS_2) holds a special importance. Like others, it is a lamellar solid material that consists of individual atomically-thin planes that can easily slide against each other [143] and can be applied directly between surfaces (plain MoS_2) or can be applied in the form of a polymer-bonded solid lubricant. The low frictional behaviour of MoS_2 is said to be intrinsic to the crystal structure of the material through the easy cleavage and shear of the basal planes [142]. The tribological performance of MoS_2 is credited to this inter-lamellar shear and under shearing forces, the basal planes are able to slide over one another [56], [144]. The intrinsic property of easy inter-lamellar shear provides low coefficient of friction both in vacuum and atmosphere since (unlike some other solid lubricants) it does not rely for its performance on adsorbed water vapour or an oxidising environment [145].

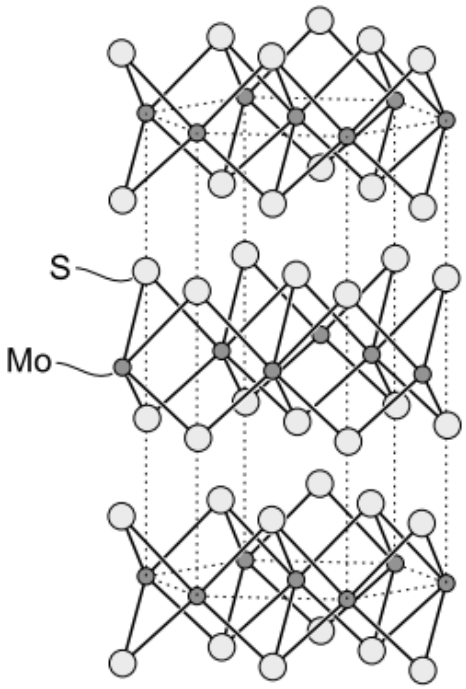


Figure 2.8 Crystal structure of molybdenum disulfide [141].

MoS_2 has a crystal layered structure by which a sheet of molybdenum atoms is sandwiched between two hexagonally packed sulfur layers (Figure 2.8) [141], [143], [146]. The layers are held together by weak Van der Waals forces while the bonding between S-Mo-S is covalent and strong [147]. The weak bonds (Van der Walls forces) between the sulfur layers enable easy movement of the lamellae over each other, resulting in a low friction in shear, whilst the strong covalent bonding between Mo and S gives the layers a high strength so that they can resist the penetration of surface asperities [131].

The lubricating properties of plain MoS_2 layers were studied by Holinski et al. [148] who explained the strong polarisation of sulfur atoms which produce the layered structure, good adhesion to metal surfaces, adhesion between MoS_2, basal planes, easy sliding of MoS_2 lamellae and the formation of homogenous continuous film. While adhesion between lamellae is highly undesirable in a solid lubricant, adhesion of lamellae to the substrate surface is essential. Material that does not adhere to the substrate surface is quickly removed by the sweeping action of the sliding surfaces [141] resulting in early failure of the system.

The mechanism of ultra-low friction of MoS_2 has been proposed in studies claiming three conditions that align to achieve low friction as follows: (i) built in MoS_2 transfer

film on the contact surface; (ii) avoids oxide contamination; and (iii) friction induced basal plane reorientation of MoS_2 grains in the interface parallel to the sliding direction [144]. As a solid lubricant, MoS_2 has been reported to have greater load carrying capacity than graphite and PTFE [148] as well as lubrication performance that exceeds that of graphite whilst it is also seen as an effective lubrication method that can be applied in a vacuum (in contrast to graphite) [149].

A comparison of coefficient of friction and lifetime of burnished, spray-bonded and physical vapour deposition (PVD) sputtered MoS_2 in vacuum is given in Figure 2.9 [150]. Burnished films can be sparse, poorly adherent, porous and significantly contaminated while the presence of the binder along with the coating thickness of bonded films can result in higher friction coefficients than the lubricating phase alone [150]. PVD films provide dense, well-adherent, uniform and pure films in the range of 0.2 – 2 µm thickness produce the lowest and steadiest friction behaviour obtainable for MoS_2 [150].

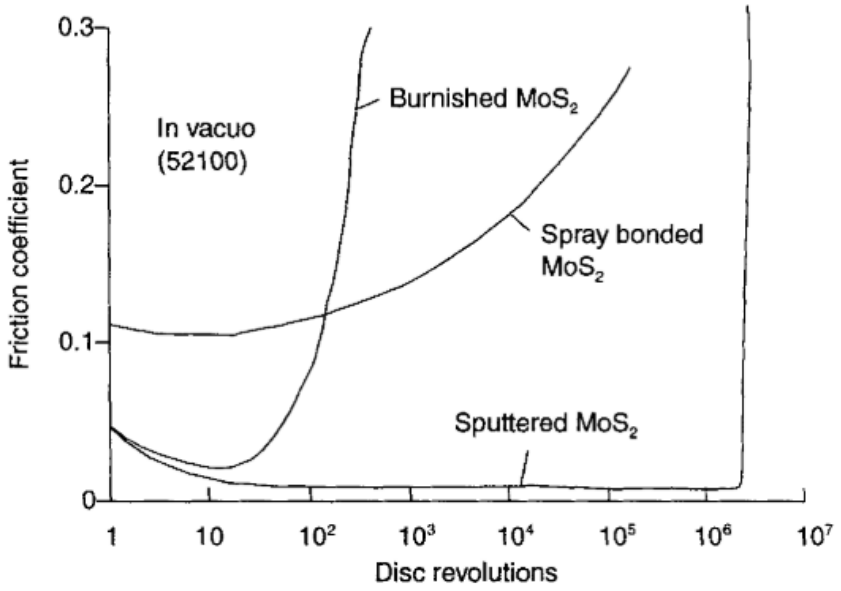


Figure 2.9 Friction coefficients of MoS_2 films deposited by various techniques [150].

The typical evolution of MoS_2 films in air has been described via the following three steps: (i) running-in period; (ii) steady-state period; and (iii) blistering delamination and film failure [141], [150], [151]. During the running-in period, the basal planes of the exposed hexagonal MoS_2 crystallites become increasingly oriented on the compacted film surface, parallel with the direction of sliding and normal to the applied load and the film rapidly becomes compacted to a fraction of its original

thickness with some film constituent being removed to form wear debris. After a few hundred to a few thousand cycles, the reduction in film thickness essentially stops and the steady state period begins. This marks the beginning of a long, smooth running friction period where the coefficient of friction attains its lowest steady-state values which represents the bulk of the useful life of the film [150], [151]. This is followed by large scale delamination and detachment of the solid lubricant from the substrate which is accompanied by an increase in the friction. Failure is sudden and indicated by a catastrophic increase in friction [151].

2.5.1.1 Effect of humidity and oxygen on the performance of MoS_2

The variations in environment such as the temperature, humidity and atmospheric gas content as well as the different materials in fretting contacts can have adverse influence on the fretting damage observed due to a strong dependence of the tribo-chemical reactions with environment and operating conditions [98], [99]. This is a vital aspect regarding solid lubricants such as molybdenum disulfide which have been reported to be highly sensitive to environmental factors such as humidity and oxygen [142], [152], [153]. The issue of environmental effects on coating performance is of particular concern given the varying atmospheric conditions in which aero-engine fan blades operate.

The detrimental effect of increased humidity on MoS_2 coatings has been attributed to water driven oxidation which causes the transformation of MoS_2 to MoO_3 [154]–[156]; MoO_3 disrupts the shear properties of the MoS_2 lubricant film, causing an increase of friction coefficient and high wear rates [156]–[159]. As sulfur is depleted, oxygen or other elements move in to fill the vacancies and the formation of molybdenum oxide and other complex salts occurs which disrupts the continuity of the MoS_2 slip planes [151]. When un-oxidised, the lamellae edges are thought to be relatively smooth, facilitating mutual sliding. After oxidation has taken place, crinkling and pitting of the edges occur and limits sliding caused by the hindrance of lamellae movement due to oxidised edges [141], [160]. The deterioration of MoS_2 films starts from the edge and progresses toward the centre when the outermost molecular layer of the sulfide is oxidised [158]. The basal planes are chemically inert whereas the edge planes are chemically reactive to oxidation, since the edge sites readily oxidize [161]. Scharf et al. [162] ascribed the high friction and extremely short wear life of MoS_2 in humid air to the dangling unsaturated bonds on the edge of the basal planes reacting with moisture and oxygen in the environment to form tribo-oxidation products such as MoO_3.

Bai et al. [163] also supported the hypothesis that dangling bonds and interlayer edges on the surface of the MoS_2 film easily react with water and oxygen in air, with the generated MoO_3 hindering the interlayer slip of the MoS_2. Thus, it exhibits a high coefficient of friction, and the wear resistance drops sharply in humid environments.

However, these hypotheses need to be considered in light of the work of Windom et al. [164] who, through Raman spectroscopic studies, showed that humidity does not play a role in the oxidation of MoS_2 as no effect or transformation to MoO_3 was realised in the presence of water vapour as compared to dry air or O_2 under ambient conditions. Lince et al. [165] however found the reduction in MoS_2 coating endurance to correlate with oxidation of lubricating MoS_2 to non-lubricating MoO_3 at the surface of the coatings. XPS line scans across wear tracks of MoS_2 based sputtered coatings that has been stored in humid air supported the idea that the reduction in endurance is likely due to third body effects, specifically the flow of non-lubricating MoO_3 wear debris back into the contact region during testing.

Rotational fretting wear tests of an epoxy-bonded MoS_2 coating conducted in a humidity of 50 ± 10% [166] suggested that the oxidative transformation of MoS_2 was caused both by mechanical and thermal effects which has a negative effect on the lubricating performance of the pure MoS_2 coating; XPS analysis shows that the oxidation of MoS_2 film occurred during the formation of debris. One the one hand, MoO_3 can display reasonably low coefficient of friction (but not nearly as low as that of MoS_2) whilst on the other hand, an increase in brittleness accompanied the oxidation of the MoS_2 crystals, which led to the occurrence of the ruptures and detachments of the tribologically active layers. Therefore, it was argued that the oxidation of MoS_2 during the wear process hastened the wear of the MoS_2 coating.

This proposed mechanism of water-mediated oxidation of MoS_2 has been disputed in other studies and different mechanisms have been proposed; these are more related to the physical bonding of water to the edge sites, and thereby, disruption of easy lamellae shear of MoS_2, and therefore modification of the easy shear between the basal planes [144], [167], [168].

By investigating rubbed MoS_2 films in dry argon, dry air and moist air, Fusaro [169] found that friction coefficient and wear rate were the highest in moist air, suggesting that water causes the reduction of MoS_2 lubricity. Longer wear life, lower wear rates and lower coefficient of friction were observed in argon and dry

air and higher wear rate, lower wear life and increased coefficient of friction were seen in moist air.

Pritchard and Midgley [170] investigated the friction characteristics of un-bonded MoS_2 powder by testing under different humidities and concluded that the friction is governed by the amount of water physically adsorbed onto the film. Indications that the water is physically adsorbed included the fact that the wear rate of the lubricant layer also increased as more water is adsorbed, the reversible effects of humidity on the friction and the friction coefficient being a monotonic function of the volume of adsorbed water which was consistent with physical adsorption rather than chemical adsorption. It was thought that the water vapour affects the adhesion component of friction and therefore the inter-crystallite forces.

Khare et al. [168], [171] aimed to understand the role of water, oxygen and temperature on tribological behaviour of a sputtered MoS_2 coating on 440C stainless steel. Sliding tests were performed in dry nitrogen (< 300 ppm), humid nitrogen (24 % RH), dry air (< 300 ppm), and humid air (60 % RH) at a range of temperatures (25 – 250 °C) as shown in Figure 2.10. It was found that water did not promote MoS_2 oxidation at room temperature as EDS was unable to detect any oxidation following sliding in the humid environment devoid of oxygen. It was concluded that water drives the increased friction coefficients through reversible physical-sorption below transitional temperature of 100 °C by physically bonding to the near surface and directly impeding inter-lamellar shear. Increasing the temperature from ambient to the transition temperature improved the tribological response of the coating [168] in high humidity conditions. At high temperatures above 300 °C, oxygen drives increased friction due to direct oxidation which can result in a rapid deterioration of tribological properties of MoS_2 due to the high shear strength of MoO_3 [172]–[174].

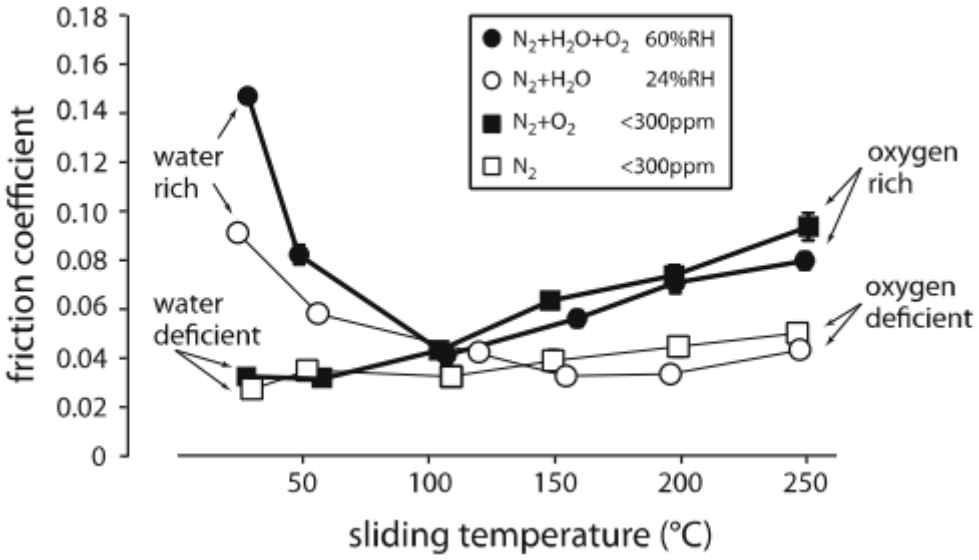


Figure 2.10 Friction of conditioned sputtered MoS_2 coatings in dry nitrogen, dry air, humid nitrogen and humid air as a function of temperature. Water increases friction at low temperatures with or without oxygen. Oxygen increases friction at high temperature with or without water [168].

Serpini et al. [175] proposed a similar hypothesis that ambient humidity mainly causes physisorption of water onto the MoS_2 surface with no appreciable oxidation of the coating. This conclusion was based upon work where a thin MoS_2 layer with a thickness of 200 nm was deposited by RF magnetron sputtering onto a Si substrate. Tribological tests were conducted in humid air (65 % RH), dry air (8 % RH) and nitrogen at room temperature (27 °C) and in humid air (65 % RH) at 75 °C. Tests in nitrogen at room temperature exhibited a stable low coefficient of friction below 0.1 throughout and did not fail, while an unstable but generally high friction coefficient (> 0.3) was observed in humid air with the associated shortest coating lifetime. At higher temperatures, however, tests in humid air, albeit still exhibiting frictional instability, exhibited a lower coefficient of friction below 0.1 and did not reach failure during the test programme. By increasing the temperature, water molecule desorption is activated which greatly improves the tribological properties of the coating. Below 100 °C, the physisorbed water drives the frictional behaviour of MoS_2. It was noted that it was still possible that some degree of oxidation occurs, but to an extent, this does not cause deterioration of the tribological properties of the coating; the authors thus concluded that adsorbed water causes the deterioration of the lubricating properties of the films, while oxidation plays only a marginal role.

Holinski and Gänsheimer [148] attributed the increase of MoS_2 friction to the bonding forces between the hydrogen atoms of the water molecules and the sulfur atoms on the basal planes of MoS_2. Polar bonding between the sulfur and water was said to increase the shear strength of the material, which increases the observed coefficient of friction. The number of hydrogen bonds corresponds proportionally to the amount of adsorbed water which is related to the humidity. Further works have also proposed the formation and presence of hydroxyl molecules to form clusters bonded by hydrogen [176], [177]. The formation of these S-H bonds increases the energy required to generate a shearing displacement between MoS_2 layers [178].

Zhao et al. [179] proposed a model to explain the tribological behaviour and instantaneous influence of humidity on magnetron sputtered MoS_2 on stainless steel during reciprocating sliding tests with a ball-on-disk configuration at varying humidity levels from 10 – 70% and under different atmospheric (inert and active) environments. Results showed increased humidity to be the driving force for an increased friction coefficient in all atmospheric environment including air, oxygen and nitrogen. It was suggested that water molecules are adsorbed on the active sites and dissociate into hydroxyl groups which exhibit a strong interaction with the counter-surface. The friction coefficient was thought to be largely dependent upon the adsorbed water which was determined by the environmental humidity level; as humidity increases, more water molecules are adsorbed onto the surface and dissociate into hydroxyl groups and the attraction from hydrogen bonds becomes stronger. In active atmospheres such as oxygen, more oxides are formed which provided additional active sites for water adsorption and further increase in the observed coefficient of friction.

Upadhyay et al. [180] studied the tribological properties of epoxy/MoS_2/graphene composites with different particle concentrations of 5, 10, and 20 wt. % as a function of relative humidity (40 %, 60 % and 80 %). There was an increase in the coefficient of friction and wear rates of the binary epoxy/MoS_2 composites as humidity increased. The effects of humidity were found to affect both the behaviour of the epoxy polymer base and the behaviour of the dispersed MoS_2 particles themselves. Adsorbed layers of water and the presence of hydroxyl groups on the polymer surface increases the adhesion forces and thereby increases the friction coefficient and the wear rate of the epoxy binder. A reaction of the MoS_2 with water molecules also produces trioxides of molybdenum, which was proposed to restrict the lubrication ability of MoS_2. It was recommended that the use of MoS_2 in epoxy

should be controlled to avoid the formation of molybdenum oxides in humid environments.

The combination of physical adsorption of water and oxygen followed by a chemical reaction and the formation of molybdenum oxides have also been suggested to be the driving influence in the tribological deterioration of MoS_2 [173]. The study of surface contamination of molybdenum disulfide by Johnston et al. [176] indicated that MoS_2 which has been exposed to damp air will contain, in addition to physically adsorbed water, sulfuric acid, molybdenum trioxide, and chemisorbed water as surface contaminants.

As can be seen, there are a wide range of differing theories and proposed mechanisms which describe how humidity and oxygen effects and deteriorates the frictional capabilities of molybdenum disulfide coatings; however, the behaviour will depend upon the specific nature of the MoS_2 and the tribological environment (including contact pressure, nature of contact motion etc). Accordingly, additional insights are required into the influential role atmospheric environmental factors have on the frictional and wear behaviours of MoS_2 coatings and particularly, on polymer bonded MoS_2 based DFL coatings under conditions that are representative of their application in aerospace dovetail joints.

2.5.2 Graphite solid lubricant

Graphite consists predominantly of carbon atoms arranged in a hexagonal planar array [141] (Figure 2.11) which are held with strong covalent bonds, while the basal planes are held together by weak Van der Waals and are weakly coupled together [181] resulting in inter-planar mechanical weakness which under shear are capable of sliding relative to each other [56]. The frictional properties of graphite are similar those exhibited by MoS_2 with weak Van der Waals which enable the shear between the layers [141].

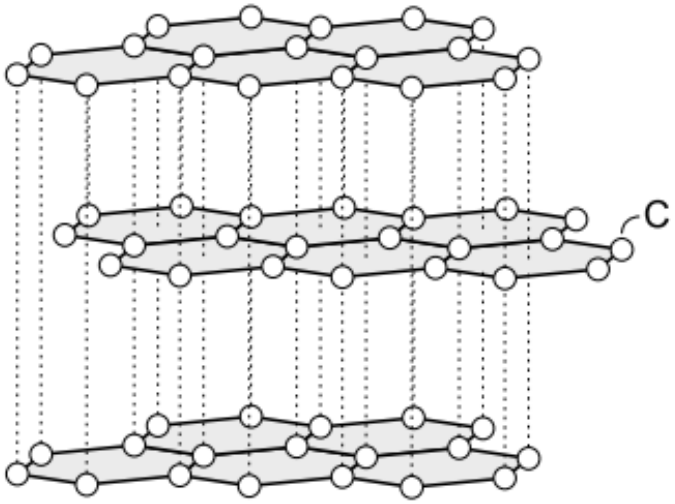


Figure 2.11 Crystal structure of graphite [141]

The drawback of graphite is the reported tendency of the lamellae to rupture at high mechanical loads, therefore yielding a limited lifetime and a higher coefficient of friction [182]. In general, graphite films fail at lower loads and exhibit shorter lifetimes than MoS_2 films. It has been stated that the limiting contact stresses are a little over half those of MoS_2 [141] although sliding speed does not seem to have an influence on the coefficient of friction, the lifetime of the solid lubricant film is greatly reduced by increases in sliding speed.

The good lubricity of graphite is however not an intrinsic property of the material but one proposed to be influenced and dependent upon environmental factors [152]. Graphite has been reported to be reliant on external environmental factors for effective lubrication [140] with the presence of water vapour and oxygen in the environment believed to facilitate the inter-lamellar shearing of graphite crystals [141], [181]. The lubricating layers result from an adsorption of water vapour and therefore relies on this adsorption for enhanced lubricating properties [183]. The intrinsic structural characteristics were first thought to enable graphite to function as an efficient and highly stable solid lubricant; however, it was later argued that the ability of layers to slide easily over each other is due to adsorbed species [142], [182]. In graphite, the inter-planar bonding is primarily from Van der Waals forces. Whilst in molybdenum disulfide, the bonding between the layers of sulfur atoms is again due only to Van der Waals forces, it is rather weaker than the Van der Waals bonding in graphite [184].

To explain the tribological responses of graphite in different environments, various mechanisms have been proposed which underline how water vapour and oxygen transform the lubricating properties of graphite. Savage et al. [185], [186] investigated the tribological properties of graphite in different atmospheric environments; increased wear rates were associated with dry and vacuum conditions whilst with higher humidity, low friction and low wear rates were observed. With these results, it was proposed that the surfaces of graphite are covered by a monolayer of condensable water molecules, which presents a surface of low cohesive energy. A physisorbed layer was proposed which was assumed to enable free motion of graphite layers resulting in low friction.

By conducting tests on a graphite coated pin and ring apparatus in a controlled environment chamber with a variety of gases and vapours, Lancaster et al. [187] suggested the mechanism of physical adsorption of water molecules on the basal plane of graphite and concluded that the adsorbed vapour on the basal plane of graphite functions as a reservoir from which molecules can migrate to neutralize edge sites being continuously exposed during the normal, low wear regime. Graphite dusting is initiated when the partial pressure of water vapour relative to the saturation vapour pressure falls below some critical value which depends on the environment and the contact temperature. Friction and wear then only remain low if these edge sites can be neutralised by the adsorption of water.

Another leading hypothesis by Rowe and Bryant [188], [189] proposed the chemisorption of water molecules in graphite formed intercalated products between the basal plane lamellae and therefore weakened the interlayer bonding to make sliding easier. It has been suggested that such an intercalation reaction would result in the expansion of the lattice [190]; however, this has been disputed following examination by X-ray diffraction which failed to reveal any increase in lamellae spacing which would necessarily accompany intercalation [191]. The interlayer distance in graphite was observed to stay the same whatever the gas phase composition [192], [193].

In investigating the frictional mechanism and lubricity of graphite, Bowden and Young [194] found that oxygen and water vapour were both immediately effective as ad-sorbates in reducing the friction. Both physical and chemical adsorption are proposed to be active in the lubricating mechanism of graphite in atmospheric humid conditions with oxygen most likely being chemisorbed; however, the friction response for both oxygen and water vapour is reversible which suggests that some physical adsorption occurs on top of the chemisorbed layer.

Deacon and Goodman [195] attributed the low friction of graphite to the low surface adhesion forces between the crystallites which occurs when dangling bonds at the edge planes react with water molecules to form oxides with weak attraction and results in weak inter-crystallite adhesion and low friction. The friction between graphite lamellae in their plane appears always to be low; they are low-energy surfaces and show little adhesion. But it was argued that the edges of the lamellae contain high-energy 'dangling bonds' which will bind strongly to other edge sites or to basal planes [184]. Yen et al. [193] was in agreement with this hypothesis and concluded that water vapour molecules are required to saturate dangling bonds at edge sites to maintain low friction behaviour. It is recognised that this is significantly different from the hypothesis that the low friction behaviour of graphite in air is due to the weakening of bonding forces between basal planes near the surface by either intercalation or basal-plane chemisorption thereby facilitating the shear of the lattice.

The lubricating nature of graphite with the reliance upon adsorbed water vapour to be an effective lubricant is a concern for aerospace applications where atmospheric conditions may vary in operating service (potentially very low humidity at cruising altitude). This dependency on the environment and the implications this might have on the performance of graphite as a suitable solid lubricant for a fan blade dovetail joint needs to be further explored.

As a promising method for enhancing anti-friction and anti-wear properties of MoS_2, the use of a MoS_2-graphite mix has been seen to confer satisfactory wear durability and moderated friction in open air, while the MoS_2 provides superior durability with extremely low friction coefficients in a vacuum or dry nitrogen [141]. In a study conducted by Li et al. [196], the combination of graphite and MoS_2 in an epoxy based coating was found to result in a reduction in the friction coefficient and increase the wear resistance with the graphite forming a layered structure with the MoS_2. The addition of graphite to MoS_2 films was also observed to effectively improved the friction reduction and anti-wear properties of MoS_2 at high temperatures [174].

Using literature data, Gardos et al. [151] explained the degradation mechanism of MoS_2 films rubbed in air and the synergistic effect of graphite in extending the wear life of such films and suggested that the beneficial effect of graphite addition has been explained in terms of graphite forming a layered structure with the MoS_2. Since the graphite lamellae are considered to be more resistant to distortion by oxidation than the MoS_2 lamellae, a mix of distorted and undistorted lamellae is

less prone to blistering than distorted lamellae acting alone [151]. Bartz et al. [197] found that MoS_2 with graphite in a resin bonded system exhibited the lowest friction coefficients (0.02 – 0.04) and the most stable friction levels in the steady-state regions at all PV (pressure × velocity) levels investigated when compared to formulations comprised by MoS_2 alone. By itself graphite was shown to have very poor lubricating properties whilst the wear life of MoS_2/graphite films is longer.

2.6 Fretting wear behaviour of polymers

Dry film lubricants are suspensions of solid lubricants (MoS_2, graphite and PTFE) and other additives in a solution of inorganic or organic binding agents (acrylic, phenol, epoxy, silicone, and urethane) which can be applied by dipping and various types of spraying procedures [131]. The hardening process depends on the type of binding system and typically takes place at ambient temperature or in a stove [132]. As soon as the coating is hard, it leaves a thin, dry, lubricant film which is firmly bonded to the surface of the component [198]. The film performs to separate surfaces with a lubricating layer between the components and to reduce friction and wear [132]. The bonded coating can be gradually worn off the component surface and therefore the life of the bonded coating is limited [198].

The binder is an important part of the formulation of dry film lubricants and the purpose of the binder is to hold the functional solid lubricant pigment on the surface [132]. Binders requiring heating in order to harden are termed thermosets and include phenolic and epoxy resins [141]. Polymeric coatings can fail by de-bonding from the substrate, general plastic wear, chemical degradation, or by the formation of cracks in the film allowing access to the substrate [38]. The mechanical properties of all polymers and composites change dramatically as the temperature is increased so that their wear rates would be expected to increase with temperature [199]. By utilising a polymeric binder as the solid lubricant carrying medium, the relationship between fretting wear of polymers with a particular focus on thermoset polymeric coatings such as epoxy is a subject of interest.

Briscoe et al. [200] classified the complex wear processes of polymers and the underlying wear mechanism under three broad approaches which primarily reflect the way sliding wear of polymers have been studied as shown in Figure 2.12. The generic scaling approach emerges from the two-term interacting model which describes that frictional work may be dissipated in two distinct regions as shown in Figure 2.13; an interface zone and a subsurface zone. The two-term model

facilitates the separation of the contributions of the interface and the subsurface to the total frictional force. The interfacial frictional work is the result of adhesive interactions and the magnitude of this depends upon factors such as hardness of the polymer, molecular structure, glass transition temperature and crystallinity of the polymer, surfaces roughness of the counter-face and chemical-electrostatic interactions between the counter-face and the polymer. Soft elastomeric solids tend to have very high adhesive components leading to high friction. The friction energy in the cohesive zone depends on the tensile strength and the elongation before fracture (or toughness) of the polymer and, the geometric parameters of the asperities on the counter-face [201].

The phenomenological approach lists the perceived origins and consequence of the wear processes related to polymers which can include abrasive wear, adhesive wear, fatigue or fretting wear as well as chemical, erosion and delamination wear. The material response approach states that the nature of the wear is based on the type of polymer being considered (e.g. elastomers, thermosets and semi-crystalline polymers) which strongly influence their mechanical properties (e.g. toughness, tensile strength, elastic modulus), all of which exert influence on the wear characteristics of the polymers [201].

Semi-crystalline linear thermoplastics give the lowest coefficient of friction, whereas elastomers and rubbers exhibit larger values. This is because of the molecular architecture of the linear polymers that helps the molecules stretch easily in the direction of shear giving least resistance to shear. Thermosetting polymers, although they possess high hardness and strength among polymers, show very high wear rates and high coefficients of friction as a result of their very low elongation to failure values as listed in Table 2.3 [201].

The wear of polymers is influenced by the contact conditions, the bulk mechanical properties of the polymer and the properties of the third body, which generally appears in the form of transfer film or degraded polymer particles between two sliding surfaces [200]. The tribological characteristics of polymers are also greatly influenced by the effects of temperature, relative speed of the interacting surfaces, normal load and the environments [201]. High tensile strength coupled with high elongation to failure promotes wear resistance in a polymer. High elongation to failure of a polymer means that the shear stress in a sliding event can be significantly reduced due to extensive plastic deformation of the polymer within a very thin layer close to the interface [201].

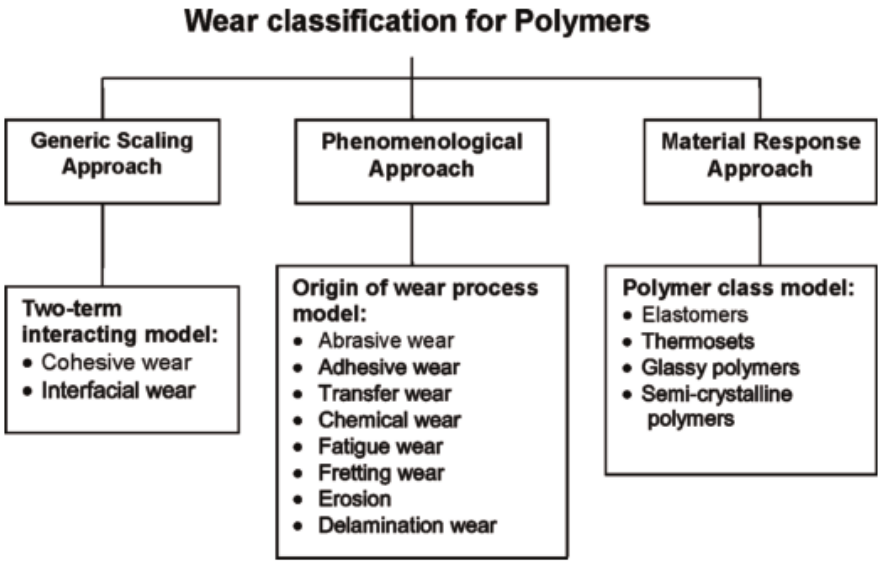


Figure 2.12 Simplified approach to classification of the wear of polymers [200]

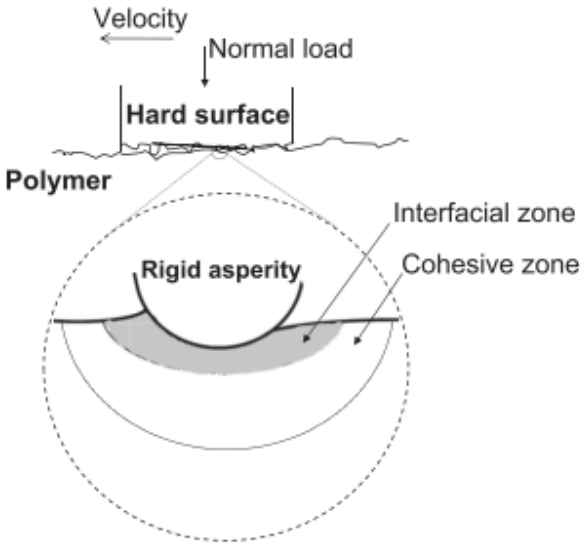


Figure 2.13 Two-term model of friction and wear process. Total friction is the sum of the forces required for interfacial and cohesive energy dissipations. Likewise, the distinction between interfacial and cohesive wear processes arises from the extent of deformation in the softer material (usually polymer) by rigid asperity of the counter-face. For interfacial wear, the friction is dissipated mainly by adhesive interactions while for the cohesive wear, the energy is dissipated by adhesive and abrasive (sub-surface) interactions [200].

Table 2.3 Friction coefficient of selected polymers when slid against a steel disk counter-face (surface roughness, R_a = 1.34 µm) with the corresponding specific wear rates and Pressure *(P)* × Velocity (*V*) conditions [201].

Polymer	Coefficient of Friction	Specific Wear rate ($x10^{-6}$ mm^3 Nm^{-1})	PV Value (Pa m s^{-1})
PMMA	0.48	1315.9	145 560
PEEK	0.32	31.7	149 690
UHMWPE	0.19	15.5	187 138
POM Poly(oxymethylene)	0.32	168.2	149 690
Epoxy	0.45	3506.6	153 997

Polymers are visco-elastic materials and due to their specific structure and mechanical behaviour, polymers are more sensitive to factors of mechanical stresses, temperature and chemical reactions of the surface layer [202].

To deal with the effects aggressive conditions such as elevated temperature, high relative speed of the contacting surfaces, high normal load, appropriate fillers may be introduced to better control the tribological responses [201]. Good mechanical strength, hardness, as well as thermal and chemical resistance, favour the application of epoxy resins as commercially used engineering materials [203]; however the improvement of friction and wear behaviour of the epoxy is required and is commonly achieved by incorporating such fillers and solid lubricants [203]–[205].

Additional composite fillers can include ceramic nano-particles, mainly metal and some non-metal oxides such as SiO_2, TiO_2 and Al_2O_3 [201], [204], carbon fibre [206] or powdered solid lubricant particles [207], which are added in polymer matrices such as epoxy with the aim to improve load-bearing capacity and wear resistance of the material against the counter-face [201], [203].

The tribological performance of such composite, i.e., matrix and fillers in humid environments can define the overall performance of such composite in practice [159]. The variation of wear rate with temperature will also depend on the influence of fillers and the way in which they modify the counter-face during sliding and on the formation of oxides or other films on the counter-face [199].

2.6.1 PV limit

In polymer tribo-systems, polymers often experience significant frictional heating during sliding. They undergo both physical and chemical changes, resulting in unwanted changes to the properties of the material [208]. For a given contact pressure and friction coefficient, the frictional heat generated at the contacting surface increases in proportion to the sliding velocity. One of the principal effects of sliding velocity on the wear rate of a polymer occurs through its influence on the temperature at the sliding surface [208].

The PV factor (the product of the nominal pressure and the linear velocity) is a commonly employed measure to characterise the thermal and wear resistance of the polymer [209] and is used to describe the critical operating conditions under which the material fails [210]–[213]. The concept of PV is related to frictional heating where P is the nominal contact pressure (Pa) and V is the sliding speed (m/s); a critical value of PV exists (commonly termed the PVlimit) above which the polymer starts to melt or rapidly wear due to overheating [199], [208]–[210], [214]. Below the PV limit, wear is envisioned as a much slower, fracture process involving crack growth and the release of small wear particles [208], [210]. The limit is affected by the friction heating at the sliding interface, as well as the rate of dissipation of heat away from the interface. Above a given PV limit, a very severe form of wear may occur with each polymer having its own PV limit [208].

Bassani et al. [215] analysed the individual influence of sliding velocity and nominal pressure on the tribological behaviour of epoxy resin against stainless steel in dry sliding conditions using a pin-on-disc configuration. Differences in the action of the two variables result from the particular thermal state induced in the polymer, as well as from the quantity and morphology of wear debris. Sliding speed was reported to affect the deformation mode, frequency, transfer film renewal rate, heat production and cooling conditions. Nominal pressure was found to exert its influence mainly by determining the basis interfacial stress level and consequently the depth of the damaged sub-surface layers, crack propagation, adhesive wear and stability of transfer films. The main difference with respect to the action of velocity appears to originate from the different thermal state induced in the polymer surface. The study suggested that improving fatigue resistance of epoxy resins can have beneficial effect on their wear behaviour if mechanical resistance is preserved to suitably control adhesive wear

The PV concept, although simple and convenient, takes account of neither the temperature at the bearing surface nor the temperature of the environment which surrounds the bearing [199]. The temperature at the bearing surface can arise due either to a high environmental temperature or to the generation of frictional heat at the sliding surface. In the latter case, sliding speed is particularly important. In addition to raising the mean temperature of the surface, high transient temperature at asperity contacts (flash temperatures) can substantially affect the wear rates at high sliding velocities [199].

The PV value is generally used as a guiding factor in the design of tribological applications [208] and enhancing the limiting PV value are the general targets of the design of wear resistant polymer composites [204], [209], [216]. The effects of fillers on the mechanical and thermal properties of polymers are inter-related with those on the friction and wear properties and each type of polymer-based material will therefore exhibit a characteristic curve relating the maximum permissible pressure to the maximum permissible velocity [212].

Chang et al. [217] utilised PV to assess the tribological properties of epoxy nanocomposites and the enhancement of the wear resistance by additions of nano-TiO_2. In Figure 2.14, the depth wear rate of epoxy composites filled with and without nano-TiO_2 is shown as a function of PV factor. Neat (unfilled) epoxy at a low PV value (1 MPa m/s) showed very high depth wear rate which indicates that material cannot be operated under these conditions in service. The depth wear rate generally increases with an increase in the PV factor, and the wear rate is significantly reduced by incorporating micron fillers of graphite and PTFE. For the composite containing only these traditional micron fillers, the wear rate rises to quite a high value when the PV factor reaches 4 MPa m/s; with the further addition of nano-TiO_2 fillers, reduced wear rate and enhanced PV limits were observed as lower depth wear rate was shown even at higher PV factors.

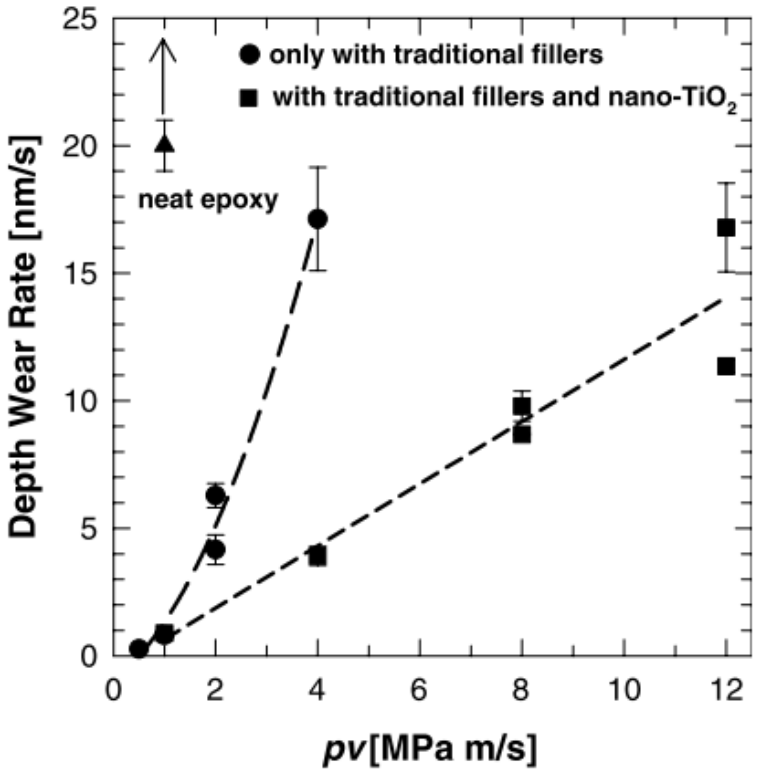


Figure 2.14 Comparison of the time-related wear depth wear rate if epoxy composites filled with and without nano-TiO_2 as a function of PV factor. [204] [217].

2.6.2 Transfer film mechanism

The formation of transfer films plays an important role in the friction and wear reduction in polymer tribology [90], linked to the low coefficient of friction and steady state realm in fretting. Formation mechanisms of transfer film, adhesion strength between the transfer film and counter surface and effects of fillers and reinforcement are among the most widely debated subjects. Strong adhesive interaction between polymers leads to an increase in the friction force which may cause the asperities of the material to be removed to form wear particles or transfer layers on the counter-face [218]. Transfer films are found to form more readily on roughened surfaces while also existing in a solid, low viscosity or fluid state which each state controlling the friction and wear of the polymer in a different way [219].

In the study of sliding mechanics of polymers, Abdelbary et al. [208] referred to three factors that determine the formation of the transfer film as: (i) the deformation of surface asperities under load; (ii) the fracture of material in the substrate; and, (iii) the adherence of this material to another surface. The effectiveness of lubrication depends on the formation of a complete film protecting the surface [220]; however, the formation of the transfer film can increase or decrease wear resistance. If the transfer film causes an increase in the counter-face roughness and results in increased frictional heating of the polymer and thus altering its mechanical properties, the wear factor will increase. On the other hand, if the initial contacting surface roughness is high, the transfer film will modify the counter- face roughness and decrease the rate of wear [208].

High wear of polymers mainly occurs in the initial stages of sliding with the majority of the material being removed at the beginning of the test and thus, whilst exhibiting higher friction coefficient and wear rate, transfer films are being formed on the contacting surface. This transitional period of material removal and high coefficient of friction to the formation of a smooth transfer film and low friction coefficient varies depending on the roughness of the counter-face. The polymer material requires more time to fill rougher surfaces [221], [222].

Once a stable transfer film is formed on the counter-face, it typically acts as a lubricating layer on the interface by protecting the soft polymer from further damage by hard and sharp metal asperities on the counter-face [222]. Polymer to metal sliding was documented in two steps: flattening of the rough metal surface by transferred material during the transient period; and then, self-lubricating effects of the transfer film during steady state sliding [222]. The resulting wear rates is directly related to the transfer film formation mechanism with a balance being established between its rate of formation and degradation. A degree of wear is required to form and maintain a smooth transfer film which helps to maintain low coefficients of friction. Minimal wear rates impede on the formation of transfer films and high wear rates increases the risk of substrate contact and material fretting damage [221].

2.6.3 Fretting wear behaviour of polymer-bonded MoS_2-based dry film lubricant

The key attributes which control the performance of dry film lubricants were categorised by Busch et al. [131] as follows: (i) their composition and in particular, the type of binding agent, the ratio of solid lubricant to the binding agent, the types of solid lubricant and the film thickness; (ii) the properties of the substrate to which the lubricating varnish is applied, in particular, the cleanliness, roughness and hardness of the surface; and (iii) environmental conditions, in particular the demands placed on the lubricant such as load and the type and speed of the movements, the temperature, atmospheric pollution (humidity, dust, radiation), atmospheric pressure, and the surrounding media (gases, liquid).

Polymer-bonded MoS_2-based dry film lubricants (DFLs) are often deployed on aero-engine fan-blade dovetail joints as a sacrificial barrier [11], [114] and in conjunction with a variety of surface treatments to reduce the effects of fretting at the contacting surfaces by reducing friction and suppress wear and fatigue and subsequent system degradation [223]–[225].

Bonded MoS_2-based solid lubricant coatings have been widely applied onto contacting interfaces experiencing fretting oscillation due to them being deposited by an inexpensive and simple process [111]. This lubrication system extends the component's life and can in certain cases be deployed to ensure lifetime lubrication depending on the combined load / stress factors of the individual tribological system [198]. Bonded solid lubricant coatings can provide a dry, clean, easy, low-cost method of lubrication for bulk manufactured components which can offer protection against wear, surface damage, and corrosion and reliable lubrication at low and high temperatures and when exposed to aggressive media, radiation or vacuum conditions [198].

This palliative method however, imposes limitations concerned with lifetimes and longevity of the coating which are critically influenced by the severity of fretting and environmental conditions [110], [111]. The Fretting wear tests of epoxy bonded MoS_2 solid lubricant were carried out at a given temperature range from 23 to 300 °C by Xu et al. [111]. Higher wear life was obtained at 100 °C. The rise the wear life value may be illustrated by a reduction in relative humidity due to the heating from 23 to 100 °C. As the temperature increased from 100 to 300 °C, fretting wear life diminished. At higher temperatures, MoS_2 lubricating pigment tended to oxidise more rapidly and the lubricating effect dropped. In addition,

mechanical properties of the coatings may weaken. High temperatures over 200 °C may accelerate oxidation and weaken lubrication effect.

The degradation process of polymer-bonded MoS_2-based solid lubricant in fretting wear has been described to exhibit a first stage where the coating undergoes plastic deformation. During this stage, the asperity peaks of the coatings are sheared off and the lubricating particles flow to form a continuous plastic flow layer [226]. Following this, micro-cracks initiate and propagate in the coatings with the detachment of particles from the surfaces resulting in the progressive elimination of the coating along with the oxidation of the MoS_2. Final failure occurs with severe detachment of the coating layers where metallic asperities emerge through the coating, making direct contact with the metallic counter-face, resulting in high coefficient of friction [110], [227], [228].

In the work by Barman et al. [225], the damage mechanisms throughout the MoS_2 DFL coating system lifetime were categorized into three stages. The initial Stage I is characterised by a high ECoF (energy coefficient of friction) which gradually reduces to a durable low ECoF phase termed Stage II where a thin layer of mixed DFL-metal is proposed to exist. The degradation of this mixed materials eventually gives way to Stage III where metal-metal contact with limited influence of DFL dominates. In this unstable regime, there is a rapid increase of ECoF until the failure point is reached.

A study was reported on rotational fretting wear of bonded MoS_2 solid lubricant coating prepared on medium carbon steel [166] where MoS_2 particles were homogenously dispersed in novolac-epoxy resin. With a constant load of 20 N, the results showed that the friction coefficients of MoS_2 were lower than those of the substrate and in the partial slip regime at lower angular displacement of 0.125°, the damage of the MoS_2 coating was very slight. With an increase in angular displacement to 0.5° and 1°, increased degradation of the coating system was observed with more debris and the main damage mechanisms of the coating in this gross-slip regime was abrasive wear, delamination and tribo-oxidation.

Using a flat and rounded geometry contacts, Kim et al. [11] investigated the effect of displacement amplitudes on epoxy bonded MoS_2 DFL which was deposited on a thermally sprayed Cu-Ni-In interlayer. Four different peak-to-peak displacements (0.6 mm, 0.5 mm, 0.4 mm and 0.15 mm) with a contact pressure of 125 MPa and a frequency of 2.5 Hz were applied for fretting wear tests where the number of cycles was shown to decrease with increasing displacement (Figure 2.15). The number of cycles decreased with increased imposed peak-to-peak displacement.

At higher displacement of 0.4mm to 0.6 mm, the evolutions of friction are similar to each other with an initial low friction state followed by increased friction and subsequent failure. At the lowest applied peak-to-peak displacement of 0.15 mm, the friction behaviour was completely different and remained below 0.2 throughout the test and no increase in friction occurred until the test was terminated at 15,000 cycles.

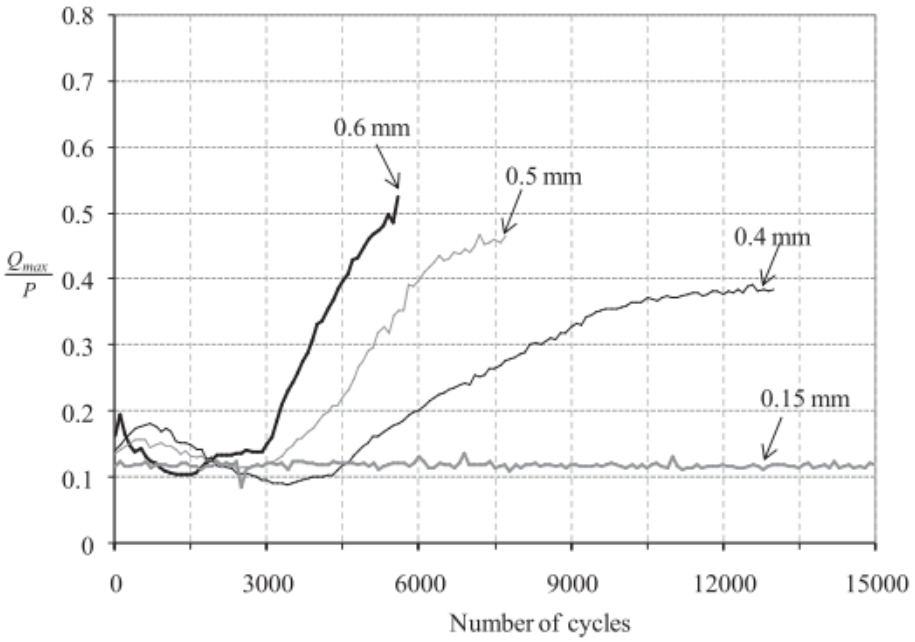


Figure 2.15 Evolution of the ratio of the maximum tangential force (Q_{max}) to normal force (P) at various imposed displacements. Q_{max} /P corresponds to friction coefficient in a gross slip regime. Labels denote imposed displacement magnitudes [11].

Excellent anti-friction, wear resistant performance and load bearing capacity of the bonded coating were observed in the evaluation of the friction and wear performance of epoxy resin bonded molybdenum disulfide with Sb_2O_3 fillers conducted on a ball on disc contact configuration by Ye et al. [112] with a counterpart steel ball. In this study, a wide load range between 20 N and 800 N which corresponded to a contact stress of 1.28 to 4.38 GPa was examined along with a wide oscillatory frequency range between 5 Hz and 30 Hz. The coefficient of friction decreased rapidly with increasing applied load and reduced to the minimum of 0.033 at a load of 250 N, and then increases slowly with further increase of the applied load within an applied load range between 250 N and 800 N. With a load carrying capacity of 800 N, the bonded MoS_2 solid film lubricant exhibited a coefficient of friction less than 0.05. The reduction of friction as a

function of increasing applied load was explained by the Bowden and Tabor friction theory [112], [139] :

$$\mu = \frac{A_r S}{N}$$

Equation 2.6

The friction force is a product of the real contact area, A_r, and the shear strength, S. The friction coefficient is the ratio of the friction force to the applied normal load, N [112] [56]. The area of real contact increases with increasing applied load. Increasing extent of the area of real contact is much less than that of the applied load in the range 20 – 250 N so the coefficient of friction was reported to decrease rapidly with increasing applied load, before the coefficient of friction starts to increase slowly with increasing applied load above 250 N [112]. Recent studies on the mechanism of graphite lubrication [182] also observed a decrease in CoF with increasing load which was said to be consistent with the friction theory of Bowden and Tabor [139] whereby the CoF will decrease with increasing load upon lubrication with solid lubricants as there will only be a small increase the real surface A_r. The lowest coefficient of friction of 0.12 was achieved by using a graphite coating with a minimal thickness of 0.2 um and the highest normal force of 402 mN which corresponded to a Hertzian contact pressure of 1008 MPa.

A deviation from this expected behaviour has been reported before, where friction increased with increasing normal force [56]. Fouvry et al. [114] showed that different friction responses could be activated depending on contact pressure and sliding amplitude conditions on a bonded MoS_2-based solid lubricant coating deposited on a Cu-Ni-In under-layer. A PV power factor was used to formalise the friction transition processes from *friction response I* which had low pressure (< 500 MPa) and small sliding amplitudes ($<$ 50 µm) and induced a stable lubrication plateau before failure to *friction response II* which had high contact pressure ($>$ 500 MPa) with large sliding amplitudes ($>$ 50 µm) and induced a continuously rising friction combined with titanium transfer at the contact interface.

2.6.4 Effect of surface condition on polymer-bonded MoS_2-based dry film lubricant

For solid lubricant coatings, strong adhesion between the coatings and the substrate is critically important to achieve long service life [134]. The pre-treatment of the substrate surface plays a particularly important role in the successful use of bonded dry film lubricants and pre-treatment of the material surface is commonly - used to help create, or improve, their adhesive and film creating / retaining properties [131].

Previous studies have also suggested that enhancing the substrate hardness, increasing dry film lubricant coating thickness, grit blasting the substrate surface, increasing the temperature to solidify coating and reducing relative humidity were favourable to improving fretting behaviour of bonded-MoS_2 dry film lubricant coating [229],[240],[241]. Mechanical properties of the substrate, surface morphology, distribution of contact stress and the adhesion strength of MoS_2 polymer bonded dry film lubricant coatings are all thought to affect fretting wear [229]. The performance and lifetimes of such dry film lubricants have been linked to various substrate conditions, with roughness being a key factor [137].

Zhou et al. [227] conducted several investigations on the friction and wear properties of MoS_2-bonded resin coatings with varying thicknesses under fretting conditions. The work reiterated the vital aspect on the surface treatment prior to the deposition of the solid lubricant with the results garnered suggesting; enhancing substrate hardness, increasing coating thickness, sandblasting substrate surface, increasing the temperature to cure the coating and reducing relative humidity were favourable for improved fretting behaviour of these coatings.

Xu et al. [111] performed a series of fretting wear tests to investigate the life of bonded MoS_2 dry film lubricant coatings deposited directly onto steel substrates with different substrate hardness (~ 275 HV and ~440 HV) and surface roughness, (Ra of 0.5 µm and 2.0 µm). Against their criterion of failure (based upon the coefficient of friction reaching a value of 0.25), they observed an increase in lifetime of the heat cured dry film lubricant of ~ 10% on changing from the softer to the harder steel substrate for fretting displacement amplitudes of both 20 µm and 40 µm. A similar increase in lifetime of the heat cured dry film lubricant of ~ 10% was observed on increasing the surface roughness of the (harder) substrate onto which the dry film lubricant was deposited. It was suggested that rougher substrates resulted in an increase in bond strength between the coating and the

substrate as well as being effective against wear in the later stages of fretting due to residual MoS_2 being retained in the troughs of the rough surface.

Barman et al. [225] presented data related to wear profiles at various stages of damage of a system where a nominally 50 µm thick dry film lubricant had been deposited onto grit-blasted Ti-6Al-4V; these profiles have been used to make an estimate of the wear depth as a function of the exposure to wear which is presented in Figure 2.16. It can be seen that the rate of increase of penetration is high as the dry film lubricant itself is worn away, but that this is followed by an extended period (~ 20 – 40 $\times 10^3$ cycles) where the rate of penetration is low; it was argued that this is associated with the period where the wearing surface is made up of a mix of metal and dry film lubricant and is a significant period in the lifetime of the system.

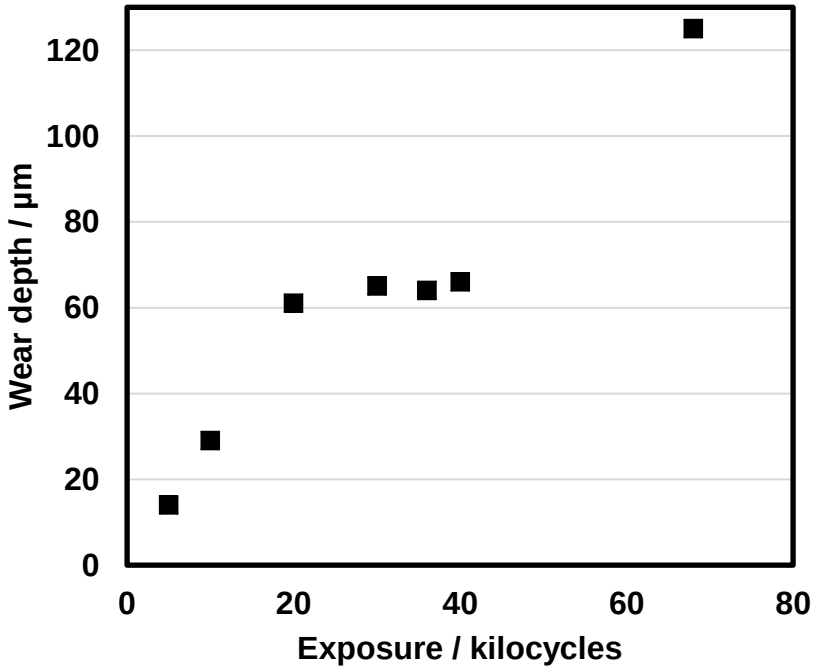


Figure 2.16 Wear depth as a function of exposure to fretting wear for a nominally 50 µm thick DFL deposited onto a grit-blasted Ti-6Al-4V substrate [225].

To actively prolong the lifetimes of fan blades, current industrial practices to ameliorate the effects of fretting include a complex surface engineering solution where the fan blade dovetail is shot peened and then plasma spray coated with a copper-nickel-indium (Cu-Ni-In) alloy coating (with a typical Ra value of ~ 9 – 10 µm [58], [230], [122] [124]), onto which a polymer-bonded molybdenum disulfide (MoS_2)-based solid lubricant coating is then deposited [5], [11]. This

surface engineering architecture is thought to provide dual advantages for the fretting system owing to the accommodating capacity of plastic deformation provided by the Cu-Ni-In coating, which limits the nucleation and propagation of cracks, and the low friction and low wear properties of the solid lubricant coating itself [66], [113].

It is well established that dry film lubricants of this type typically confer extended lifetimes before failure when deposited onto thermally spayed Cu-Ni-In. The implications of a Cu-Ni-In under-layer below polymer-bonded MoS_2 dry film lubricants were explored by Barman et al. [230] who sought to uncover the specific role that a thermally sprayed Cu-Ni-In layer plays on the tribological performance in Ti-6Al-4V dovetail arrangements. In that work, a MoS_2-based dry film lubricant was applied either on top of a thermally sprayed Cu-Ni-In coating or directly to a grit-blasted Ti-6Al-4V substrate. The soft metallic layer of Cu-Ni-In (177 ± 20 HV) displayed significantly higher roughness (Ra) of 9.0 µm compared to that of the harder (287 ± 10 HV) grit-blasted Ti-6Al-4V substrate with a Ra of 2 µm. The MoS_2 DFL exhibited significantly enhanced durability when applied on top of the Cu-Ni-In coating, with a five-fold increase in lifetime typically being observed. It was suggested that the high roughness resulted in an extended lifetime for the phase of wear where the contacting surface experiencing fretting motion was partly made up of metal and partly of DFL itself, with this mixed material exhibiting high resistance to degradation and wear. It was argued that the increased lifetime with increasing roughness could be explained by the concept of the mixed metal-DFL simply existing over an extended depth of penetration by the wear process.

Previous work [231] has stressed the strong dependency of the tribological fretting behaviour of MoS_2-based coatings on the characteristics of the Ti-6Al-4V substrate surface upon which the coating has been deposited. In particular, the substrate surface characteristics have been shown to exert influence in controlling the formation and durability of a stable low coefficient of friction phase. However, the presence of a Cu-Ni-In layer has been shown to increase the lifetime of the solid lubricant layer, with different mechanisms being proposed for this; (i) the Cu-Ni-In acts as a retainer for the solid lubricant due to its higher surface roughness; (ii) the low hardness and stiffness of the Cu-Ni-In material may result in deformation (both elastic and plastic) that reduces the severity of the contact and thus extends fretting lifetimes [122], [125].

The substrate surface conditions have been shown to influence the tribological behaviour of the coating [137] with observations that higher surface roughness

leads to an increase of dry film lubricant fretting wear lifetimes [230] with the softer plasma-sprayed Cu-Ni-In metallic later reducing the severity of the fretting conditions at the contacting interface to further extend the fretting lifetimes of the system [113], [114].

2.7 Summary

The propensity for fretting damage of titanium alloys (e.g. Ti6Al4V) is a common concern in industry, and nowhere less so than within the dovetail joint in aero-engines; in this regard, the application of dry film lubricant systems have been established as the dominant palliative method.

The literature reveals that there is a longstanding goal to understand the mechanisms by which fretting damage occurs so that its effects can be best ameliorated. Specifically, numerous reviews, hypothesis and experimental methodologies have been presented with the aim of detailing and verifying the mechanisms of fretting and how varying palliative methods can be deployed to restrict fretting damage. This has spawned further questions attested by the relentless ongoing research effort within the subject area. The literature review emphasises the complex nature of fretting by documenting the influences of the materials, loading and environmental parameters which can alter the mechanism involved.

The limitations associated with solid lubricants have often been noted to be the durability and therefore finite lifetime (since, unlike liquid lubricants, such solid lubricants cannot readily be replenished within the contact). It has been established in the literature that no solid lubricant can provide reasonably low and consistent friction coefficients over a broad range of imposed conditions, temperatures and environments [140]. Solid lubricants typically function best under certain test conditions but not under all conditions with researchers aiming to broaden the operational range; however, to date, in most cases the improvements were either transitory or short-lived [140], [232], [233]. The effort to extend the durability and performance of MoS_2-based dry film lubricants to resist fretting damage has unveiled certain limitations associated with the system. In addition, the environmental effects on the performance of MoS_2-based systems has also been reported to be a limiting factor in limiting the use of dry film lubricants.

This review highlights the numerous investigations that have documented the degradation behaviour under fretting conditions of the most favoured and deployed solid lubricants currently in used in industry (MoS_2 and graphite) in order to identify the strength and weaknesses associated with these solid lubricants so that systems can be tailored for their applications. There is, however, a need to understand the fretting wear mechanisms of the polymer-bonded dry film lubricant systems across a range of different fretting conditions of the aero-engine fan blades in order to highlight the pathways where the extension of fretting lifetimes could be achieved. The combination of different solid lubricants in a coating system has also been highlighted as a means to improve the performance of the coating. Further investigation of the performance under various environments and loading conditions is required to understand the benefits and limitations of a graphite modified polymer-bonded MoS_2 films for in-service applications.

2.7.1 Basis for current work

Despite commercial use of a complex solid-lubricant system, aero-engine dovetail joints are exposed to conditions that require expensive maintenance and repair of the coatings in order to avoid significant fretting damage of the blade or disc themselves. More robust coatings are required to withstand the fretting wear damage incurred and allows the inter-maintenance intervals to be extended. This in turn calls for the testing and development of the aero-engine dry film lubricant system under a range of fretting conditions as a means of developing and understanding of the mechanisms of degradation with a view to then making modifications which allow the coating system to be improved. The basis of this work is to investigate the underlying wear mechanisms and failure modes that occur on the polymer-bonded MoS_2-based dry film lubricant (DFL) coating which is currently used to prevent the damaging effect of fretting wear on aero-engine fan blade/disc interface across different fretting conditions. Experimental fretting wear tests are needed to understand how influences of the following on the aero-engine dry film lubricant system:

- Environment (namely humidity and oxygen);
- Substrate type and roughness upon which the bonded solid lubricant coating is deposited;
- fretting conditions (focussing on applied load and stroke);
- Contact geometry.

This work aims to understand the pathways to which the extension of fretting lifetimes of the polymer-bonded MoS_2 could be achieved. The inclusion of graphite to the currently applied polymer-bonded MoS_2-based dry-film lubricant have previously delivered initial favourable low friction capabilities and extension of fretting lifetimes [234]. Questions however remain about the effectiveness of the graphite-modified dry-film lubricant and if the low friction capabilities of the graphite-modified dry-film lubricant can be sustained in more demanding fretting conditions.

Chapter 3. Experimental Methodology

This chapter details the materials employed, sample preparation processes, the fretting wear testing configurations and rigs used and the material characterisation techniques that were employed across the experimental programme carried out in this work.

3.1 Specimen preparation

Fretting tests were conducted with Ti-6Al-4V as the substrate material which is reported to have an elastic modulus of 115 GPa and a Poisson's ratio of 0.342 [230]. The material was provided in the form of 10 mm thick plate by Rolls-Royce plc to represent the material of the fan blade and disc in an aero-engine dovetail joint.

A cylinder-on-flat fretting contact configuration was employed as indicated in Figure 3.1. This resulted in a contact length (w) of 10 mm (determined by the width of the flat sample) with the cylindrical sample having a radius,R of 15 mm. This configuration offers good alignment whilst also facilitating the simulation of the contact pressures of the highly loaded fan blade root contacts which could be achieved within the loading capacity of the fretting testing rig. This contact also allows direct comparison with previous work conducted at The University of Nottingham [234].

Both cylindrical and flat samples for the fretting pairs were cut from the Ti-6Al-4V plate by electrical discharge machining (EDM). The manufactured fretting couples were made up of a flat specimen which had a test surface width (w) of 10 mm and a counterpart with a cylindrical surface (with a radius,R of 15 mm) as shown in the flat and round specimen drawings in Appendix A. After machining, a surface grinding machine was used to for the surface finish of 0.4 – 0.7 µm Ra on the flat and cylinder samples as specified in Appendix A.

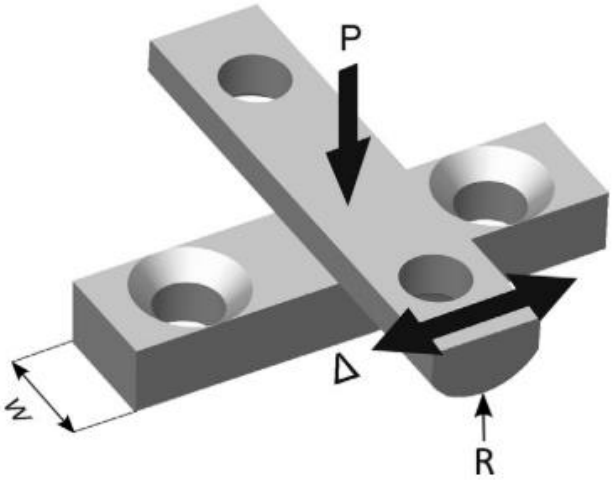


Figure 3.1 Cylinder-on-flat specimen configuration used in fretting tests where P is the applied normal load is, and Δ is the applied displacement.

A commercially available polymer-bonded MoS_2-based dry film lubricant with the trade name PL237-R2 (Appendix B) and a polymer-bonded graphite-based DFL (Appendix C) with the trade name IP9136-R1 were procured from Indestructible Paint Ltd., Birmingham, UK. The MoS_2-based DFL will be referred to as Mo-DFL and the graphite-based DFL will be referred to as Gr-DFL. The commercially available MoS_2-based DFL coating (Mo-DFL) was further modified with 4.76 % graphite powder as an additive (Appendix D). This powder was acquired as free-flow powder from Sigma Aldrich and had a granular size of 1<10 µm. The mixing process of the graphite-modified MoS_2-based DFL is discussed in Section 3.3. The graphite-modified MoS_2-based DFL is hereafter referred to as Gr-Mo-DFL.

Compressed dry air (Appendix E) and dry argon cylinders (Appendix F) used for environmental control purposes were acquired from BOC, Manchester, UK. Materials used are listed in Table 3.1.

Table 3.1 Raw material specification

Material	Form	Specification	Supplier
Ti-6Al-4V	Plate	500 × 500 × 10 mm	Rolls-Royce plc. UK
Grit-blast alumina	Aluminium oxide grit	0.125 – 0.149 mm	Airblast, UK
MoS_2-based DFL	Paint	PL237 – R2	Indestructible Paint Ltd, UK
Graphite-based DFL	Paint	IP9136 – R1	Indestructible Paint Ltd, UK
Graphite powder	Powder	1<10 µm	Sigma Aldrich, UK
Compressed dry air	Gas	Nitrogen – 79 % Oxygen – 21 %	BOC, UK
Compressed dry argon	Gas	Argon– 100 %	BOC, UK

3.2 Substrate surface preparation

3.2.1 Cylindrical specimen

In industrial practice, Ti-6Al-4V dovetail disc surfaces are typically shot-peened to promote fretting fatigue strength by introducing residual stresses on the surfaces of the component in order to delay crack initiation and propagation [107]. Accordingly, the majority of cylindrical Ti-6Al-4V counter-body specimens which represent the disc surface underwent a commercial steel-shot peening process (courtesy of Rolls-Royce plc) as listed in Table 3.2 with an intensity of 6-10A, 230 R shot size and 200% coverage (Appendix A) [235] which resulted in a roughness (Sa) of 0.6 µm; the DFL was then applied directly to this surface. A topographical image of the shot-peened Ti-6Al-4V surface can be seen in Figure 3.2 which were obtained using an Alicona G4 focus variation measuring instrument as discussed in Section 3.6.2.

There was a need to understand the behaviour of systems in light of previous work conducted at The University of Nottingham [234]. As such, in some tests, the cylindrical samples were grit-blasted with aluminium oxide grit (Airblast, UK) with a grit size of 0.125 – 0.149 mm and a blast pressure of 3 bar in a manual grit-blast cabinet at the University of Nottingham.

Table 3.2 Surface processing and surface characteristics of the various forms of the cylinder fretting specimens onto which the DFL was applied which were employed in the experimental programme

Surface condition of cylinder sample in pair	**Surface processing applied**	**Surface roughness (Sa) / µm**	**Maximum height (Sz) / µm**
Grit-blasted Ti-6Al-4V cylinder	Uncoated Ti-6Al-4V sample first ground using a surface grinding machine post sample machining and then subsequently grit-blasted.	0.9	11.7
Shot-peened Ti-6Al-4V cylinder	Uncoated Ti-6Al-4V sample first ground using a surface grinding machine post sample machining and were shot-peened	0.6	7.3

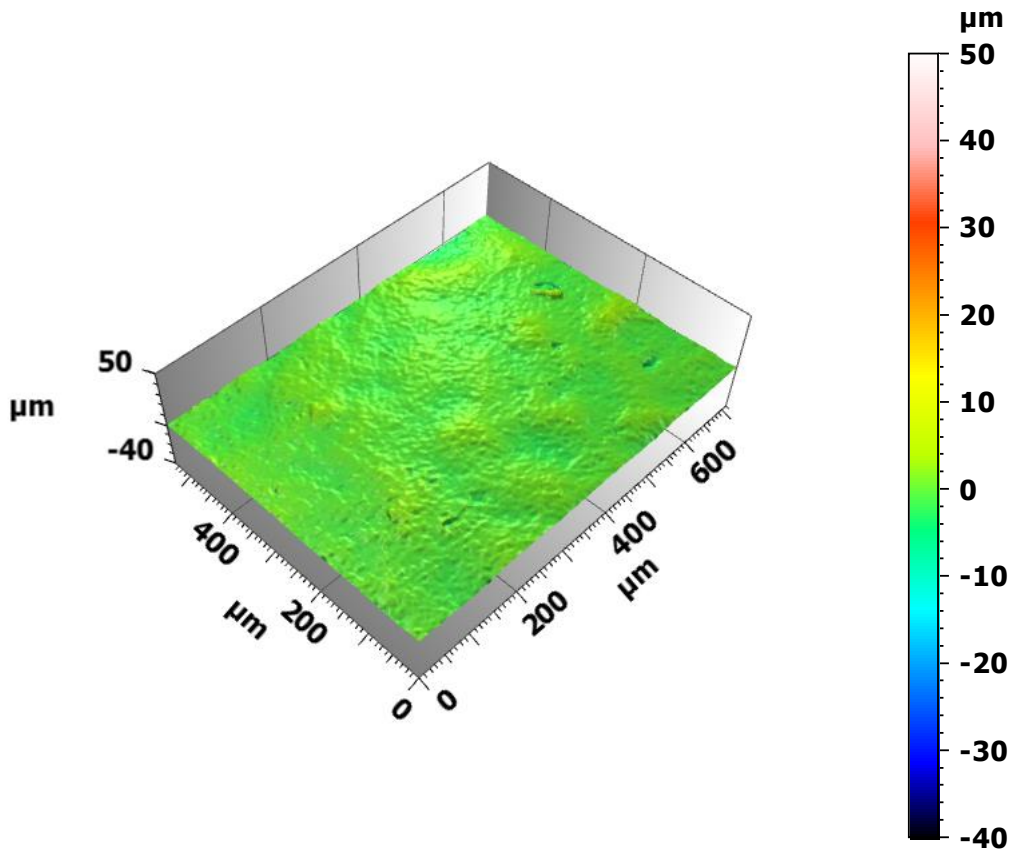


Figure 3.2 Topographic 3D profile of the shot-peened Ti-6Al-4V substrate surface prior to DFL coating application.

3.2.2 Flat specimens

The flat specimens were selected to represent the blade in the dovetail joint. To match industrial practice, selected Ti-6Al-4V flat samples were first shot peened (Appendix A), grit-blasted and then plasma sprayed with a Cu-Ni-In metallic layer with an approximate thickness of 100 - 190 µm by an external contractor (courtesy of Rolls-Royce plc) with this process representing current industrial practice.

Plasma spraying was conducted with a gas atomised feedstock powder (Metco 58 supplied by Oerlikon Metco) with a composition of 59 wt.% copper, 36 wt.% nickel and 5 wt.% indium and a nominal size distribution of -75 + 46 µm, indicating that 90% of the particles lie in this size range [236]. An equivalent plasma-sprayed Cu-Ni-In layer has been shown to have an elastic modulus of 66 GPa and a Poisson's ratio of 0.15 [114]. Vickers micro-hardness tests (with a 200 gf load) have shown

that the hardness of the Ti-6Al-4V substrate and the Cu-Ni-In deposit deployed in this work were 287 ± 10 HV and 177 ± 20 HV respectively [230].

To understand the role of surface material and topography on the DFL lifetimes, other preparations for the surface of the flat specimen were examined, with the DFL being deposited then onto these various surface types as detailed in Table 3.3. Manual surface grinding involved surface material removal with successively finer SiC (silicon carbide) grinding paper down to P800, whilst grit-blasting was conducted with aluminium oxide grit (Airblast, UK) with a grit size of 0.125 – 0.149 mm and a blast pressure of 3 bar in a manual grit-blast cabinet at The University of Nottingham. Topographical images of the flat specimen surfaces on both the Cu-Ni-In layer and the Ti-6Al-4V substrate are shown in Figure 3.3. Figure 3.4a shows a plan-view SE SEM image of the as-sprayed Cu-Ni-In interface and Figure 3.4b shows the grit blasted Ti-6Al-4V surface.

Table 3.3 Surface processing and surface characteristics of the various forms of the flat fretting specimens onto which the DFL was applied which were employed in the experimental programme.

Surface condition of flat sample in pair	**Surface processing applied**	**Surface roughness (Sa) / µm**	**Maximum height (Sz) / µm**
As-sprayed Cu-Ni-In (industrial practice)	Plasma-spray coated with Cu-Ni-In. No further processing of the as-sprayed coating.	9	84
Grit-blasted Cu-Ni-In	Plasma-spray coated with Cu-Ni-In. Coating then manually ground using SiC papers and then subsequently grit-blasted.	1.0	12
Ground Cu-Ni-In	Plasma-spray coated with Cu-Ni-In. Coating then manually ground using SiC papers.	0.4	4.7
Grit-blasted Ti-6Al-4V	Uncoated Ti-6Al-4V sample first ground using a surface grinding machine and then subsequently grit-blasted.	0.9	12.3
Ground Ti-6Al-4V	Uncoated Ti-6Al-4V sample ground using a surface grinding machine	0.5	5.8

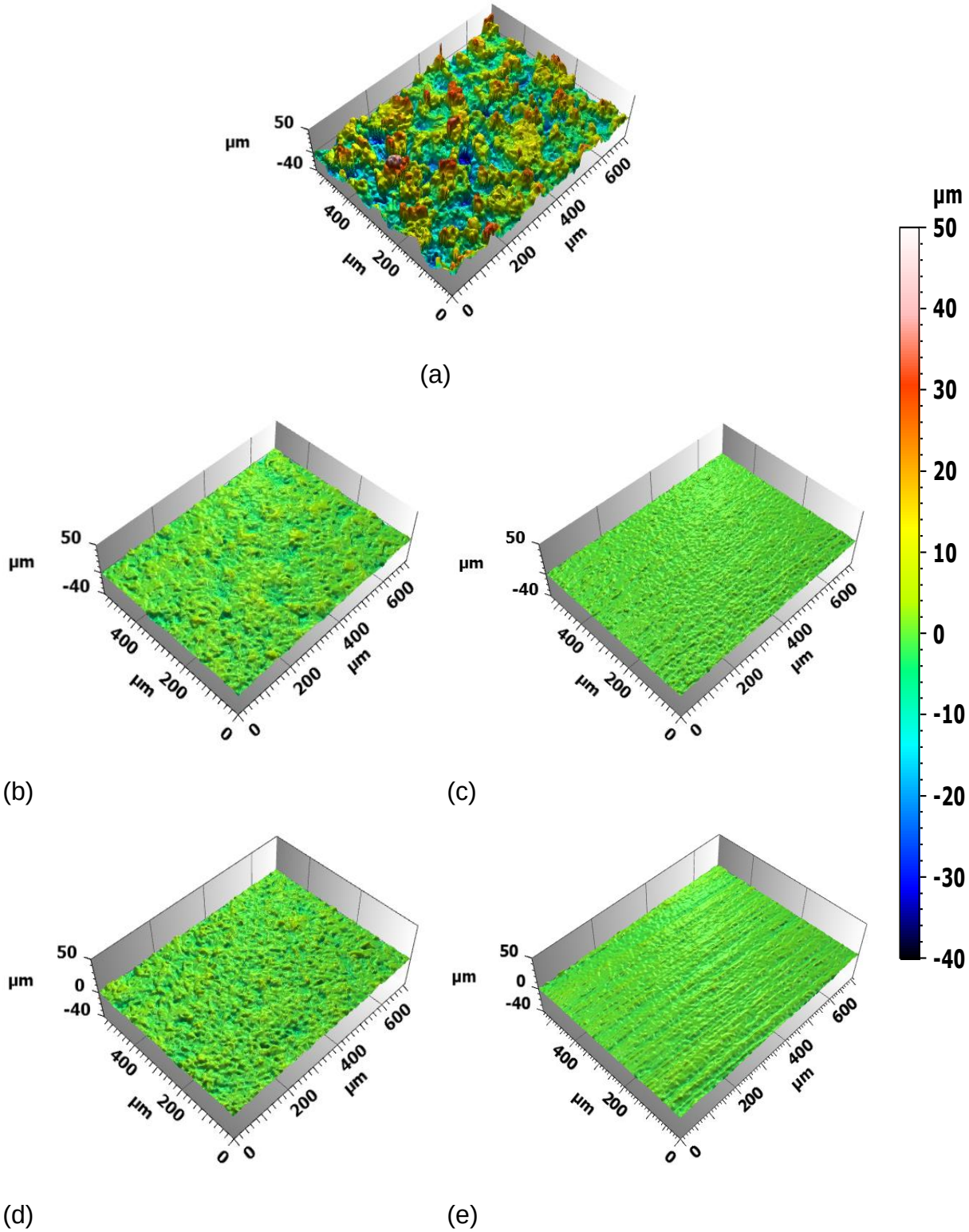
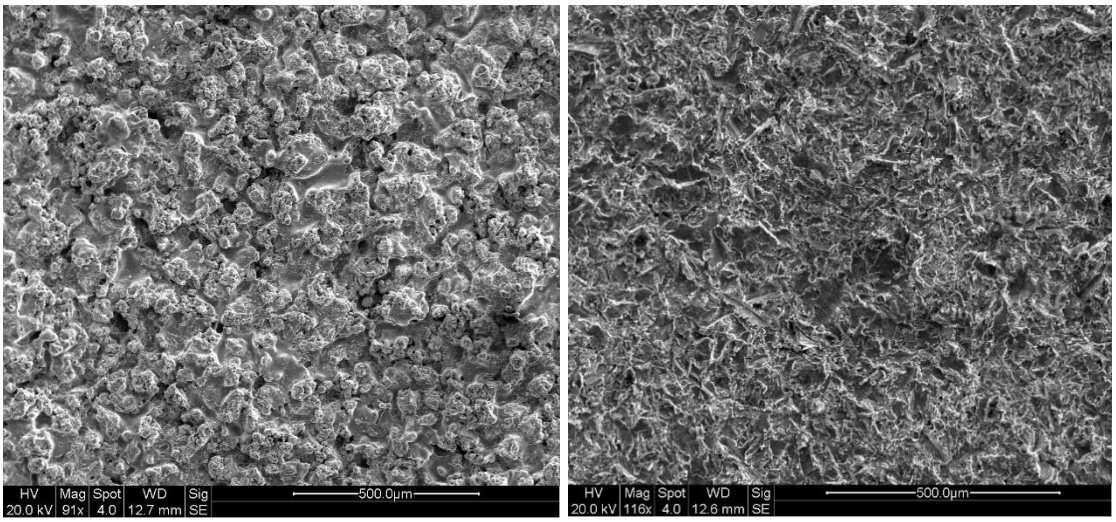


Figure 3.3 Topographic 3D profiles of the flat Cu-Ni-In layer and Ti-6Al-4V substrate surfaces prior to DFL coating application. (a) As-sprayed Cu-Ni-In, (b) Grit-blasted Cu-Ni-In, (c) Ground Cu-Ni-In, (d) Grit-blasted Ti-6Al-4V, (e) Ground Ti-6Al-4V.



(a) (b)

Figure 3.4 SE SEM images of (a) plasma sprayed Cu-Ni-In coating (b) grit-blasted Ti-6Al-4V

3.3 DFL spray deposition process

Following surface preparation of the specimens, the various DFLs (as discussed in Section 3.1) were spray deposited on the working surfaces of both the cylindrical and flat fretting samples to align with industrial practice. The graphite-based (Gr-DFL) and MoS_2-based (Mo-DFL) paints were mixed by first stirring with a glass rod and then shaking by hand thoroughly for 15 - 20 minutes before use. Prior to pouring into the spray gun, the paint was sieved through a fine mesh filter (180 µm).

In light of previous work [234], additional graphite powder with a particle size of 1<10 µm was mixed with the as-supplied Mo-DFL paint to investigate the implications this has on the fretting lifetimes (this paint is termed Gr-Mo-DFL). The details of the graphite powder are presented in Table 3.1.

Prior to adding the graphite powder, the paint is thoroughly mixed for half an hour by a glass rod and by manual shaking to ensure uniform viscosity. 100 ml of DFL paint was weighed in a 250 ml glass beaker which was sieved through a 180 µm before being poured. According to the mass of the paint (~55 g), 5 % of graphite powder was slowly added (~ 2.75 g) in small quantities into the initial DFL and mixed. The graphite fraction in the final paint (including solvents) was 5 parts in 105 (4.76 %).

To ensure good dispersion of the graphite, the mixture is stirred with an ultrasonic immersion vibrator at 20 second intervals to avoid heat generation within the mixed paint. Once all the graphite powder has been added to the DFL paint matrix, a final stir with the ultrasonic immersion vibrator was conducted which completes the additive mixture procedure.

Spray deposition of the DFL, in line with industrial procedure, was conducted in a painting facility at The University of Nottingham. A spray gun was used to apply the paint; temperature in the spray booth remained within 15 – 30 °C and the air pressure of the spray was maintained at 30-40 psi (206.8 – 275.7 kPa). Sample surfaces were first swabbed with solvent, IP9151 (Appendix G) and left to dry in air. Specimens were fixed upon a wooden board using double sided tape to keep them in position. The wooden board is held vertically and a guide board (to promote) consistency in the manual spraying process is fixed a distance of 150 mm from the specimen board; the sprayer then ensures that the distance from the spray nozzle and specimens is maintained within a certain range.

As seen in Figure 3.5, spraying is done by hand using a zig-zag motion to cover the fretting specimens. A target coating thickness of approximately 50 ± 10 µm was aimed for and achieved through a number of painting passes, which was initially determined by trial and error; the paint is left to dry for a minimum of 10 minutes at room temperature after each successive pass.

To cure the DFL-coated specimens, they were placed in a circulatory air oven at 100 °C, with the temperature then being increased by 6 °C min^{-1} to 190 ± 1 °C followed by holding at this temperature for 2 hours, following which, they were removed from the oven and cooled to room temperature. The target DFL coating thickness (t) measurement ensued using a DeFelsko PosiTector 6000 eddy current thickness measurement gauge to confirm the coating thickness. Specimen pairs (flat and cylindrical) were painted in batches to ensure coating thickness and quality consistency for each set of tests planned.

Due to the complexities of making DFL thickness measurements when deposited onto an as-received Cu-Ni-In interlayer which can affect accuracy of the measurement, DFL coating procedures were first defined via coating of the flat Ti-6Al-4V substrate to establish the desired DFL thickness. The same coating process parameters which were used to achieve a thickness of 50 ± 10 µm on the Ti-6Al-4V samples were then employed for DFL deposition onto the Cu-Ni-In coated samples.

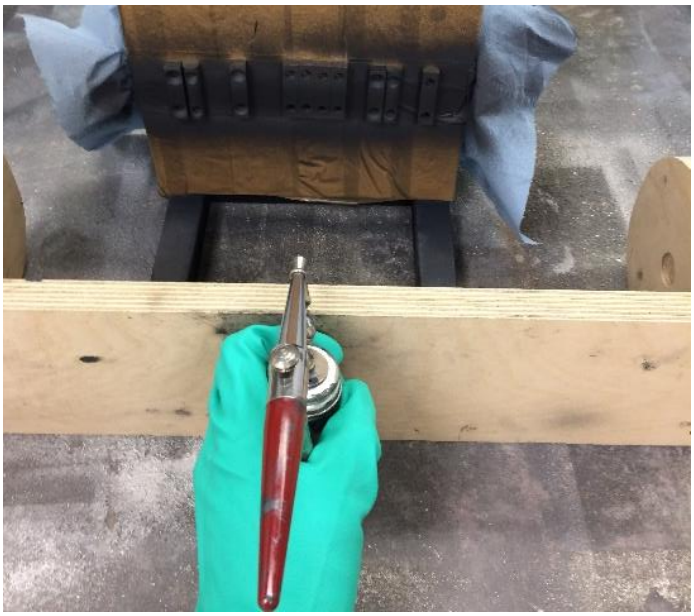


Figure 3.5 Image of the DFL coating process in progress

3.4 Fretting wear test

Fretting wear tests were carried out on an electro-servo hydraulic fretting testing machine which was based at The University of Nottingham.

A schematic diagram of the test setup is presented in Figure 3.6. In this arrangement, two pairs of identical specimens are fretted simultaneously on the same fixture. A linear variable displacement transducer (LVDT) is mounted to the base of the hydraulic actuator to continuously measure the far-field applied displacement whilst a load cell measures the total shear force (i.e., the sum of that associated with the two individual fretting contacts). The fretting test machine is equipped with a central hydraulic ram which has a 10 kN load cell, two horizontal hydraulic cylinders with a 1 kN maximum load housed within the diaphragm, two specimen pair holders and a LVDT (linear voltage displacement transducer) used for displacement measurements and feedback to the accompanying control unit.

A summary of the fretting test parameters and conditions are presented in Table 3.4; these conditions were selected to deliver contact pressures and relative displacements representative of those experienced within aero-engine dovetail joints [11], [225].

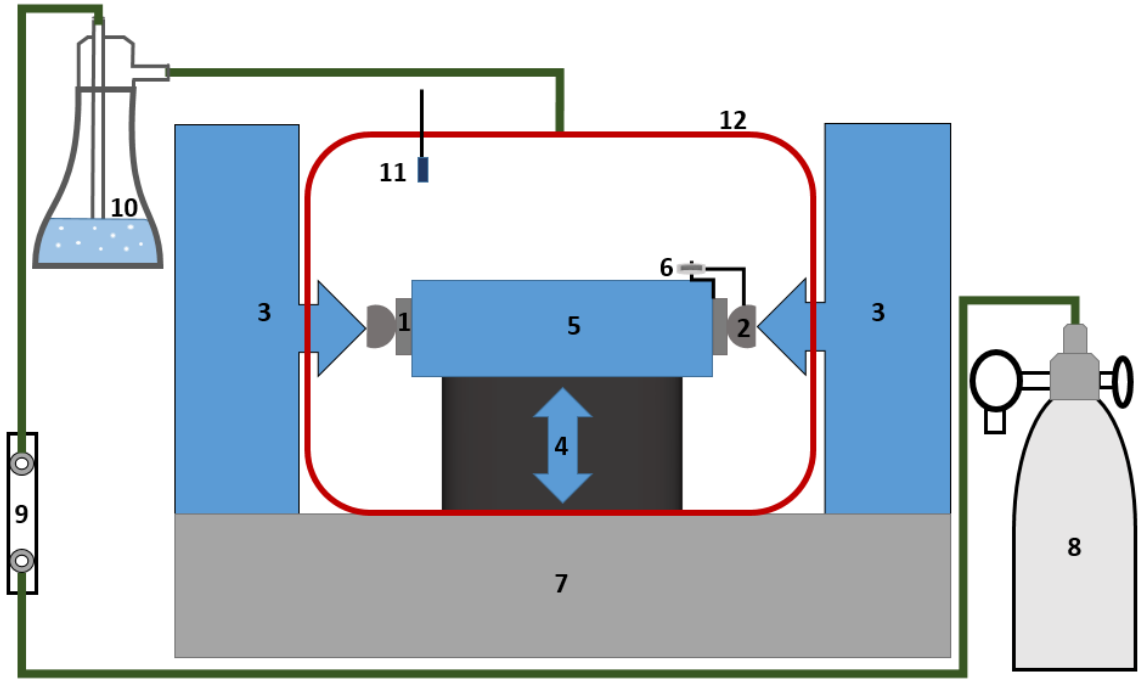


Figure 3.6 Electro servo hydraulic fretting rig operating schematics and environmental set up (1) Ti-6Al-4V flat specimen with contact length w = 10 mm (2) Ti-6Al-4V cylindrical specimen with radius R = 15 mm (3) Fixed position hydraulic cylinder for applied normal load P = 575 N (4) Vertical controlled actuator for applied displacement amplitude Δ* = 0.3 mm (5) Load cell (6) LVDT (7) Mounting block (8) Dry air or argon cylinder (9) Flow meter (10) Water bubbler (11) Humidity sensor (12) Environment chamber.

Cylindrical samples were screwed to the hydraulic pistons and pressed against the flat specimen through a pair of floating hydraulic cylinders capable of moving horizontally along a line perpendicular to the specimen axis. The flat specimen then moved vertically within the prescribed cross-head displacement range. The vertical movement of the specimen induced slip between the contacting surfaces. The prescribed cross-head displacement range was sufficiently large enough to exceed displacement due to elastic deformation in the system; however, it is recognised that the slip amplitude in the contact is less than the far-field displacement amplitude. During the test a normal force was applied to both pads, this was maintained as constant and equal through the use of a hydraulic accumulator. The sum of the tangential force at the two contacts was measured with the load cell of the testing machine. Coefficient of friction (CoF) in slip was computed as the ratio of the tangential force to the normal load induced by the hydraulic cylinder onto each pad. Relative displacement was continuously measured with a LVDT.

Before alignment and testing, the specimens were cleaned with industrial methylated spirit. For a single fretting test, two specimen pairs (two flats and two cylinders) must be assembled to maintain lateral balanced forces on the main ram due to the dual running configuration.

The flat specimens are attached to the central hydraulic loading ram which controls the displacement amplitude and frequency with vertical motion to replicate the vibration and fretting motion. An oscillatory displacement amplitude and a frequency were applied to the central ram.

The round specimens are attached to the side loading hydraulic pistons which apply a constant normal load, P, against the flat specimen attached to the central ram. In operation, the specimen will be in contact under an applied load, P. The loading conditions are applied through the accompanying control unit while the sum of tangential traction forces from the paired specimens are measured using a machined strain gauge load cell on the central ram.

Table 3.4 Fretting test conditions employed

Normal Load (P) / N	575, 1000
Displacement amplitude Δ* / mm	0.3, 0.4
Frequency (f) / Hz	2.5

The control and data acquisition system used an NI USB 6000 multifunction I/O device along with a written program in LAB-VIEW^{TM} which permitted real time monitoring and continuously recorded the tangential force and applied relative displacement at 500 Hz sampling rate garnering 200 sampling points per fretting cycles, an assumption was made that the tangential force associated with each of the two fretting contacts was equal, and therefore the tangential force on each specimen was assumed to be a half of the total tangential force measured by the load cell.

The tangential force-displacement data were plotted to form fretting loops of the type presented in Figure 3.7. The coefficient of friction (CoF) (μ) is given by:

$$\mu = \frac{Q^*}{P}$$

Equation 3.1

where $Q*$ is the maximum tangential force per specimen recorded in each cycle and P is the constant normal load applied. CoF can be calculated on-the-fly (i.e. during the test) and is therefore used for in-test monitoring. Previous work looking at the behaviour of DFLs with this test geometry had shown that the CoF increased rapidly towards the end of the test and that this was associated with the failure of the coating system [225]. In light of that work, failure of a test pair in the current work was defined to have occurred when $\mu \geq 0.7$ and for each material pairing type examined, tests to failure (i.e., to completion) were automatically terminated when that condition was first satisfied.

It is known that alongside the coefficient of friction (CoF) itself, geometrical evolution of the contact also affects the maximum force recorded in a fretting cycle [72]. Accordingly, in this work, on fretting tests that were conducted on the in-house cylinder-on-flat fretting wear rig, the energy coefficient of friction (ECoF) (μE) [73] has been derived in post-test analysis of the data as follows:

$$\mu_E = \frac{E_d}{4\ P\ \delta^*}$$

Equation 3.2

where E_d is the energy dissipated over a fretting loop and $\delta*$ is the slip amplitude (as distinct from the applied displacement amplitude,$\Delta*$).

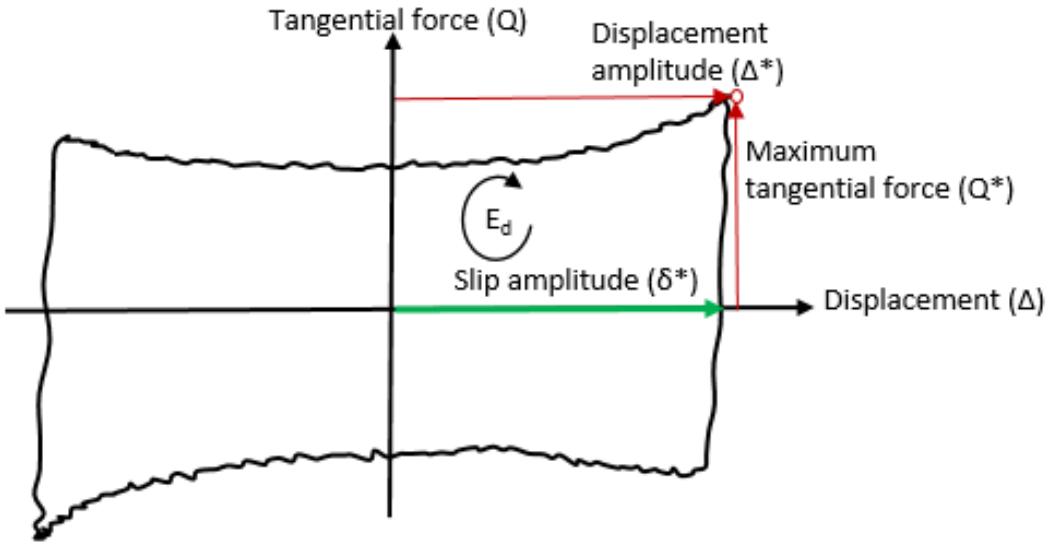


Figure 3.7 Annotated schematic diagram of fretting loop

Once the number of cycles to failure of the various fretting pairing types had been determined, interrupted tests (i.e., tests which were stopped before failure took place) were conducted on selected sample pairing types from the test matrix. Such tests were conducted to facilitate a better understanding of the wear process in the various stages of fretting degradation of these systems.

Raw data files that are obtained from the rig contain information regarding the tangential forces and displacement amplitudes which are recorded during fretting tests were post-processed using written LAB-VIEW^{TM} software scripts. This includes Batch process script and Get Data scripts which help determine the fretting loops, and clean the signals by removing drift and noise and expand the displacement and force values into CoF (μ) and ECoF (μE).

3.4.1 Environmental chamber

Fretting wear tests were first conducted in atmospheric ambient conditions and were then repeated in different controlled environmental conditions made possible by outfitting the fretting wear rig with environment control capabilities as illustrated in the fretting rig schematic (Figure 3.6). This was implemented with dry compressed air and argon gas cylinders which were purged into a purpose built sealed environment chamber at a constant flow rate of 2 litres/minute to maintain a consistent gas environment. A Honeywell HIH-4000 series humidity sensor was used for the duration of the tests to measure the relative humidity inside the chamber. The NI USB 6000 and written LAB-VIEW^{TM} program was also used for the humidity data acquisition and meant the simultaneous acquisition of the fretting wear rig data and the humidity data occurred. During selected tests, the constant flow gas purge was switched off and the environment chamber was opened to monitor the effects of the increased relative humidity during ongoing fretting tests. Further examinations on the effect of humidity required the identification of the dominant environmental mechanism that affects the wear behaviour of the coating, and thus, it was needed to isolate the effects of oxygen and that of humidity on the performance and wear behaviour of the various DFLs. In order to test the influence of water vapour without the presence of oxygen, humidified argon was employed by passing dry argon gas at 2 litres/minute through a water bubbler to increase its humidity before directing it into the environment chamber. This achieved a humidity level of around 60 – 75 % inside the chamber. This was repeated for dry air to obtain a high humidity environment with oxygen content. A summary of the environmental fretting test conditions can be seen in Table 3.5.

Table 3.5 Environment fretting test conditions

Environment conditions	Relative Humidity (%)	Temperature (T) / °C
Dry Argon	0.5 - 3 ± 3	30 ± 5
Humidified argon	60 - 75 ± 3	30 ± 5
Dry air	0.5 - 3 ± 3	30 ± 5
Ambient air	25 - 40 ± 3	25 ± 5
Humidified air	60 - 75 ± 3	30 ± 5

3.5 Flat-on-flat (Scitek) Fretting wear test rig

The testing at the University of Nottingham was compared with testing which was being conducted elsewhere (Scitek) by the research sponsor (Rolls-Royce plc). The key difference between the two test types was in specimen contact configuration; the Scitek test machine had a much larger load capacity and thus flat-on-flat contact geometry could be employed with a similar contact pressure. Figure 3.8 shows a schematic diagram of the Scitek testing rig. The testing programmes at University of Nottingham and Scitek allowed the expansion of testing parameters to give further insight on the wear behaviours and the mechanisms which will further facilitate the development of the enhanced performance DFL. The Scitek testing rig is capable of 75 kN sliding force and controlled by the existing Parker D1FP valve & DSCC-100kN load cells on both cylinders for normal and frictional force measurement. An OptoNCDT 1700/10 laser triangulation system is used for displacement measurements and a Gobi640-GigE-6484 thermal camera records the temperature measurement of the samples during fretting wear tests.

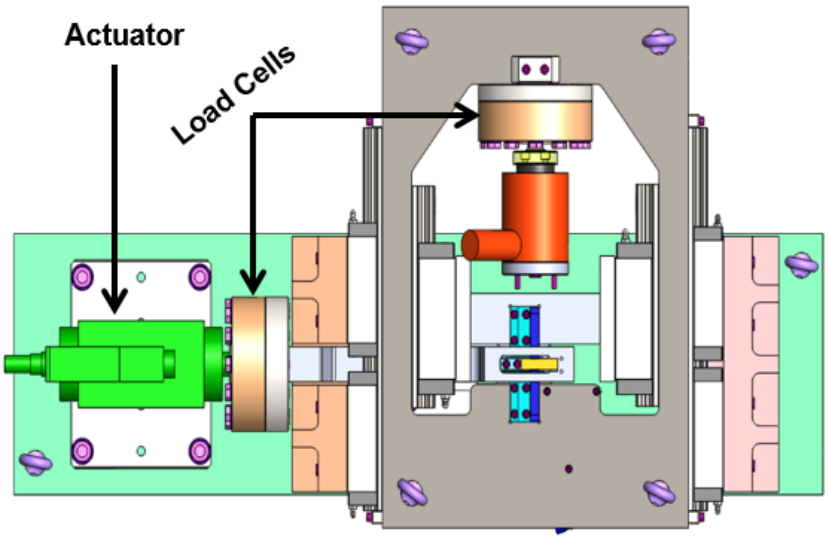
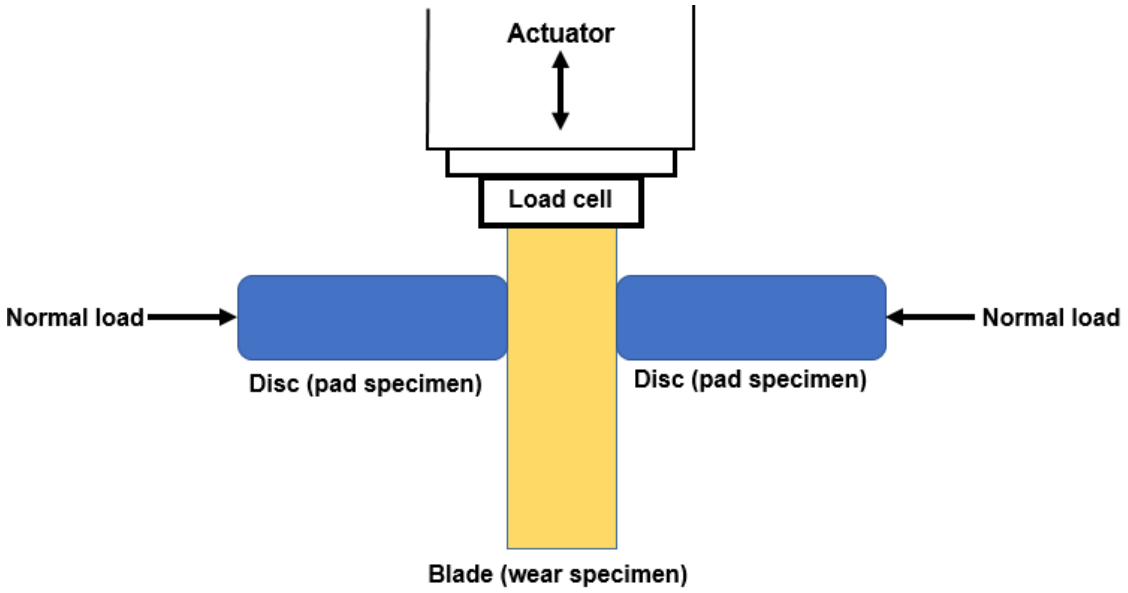


Figure 3.8 Scitek Flat-on-Flat fretting wear test rig

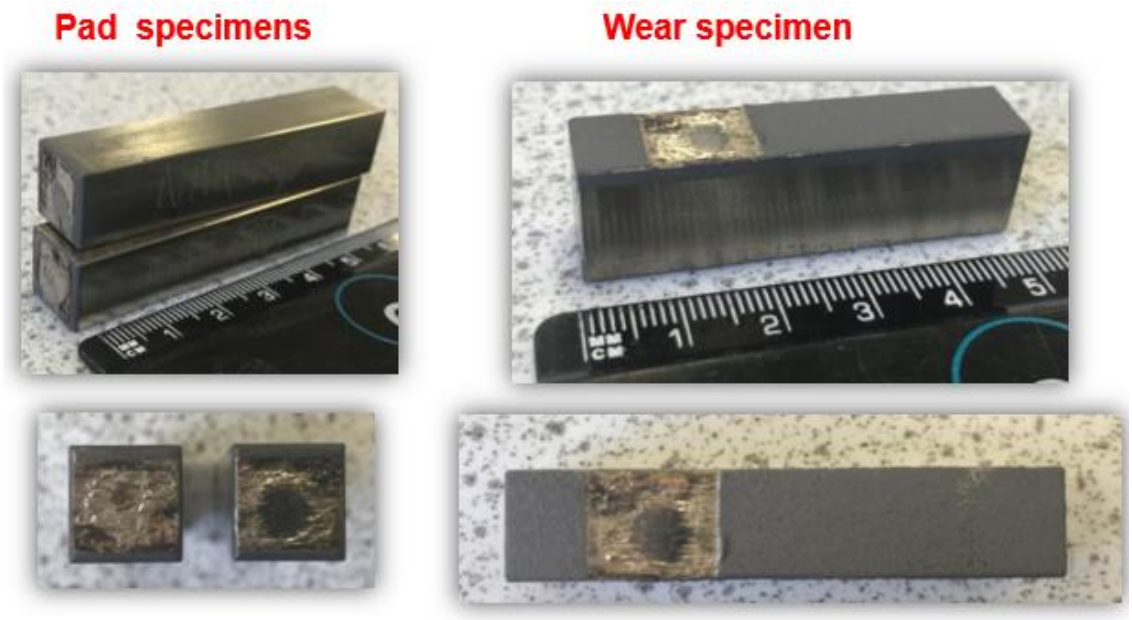
In Figure 3.9, the corresponding pad and wear testing samples can be observed. The contact configuration employs a single flat wear sample that represents the fan-blade root. Prior to the deposition of the bonded DFL coating, the sample

undergoes the surface preparations as described in Section 3.2 to match the surface architecture of the fan blade root which are plasma-sprayed with a Cu-Ni-In under-layer. Two adjacent pad samples represent the disc counterparts which are shot-peened and DFL coated. This results in a flat-on-flat contact with a surface area of 10 x 10 mm.

During the fretting wear tests, a force is applied on either side of the two pad samples which are pushed against the wear sample in the middle to establish a contact pressure at the contacting surface. A displacement is applied on the wear sample at a certain frequency by actuator control resulting in a force displacement action and thus, a tangential force at the contacting surface. The coefficient of friction from the fretting wear tests were calculated by utilising the ratio of the peak to peak frictional force (i.e., the highest forces in each fretting loop) to the applied normal load. Selected tests were conducted under controlled specimen temperature and humidity during the experiment. The temperature of the fixtures was controlled to allow a specimen temperature of 30 °C to be achieved. The relative humidity was controlled and monitored in the range of 10 ± 5 % with a dry air gas purge.



(a)



(b)

Figure 3.9 (a) Schematic of Scitek fretting wear testing sample configuration, (b) photographic images of the flat-on-flat fretting wear testing samples showing the wear specimen which represent the fan blade root and the pad specimen which represent the disc after a test.

3.6 Fretting wear scar assessment

3.6.1 Sample preparation for characterisation

A cut-off machine operating at a cutting speed of 0.020 mm s^{-1} and fitted with an alumina abrasive wheel was used to section selected worn specimen samples. Samples were then cold-mounted in non-conductive metallographic preparation resin; epo-fix cold mount resin and epo-fix hardener resin were mixed at a ratio of 5:1 (15 ml – 3 ml) which has an 11 hour setting time. Once mounted, the specimen is ground using different grades of silicon-carbide abrasive paper (starting at P240 grit up to P4000 grit). This step is followed by 0.1 µm cloth polishing with an MD-CHEM Colloidal silica disc with silica oxide final polishing suspension. Samples were cold mounted rather than mounted using the traditional conductive hot mounting method to avoid any concerns of thermal damage to the DFL during the mounting process. Cold mounting material is non-conductive which meant that before characterisation analysis on the SEM machine could begin, the specimen and the mount were sputtered with a conductive carbon layer (~ 10 nm) using the Quorum evaporative carbon coater.

3.6.2 Surface topography and profilometry

Surface characterisation and profilometry was carried out by focus variation microscopy using the Alicona G4 Infinite Focus. A defined area of 710 × 539 µm was measured for determination of various surface parameters (of the type presented in Table 3.3) which were calculated in accordance with ISO 25178 using a cut-off wavelength of 250 µm for S-L filters. The Alicona G4 is a focus variation measuring instrument which vertically scans the surface to capture a full surface profile through a stack of 2D microscope images. For each image, the sharpness of each pixel is calculated to detect the varying depths associated to the surface. The software, MountainsMap™ was used to process the raw data of the surface profiles. Further 3D measurements (also with the Alicona system) were employed in this work to carry out surface profilometry of the wear scars from the flat and cylindrical specimens after fretting tests, data again being processed using MountainsMap™ software. Before analysing the wear volumes of cylindrical samples, the surface form was first removed. From these measurements, average depth profiles and the maximum depths of the averages profiles across the scars

were derived by taking the average of 50 individual profile lines across a scar. An error margin of ± 2 µm is applied for the wear scar depth plots.

3.6.3 Scanning electron microscopy and energy dispersive x-ray (EDX) analysis

After fretting tests, scanning electron microscopy (SEM) was utilised for the analysis of the wear scar features; wear scars were examined both in plan-view and in cross-section. Energy dispersive X-ray (EDX) analysis was performed in the SEM for semi-quantitative chemical characterisation of the various features observed in the fretting wear scars.

An FEI Quanta600 MLA SEM scanning electron microscope was used for the majority of this study which was fitted with a thermal field emission gun. The SEM was operated with an accelerating voltage of 20 kV and a working distance of ~ 13 mm. Images were taken using both secondary electron (SE) and back scattered electron (BSE) mode. SE images give information about surface topography, scar orientation, wear scar direction, presence of debris or any presence of layer structure. Backscattered electrons give contrast based upon average atomic number; they have a greater energy than secondary electrons and can escape from deeper within the specimen, and thus BSE images have lower lateral resolution than SE images. Due to its atomic number contrast, BSE can be used to distinguish oxide and DFL from metallic materials, as both DFL and oxide (generally the main constituent of the debris formed within the wear scar) have a lower average atomic number (resulting in lower brightness in BSE imaging) than titanium. In addition, BSE imaging can be used to identify the high-brightness MoS_2 particles within the DFL itself.

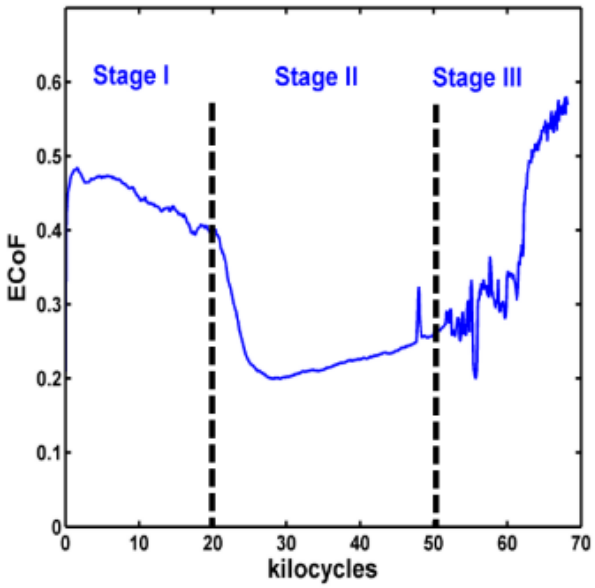
EDX analysis was conducted with an EDAX^{TM}CDU LEAP detector with a 10 kV beam accelerating voltage being employed.

Chapter 4. Effects of humidity and oxygen on the performance of polymer-bonded MoS_2-based; graphite-based; and graphite-modified MoS_2-based DFL coatings

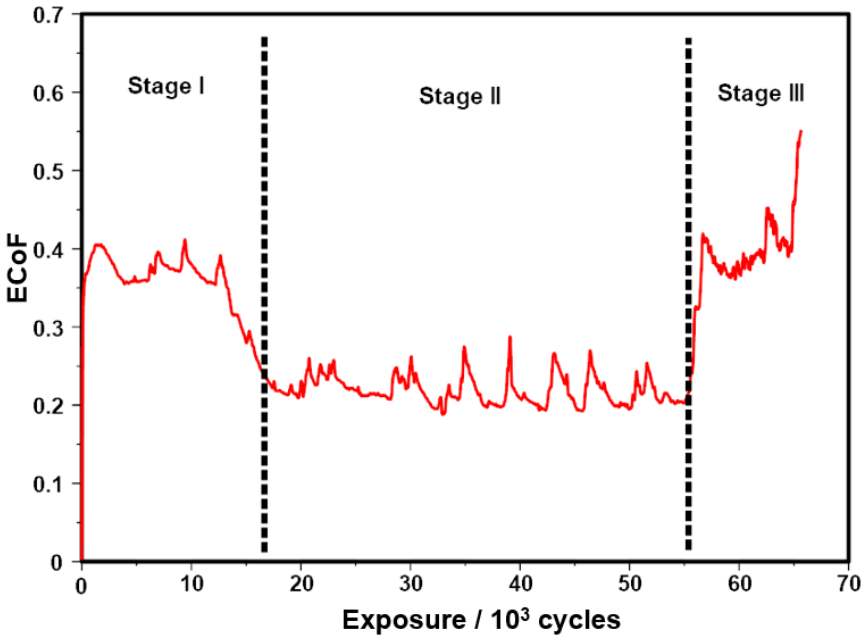
4.1 Background – Initial results of the polymer-bonded MoS_2-based DFL (Mo-DFL) and graphite-modified MoS_2 DFL (Gr-Mo-DFL)

Previous work [234] conducted at University of Nottingham by Barman et al. investigated the fretting wear behaviour of a polymer-bonded MoS_2-based dry film lubricant including a variety of additives. In that work, fretting tests were conducted in a like-on-like configuration. As one of the additives, 4.76 wt. % carbon powder was added to the commercially available MoS_2-based polymeric DFL paint prior to its deposition (the resulting modified DFL coating system is termed Gr-Mo-DFL). Fretting tests were conducted on Mo-DFL and Gr-Mo-DFL coated Ti-6Al-4V samples (which had been grit-blasted prior to DFL deposition) using a cylinder-on-flat contact configuration with a cylinder radius of 15 mm. An applied normal load of 575 N, 0.3 mm displacement and a frequency of 2.5 Hz were employed for the fretting tests.

To confirm the repeatability of the earlier work on the test apparatus employed in this work (different from that of the previous work), repeats of the initial experiments with the as-received MoS_2 DFL (Mo-DFL) and the modified version with 4.76 wt. % graphite powder additive (Gr-Mo-DFL) were conducted using an electro-servo hydraulic fretting testing machine (Figure 3.6) with the same cylinder-on-flat contact configuration (Figure 3.1) and fretting conditions as used in the previous work [225]; in both cases, like-on-like sample configurations were employed. Figure 4.1a shows the evolution of friction of the as-received MoS_2 DFL (Mo-DFL) coating which had been sprayed onto grit-blasted Ti-6Al-4V samples (both cylinder and flat) from the previous work and Figure 4.1b shows a repeated test in the current work with the same fretting conditions applied. The Mo-DFL system failed at ~ 65 k cycles with three stages of wear behaviour as previously observed by Barman et al. [225] again being observed in the current work.



(a)



(b)

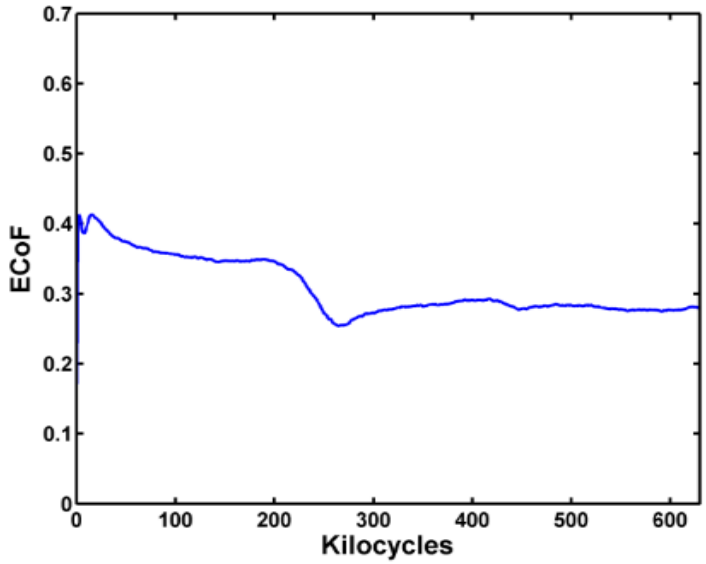
Figure 4.1 (a) Evolution of friction coefficient against number of cycles for polymer-bonded MoS_2-based DFL (Mo-DFL) on grit-blasted self-mated Ti-6Al-4V samples conducted in atmospheric conditions from previous work [225], (b) Repeat of the Mo-DFL test conducted on self-mated grit-blasted Ti-6Al-4V samples at a load of 575 N, 0. 3mm applied displacement and 2.5 Hz frequency at atmospheric conditions (25 – 40 % RH) to verify previous results on a new testing rig which compares the lifetime.

In Figure 4.2a, Gr-Mo-DFL tests from previous work [234] is presented where it can be seen that an initial ECoF of ~ 0.42 was observed which then fell slowly and steadily to ~ 0.28 over the test duration. This low steady state friction was maintained until 658 k cycles when the experiment was terminated (before coating failure). This result showed an increase of *at least* approximately 10 times the lifetime previously seen with the unmodified MoS_2 dry film lubricant (hereafter termed Mo-DFL). It was found that following the test (658 k cycles), the DFL had worn to a depth greater than the original thickness (~ 50 µm) indicating that there has been substantial removal of material from the titanium alloy substrate, despite still exhibiting the low coefficient of friction. However, analysis via high magnification BSE SEM imaging (Figure 4.2b) revealed ploughing effects on the surface but with no indication of exposure of the metallic surface on the wear scar in that work. Overall observations showed that the addition of 4.76 wt. % graphite powder into the MoS_2-based (Mo-DFL) paint matrix significantly extended the lifetime and durability of the fretting system. Remnants of graphite modified DFL coating was preserved over the titanium substrate and a low friction surface was maintained in the fretting contact which kept a stable and steady coefficient of friction and extended the fretting lifetime of the coating system.

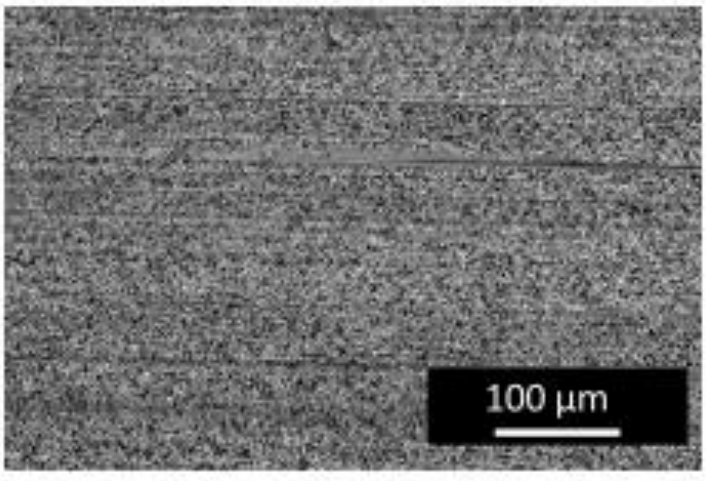
Figure 4.3 shows the evolution of the coefficient of friction of the as-received MoS_2 DFL (Mo-DFL) and the graphite modified MoS_2-based DFL (Gr-Mo-DFL) coatings obtained in the current work. A significant extension of fretting lifetime was observed for the modified Gr-Mo-DFL system where a low and steady ECoF was present for a majority of the fretting test which was terminated at 2300 k cycles before failure occurred. Wear depths greater than the original DFL thickness (~ 50 µm) were also observed on the surface profilometry of the testing samples. These results demonstrate that similar extended low friction performance and wear characteristics as observed in previous work were also observed with tests conducted as part of this research programme, with a significant extension of lifetime (in this case, more than a 35 times extension to lifetime) observed for the graphite modified Gr-Mo-DFL system when compared to the Mo-DFL system.

With the aim of extending the lifetime of the original MoS_2-based (Mo-DFL) coating system employed for in-service fan blade roots, the initial results of the graphite modified (Gr-Mo-DFL) coating system appeared to offer a low-cost solution to maintain low friction and durability at the fan blade roots and reduce the ongoing need for regular recurring interim services. To expand the testing envelop, this chapter focuses on the atmospheric environmental challenges and limitations which are imposed on polymer-bonded MoS_2 dry film lubricant (Mo-DFL). As part

of this, the performance of the Mo-DFL will be compared to that of the graphite modified MoS_2 DFL (Gr-Mo-DFL) coating system across different environmental conditions.



(a)



(b)

Figure 4.2 (a) Evolution of friction coefficient against number of cycles for graphite modified polymer-bonded MoS_2-based DFL (Gr-Mo-DFL) on grit-blasted self-mated Ti-6Al-4V samples conducted in atmospheric conditions from previous work [234] interrupted at 658 k cycles, (b) Plan-view BSE SEM images of the Gr-Mo-DFL testing sample which was stopped at 658 k cycles from previous work [234].

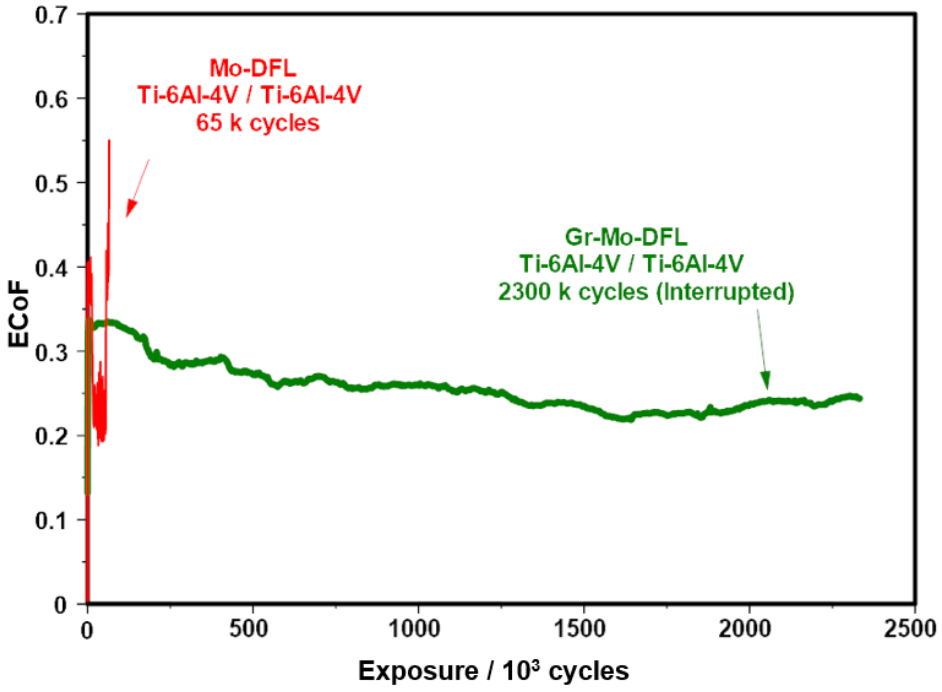


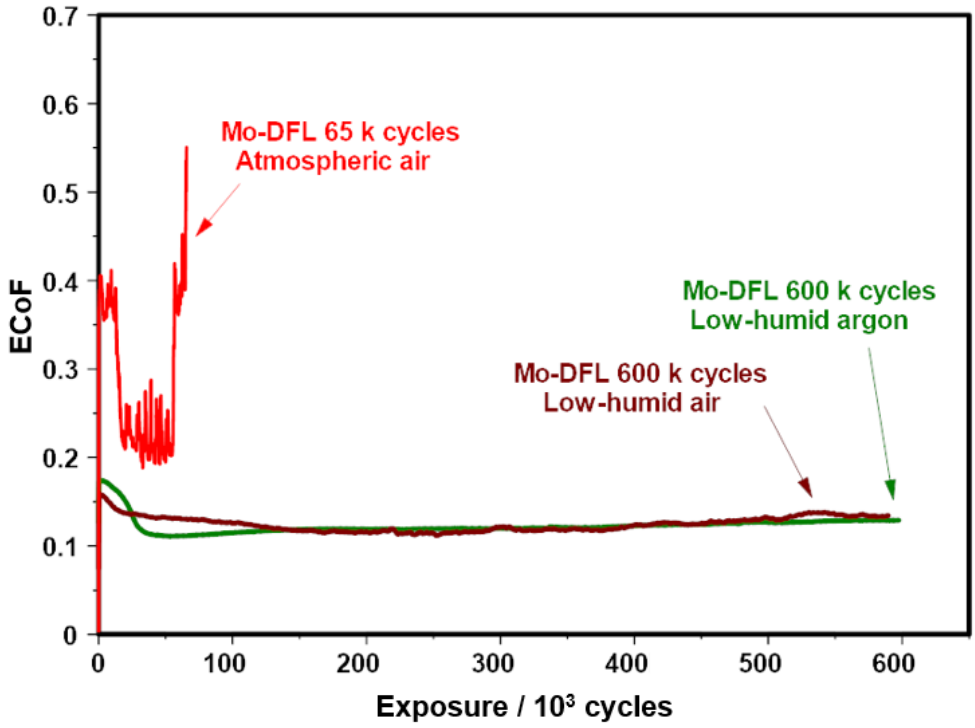
Figure 4.3 Repeat of the original MoS_2 DFL (Mo-DFL) and graphite modified (Gr-Mo-DFL) equivalent tests conducted on self-mated grit-blasted Ti-6Al-4V samples at a load of 575 N, 0.3mm applied displacement and 2.5 Hz frequency at atmospheric conditions (25 – 40 % RH) to verify previous results on a new testing rig which compares the lifetime.

4.2 Polymer-bonded MoS_2-based DFL (Mo-DFL) performance in low-humidity environments

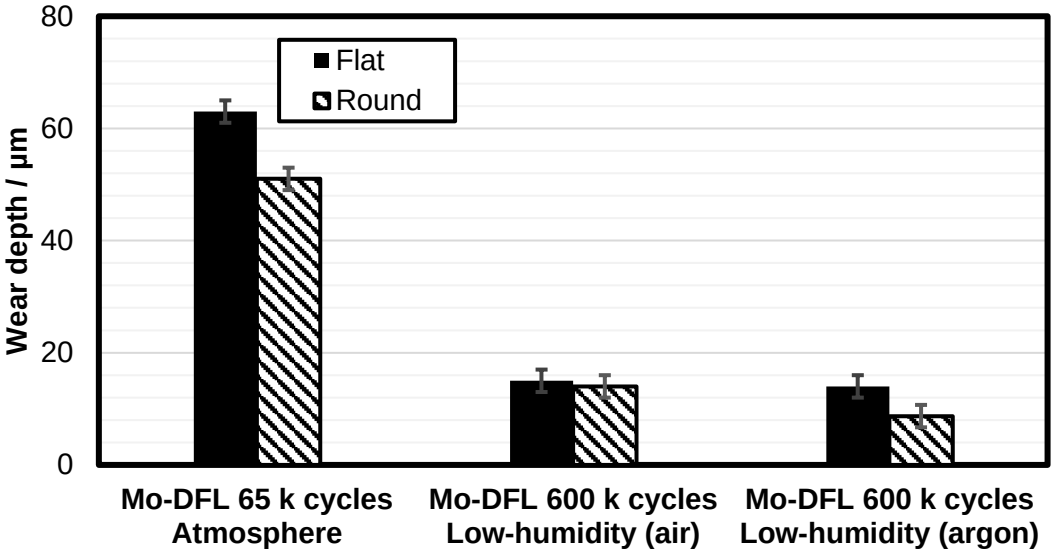
The performance of the Mo-DFL coating system was investigated with an emphasis of the role that oxygen and humidity have on the fretting wear behaviour of the coating. Fretting tests were conducted using a cylinder-on-flat testing configuration as seen in Figure 3.1 on the ESH fretting test rig (Figure 3.6) where a normal load of 575 N, an applied displacement of 0.3 mm and a frequency of 2.5 Hz were imposed. Both the flat and cylinder Ti-6Al-4V specimens for the tests reported in this section were grit-blasted prior to the application of the DFL coatings and featured an initial surface roughness (Sa) of 0.9 µm as listed in Table 3.3. Tests were conducted with a constant purge of dry argon or dry air (2 litres / minute flow rate) which resulted in a measured humidity of 0.5 – 3%.

Figure 4.4a shows the evolution of ECoF against test duration for tests conducted in the various environments. In atmospheric conditions (air with ambient humidity of ~ 30%), failure was reached at ~ 65 k cycles; the three distinct stages of wear behaviour as outlined in previous works [225] were again observed (Figure 4.1) where the beginning of the test (Stage I) featured an initial period of high friction followed by a low friction phase (Stage II) which lasts for approximately 40 k cycles and subsequently leads to failure phase of the coating (Stage III) which is characterised by instability and the increase of friction until the imposed limit (when $\mu \geq 0.7$) was reached. The test conducted in low-humidity air was deliberately stopped at 600 k cycles before failure was reached. The test conducted in a low-humidity, oxygen-free environment (dry argon gas purge) was similarly stopped at 600 k cycles before failure occurred. In the low-humidity conditions (with or without oxygen), a low stable friction dominated the test exposure where an ECoF of ~ 0.13 was maintained until the tests were stopped (this is much lower that ECoF at any stage in the test conducted in air with ambient humidity.

In Figure 4.4b, wear depths taken from averaged wear profiles on the flat and cylindrical specimens are shown; upon failure at ~ 65 k cycles, the test conducted in ambient atmosphere has worn to depths of > 50 µm on both the flat and round specimen, indicating that the DFL had been removed to its full thickness (this being 50 ± 10 µm). In low-humidity conditions, the flat and cylindrical samples have worn to depths of < 15 µm in both air and argon environments, despite the test exposures being more than nine times greater than that of the test conducted in ambient atmosphere; the small wear depths indicate that the DFL layer has not been penetrated during the test.

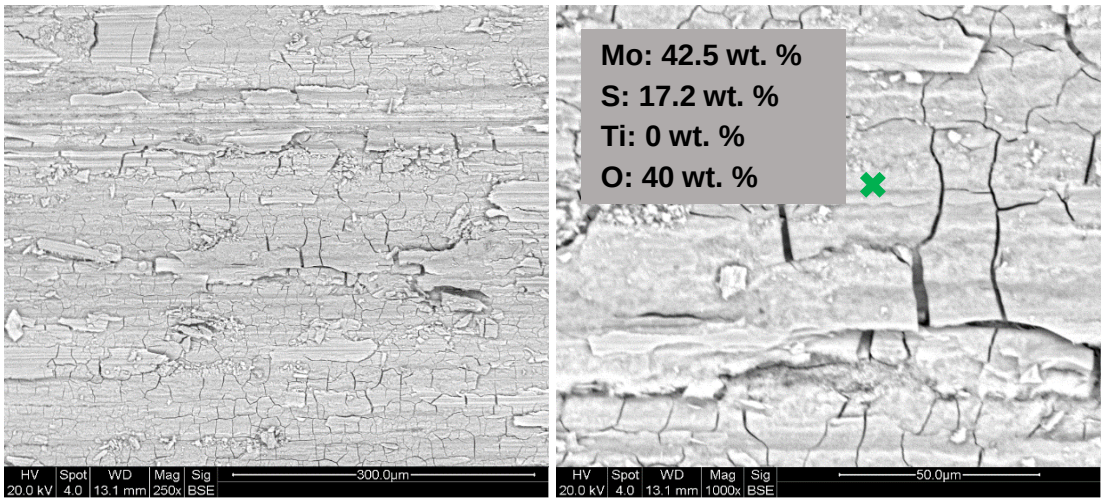


(a)



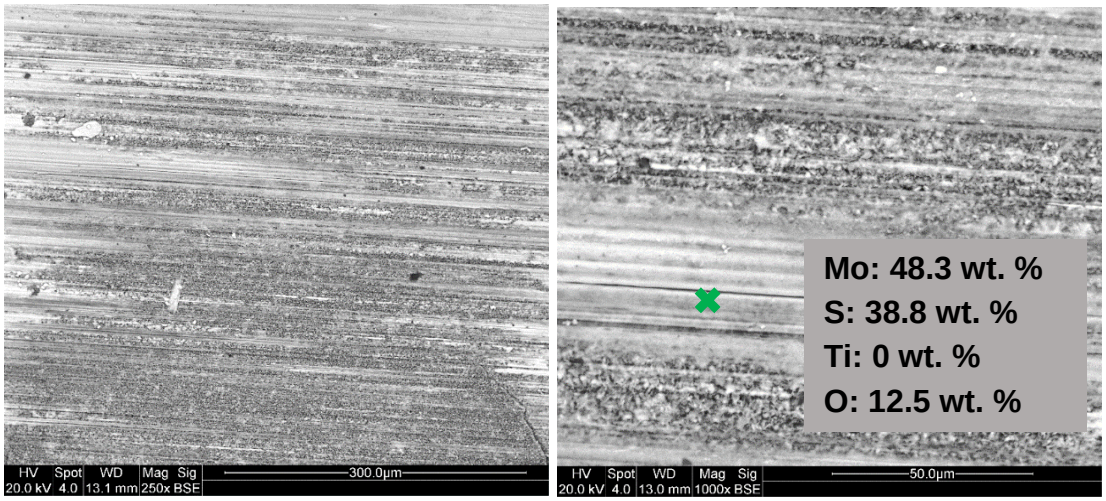
(b)

Figure 4.4 Performance of the as-received MoS_2 bonded DFL coating (Mo-DFL) in tested ambient (~ 30% RH) air and in low humidity air and argon. (a) ECoF evolution against test exposure of self-mated grit-blasted Mo-DFL coating system in different atmospheric conditions (b) The maximum depths of the averaged wear profiles taken from the wear surface upon failure for the Mo-DFL upon failure at 65 k cycles in atmospheric air and at 600 k cycles upon test interruption in different atmospheric conditions.



(a) (b)

Figure 4.5 Plan-view BSE SEM images of the flat specimen of the Mo-DFL coating in low-humidity air conditions which was interrupted at 600 k cycles (a) Low magnification image (b) High magnification image with EDX point analysis.



(a) (b)

Figure 4.6 Plan-view BSE SEM images of the flat specimen of the Mo-DFL coating in low humidity argon conditions which was interrupted at 600 k cycles (a) Low magnification image (b) High magnification image with EDX point analysis.

Plan-view BSE SEM images of the flat wear surface tested in low-humidity air (stopped at 600 k cycles) are shown in Figure 4.5 where a cracked-paved structure is present on the wear surface. EDX point analysis of this surface details a high composition of Mo (~ 42.5 wt. %), S (~ 17.2 wt. %) as well as a high oxygen content of ~ 40 wt. % with no titanium detected.

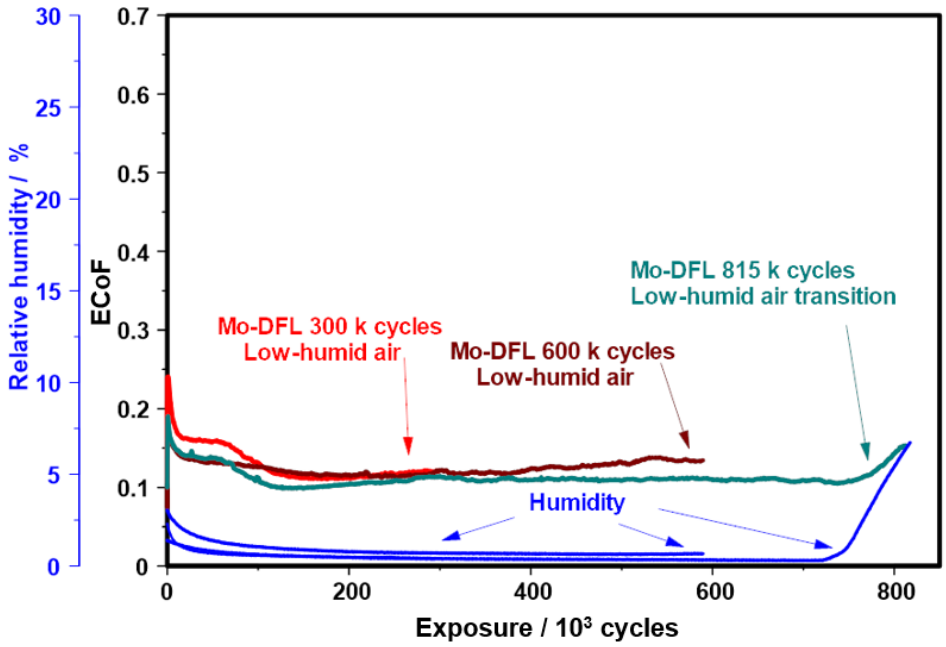
Plan-view BSE SEM images of the flat specimen wear surface tested in low-humidity argon (and stopped at 600 k cycles) are shown in Figure 4.6. Here, a very different surface appearance is evident; the cracked-paved structure seen after testing in low-humidity air condition was absent, with instead a relatively featureless surface. EDX point analysis (Figure 4.6b) indicated a relatively low oxygen content of 12.5 wt. % on the wear surface with high Mo (48.3 wt. %) and S (38.8 wt. %) content and again no evidence of titanium. It is assumed that the oxygen detected was due to reaction of the surface following testing when the samples were brought into an air atmosphere.

Results shown in Figure 4.7a detail traces of the evolution of friction against cycles alongside the recorded relative humidity for fretting tests that were conducted in low-humidity air conditions and stopped at both 300 k and 600 k cycles to assess the wear evolution of Mo-DFL coating system in low-humidity conditions and gain additional insight into the influence of humidity on the wear performance. Here, a steady-state low friction is maintained until the point of interruption. The repeatability of the fretting tests can also be observed as the friction traces of the test interrupted at 300 k cycles in the low-humidity air conditions closely follow the friction traces of the test that was interrupted at 600 k cycles also conducted in the low-humidity condition.

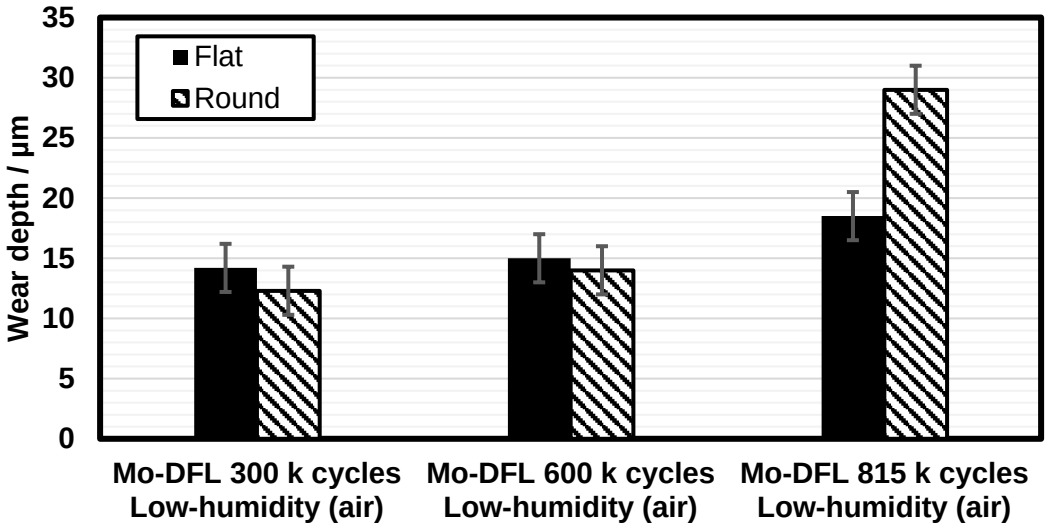
A further test was conducted where which was stopped at 815 k cycles; the dry air gas purge was maintained until 720 k cycles but then turned off whereupon the humidity increased slowly due to air exchange with the laboratory atmosphere driven by the movement of the servo-hydraulic ram. As the humidity increased from 0.5 to 6.7% (at a rate of approximately 0.6% per hour), a rise in ECoF from 0.1 to 0.15 was observed. The ECOF started to rise after ~ 765 k cycles by which time the humidity had risen to 2.5%, and it is thus proposed that this is a maximum humidity below which the low friction-low wear state can be maintained.

In Figure 4.7b, wear depths of the corresponding tests are presented, it shows that the low-humidity tests that were stopped at 300 k cycle and 600 k cycles had very similar wear depths of between 12 and 15 µm on both the flat and cylindrical specimens. In the test where the humidity had been allowed to rise, it is noted that ECoF began to rise after 765 k cycles and that the test was terminated at 815 k cycles (before failure was deemed to have taken place). Thus, it ran for only 50 k cycles at the end of the test with the elevated ECoF and yet the observed wear depths were much larger, being ~ 19 and 29 µm on the flat and cylindrical specimens respectively. In Figure 4.8, plan-view BSE SEM images of the flat

specimens from the three tests are presented. Here, a cracked paved-like structure is present in all these surfaces tested in low-humidity air (with oxygen), irrespective of duration; however, the surface following the extended tests with rising humidity shows much more surface damage (with coarser features) than the surfaces seen following the other two tests.



(a)



(b)

Figure 4.7 Performance of the as-received MoS_2 bonded DFL coating (Mo-DFL) which were interrupted and failure had not occurred at test duration intervals of 300 k cycles, 600 k cycles in low-humidity air and at 815 k cycles at low humidity to atmospheric air transition. (a) Friction evolution against cycles of fretting tests of self-mated grit-blasted Mo-DFL coating system in low-humidity air at 300 k cycles, 600 k cycles and 815 k cycles (in low-humidity to atmospheric transition) (b) The maximum depths of the averaged wear profiles taken from the wear surface upon interruption at 300 k cycles, 600 k cycles in low-humidity air and at 815 k cycles in low humidity to atmospheric humidity transition

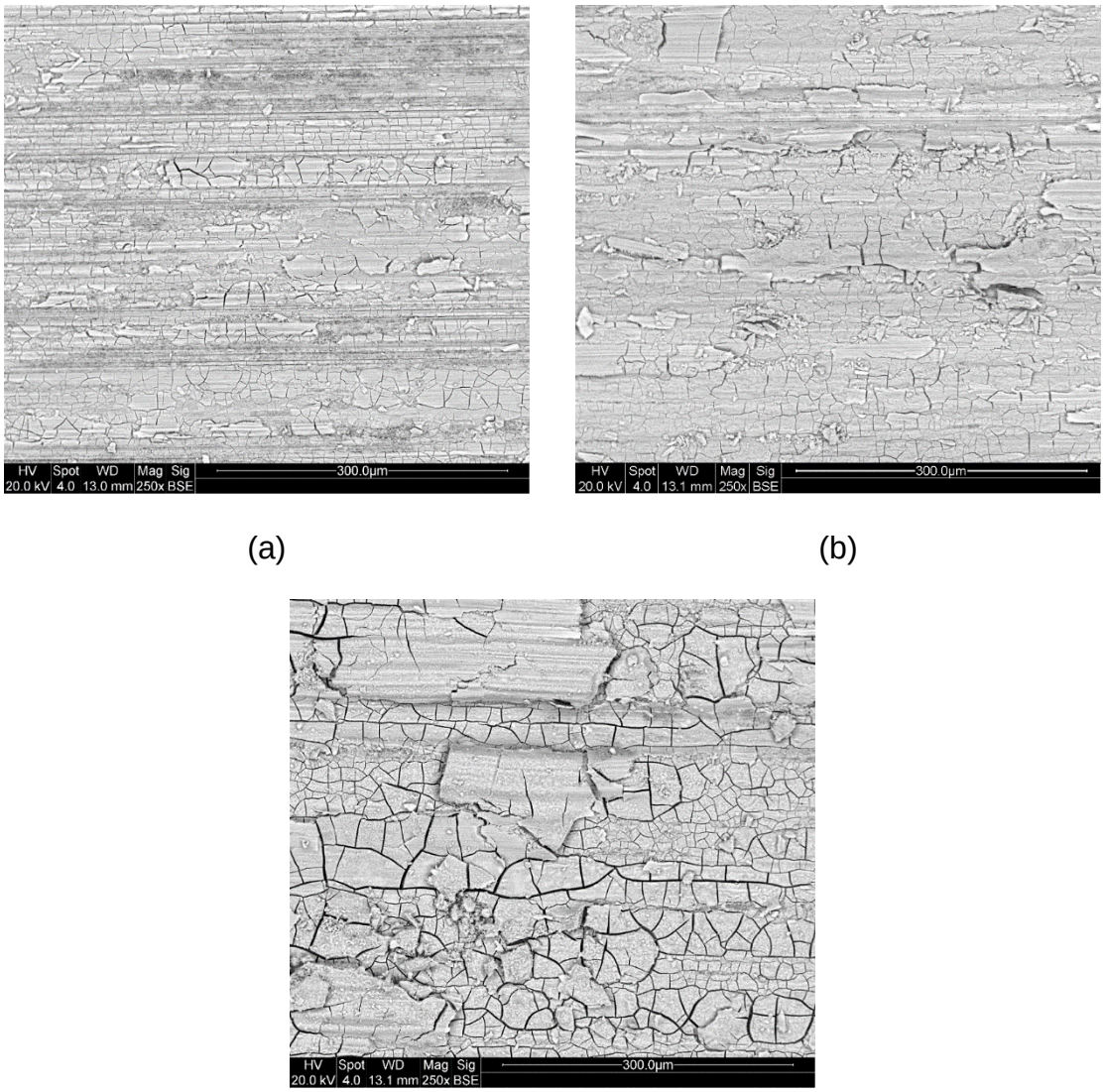


Figure 4.8 Plan-view BSE SEM images of flat specimen of Mo-DFL low-humidity air tests interrupted at various test duration intervals. (a) 300 k cycles (b) 600 k cycles (c) 815 k cycles which was terminated after a period of continuously increasing humidity had been imposed

In light of these observations, a test was conducted where the first 416 k cycles were performed in low humidity air (dry air gas purge), whereupon the gas purge was turned off and the humidity was rapidly raised to that of ambient laboratory air (~38%) by opening the environmental chamber to the air. As can be seen in Figure 4.9, a sharp rise is relative humidity occurred (blue line) which directly correlated with a sharp rise in friction coefficient from 0.1 to 0.38 (orange line). It is also noted that upon the exposure of the surface which had been tested in low humidity condition to the higher ambient humidity (~38%), the ensuing fretting wear

behaviour closely emulates the wear behaviour of a sample which had been tested in that ambient environment from the start (also included as the red line in Figure 4.9 for comparison). Specifically, it is noted that the three wear stages are observed in both tests once they are exposed to humid air. For the sample initially tested for 416 k cycles in dry air and then exposed to humid air, failure occurred after 483 k cycles. The period in humid air was therefore 67 k cycles, and it is noted that this was very similar to the failure lifetime of the sample tested in humid air alone (65 k cycles), suggesting that the damage incurred by the DFL during fretting in very low humidity was almost negligible and again, demonstrating the repeatability of the test in atmospheric humidity conditions.

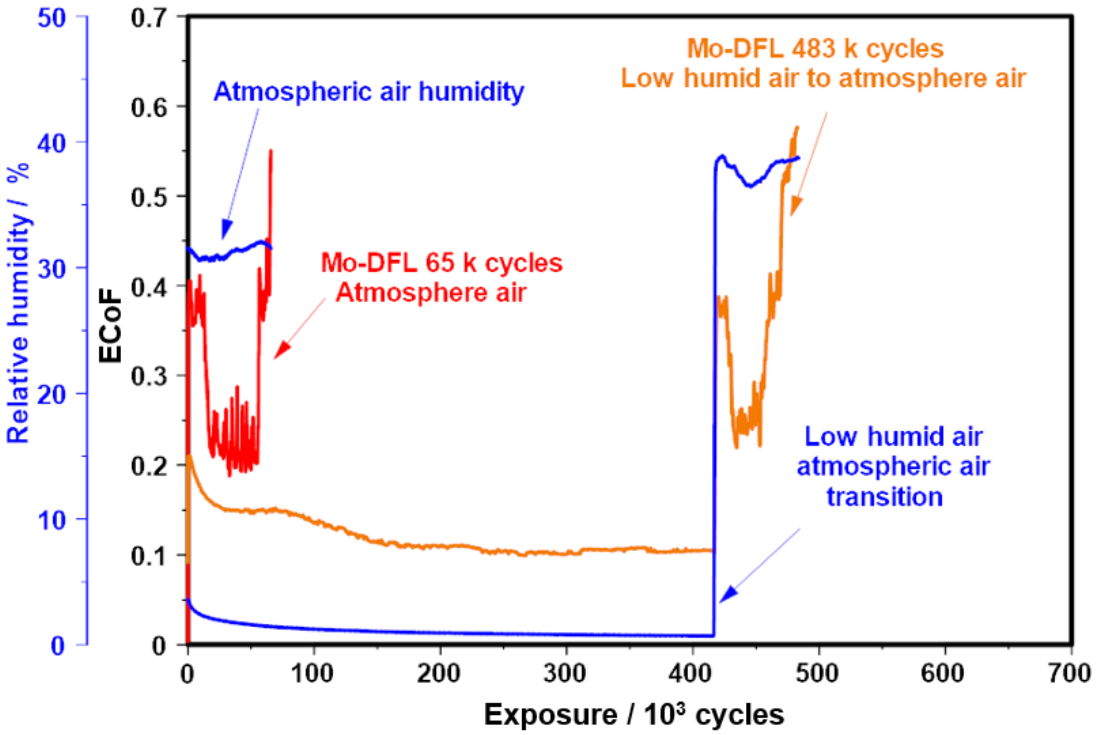


Figure 4.9 Friction evolution against cycles showing fretting tests of self-mated grit-blasted Mo-DFL coating tests in atmospheric air conditions and a test initially conducted in low-humidity air and transitioned to atmospheric air condition.

4.3 Polymer-bonded MoS_2-based DFL (Mo-DFL) in high-humidity environments

Fretting wear behaviour in atmospheric, low-humidity air and low-humidity argon conditions have been shown in Figure 4.4 where the water content in the environment can be seen to have considerable effects on the friction and wear durability of the polymer-bonded MoS_2-based DFL (Mo-DFL) coated fretting system. To gain additional insight into how the increase of humidity in the surrounding environment further influences the wear behaviour of the Mo-DFL fretting system, tests were conducted with increased humidity levels of 60 – 75 %. Increased humidity conditions in both oxygen-containing and oxygen-free environments were established by passing the compressed dry air or dry argon gas flow through a water bubbler system before directing the mixture into the rig environmental chamber. In Figure 4.10, the evolution of ECoF in fretting tests in ambient laboratory air and in high humidity air and argon are presented. In ambient atmosphere (~ 25 – 40 % RH), a fretting lifetime of 65 k cycles was observed before failure ($\mu \geq 0.7$). As noted previously, the three distinct stages of wear were observed in this system [225], whereby, stages; I, II and III are ascribed to the initial high friction phase followed by a low friction period and finally rising friction to failure.

By increasing the humidity levels to 60 – 75 % in air, similar fretting wear behaviour was observed, with the three stages again being observed, but with a reduced lifetime of 44 k cycles (Figure 4.10). Most notably, the low friction phase (Stage II) when ECoF drops to ~ 0.25 exhibits a considerably shorter duration of only ~ 8 k cycles compared to the 40 k cycles observed in ambient atmospheric conditions.

A very different evolution of ECoF is observed in high humidity (60 – 75 % RH) argon with the low friction steady state phase (Stage II) previously observed in ambient atmosphere and high humidity air being absent. In this test, an initial increase of friction from ~ 0.24 to ~ 0.43 takes place which is then maintained for the majority of the fretting test until failure is reached at 54 k cycles.

To examine the development of wear occurring in ambient atmospheric air and high-humidity argon environments, additional tests, as shown in Figure 4.11a, were conducted which were interrupted before the failure; specifically, these were interrupted at 23 k cycles (during the low-friction Stage II phase) in the test in

ambient air and at 27 k cycles in the test in high-humidity argon when ECoF was 0.4.

Wear depths (taken from the averaged wear profiles) of the resulting flat and cylindrical wear samples following interruption can be observed in Figure 4.11b. In all cases, the wear depths were greater than 40 µm, with the wear on the cylinder in the ambient air test being just about 50 µm. These depths indicate that the majority of the ~ 50 µm thick DFL had been penetrated by the time the tests were interrupted, despite the interruption point being around a third and a half of the total lifetime for the ambient atmosphere test and high humidity argon test respectively.

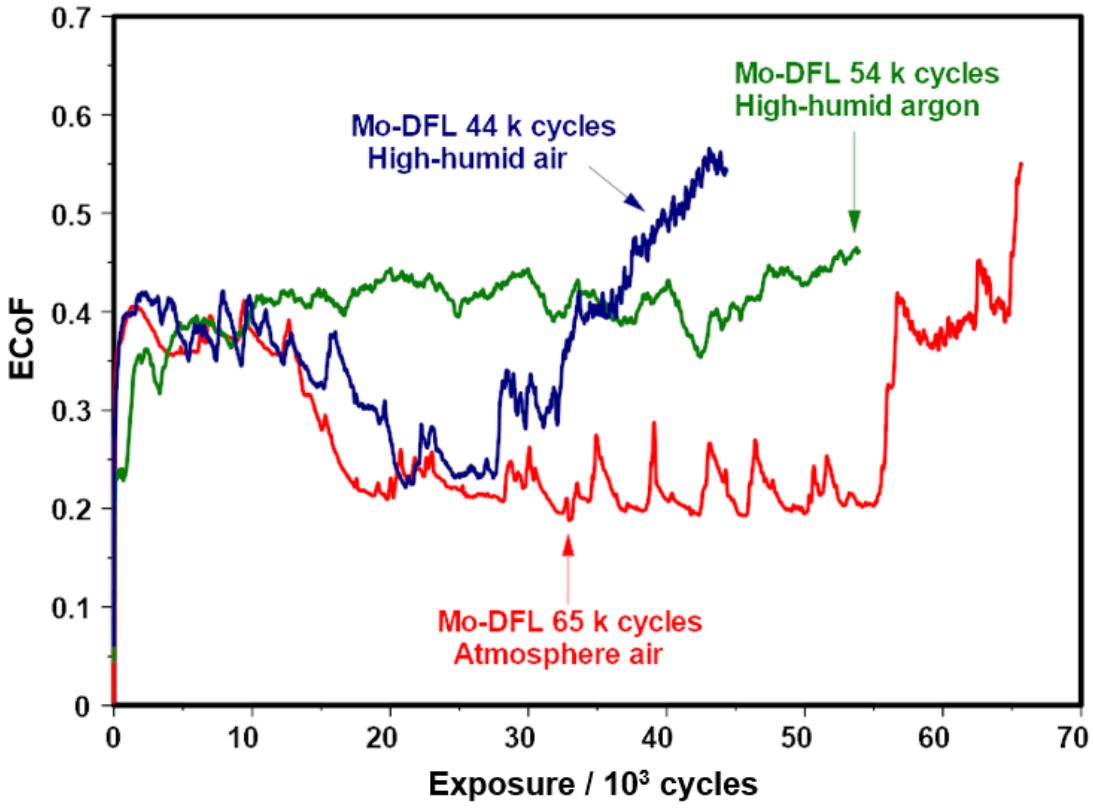
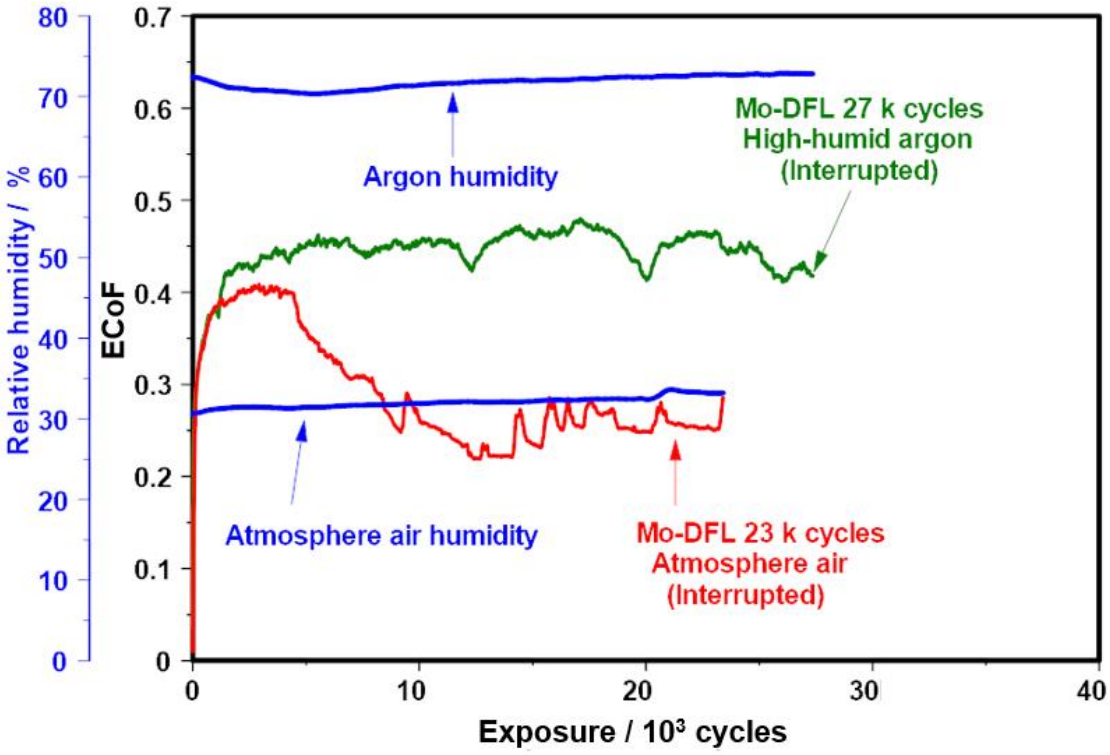
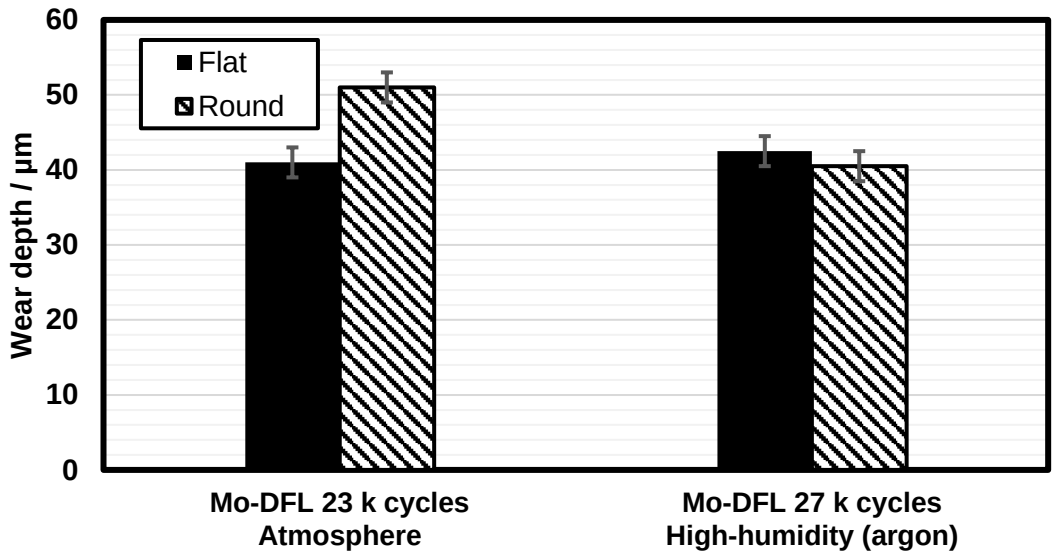


Figure 4.10 Friction evolution against cycles showing fretting tests of self-mated grit-blasted Mo-DFL coating in atmospheric air, high-humidity air and high-humidity argon conditions.



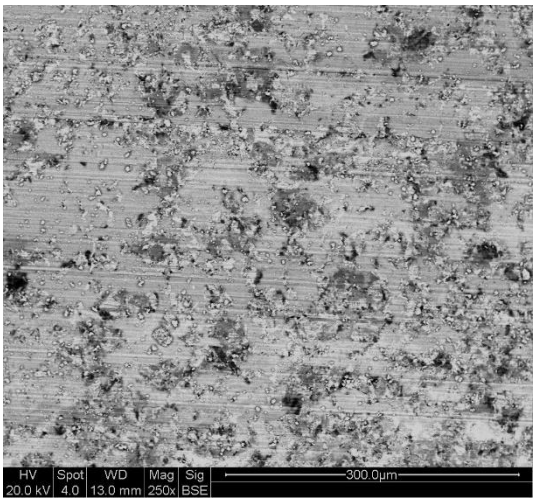
(a)



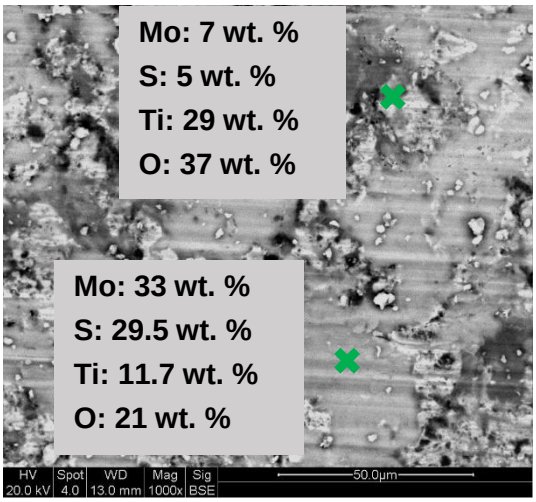
(b)

Figure 4.11 (a) Interrupted friction evolution against cycles of fretting tests of self-mated grit-blasted Mo-DFL coating in atmospheric air which was stopped at 23 k cycles and high-humidity argon environment stopped at 27 k cycles before the point (b) Wear depths of corresponding interrupted tests.

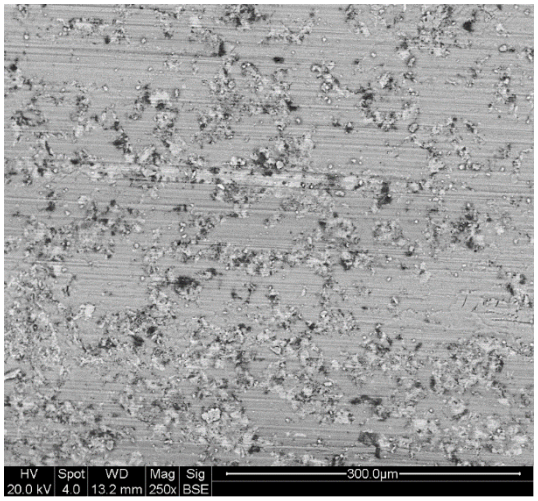
In Figure 4.12, plan-view BSE SEM images of the flat specimens tested in atmospheric air (Figure 4.12 a and b) and high-humidity argon (Figure 4.12 c and d) which were stopped before their failure point (at 23 k cycles and 27 k cycles respectively) are shown. The micrographs along with the EDX point analyses show different phases on the wear surfaces on both of the tests. There are regions rich in Mo and S (indicating that the DFL remains here) and rich in titanium from the underlying alloy substrate, indicating that the DFL has been removed in places. A high oxygen content was found to be present in all cases. Perhaps most notably, the cracked-paved like appearance of the worn surfaces observed in the low humidity conditions (see Figure 4.5) is not observed here at all, indicating a different mechanism of material degradation operates in the two cases.



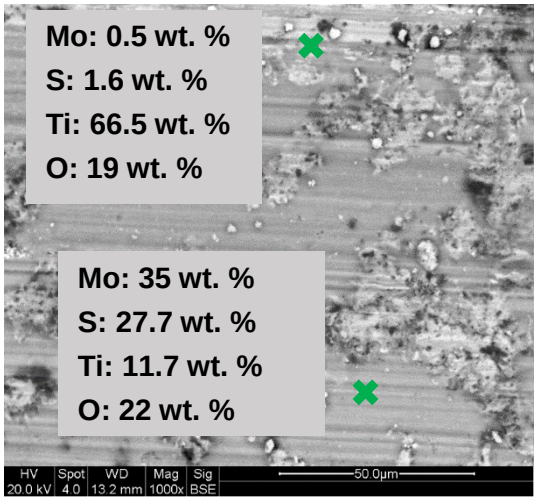
(a)



(b)



(c)



(d)

Figure 4.12 Plan-view BSE SEM images of flat specimen of interrupted Mo-DFL tests. (a) Low magnification of interrupted atmospheric air test (b) high magnification and EDX point analysis of interrupted atmospheric air test stopped at 23 k cycles. (c) Low magnification of interrupted high-humidity argon test (d) High magnification and EDX point analysis on interrupted high-humidity argon test stopped at 27 k cycles.

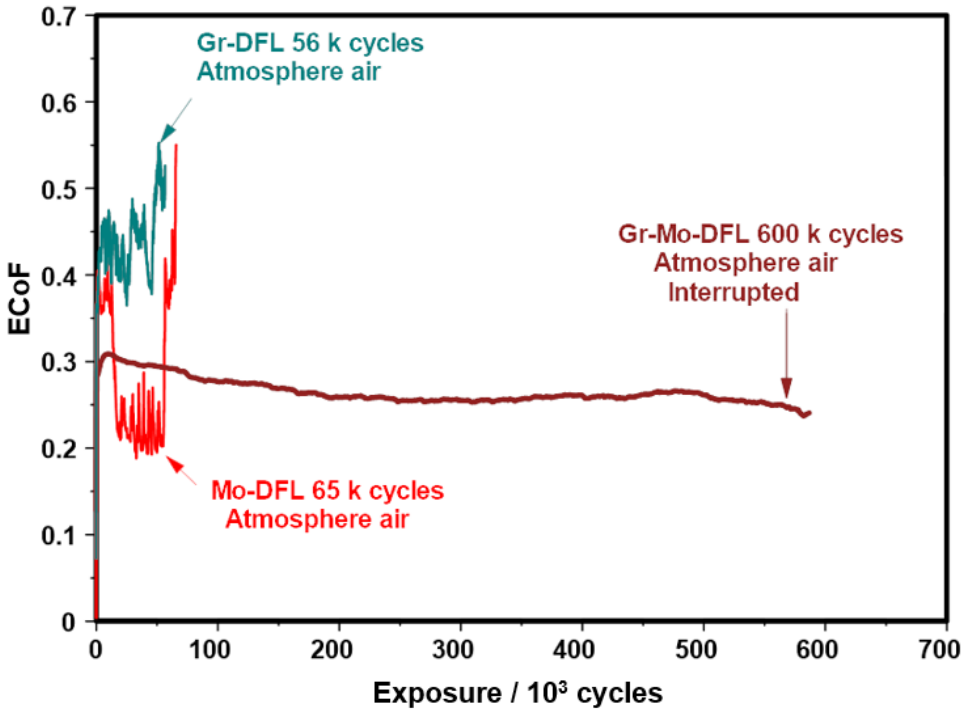
4.4 Graphite-based DFL (Gr-DFL) and graphite-modified MoS_2-based DFL (Gr-Mo-DFL) in high humidity environments

In ambient (25 – 40 % RH) and high-humidity (60 – 75 % RH) conditions, the Mo-DFL coating system has been observed to have reduced fretting lifetimes and durability in both air and argon environments compared to the very long lifetimes observed in low humidity environments. It is recognised that different lubricating phases (MoS_2 and graphite) behave differently in different atmospheric conditions, and so this work is extended to the Gr-Mo-DFL and Gr-DFL systems in the regime where the Mo-DFL exhibits limited lifetime (i.e. above 2.5% RH).

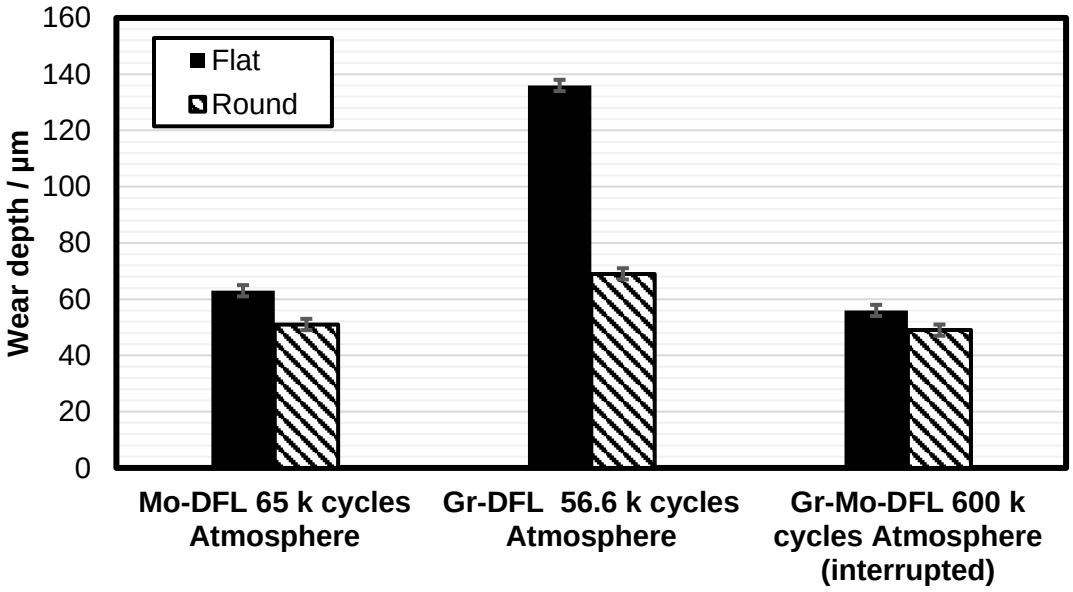
In Figure 4.13a, the evolution of friction of Mo-DFL, Gr-DFL and Gr-Mo-DFL in atmospheric conditions can be observed. Here, it is evident that different fretting wear behaviours are exhibited. As previously noted, the Mo-DFL exhibits three stages of wear (Stages I, II and III) with eventual failure of the coating at 65 k cycles. Like the Mo-DFL, the lifetime of the Gr-DFL system is fairly short (~ 57 k cycles) and ECoF does not display a low friction Stage II (as was observed for the Mo-DFL); instead, ECOF remains above ~ 0.4 for the majority of the test. In contrast to both of these, the Gr-Mo-DFL exhibits a steady state low friction for the entire duration of the test to which ECoF was maintained between 0.25 and 0.3 prior to the test being stopped at 600 k cycles (interrupted before failure).

The corresponding wear depths of Mo-DFL, Gr-DFL and Gr-Mo-DFL coating systems can be observed in Figure 4.13b. For the Mo-DFL and the Gr-Mo-DFL, the wear depth is very similar to the original thickness of the DFL; in the case of the Mo-DFL, this is linked to the failure of the system whilst in the case of the Gr-Mo-DFL, it is noted that the test was interrupted before failure occurred. However, the wear depths in the Gr-DFL system at failure (136 and 69 µm on the flat and cylindrical specimens respectively) is much higher than the original DFL thickness, indicating that significant substrate removal has occurred before the failure criterion (μ) > 0.7) was reached.

.



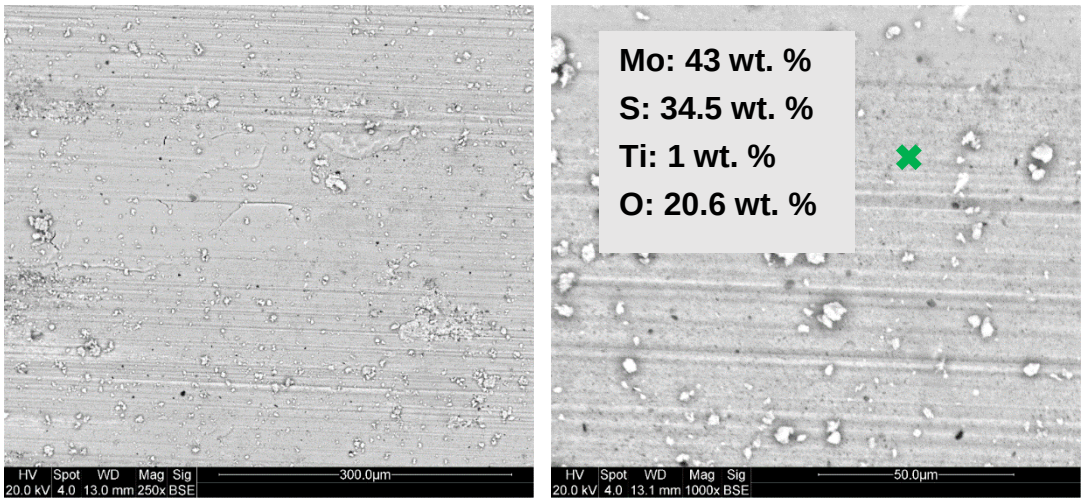
(a)



(b)

Figure 4.13 Performance of the MoS_2 bonded DFL coating (Mo-DFL), graphite bonded DFL coating (Gr-DFL) and graphite modified MoS_2 bonded DFL coating (Gr-Mo-DFL) which was interrupted at 600 k cycles in atmospheric air environment (a) Friction evolution against cycles of fretting tests (b) Wear depths of the corresponding tests.

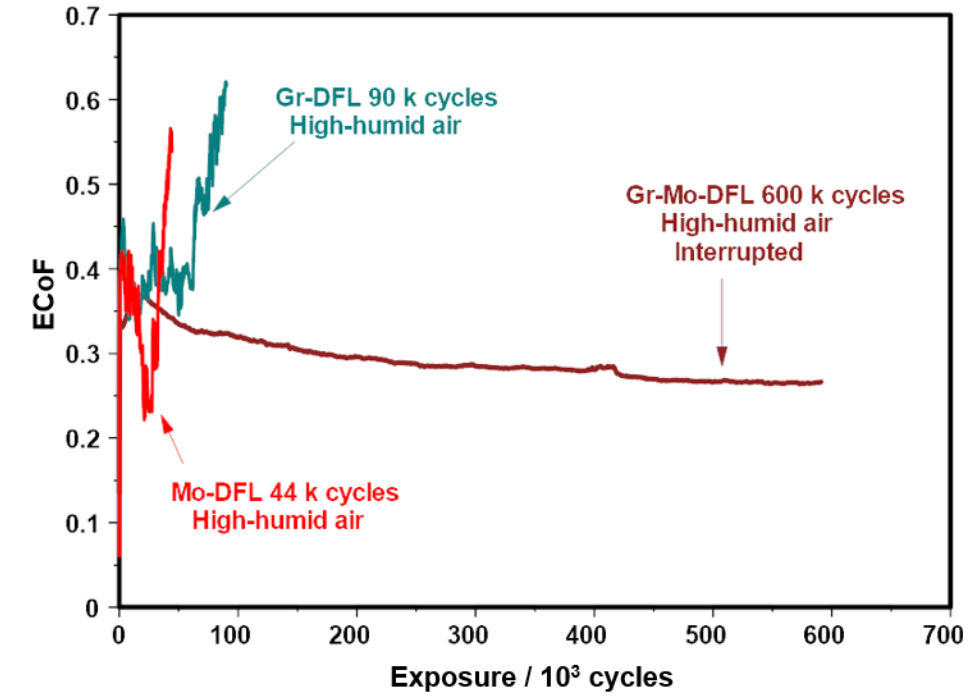
SEM images of the active low friction surface of the Gr-Mo-DFL coating system in atmospheric condition which was interrupted at 600 k cycles (before failure) are presented in Figure 4.14. A very smooth surface morphology is observed with some evidence of scoring being present. EDX point analysis on the wear surface found high Mo (43 wt, %), S (34.5 wt. %) and O (20.6 wt. %) contents on the surface with only a very small fraction of Ti (1.2 wt. %); whilst the wear depth indicates that most of the DFL had been removed by this point, the small Ti EDX signal indicates that the coating does remain intact at this point. The Mo:S ratio of 1.25:1 is slightly lower than that expected for MoS_2 (1.5:1) providing evidence that wear has not resulted in a surface layer rich in molybdenum oxide (where the Mo:S ratio would be expected to be larger).



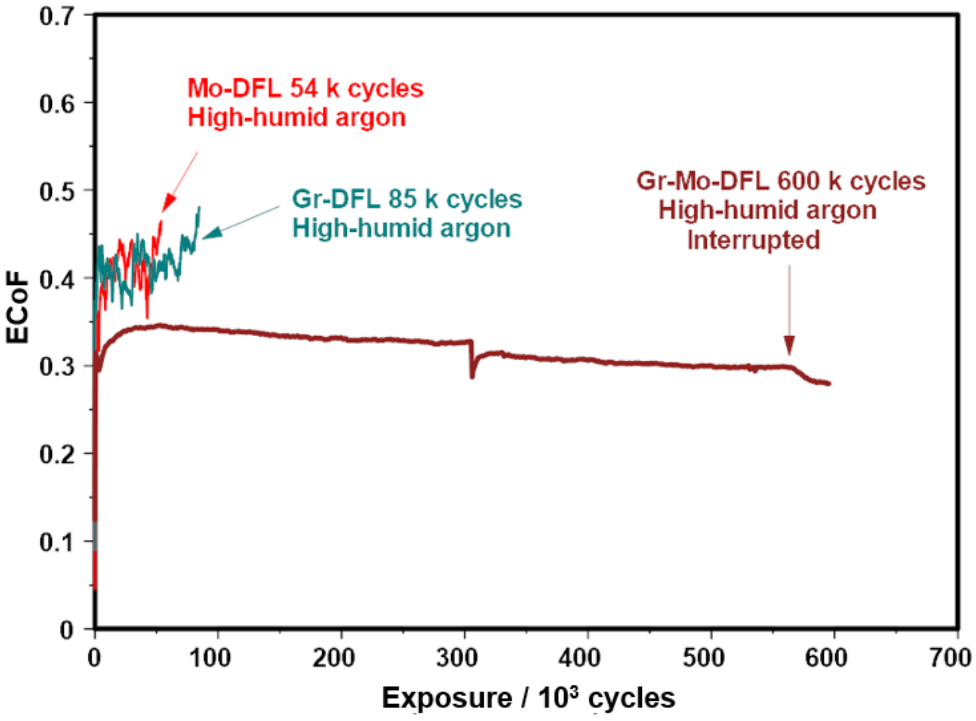
(a) (b)

Figure 4.14 Plan-view BSE SEM images of the flat specimen of the Gr-Mo-DFL coating atmospheric air condition which was interrupted at 600 k cycles (a) Low magnification image (b) High magnification image with EDX point analysis.

The evolution of ECoF in fretting tests for the three coatings (Mo-DFL, Gr-DFL and Gr-Mo-DFL) in both high humidity air and high humidity argon environments are presented in Figure 4.15a and Figure 4.15b respectively. In both conditions, the Gr-Mo-DFL exhibited an extended lifetime (neither had failed when the tests were interrupted at 600 k cycles) with ECoF around 0.3; however, the Mo-DFL and the Gr-DFL failed in both conditions with lifetimes of less than 100 k cycles. It should be noted that there is a marginal increase in lifetime for the graphite-based DFL coating (Gr-DFL) in the high-humidity air (90 k cycles) and high-humidity argon (85 k cycles) when compared to the fretting lifetime (56 k cycles) in atmospheric air conditions.



(a)



(b)

Figure 4.15 Performance of the MoS_2 bonded DFL coating (Mo-DFL), graphite bonded DFL coating (Gr-DFL) and graphite modified MoS_2 bonded DFL coating (Gr-Mo-DFL) which was interrupted at 600 k cycles in high-humidity air environment (a) Friction evolution against cycles of fretting tests (b) Wear depths of the corresponding tests.

4.5 Discussion

4.5.1 Effect of humidity on polymer-bonded MoS_2-based DFL (Mo-DFL) in air and argon environments

The evolution of friction of Mo-DFL in low-humidity conditions (0.5 – 3 % RH) and system durability as observed in Figure 4.4a indicate that very different wear mechanisms operate when compared to ambient atmospheric air conditions (25 – 40 % RH). A steady state low friction phase was maintained at an ECoF ~ 0.13 in low-humidity conditions (in both air and argon environments) until the tests were deliberately stopped at 600 k cycles. In ambient atmospheric air (25 - 40 % RH), a dynamic wear behaviour was initiated whereby three distinct wear stages of MoS_2 wear [151], [225] occurred before the coating failed at 65 k cycles. These results are in accord with those observed in literature with the majority of studies maintaining the narrative that MoS_2 has low friction and low wear characteristics in low-humidity conditions [142], [143], [152], [154], [159], [237].

The driving wear mechanism that spurs this humidity-dependent behaviour of MoS_2 however remains a point of contention in literature where two main mechanisms have been proposed [152]. This includes the tribo-oxidative degradation of the MoS_2 to MoO_3 in a moist environment as a product of oxidation to disrupt the shear properties of the MoS_2 lubricant film, causing an increase of friction coefficient and high wear rates [156]–[159]. This disrupts the basal layer during sliding and limits the effectiveness and lifetime of MoS_2 as a solid lubricant [164], [165]. The second proposed mechanism is physisorption which entails the adsorption and physical bonding of water molecules to the edge sites which increases the adhesion forces between the sliding interfaces and disrupts the easy lamellar shear [170], [171], [176]. In this work, the effects of oxygen in low-humidity conditions have been observed to be marginal in regards to the influence of friction, wear durability and lifetime of the Mo-DFL coating. As shown in Figure 4.4a, a steady state low friction and low wear phase is preserved for the duration of the tests (before the tests were deliberately stopped at 600 k cycles) in low-humidity air and in low-humidity argon environments. The low friction and low wear capabilities of Mo-DFL are evident irrespective of the oxygen content in the environment. This leads to the conclusion that it is the water content in the environment and not the oxygen which is the driving factor behind the friction and

wear behaviours of the MoS_2-based lubricant coating which is in agreement with previous studies [168], [169], [171], [175].

Although oxygen has been shown not to affect the low friction and low wear capabilities of the Mo-DFL coating system in low-humidity conditions (Figure 4.4), it is clear that oxygen does have an effect on the wear surface chemistry and subsequently, the tribo-oxidative mechanism as seen when analysing the plan-view BSE-SEM images of the flat wear specimen tested in low-humidity air environment (Figure 4.5) which shows a cracked-paved structure at the surface interface. On the surface of the test conducted in low-humidity argon (Figure 4.6), the cracked-paved structure was absent. The gravimetric ratio of Mo:S in MoS_2 is 1.5:1. After testing in dry argon, the ratio at the surface is 1.25:1 whereas after testing in dry oxygen, it is 2.47:1. This increased ratio of Mo:S along with the high oxygen content (Figure 4.5b) suggests that the surface is composed of molybdenum oxide when tested in dry air, which indicates that whilst the extended low friction and low wear characteristics of Mo-DFL are not affected by oxygen in low humidity conditions, different tribo-chemical interactions are apparent.

Further evidence of the sensitivity of Mo-DFL to moisture is presented in Figure 4.7a where fretting tests conducted in low-humidity air conditions until the point of interruption at testing durations of 300 k cycles and 600 k cycles maintain a steady state low friction phase (ECoF ~ 0.13) and low wear depths < 15 µm (Figure 4.7b). Low-humidity air conditions were maintained until 720 k cycles whereupon the dry air gas purge into the environmental chamber was stopped and the humidity increased from 0.5 to 6.7% (at a rate of approximately 0.6 % / hour). ECoF was observed to also rise from 0.1 to 0.15 and the wear depth had increased to ~ 19 and 29 µm on the flat and cylindrical specimens respectively upon interruption at 815 k cycles. An additional test was conducted where the first 416 k cycles were performed in low-humidity air with the environment then being changed to ambient laboratory air (~38%) by opening the environmental chamber to the air as seen in Figure 4.9. This resulted in a rapid rise of ECoF from 0.1 to 0.38 with the following progress of friction and wear closely following that in a fretting test that had only been conducted in an ambient atmospheric air environment (Figure 4.9), approximately 67 k cycles after the low-humidity air test was exposed to the ambient air which is also a similar lifetime to a test solely conducted in ambient atmospheric air which failed at 65 k cycles. This indicates that, prior to ambient air exposure, limited damage had occurred on the Mo-DFL coating system and it is only after air with increased humidity was introduced to the system that the progression of fretting wear damage resumes.

The demonstrated sensitivity and the observed behaviours of the Mo-DFL in low and high humidity conditions (with and without the presence of oxygen) suggests a water driven physisorption as proposed in previous studies [148], [168], [176], [179], is likely to be a driving factor which causes increased friction, increased wear and degradation of the polymer-bonded MoS_2-based DFL coating and not an effect of oxygen.

As observed in Figure 4.10, further increasing the humidity from ambient atmospheric air (25 – 40 % RH) to high-humidity air (60 - 75 % RH) led to further reduction in the overall fretting lifetimes from 65 k cycles to 44 k cycles respectively. Although, similar fretting wear behaviours were still maintained, the increase of humidity led to a shorter duration of the low friction (Stage II [225]) phase (~ 8 k cycles) when compared to the extended low friction duration of ~ 40 k cycles observed in ambient atmospheric air. This suggests that increasing humidity in the Mo-DFL coating system further limits the overall lifetime and the sustainment of a low friction phase.

In high-humidity argon environment a different wear mechanism was perceived to be active where the low friction phase (Stage II) was absent from the evolution of friction as was observed in the ambient and high humidity air (Figure 4.10a). To chart the friction evolution and the physical wear evolution of the Mo-DFL coating occurring at the contacting surfaces during the fretting wear tests, interrupted tests before failure were conducted in ambient atmospheric air conditions which was stopped during the low friction phase (Stage II) at 23 k cycles (at an ECoF ~ 0.25), and, in high-humidity argon environment which was stopped at 27 k cycles (at an ECoF ~ 0.4) as shown in Figure 4.11a.

The diverging paths of the evolution of friction in atmosphere air and high-humidity argon conditions can be observed as well as the comparable wear depths presented in Figure 4.11b which suggests similar progression of wear was occurring in the two different environments, despite the differences in evolution of friction traces shown (Figure 4.11). Further evidence of the comparable wear evolution is presented through plan-view SEM micrographs of the interrupted flat specimens of tests conducted in atmospheric air (terminated at 23 k cycles) shown in Figure 4.12a & b and in high-humidity argon (terminated at 27 k cycles) shown in Figure 4.12c & d. Regions of molybdenum and titanium were observed at the wear interfaces (as confirmed by EDX point analysis) on both fretting wear scars indicates that although differing evolutions of friction are active in the two different environments, the physical wear process of the Mo-DFL coating in both

environments are comparable. However, the differences in evolution of friction (in particular, the absence of Stage II in the test conducted in argon) indicate that oxygen plays a role in enabling the low friction phase (Stage II) within the wear process of the polymer-bonded MoS_2-based coating system in higher humidity environments; however, the mechanism behind this difference remains unclear at the present time.

In this work, different types of Mo-DFL low friction behaviours have been identified. Firstly, an extended, steady state low friction (< ~ 0.15) is exhibited in low-humidity conditions (0.5 – 3 % RH) which is active throughout the thickness of the bulk DFL coating thickness (Figure 4.7) which generates a cracked-paved oxygen-rich interface in air (oxygen containing) environment (Figure 4.5); however, it is also observed in oxygen-free dry environments, although the oxygen-rich interface is not observed in this case. The second type of low friction behaviour (> ~ 0.2) is observed only when the Mo-DFL was worn so that the surfaces in contact are made up of a mixture of Mo-DFL and titanium (Stage II [225]); this type of low friction behaviour is only observed in air conditions (i.e. not in argon) as observed in Figure 4.11a and Figure 4.12a & b.

4.5.2 Effect of ambient and high-humidity on graphite-based DFL (Gr-DFL) and graphite-modified MoS_2-based DFL (Gr-Mo-DFL) in air and argon environments.

The graphite modified MoS_2-based DFL (Gr-Mo-DFL) far exceeded (> 10 fold) the durability of both the graphite-based DFL (Gr-DFL) and MoS_2-based (Mo-DFL) coating systems in ambient atmospheric air (Figure 4.13a), high-humidity air (Figure 4.15a) and at high-humidity argon (Figure 4.15b) conditions. The Gr-Mo-DFL coating system maintained a stable, but relatively high, ECoF of ~ 0.25 - 0.3 until the tests were terminated at 600 k cycles in all conditions tested. The worn surfaces in interrupted tests were also very different; for the Mo-DFL, a roughened surface with indentations suggesting pull-out was evident (Figure 4.12a and b) whereas for the Gr-Mo-DFL, the worn surface of the DFL was relatively smooth with some fine scoring evident, indicative of abrasion (Figure 4.14). The poor performance exhibited by the graphite-based DFL (Gr-DFL) and MoS_2-based DFL (Mo-DFL) in ambient humidity and above suggests that the synergistic behaviour of the combined MoS_2 + graphite is what enables the continued low friction and wear capabilities at the fretting interface in atmospheric air and high-humidity

environments. However, given that the Gr-Mo-DFL was made by addition of graphite to an already existing DFL system, it is recognised that the enhanced performance of Gr-Mo-DFL may also be an effect of the increased volume fraction of lubricating phases within the DFL paint matrix rather than the specific mixture of MoS_2 + graphite. The commercially available DFLs do not provide information with regard to the fraction of components in the DFL, and so to resolve this, further work would be required with pure and mixed DFLs being constructed from basic components.

The extended stable friction phase (ECoF ~ 0.25 - 0.3) of the Gr-Mo-DFL coating system is markedly different from the extended low friction phase observed in the low-humidity condition for the Mo-DFL coating which maintained an approximate ECoF of 0.13 for the testing duration as observed in Figure 4.4a and Figure 4.7a. For the graphite modified Gr-Mo-DFL coating system tested in ambient atmospheric air, corresponding wear depths (Figure 4.13b) at 600 k cycles were very similar to the original thickness of the DFL ~ 50 µm for both the flat and round specimen; however, for the Mo-DFL system in low-humidity air (Figure 4.4b), the wear depth was less than 15 µm. Moreover, the worn surfaces exhibited very different morphologies too; the worn surface of the Mo-DFL in low humidity conditions exhibited a cracked-paved morphology (associated with formation of an oxide of molybdenum) (Figure 4.5) whereas the worn surface of the Gr-Mo-DFL was relatively smooth with some fine scoring evident, indicative of abrasion (Figure 4.14). All these evidence together suggest that there are distinct differences in the way that the surface slide (and the coefficient of friction associated with that sliding) and in the mechanism by which wear takes place.

Mo-DFL exhibited a three stage ECoF development in ambient and high-humidity air while graphite-based Gr-DFL coating maintains an ECoF of ~ 0.4 with no distinct low friction phases until failure occurred (Figure 4.13a and Figure 4.15a) which indicates that different mechanisms are driving the behaviours of the individual DFLs. It is also noted that with increased humidity, the fretting lifetime of Gr-DFL marginally increased also from 56 k cycles in ambient atmospheric air (25 – 40 % RH) to 90 k cycles in high-humidity air and 85 k cycles in high-humidity argon (60 – 75 % RH). The tendency of graphite to display increased performance in higher humidity conditions has been observed in previous works [185] however, only the lifetime is shown to have increased while high friction is maintained in the current work.

4.6 Conclusion

In this chapter, the effects of humidity and oxygen on the tribological performance of the polymer-bonded (Mo-DFL) was examined to better understand the mechanisms that drive fretting wear behaviours in low-humidity air and argon environments, ambient atmospheric air and high-humidity air and argon conditions. Additional fretting wear tests were performed on a graphite-based DFL (Gr-DFL) and a graphite modified MoS_2-based DFL (Gr-Mo-DFL) in atmospheric ambient air and high-humidity conditions. The following conclusions could be made:

- In low-humidity conditions, (0.5 – 3 % RH) a steady-state low friction and low wear phase is active and maintained for the entire fretting duration until tests were stopped at 600 k cycles (approximately x10 the lifetime attained in atmospheric ambient air).
- Minimal damage was incurred on the ~ 50 µm thick DFL during fretting in very low humidity conditions (both air and argon) even with an extended lifetime period of 600 k cycles.
- The Mo-DFL coating was observed to be highly sensitive to the water content in the environment. With the exposure to ambient atmospheric humidity, the wear progression follows three distinct wear stages; a rapid increase of ECoF, followed by a short-lived low friction phase which is different to the low friction phase experienced in low-humidity conditions before the onset of coating failure.
- Oxygen was observed to not affect the low friction and low wear capabilities in low-humidity conditions however, a cracked-paved interface is formed on the top surface on the Mo-DFL coating in low-humidity air but not in low-humidity argon. Lower oxygen content was recorded on the surface sample of tests conducted in low-humidity argon environment which suggests different tribo-chemical interactions occur at the interface.
- In atmospheric and high-humidity conditions, oxygen appears to contribute to the formation of a low friction phase (Stage II) within the evolution of friction of Mo-DFL.
- Graphite modified MoS_2-based Gr-Mo-DFL exceeded the performance of both graphite-based (Gr-DFL) and MoS_2-based (Mo-DFL) coating systems in ambient and high-humidity environments and provided an extended stable friction phase with ECoF ~ 0.25 – 0.3; wear occurred throughout this at a rate much higher than that observed in low humidity conditions.

Chapter 5. Lifetime of MoS_2-based DFL systems in fretting with and without a Cu-Ni-In under-layer: the dependence on the topography of the surface onto which the DFL is deposited

5.1 Background

In Chapter 4, self-mated grit-blasted Ti-4Al-4V testing samples were utilised to test the fretting wear behaviour of a polymer-bonded MoS_2-based (Mo-DFL) coating system in different humidity and oxygen environments. The lifetime of the Mo-DFL coating was significantly extended in low humidity conditions and failed in ambient and high-humidity conditions. To further understand the conditions and wear mechanisms that facilitate the extension of fretting lifetimes of the Mo-DFL coating, this section investigates how the surface conditions onto which the polymer bonded Mo-DFL coating is deposited affect the lifetime and durability of the coating system.

Current industrial practice utilises a thermally-sprayed Cu-Ni-In under-layer on the fan blade root which is followed by the deposition of a bonded MoS_2-based DFL coating. The Cu-Ni-In under-layer changes both the material and the topography of the surface onto which the DFL is applied (when compared to the DFL being applied directly to a suitably prepared Ti-6Al-4V surface). The mechanism of how the DFL/Cu-Ni-In interface improves fretting performance is investigated. Fretting wear tests were conducted in ambient atmospheric air conditions (~ 25 – 40 % RH).

There is a need to understand the dominant mechanisms behind the extended lifetimes that are observed when thermally sprayed Cu-Ni-In is employed as an under-layer in the application of a DFL to a Ti-6Al-4V component. It is noted that there are many differences between a thermally sprayed Cu-Ni-In surface and a prepared Ti-6Al-4V surface for deposition of a DFL, with these being broadly categorised as (i) differences in topography (roughness); (ii) differences in the nature of the materials (such as chemical affinity for the DFL, hardness and Young's modulus etc.). To identify the dominant causal mechanism, the aim of this work is to isolate the separate effects of surface material type and surface

topography to understand their distinct influences to aid the optimisation of anti-fretting systems.

Figure 5.1 shows the cross-sectional BSE SEM images of the different surfaces onto which the DFLs were deposited, along with information regarding the roughness of those surfaces derived from the Alicona measurements. Three distinct surface topographies have been generated for the Cu-Ni-In onto which the DFL was applied as shown in Figure 5.1a, b & c (as-sprayed, ground and grit-blasted respectively). Two equivalent surface topographies have been generated for the Ti-6Al-4V onto which the DFL was directly applied; as can be seen by comparison of Figure 5.1c and Figure 5.1d, the grit-blasted Ti-6Al-4V has similar surface roughness and topographical features as that of the grit-blasted Cu-Ni-In surface. All three preparations exhibit a broadly symmetrical distribution of peaks and troughs. The as-sprayed Cu-Ni-In surface has the highest roughness and surface height parameters ranging from a peak of 46 µm to a depth of -38 µm.

As shown seen in Figure 5.1a, the DFL coating contours around the rough substrate (Cu-Ni-In) surface resulting in high variation in the DFL coating thickness on this substrate type. In some areas, a thinner layer (~ 25 µm) of DFL exists when covering the high points of the surface and in other areas, a deposit with a much higher local DFL thickness exists, the thickest of these being approximately 60 µm.

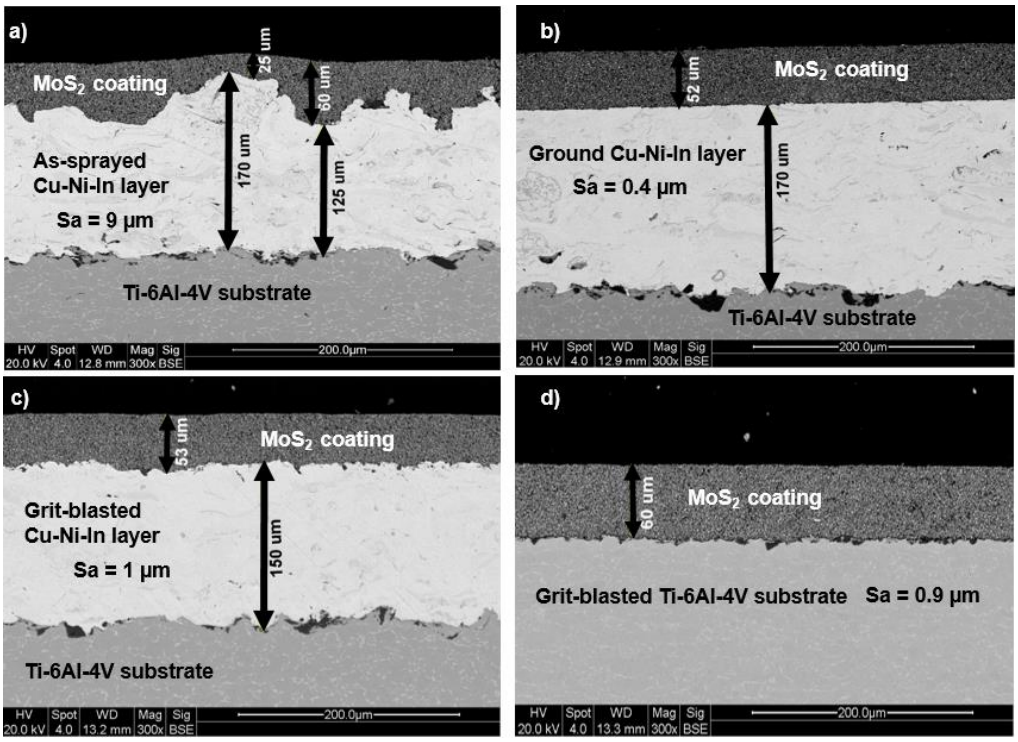


Figure 5.1 Cross sectional BSE images of flat specimens with a layer of MoS_2 DFL coating before fretting test with the thickness measurements of layers as indicated. DFL deposited onto the following surface types: a) as-sprayed Cu-Ni-In layer, b) ground Cu-Ni-In layer, c) grit-blasted Cu-Ni-In layer, d) grit-blasted Ti-6Al-4V.

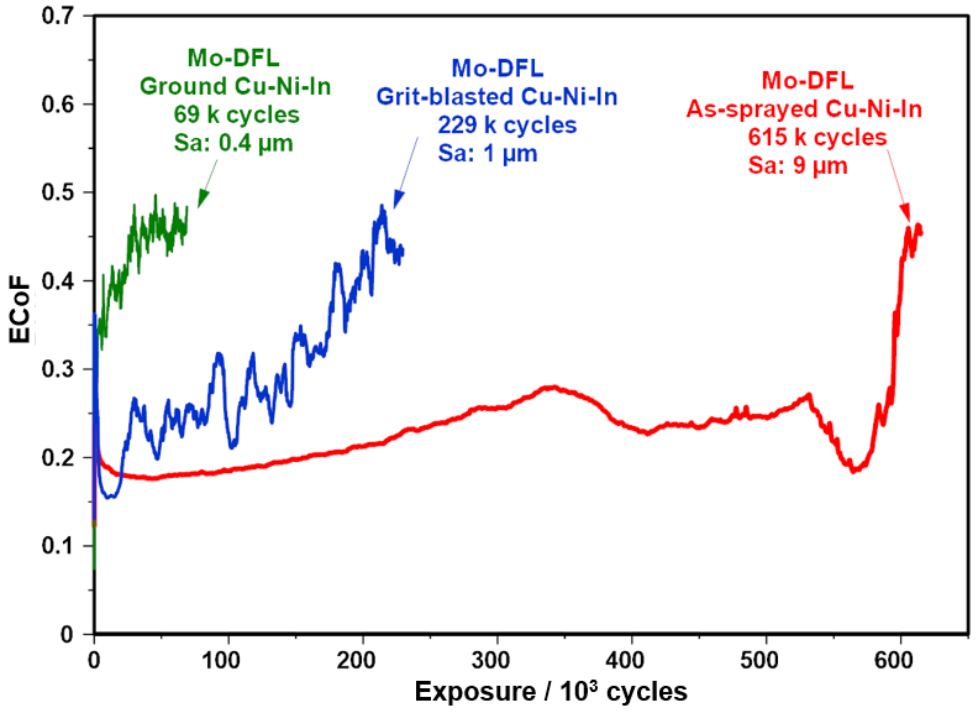
5.2 Effect of Cu-Ni-In interface roughness on system failure

The evolution of ECoF in the fretting wear tests conducted to failure where flat samples had the DFL applied to a Cu-Ni-In under-layer with the three different surface characteristics is presented in Figure 5.2a (these tests were terminated when the CoF first exceeded 0.7, although it is noted that the ECoF values are always much lower than that due to their averaging effect over the slip within any one cycle). It is seen that the DFL fretting lifetime increased with increasing surface roughness of the Cu-Ni-In under layer. A low friction coefficient (ECoF < 0.25) is observed for the vast majority of the DFL lifetime of the system where the DFL was deposited onto the roughest (as-sprayed) Cu-Ni-In under-layer; in the case presented, a lifetime of 615 k cycles was observed. In the system where the DFL was deposited onto a grit-blasted Cu-Ni-In surface, a low ECoF of < 0.2 was again observed soon after the beginning of the test; however, this low friction phase was short lived with the friction coefficient steadily increasing throughout the test with a

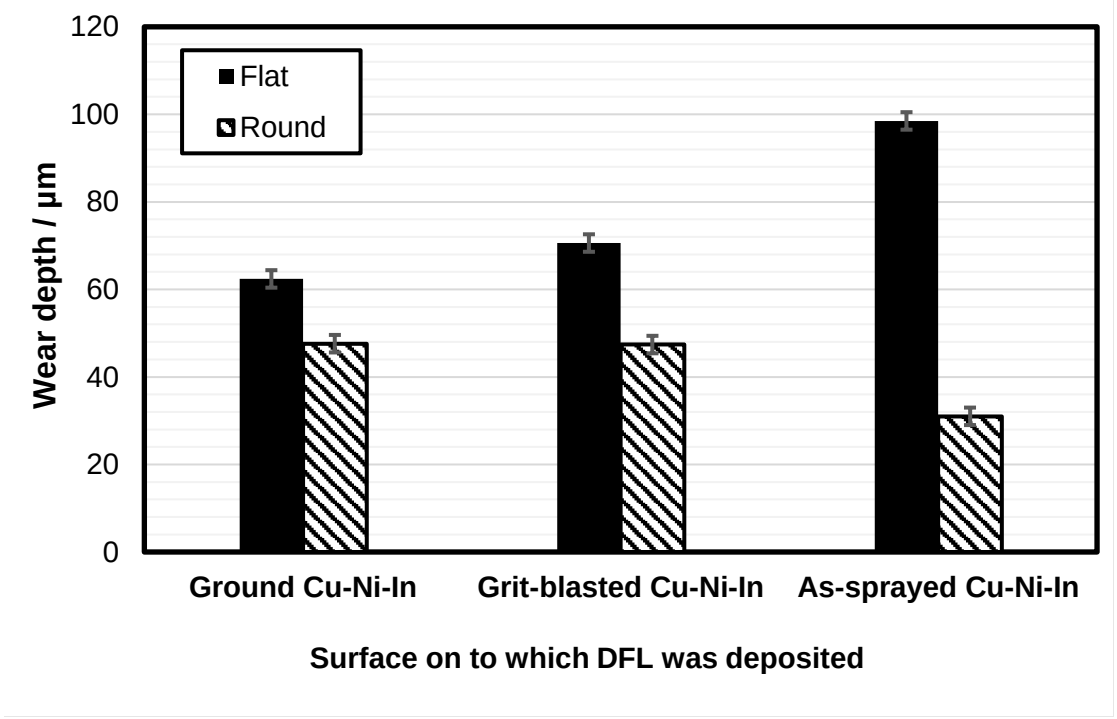
significantly smaller number of fretting cycles to failure (229 k cycles) being observed.

A significant difference in fretting behaviour was observed for the system where the DFL was deposited onto the smoothest (ground) Cu-Ni-In under-layer; no low friction phase was observed in the test, and instead the coefficient of friction rapidly rose until failure was reached after only 69 k cycles.

Profiles of the wear scars were made following tests to failure (i.e. when the CoF reached 0.7); Figure 5.2b shows the maximum depths of the average profile of both the flat samples with the Cu-Ni-In layer with varying surface conditions and the mating cylindrical samples. The maximum depth at failure of the flat samples (i.e. the sample with the Cu-Ni-In interlayer) increased with increasing roughness of the Cu-Ni-In layer onto which the DFL was deposited. It is noted that the scars on the mating round specimens always exhibit a smaller depth of wear at failure than that of the flat counterpart; moreover, the ratio of the scar depth of the cylindrical and flat samples decreased as the lifetime of the pair increased (as the surface roughness of the Cu-Ni-In interlayer increased).



(a)



(b)

Figure 5.2 a) Evolution of ECoF with number of cycles for fretting tests where flat samples had the DFL applied to the Cu-Ni-In layer with different surface preparations as indicated and the round counterpart was shot peened and DFL coated, b) Maximum depths of the averaged wear profiles at failure of the Cu-Ni-In coated flat samples and the shot peened Ti-6Al-4V round samples following tests to failure.

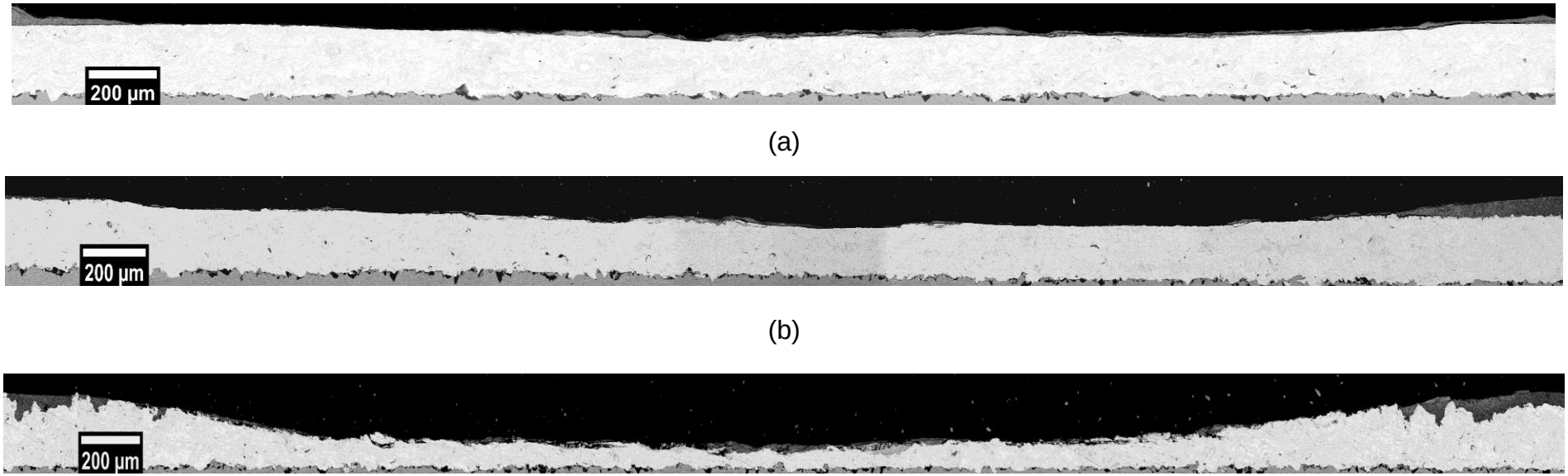
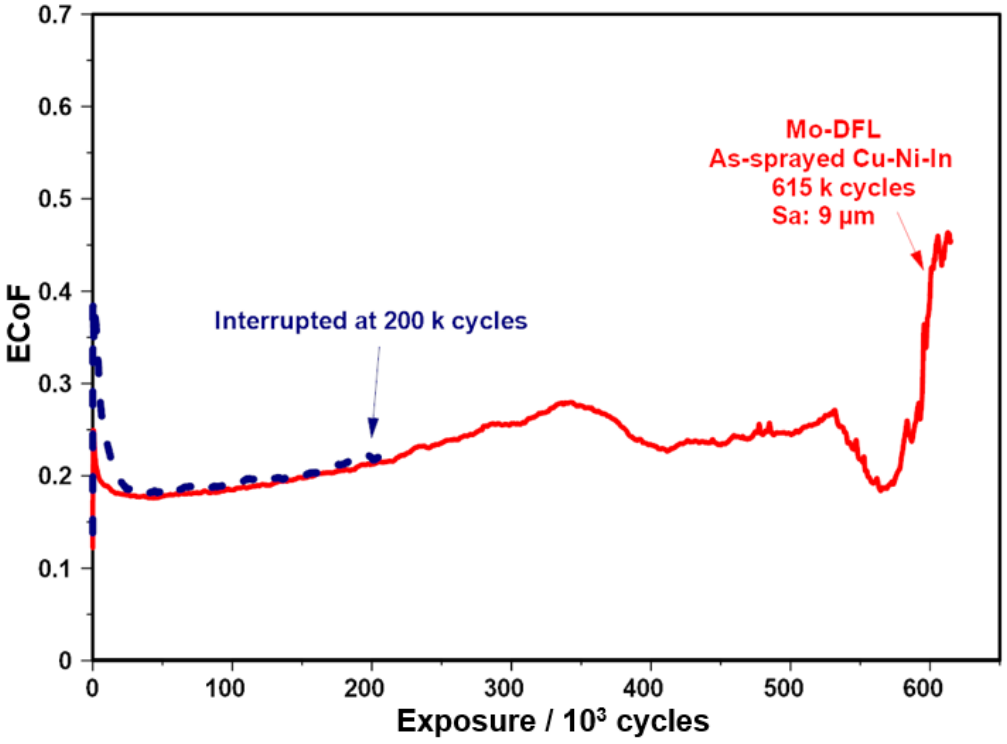


Figure 5.3 Cross sectional BSE SEM fretting wear scar images of flat samples. (a) test with DFL which had been deposited onto ground Cu-Ni-In following completed test to failure at 69 kilocycles, (b) test with DFL which had been deposited onto grit-blasted Cu-Ni-In following completed test to failure at 229 kilocycles, (c) test with DFL which had been deposited onto as-sprayed Cu-Ni-In following completed test to failure at 615 kilocycles.

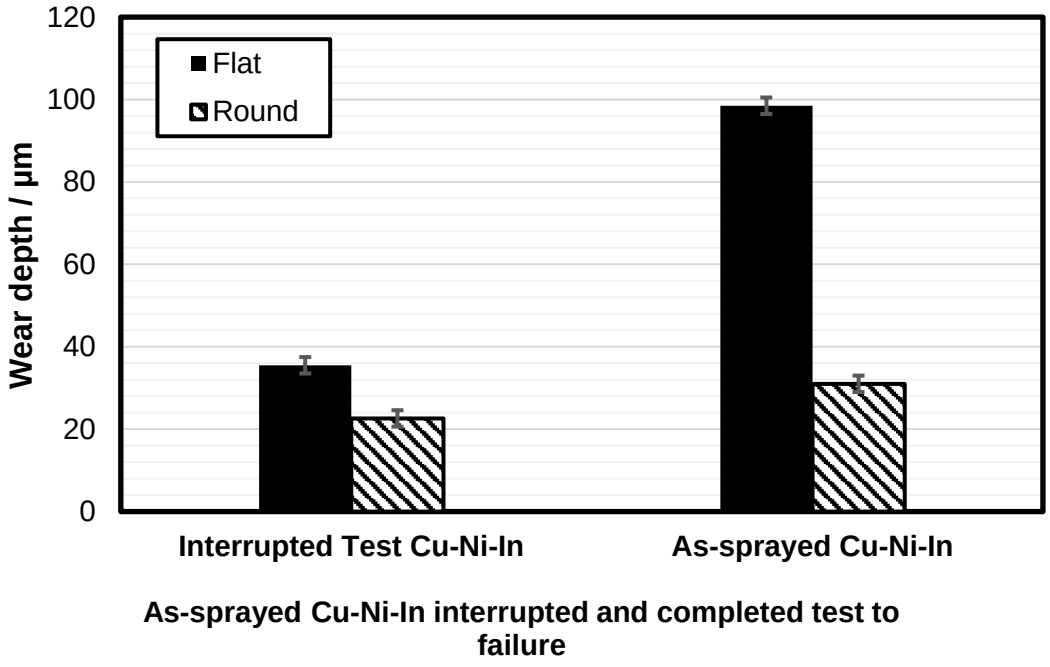
Cross sectional BSE SEM images of the flat Cu-Ni-In-coatings with the three different surface roughness following testing to failure are presented in Figure 5.3 (the reader is reminded of the different magnifications in the two directions in these images). Figure 5.3a & b show the wear scars in the flat specimens with (i) the ground Cu-Ni-In layer with the lowest initial surface roughness (Sa) of 0.4 µm which failed at 69 k cycles and (ii) the grit-blasted Cu-Ni-In layer with a surface roughness (Sa) of 1 µm which failed at 229 k cycles. In these tests, failure occurred when the wear scar had penetrated only a small way (< ~ 50 µm) into the Cu-Ni-In layer. In contrast, the wear scar in the specimen where the DFL had been applied onto an as-sprayed Cu-Ni-In with a high surface roughness (Sa) of 9 µm (which failed at 615 k cycles) indicated that much deeper penetration of the Cu-Ni-In layer had taken place when failure occurred.

For the system where the DFL was deposited onto the as-sprayed Cu-Ni-In layer, interrupted tests were also conducted. Figure 5.4a shows the evolution of ECoF from a test to failure and from an interrupted test which was stopped at 200 k cycles, which was judged to be still within the low friction phase. It is notable that the evolution of ECoF with exposure for the completed and interrupted test are very similar. The repeatability of the fretting test can also be observed as the friction traces of the interrupted test at 200 k cycles closely follow the friction traces of the completed test (which failed at 615 k cycles). Figure 5.4b displays the accompanying wear depth profiles of the respective wear scars for the flat and round specimen where (i) the maximum depth of the averaged wear profile was around 98 µm on the flat sample for the fully completed fretting test; (ii) the test stopped at 200 k cycles exhibited a wear depth of around 36 µm on the flat sample. The Ti-6Al-4V cylindrical counterpart of the interrupted test has a wear depth of 23 µm whilst that from the completed test displays a wear depth of 31 µm.

The loss of DFL coating along with the extent of wear and damage which had occurred during the fretting wear test of the DFL deposited onto as-sprayed Cu-Ni-In layer can be seen in Figure 5.5a which shows a cross sectional BSE SEM image of the fretting wear scar that had been interrupted during the low friction phase at 200 k cycles. Following 200 k cycles, the cross-sectional image (Figure 5.5a) shows that very little wear of the Cu-Ni-In layer itself is observed; however, failure following 615 k cycles has resulted in much more significant penetration of the Cu-Ni-In interlayer (Figure 5.5b).

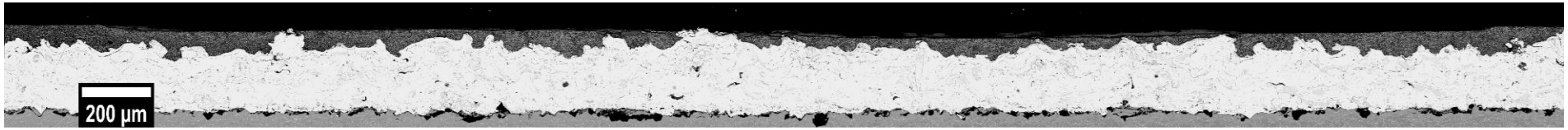


(a)

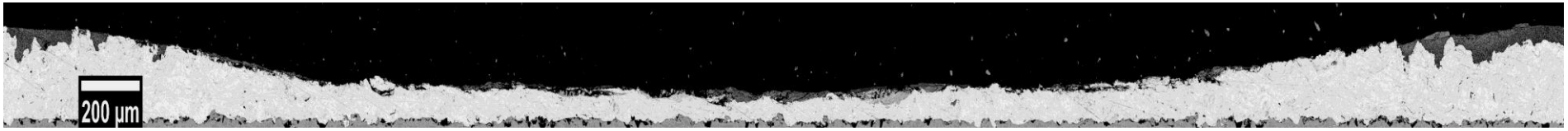


(b)

Figure 5.4 a) Evolution of ECoF with number of cycles for as-sprayed Cu-Ni-In fretting wear test which were interrupted and run to failure; b) Maximum depths of averaged wear profiles of as-sprayed flat Cu-Ni-In sample and the shot peened cylindrical Ti-6Al-4V samples of tests that were (i) interrupted at 200 k cycles and (ii) run to failure at 615 k cycles.

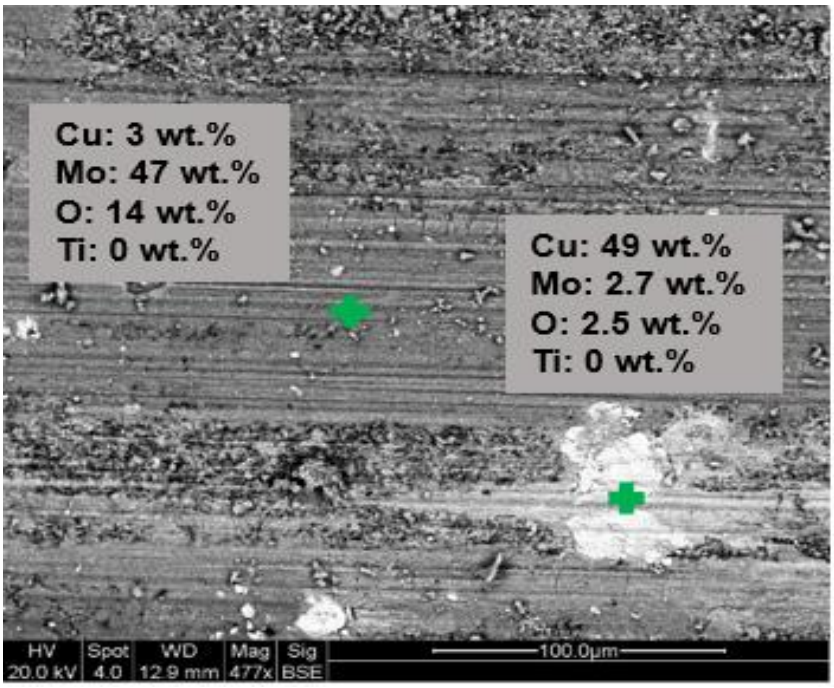


(a)

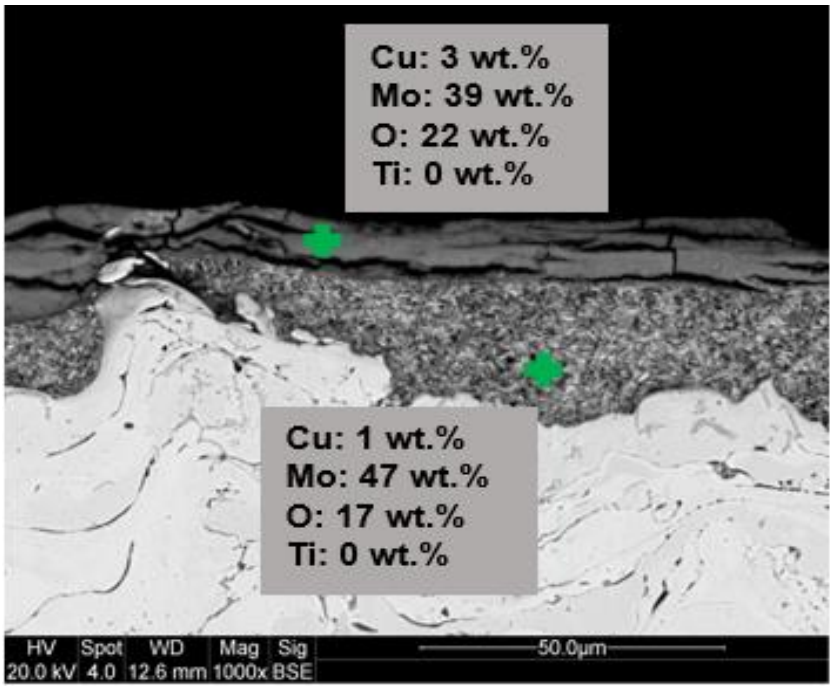


(b)

Figure 5.5 Cross sectional BSE SEM fretting wear scar images of flat samples. (a) test with DFL which had been deposited onto as-sprayed Cu-Ni-In following a test that was interrupted at 200 k cycles, (b) test with DFL which had been deposited onto as-sprayed Cu-Ni-In following completed test to failure at 615 k cycles.



(a)



(b)

Figure 5.6 BSE SEM images of fretting wear scars of a test where the DFL was deposited on an as-sprayed Cu-Ni-In flat sample that was interrupted at 200 k cycles a) plan view high magnified area, b) cross-section high magnified area.

Figure 5.6a shows a plan-view BSE SEM image of the worn surface following interruption of the test with the as-sprayed Cu-Ni-In interlayer in the low friction regime (200 k cycles). The majority of the surface is made up of a dark-contrast region (the DFL) with small areas of bright-contrast (the Cu-Ni-In under-layer) being observed. The nature of the two regions is identified via EDX analysis. Despite the cylindrical body not having a Cu-Ni-In layer (i.e. being DFL deposited onto shot-peened Ti6Al-4V), there is no evidence of titanium in the EDX analysis of either region on the surface of the flat specimens following these interrupted tests.

A high magnification cross sectional BSE-SEM image of the same surface from an interrupted test is presented in Figure 5.6b. A thin layer is observed on the outer worn surface which was not observed in the samples prior to wear (see Figure 5.1a); EDX analysis from these surface regions indicates a higher oxygen: molybdenum ratio than in the bulk of the DFL and provides evidence for formation of molybdenum oxide on the wearing surface as previously reported in the literature [114], [230]. It is also noted that minimal Cu content exists in the outer surface layer which suggests the involvement of Cu-Ni-In asperities within the formation of the molybdenum oxide surface. Below this outer layer, an approximate DFL thickness of 20 – 30 µm remains within the deepest valleys of the rough Cu-Ni-In layer. Figure 5.6 also shows areas in which the high Cu-Ni-In roughness peaks protrude through the DFL coating during the low friction stage, both in plan-view and in cross-section.

5.3 Effect of Cu-Ni-In interlayer material and Ti-6Al-4V substrate surface on systems failure

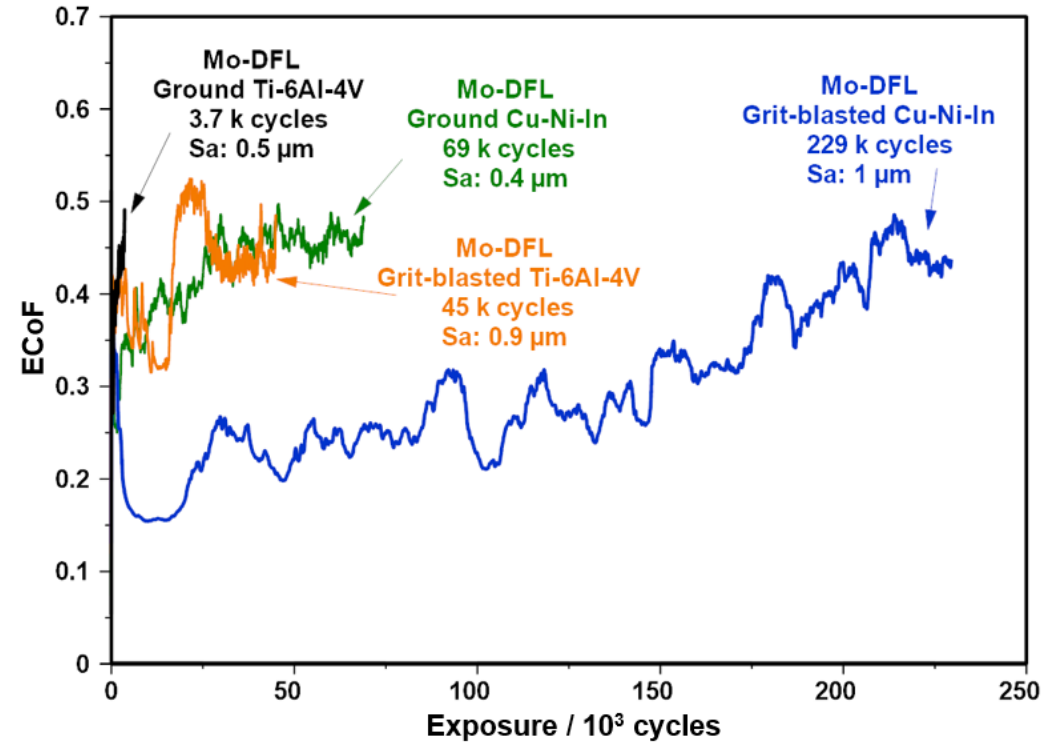
In Figure 5.7a, the evolution of ECoF through the fretting tests are presented for systems where the DFL layer had been deposited onto both the Cu-Ni-In and Ti-6Al-4V where the surfaces onto which the DFL had been deposited had two different topographies, namely that resulting from grinding and that resulting from grit-blasting. The relevant surface topographies can be seen in Figure 3.3b & c and Figure 3.3d & e for Cu-Ni-In and Ti-6Al-4V surfaces respectively.

It can be seen that the material type has a strong effect on the lifetime of the systems for both topographies, with the Cu-Ni-In interlayer resulting in longer lifetimes than when the DFL was deposited onto Ti-Al-4V for both of the surface topographies examined. The data demonstrate the effect of material type on the

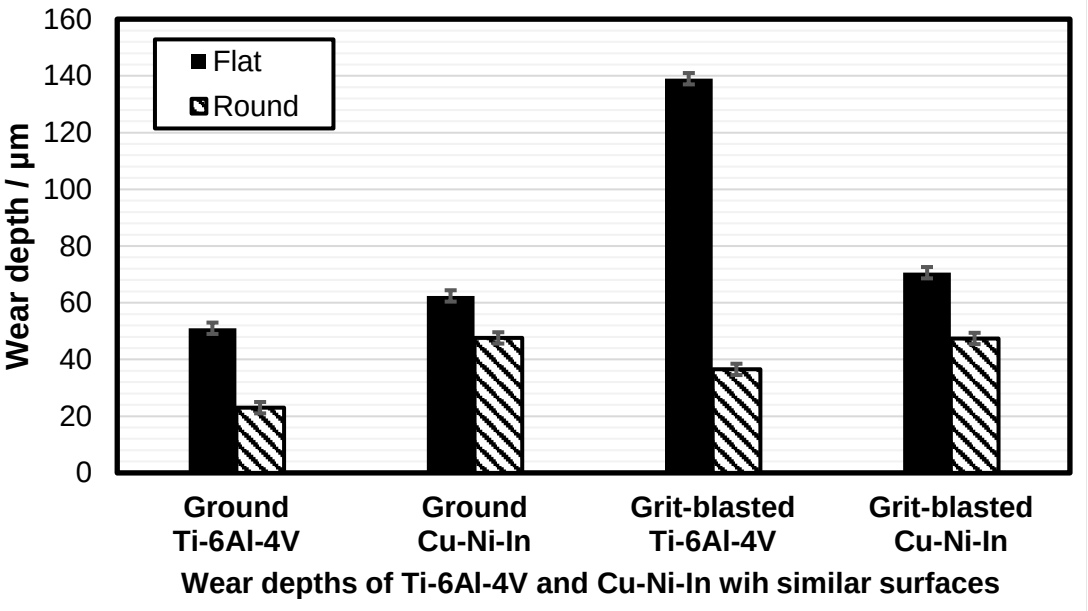
system with different responses shown through the evolution of ECoF. In tests with the DFL deposited onto the grit-blasted Cu-Ni-In substrate, ECoF fell quickly to around 0.15 soon after the beginning of the test whereupon it remained stable for a duration of 20 k cycles. After this brief low friction phase, a gradual increase in ECoF was observed until failure was reached at 229 k cycles. In contrast, when the DFL was deposited onto grit-blasted Ti-6Al-4V, the ECoF remained high throughout the test until failure was reached at only 45 k cycles.

The deposition of the DFL onto ground surfaces resulted in significantly reduced lifetimes compared to systems where the DFL had been deposited into grit-blasted surfaces. However, it is noted that again, ground Cu-Ni-In resulted in a much longer lifetime than ground Ti-6Al-4V.

Figure 5.7b shows the maximum depths of the averaged wear profiles of the fretting wear scars from these tests. It is noted that the ground Cu-Ni-In has a deeper wear depth on the flat and the ground compared to the ground Ti-6Al-4V. The fretting lifetime difference is however quite large as failure occurs at 3.7 k cycles on the ground Ti-6Al-4V and at 69 k cycles on the ground Cu-Ni-In layer. The wear scar depth for the flat samples with the DFL deposited onto grit-blasted Cu-Ni-In was 70 µm whilst that of the flat sample where the DFL was deposited onto the grit-blasted Ti-6Al-4V substrate was 139 µm. This depth range can be further observed in Figure 5.8 where the cross-sectional BSE SEM wear scar images of the completed (worn to failure) tests for the flat grit-blasted Ti-6Al-4V surface and the flat grit-blasted Cu-Ni-In surface are presented. For the grit-blasted Ti-6Al-4V substrate (Figure 5.8), there is evidence of DFL delamination (a vertical step in the DFL itself, top right of Figure 5.8a) which will have resulted in the protective influence of the DFL being curtailed. In contrast, the slope of the DFL in the Cu-Ni-In wear scar (Figure 5.8b) indicates progressive wear of the DFL itself and the absence of early delamination.

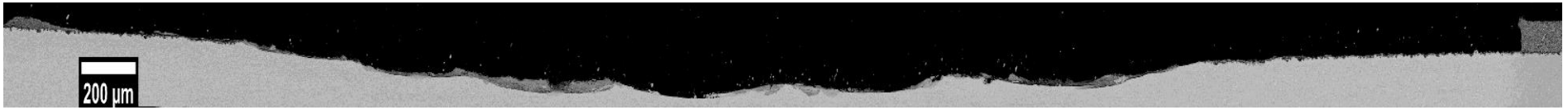


(a)

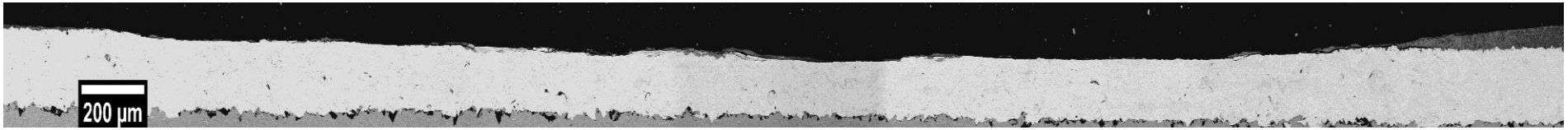


(b)

Figure 5.7 a) Evolution of ECoF with number of cycles for fretting tests to failure where the DFL was deposited onto either Ti-6Al-4V or Cu-Ni-In, both with a ground or grit-blast surface condition, b) Maximum depths of the averaged wear profiles of the flat ground Ti-6Al-4V and Cu-Ni-In and the flat grit-blasted Ti-6Al-4V and Cu-Ni-In samples as well as their round shot peened Ti-6Al-4V counterparts upon failure

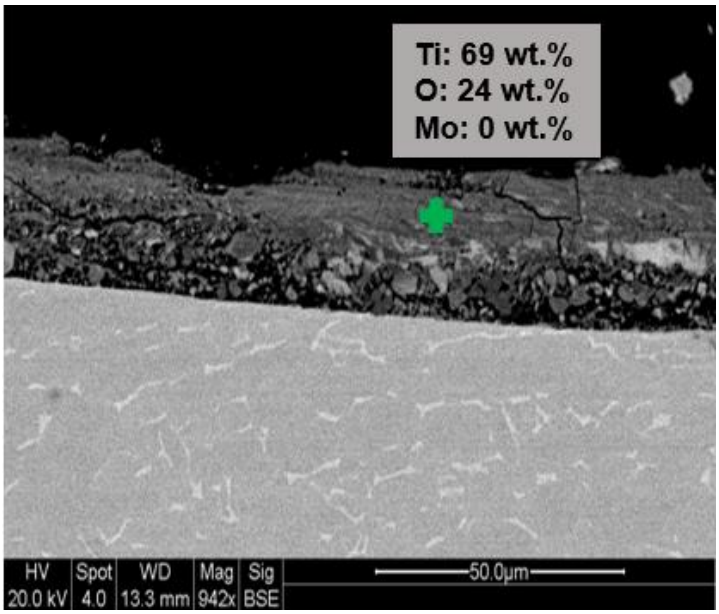


(a)

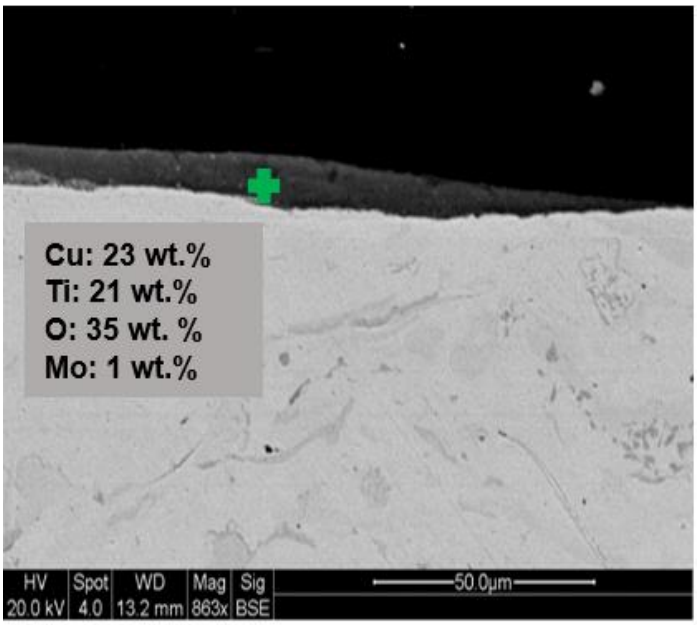


(b)

Figure 5.8 Cross sectional BSE SEM fretting wear scar images of flat samples. (a) test with DFL which had been deposited onto grit-blasted Ti-6Al-4V following completed test to failure at 45 k cycles, (b) test with DFL which had been deposited onto grit-blasted Cu-Ni-In following completed test to failure at 229 k cycles.



(a)



(b)

Figure 5.9 High magnification cross sectional BSE SEM images of flat samples from fretting wear scars, along with EDX analysis: a) test with DFL which had been deposited onto grit -blasted Ti-6Al-4V substrate upon failure at 45 k cycles, b) test with DFL which had been deposited onto grit-blasted Cu-Ni-In layer upon failure at 229 k cycles.

5.4 Discussion

5.4.1 Effect of roughness of Cu-Ni-In layer

It is well known that the addition of a thermally sprayed Cu-Ni-In under-layer for the application of a DFL to Ti-6Al-4V results in an extension to the durability of the DFL system. Whilst other studies ([111], [227], [228]) have shown that an increase in roughness of a substrate to which a DFL is applied results in an and extension of DFL system lifetime, this has tended to be in the range of roughness (Sa) values up to around ~3 µm. In this work, the roughness of as-sprayed Cu-Ni-In has been modified by further preparation and the same increase in DFL lifetime was again observed with increasing roughness (Figure 5.2a).

Previous work using the same cylinder-on-flat contact geometry has examined the behaviour of a systems where the DFL was deposited on to a grit-basted Ti-6Al-4V substrate [225]. A general form of evolution of ECoF with exposure was observed and was categorised into three stages as indicated in Figure 4.1. The following explanation was proposed: Stage I (with a high but falling ECoF) was associated with wear of the DFL itself; Stage II (where the ECoF fell rapidly and then remained relatively low and steady) was associated with wear of the mixed metal-DFL layer; Stage III was initiated when the DFL was exhausted and was associated with metal-metal contact and both instabilities with a generally rapid rise in the ECoF.

In this context, it is notable that when the DFL was deposited onto ground Cu-Ni-In (Sa ~ 0.4 µm), there was no evidence of Stages I or II in the evolution of ECoF with exposure, with behaviour similar to Stage III from the outset (Figure 5.2a) characterised by a rising ECoF with significant instability. As such, it is proposed that the DFL delaminates in this case and so it is neither worn away (Stage I absent) nor does any mixed DFL-metal layer form (Stage II absent). The fact that the DFL delaminates indicates that one of the functions of a rough surface is to provide a mechanical key for the retention of the DFL.

For the system where the DFL had been deposited onto the grit-blasted Cu-Ni-In (Sa ~ 1.0 µm), Stage I appeared to be absent (or very short) with Stage II being maintained until around 25×10^3 cycles (Figure 5.2a). In this case, Stage III was maintained until an exposure of 229×10^3 cycles; it is notable that this is much longer than the Stage III in the system where it is proposed that the DFL

delaminated (where the DFL was applied to a ground surface) and it is therefore proposed that some of the DFL must be retained into Stage II to effect that difference. Finally, when the DFL was deposited onto the as-sprayed Cu-Ni-In surface (Sa = 9 µm), no Stage I was seen again, but the low friction (Stage II) phase lasted at least ten times longer (although it is recognised that it is not clear when Stage II ends and Stage III begins in this case).

Together, these observations therefore strengthen the conclusions drawn in earlier work [230] that the mixed DFL-metal layer is both durable and confers low friction in Stage II, and that its formation and maintenance is best achieved by a high roughness metal onto which the DFL is deposited. A surface of sufficient roughness is required to act as a mechanical key for the DFL and thus prevent its delamination; if this is not achieved, low system durability is observed. The reason for the lack of Stage I behaviour with this system is not clear.

This durable nature of the mixed metal -DFL material is demonstrated by the cross-section of the test sample which was interrupted following 200×10^3 cycles (Figure 5.5a); here, despite the number of cycles being around a third of those resulting in system failure, the majority of the thickness of the DFL itself has been worn away (Figure 5.4b) but there is very little penetration and damage of the thermally sprayed Cu-Ni-In under-layer itself. The plan view image (Figure 5.6a) shows Cu-Ni-In providing support on the surface whilst the higher magnification cross-section in Figure 5.6b indicates the formation of a surface layer on top of the DFL; this upper glaze layer is rich in both molybdenum and oxygen but also contains copper, indicating that the Cu-Ni-In layer is involved to some limited degree in the formation of this upper glaze layer. The significant roughness in the as-sprayed Cu-Ni-In coating as well as the even distribution of high peaks and deep pits across the surface (Figure 3.3a and Figure 5.1a) provide reservoirs for the DFL which replenish the durable and low friction mixed metal - DFL layer as it is worn away.

Once the durable Cu-Ni-In – DFL mixed material has been removed, the Cu-Ni-In wears rapidly and wears much more rapidly than the Ti-6Al-4V. Figure 5.4b shows that after 200 kilocycles of exposure, the cylinder (which was originally made up of DFL deposited onto a shot-peened Ti-6Al-4V surface) has worn to a depth of ~ 23 µm whereas the flat specimen (with its Cu-Ni-In under-layer) has a worn to a depth of 36 µm. As the number of cycles of exposure were increased to generate system failure, the worn depth of the cylindrical specimen increased by ~ 5 µm, whereas the worn depth of the Cu-Ni-In containing flat sample increased by

~ 60 µm. This preferential wear of the Cu-Ni-In can be attributed to its low hardness compared to the Ti-6Al-4V (177 ± 20 HV and 287 ± 10 HV respectively).

As well as extending the lifetime, the increased roughness of the Cu-Ni-In underlayer also resulted in an increase in the depth of wear of the Cu-Ni-In coated flat specimen before CoF > 0.7 (the measure of test failure and the signal for the test to be stopped) and a decrease in the plain Ti-6Al-4V round specimen (Figure 5.2). Figure 5.3 shows that for all three of the Cu-Ni-In surface topographies examined, the depth of wear into the Cu-Ni-In when failure was deemed to have occurred was very much larger than the scale of the surface roughness, implying that the effect of the DFL is experienced long after the original thickness of the DFL has been worn away.

5.4.2 Comparison between Cu-Ni-In interlayer and Ti-6Al-4V substrate with similar roughnesses

Whilst it has been shown that the roughness of as-sprayed Cu-Ni-In is a key factor in extending the lifetime of the DFL, there is a need to understand if this is simply a roughness effect or if there is a dependence upon the material type. In this work, the surface of the as-sprayed Cu-Ni-In coating was further modified to be directly comparable to the topographies of TI-6Al-4V in both the ground and grit-blasted conditions. The similar nature of the surface topography of both Cu-Ni-In and Ti-6Al-4V in a smooth ground state and with a grit-blasted surface condition (as displayed in Figure 3.3 and Figure 5.1) has allowed the effect of these two substrate materials on test duration and failure mode to be examined independently of the effects of topography.

The evolution of ECoF with exposure to wear for the four surface types (two materials and two roughnesses) is presented Figure 5.7. Significant differences in behaviour are observed for the systems where the DFL was applied to a Ti-6Al-4V substrate as was seen when it was applied to the Cu-Ni-In.

When the DFL was applied to the ground Ti-6Al-4V (Sa ~ 0.5 µm), no stage I or Stage II behaviour was seen, with the system failing after just 3.7×10^3 cycles. This again indicates that the DFL delaminated from the substrate due to the lack of a mechanical key between them. In contrast, when the DFL was deposited onto a grit-blasted Ti-6Al-4V substrate (Sa ~ 0.9 µm), Stage I behaviour was observed (with a duration of ~ 10×10^3 cycles) indicating that the DFL was worn through

rather than delaminated. A short period of Stage II behaviour was then observed before Stage III commenced. For the grit-blasted systems, the wear scar depth (Figure 5.7b) for the grit-blasted Ti-6Al-4V-based system was very much larger than the DFL thickness itself (~ 140 μm) whereas for the Cu-Ni-In based system, failure occurred soon after the thickness of the DFL had been exceeded. This significant difference can also be observed in the cross-sectional micrographs presented in Figure 5.8. Higher magnification images (with EDX analysis) of cross-sections of the surfaces of the two grit-blasted systems following failure (Figure 5.9) show that in the case of the Ti-6Al-4V surface, there is no evidence of the DFL when failure occurred (i.e. no molybdenum is detected) whereas molybdenum was still present in the surface layer present when failure of the Cu-Ni-In system occurred. It is also notable in this latter case that titanium was present in the surface layer; this titanium must have come from the counter-body indicating that the DFL had been penetrated there also. The greater wear depth at failure with the Ti-6Al-4V system compared to the system with Cu-Ni-In has been observed in previous studies [230]. Niu et al. [124] credited the low depth of the Cu-Ni-In layer to delamination wear which under fretting, generates soft and large flake debris that could be easily retained in the contact area to form a third body. The effective load carrying capacity of the debris effectively inhibited the damage of the Cu-Ni-In coated specimen.

The systems where the DFL was deposited onto Ti-6Al-4V exhibited much lower durability than those where the DFL was deposited onto Cu-Ni-In with a similar topography. In the cases where it is proposed that delamination of the DFL occurred (i.e. where the DFL was deposited onto a ground surface), it is seen that Stage III (i.e. where ECoF rises steadily towards failure) lasts almost twenty times longer in the system with the Cu-Ni-In under-layer. In the cases where the DFL was deposited onto a grit-blasted surface, both Stage II and Stage III were much longer for the system with the Cu-Ni-In under-layer with a lifetime extension of approximately five times with the Cu-Ni-In under-layer.

Together, this evidence indicates that the Cu-Ni-In provides an extension to the lifetime in this system compared to Ti-6Al-4V. Although previous studies [58], [122], [124] have shown similar friction coefficients occur for unlubricated self-mated Ti-6Al-4V, and plasma sprayed Cu-Ni-In coatings mated against Ti-6Al-4V counter-body when deployed without any DFL. In the case considered in the current work, it must be remembered that the counter-body in all cases was a shot-peened Ti-6Al-4V surface to which a DFL had been applied. As such, it is argued here that in light of the observations made in the literature, the enhanced lifetimes associated

with the inclusion of Cu-Ni-In in the system do depend upon the presence of a DFL on at least one of the surfaces. However, the fact that the lifetimes of both the Ti-6Al-4V and the Cu-Ni-In were significantly longer if the DFL was deposited onto a grit-blasted surface rather than a ground surface indicates that the effect of the DFL being retained by the surface roughness is critical to lifetime extension in both cases.

5.5 Conclusion

In this study, the effects of the interfacial geometry and material type upon which a polymer bonded MoS_2 based DFL is deposited on is investigated and has permitted further understanding of the working mechanisms that enables the extension of fretting lifetimes and durability of the bonded DFL coating systems. By modifying the interfacial roughness of the as-sprayed Cu-Ni-In under-layer, the increase of DFL fretting lifetimes and system durability was found to correlate with increased surface roughness. The surface of the underlying Cu-Ni-In coating was modified to be directly comparable to the TI-6Al-4V substrate in both the ground and grit-blasted conditions. With this, the material effects of the DFL coated fretting system could be isolated. The experimental results showed that:

- In both the smooth ground state and grit-blasted conditions, samples with a Cu-Ni-In under-layer showed better durability and lifetimes when compared to Ti-6Al-4V substrate despite having similar surface topographies.
- The interfacial surface roughness plays a key role in enabling the formation of a low ECoF mixed metal-DFL phase which, regardless of material type, enhances fretting lifetime.
- The roughness of as-sprayed Cu-Ni-In is a key factor in extending the lifetime of the DFL which is proposed to provide a mechanical key for the retention of the DFL to prevent delamination of the DFL coating and increase system durability.
- When a thermally sprayed Cu-Ni-In layer is used in its as-sprayed condition, these effects of high roughness and material durability combine to significantly enhance the fretting lifetime compared to a non-roughened Ti-6Al-4V surface.

- For the results presented here, the change in material from Ti-6Al-4V to Cu-Ni-In at a fixed surface roughness of 0.9 - 1 µm increased fretting lifetime by approximately fivefold. Increasing roughness of the Cu-Ni-In layer from 1 µm to 9 µm more than doubled fretting lifetime.

Further work to determine the optimum surface would need to include a cost benefit analysis of the relevant surface engineering processes.

Chapter 6. Examining the performance of polymer-bonded MoS_2-based DFL and graphite-modified MoS_2-based DFL on different fretting contact configurations and loading conditions

6.1 Background

In Chapter 4, it was reported that fretting tests conducted on a self-mated, grit blasted Ti-6Al-4V cylinder-on-flat fretting contact in atmospheric and high-humidity air and argon conditions showed that the graphite modified MoS_2-based DFL (Gr-Mo-DFL) coating was able to maintain a stable friction coupled with a very significant (> 10 times) extension of fretting lifetimes when compared to as-received MoS_2-based (Mo-DFL) coating system which underwent rapid wear to failure in the same atmospheric and high-humidity conditions. In Chapter 5, it was reported that when a thermally-sprayed Cu-Ni-In layer is used in its as-sprayed condition as the surface onto which a DFL is deposited, the interfacial geometry and material type together provide a significant enhancement to the fretting lifetime compared to when the DFL is deposited onto a grit-blasted Ti-6Al-4V surface.

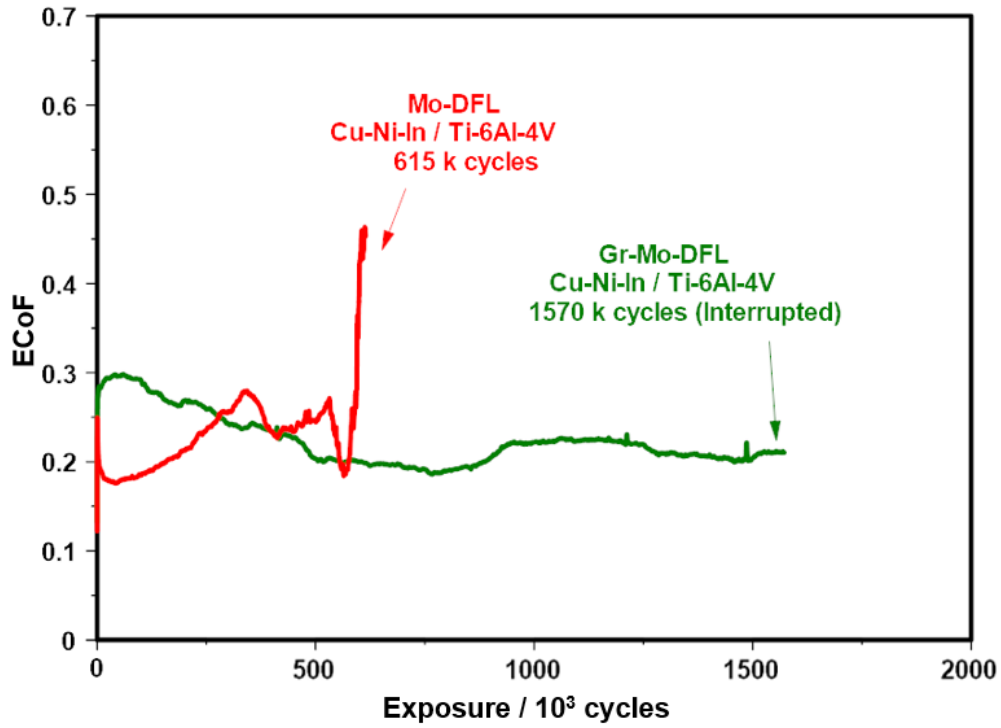
In this chapter, the aim is to provide a better understanding of the performance limits of the graphite modified MoS_2-based DFL (Gr-Mo-DLF) compared to Mo-DFL; to achieve this, further fretting wear tests were conducted with the relevant surface architectures of the fan-blade root and disc, increased fretting load capacities and alternate contact configurations.

6.2 Performance of the Mo-DFL and Gr-Mo-DFL coatings on a cylinder-on-flat contact configuration

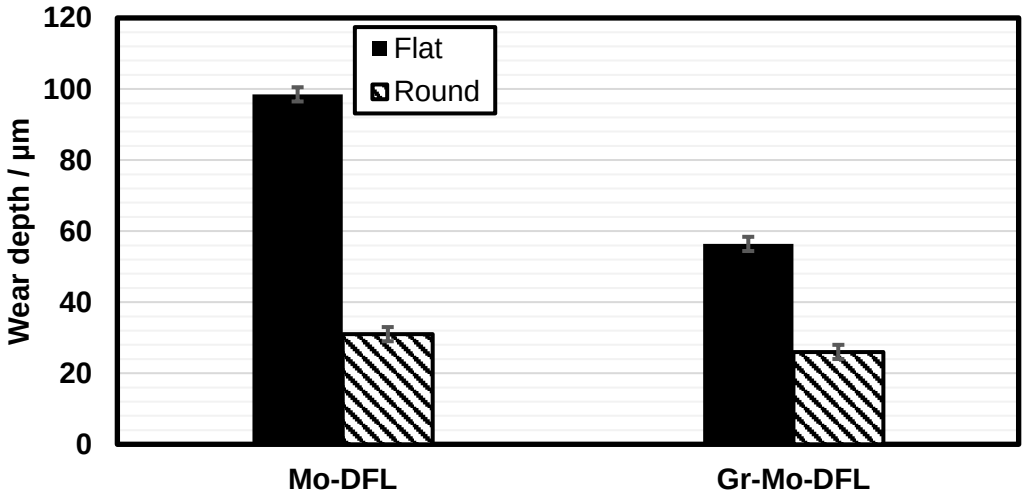
In Chapter 4 (Section 4.4) the increased performance, durability and extended lifetime of Gr-Mo-DFL (compared to Mo-DFL and Gr-DFL) has been observed following its deposition onto grit-blasted Ti-6Al-4V specimens as seen in ambient atmospheric air (Figure 4.13a) and in high-humidity air and argon environments (Figure 4.15a & b).

To understand the fretting wear behaviour of the graphite modified Gr-Mo-DFL coating system on the relevant surface architecture of the fan blade root and disc whilst still maintaining a cylinder-on-flat contact configuration, fretting wear test specimens were prepared as follows: the flat specimen of the fretting couple was thermally-sprayed with a Cu-Ni-In under-layer whilst the cylindrical counter-body was shot-peened. Both specimens were subsequently coated with a DFL coating before being subjected to a fretting test.

Figure 6.1a shows the evolution of ECoF against cycles for the Mo-DFL and the Gr-Mo-DFL coating systems with the adapted fan blade root surface architecture with the imposed fretting loading conditions of 575 N normal load (which resulted in an estimated initial Hertzian contact pressure of ~ 183 MPa), an applied displacement of 0.3 mm and a frequency of 2.5 Hz. The Gr-Mo-DFL system maintained a stable low ECoF ~ 0.25 for the duration of the test which was stopped at 1570 k cycles (prior to failure) whilst the Mo-DFL system failed following 615 k fretting cycles. Figure 6.1b shows the corresponding wear depths; the Mo-DFL system had worn to a depth of 98.5 µm on the flat sample and 31 µm on the cylinder at the point of failure, whilst the Gr-Mo-DFL system exhibited a wear depth of ~ 56 µm on the flat and ~ 26 µm on the round specimen. This shows the durable low friction characteristics of the modified Gr-Mo-DFL coating system is maintained when applied to substrates which had been prepared in a manner that reflects industrial practice and, under the test configuration employed, continues to yield significant extension of fretting lifetime (an increase in lifetime of > 2.5 times has been demonstrated).

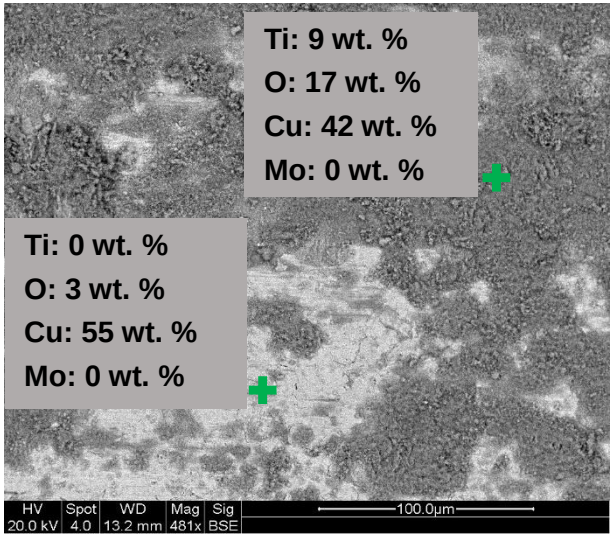


(a)

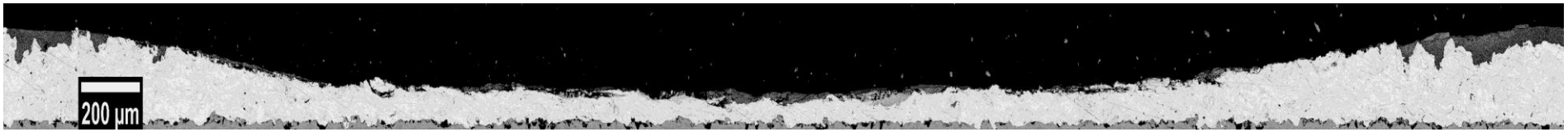


(b)

Figure 6.1 Fretting performance of the as-received MoS_2 bonded DFL coating (Mo-DFL) and the modified (Gr-Mo-DFL) version using relative fan blade root surface architecture. (a) Friction evolution against cycles of Mo-DFL and Gr-Mo-DFL deposited on top of a thermally sprayed Cu-Ni-In under-layer (b) The maximum depth of the averaged wear profile taken from the wear surface upon failure for Mo-DFL at 615 k cycles and at 1570 k cycles for modified Gr-Mo-DFL which was stopped before failure occurred.



(a)

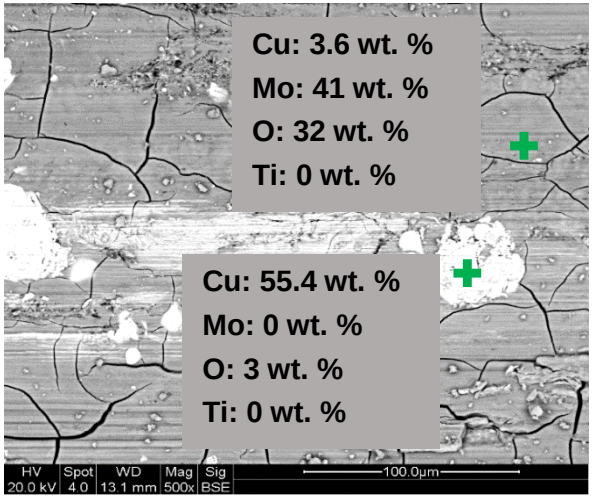


(b)

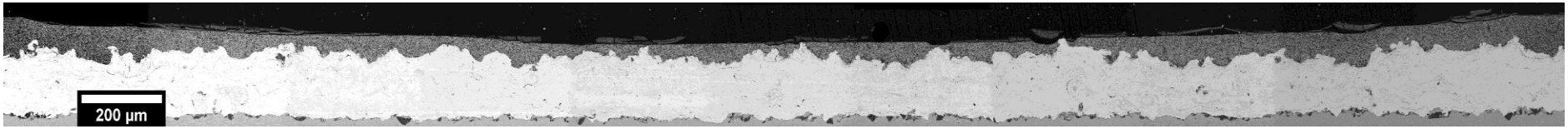
Figure 6.2 BSE SEM images of the flat specimen of the Mo-DFL system upon failure at 615 k cycles (a) plan-view image (b) cross-sectional BSE SEM fretting wear scar images of flat samples.

Plan-view and cross-sectional BSE SEM images were taken of the flat specimen from the Mo-DFL tests (which failed at 615 k cycles) and are presented in Figure 6.2. The plan-view exhibits a darker region which is shown from EDX point analysis to contain Cu (~ 42 wt. %), Ti (~ 9 wt. %) and O (~ 17 wt. %) but no Mo; this indicates that the surface is made up of oxides of Cu and Ti. A bright region also exists which again contains Cu (~ 55 wt. %) but with a much reduced O content (~ 3 wt. %) and with no Ti or Mo being detected, which indicates that the surface is made up of the Cu-Ni-In under-layer material. These compositions indicate that the Mo-rich DFL had been completely eliminated by this stage. This conclusion is supported by the cross-sectional image (with higher magnification in the vertical than in the horizontal direction) presented in Figure 6.2b which shows that significant wear has occurred well into the Cu-Ni-In layer at the point of failure.

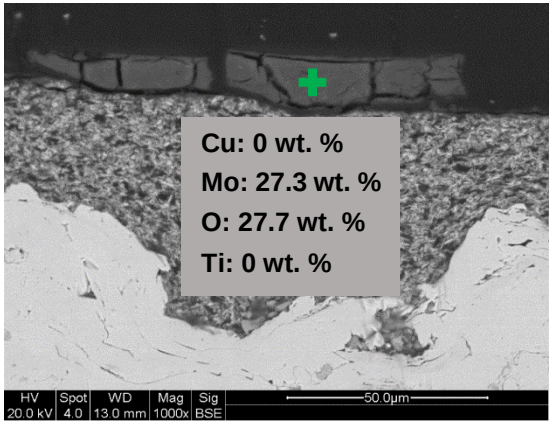
Figure 6.3 displays plan-view and cross-sectional BSE SEM images that were taken of the Gr-Mo-DFL flat specimen where the test was stopped at 1570 k cycles (prior to failure). In Figure 6.3a, a plan-view BSE SEM shows the wear surface is dominated by a region with a cracked-paved structure which has a composition of Mo (~ 41 wt. %), S (~ 21 wt. %) and oxygen content of ~ 32 wt. % (Figure 6.3a). Dotted and smeared bright regions are also evident on the surface which have a high Cu content (~ 55.4 wt. %) with low oxygen composition of ~ 3 wt. % and no molybdenum. A cracked-paved surface with a similar appearance has been previously observed in Section 4.2 , Figure 4.5, for a Mo-DFL coating system following fretting in a low-humidity air environment which had a high fraction of Mo (~ 42.5 wt. %), S (~ 17.2 wt. %) as well as a high oxygen content of ~ 40 wt. % (Figure 4.5a & b). A cross-sectional BSE SEM image with higher magnification in the vertical than in the horizontal direction (Figure 6.3b) shows that significant wear damage into the underlying Cu-Ni-In had not occurred; although significant wear of the DFL had occurred (down to the point where the Cu-Ni-In was being exposed, a reasonably thick Mo-DFL coating (~ 40 µm thick in places) was observed to remain on the wear interface along with a cracked surface layer of ~ 10 µm thickness which exists on the very top surface as presented in Figure 6.3c & d (the same material as seen in plan-view on the surface in Figure 6.3a). More severe fretting conditions (increased load and / or increased slip amplitude) were imposed on the cylinder-on-flat contact configurations for both Mo-DFL and the Gr-Mo-DFL coating systems in an attempt to be able to directly compare the cycles to failure of the two coatings. The maximum normal load capacity for the fretting rig based at The University of Nottingham is 1000 N which results in an estimated Hertzian contact pressure of ~ 241 MPa on the plasma-sprayed Cu-Ni-In material.


Cu: 3.6 wt. %
Mo: 41 wt. %
O: 32 wt. %
Ti: 0 wt. %
Cu: 55.4 wt. %
Mo: 0 wt. %
O: 3 wt. %
Ti: 0 wt. %
HV
20.0 kV
Spot
4.0
WD
13.1 mm
Mag
500x
Sig
BSE
100.0µm

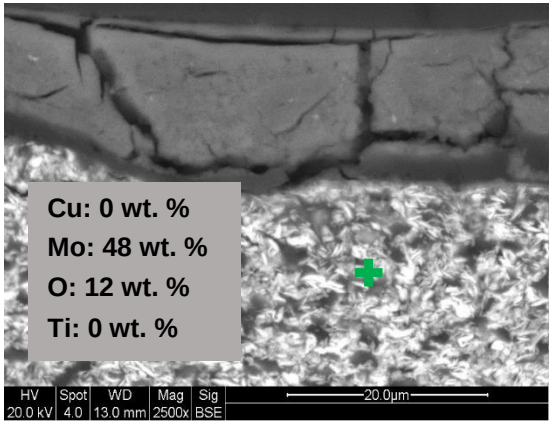
(a)


200 µm

(b)



(c)



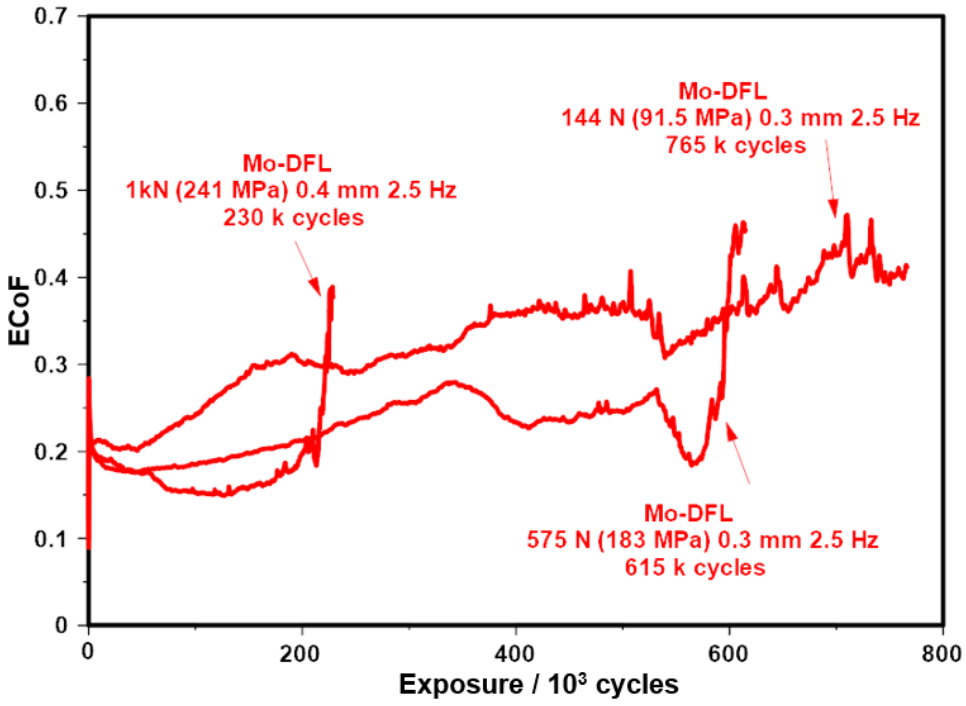
(d)

Figure 6.3 BSE SEM images of the flat specimen of the Gr-Mo-DFL system stopped at 1570 k cycles (a) plan-view image with EDX analysis (b) Cross-sectional BSE SEM fretting wear scar images of flat samples (c) High magnification of the top surface (d) Increased magnification.

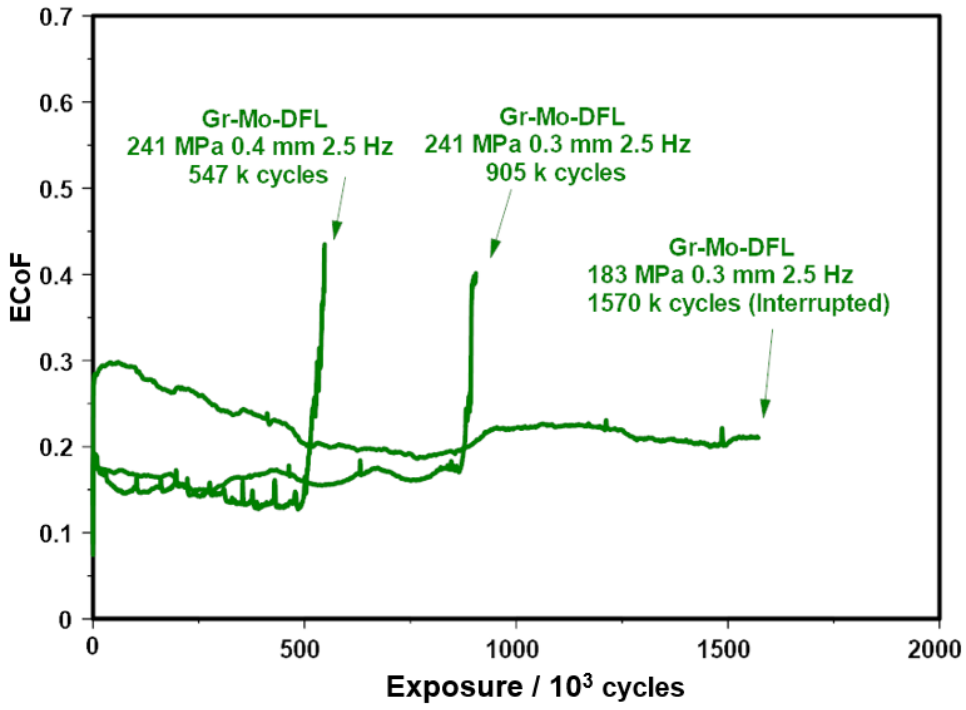
.

In Figure 6.4a, the performance of the Mo-DFL system can be observed where an increase in both normal load (from 575 N to 1000 N) and applied displacement (from 0.3 mm to 0.4 mm) were imposed for the test. With this, a reduction of lifetime can be seen leading to failure at 230 k cycles (compared to 615 k cycles with the less severe loading conditions). An initial lower ECoF phase ~ 0.15 is noted for the more severe load conditions prior to failure. When the normal load is reduced from 575 N to 144 N (which resulted in a reduction of the approximate initial Hertzian contact pressure from 183 MPa to 91.5 MPa), marginal increase of fretting lifetime from 615 k cycles to 756 k cycles was observed along with increased ECoF $\geq$ 0.2.

Figure 6.4b details the performance of the modified Gr-Mo-DFL system with more severe loading conditions. With an increase in normal load from 575 N to 1000 N (183 MPa to 241 MPa) with the same displacement amplitude of 0.3 mm, the failure occurs at 905 k cycles and with the increase of both the normal load (575 N to 1000 N) and the applied displacement (0.3 mm to 0.4 mm), an even shorter lifetime is observed with failure occurring at 547 k cycles. It is notable that under the most severe loading conditions, the ratio of the failure lifetimes for Gr-Mo-DFL and the Mo-DFL is 2.37 (still a very significant improvement in lifetime).



(a)



(b)

Figure 6.4 ECoF evolution against cycles of (a) Mo-DFL deposited on top of a Cu-Ni-In under-layer and (b) Gr-Mo-DFL deposited on top of a Cu-Ni-In under-layer, at different fretting loading conditions.

With less severe loading conditions of 575 N normal loading and 0.3 mm applied displacement, the Gr-Mo-DFL had previously yielded an extended wear lifetime (as seen in Figure 6.1a) where the test was stopped at 1570 k cycles before failure. By increasing the normal load alone or the normal load and the applied displacement amplitude, it is proposed that a threshold has been crossed where failure now occurs.

The concept of a PV value for these polymer-bonded DFL coatings is investigated where the mutual effects of applied pressure P and sliding speed V is considered with the aim of uncovering the threshold limit for the coating system. The PV limit are defined as the value above which the wear rate increases rapidly with the maximum operational PV value being the maximum value for continuous operation at a specified wear rate [208]. This limit is usually based on the maximum allowable PV value and is related to conditions when the polymer coating cannot transfer the frictional energy dissipated at the surface during wear fast enough, and its internal temperature thus increases leading to thermally-accelerated failure [208], [210].

In Figure 6.5, the measured fretting lifetimes of the Mo-DFL and Gr-Mo-DFL systems are shown against the respective PV values of the tests. With high PV values, shorter fretting lifetime are observed, however, at each PV value, the graphite modified Gr-Mo-DFL performs better with increased overall lifetime in each case. When PV = 0.274 MPa m s^{-1}, there is a distinct difference in the performance of the graphite modified Gr-Mo-DFL and Mo-DFL (as previously observed in Figure 6.1) by which a steady state low friction behaviour with a significant increase in lifetime is seen which was stopped before failure for the graphite-modified Gr-Mo-DFL coating system whereas a failure point occurred at 615 k cycles with Mo-DFL. With a higher PV value (PV = 0.361 MPa m s^{-1}), the Gr-Mo-DFL undergoes a transition from a steady state low friction behaviour to a high friction test to failure which indicates that a threshold limit between the PV values of 0.274 MPa m s^{-1} and 0.361 MPa m s^{-1} exists. However, a steady state low friction behaviour was not observed for the Mo-DFL coating system with reduced contact pressure and a lower PV value of 0.137.

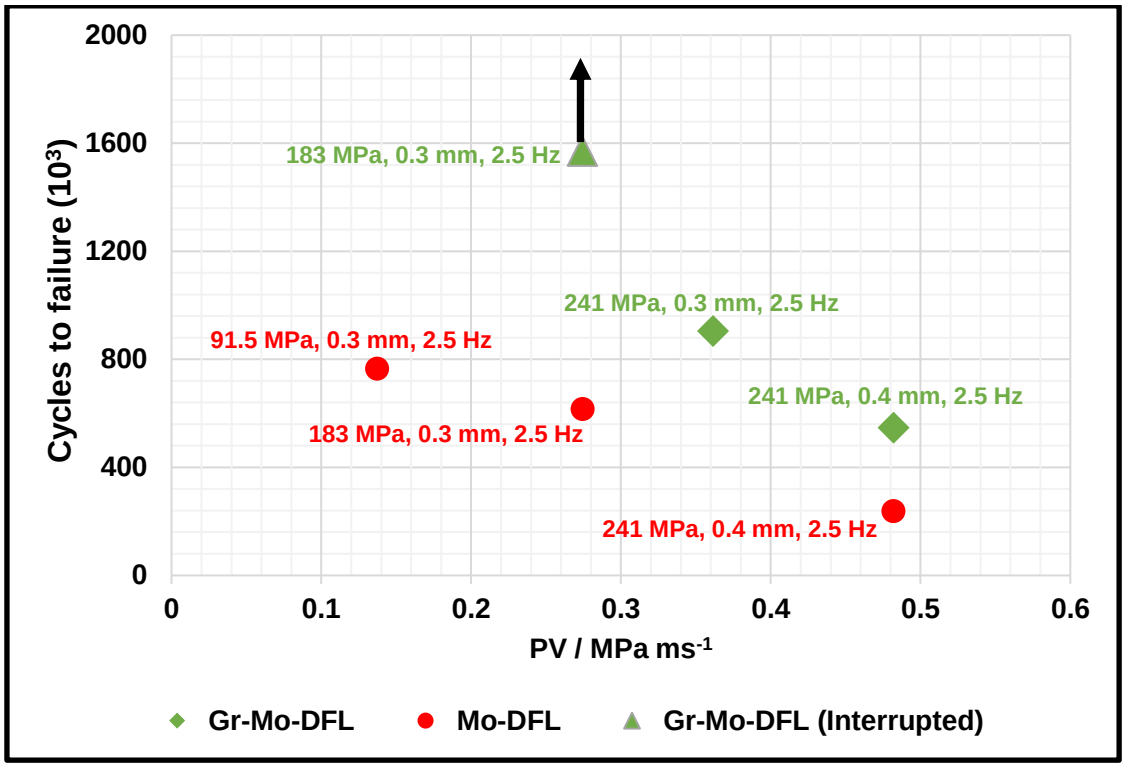


Figure 6.5 Plotted graph of the fretting wear test cycles and the corresponding PV values of Mo-DFL and Gr-Mo-DFL on a cylinder-on-flat contact. Failure was defined to have occurred when $\mu \geq 0.7$ and tests to failure (i.e., to completion) were automatically terminated when that condition was first satisfied as the critical wear depth of the DFL coating had occurred.

6.3 Comparison of performance of Mo-DFL and Gr-Mo-DFL coatings when tested with a flat-on-flat contact configuration

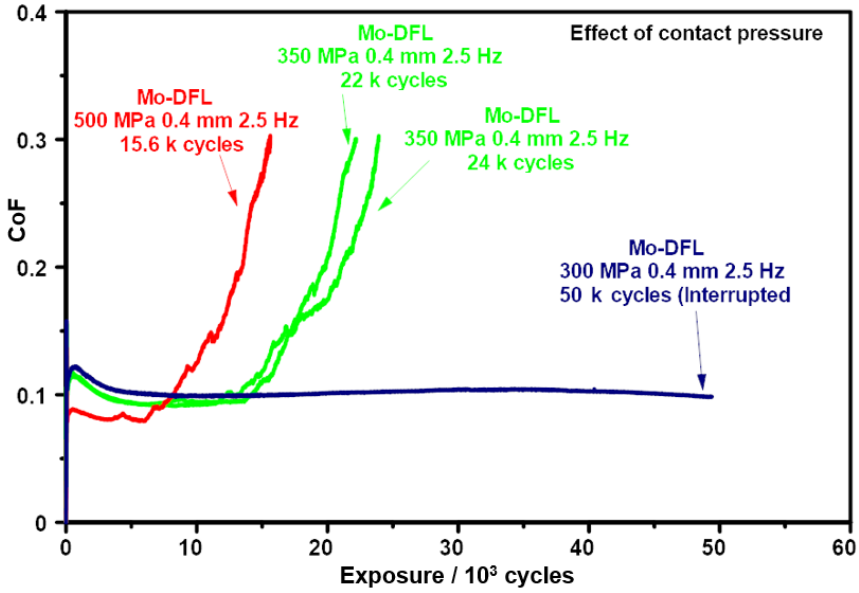
A second fretting wear rig (Figure 3.8) which uses flat-on-flat contact configuration (Figure 3.9) with higher loading and controlled environmental capabilities was employed for this section. The addition of this rig expands the testing envelop with a wider range of fretting loading conditions using an alternate flat-on-flat contact configuration which is preferred since it more closely represents the geometry of the fan blade root.

Fretting wear tests in this section were conducted elsewhere at commercial testing facilities (Scitek) where only the coefficient of friction (CoF) measurements were provided. It should be noted that CoF is used to display the evolution of friction as

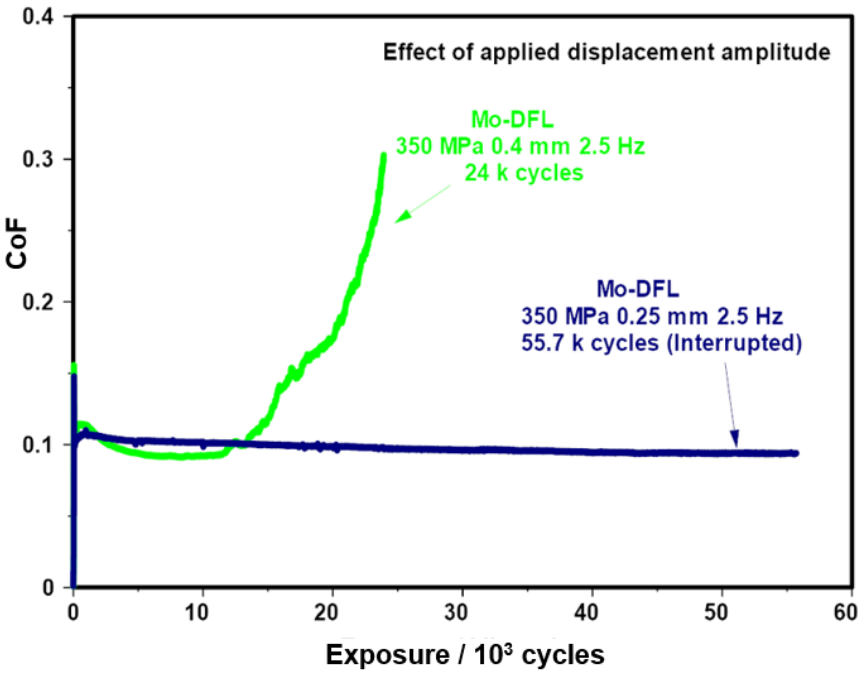
opposed to the energy coefficient of friction (ECoF) which was utilised in earlier sections of the thesis.

At various loading conditions, a series of fretting wear tests were conducted to understand the performance of the Mo-DFL system with the flat-on-flat contact configuration. Figure 6.6a displays the results of the evolution of friction against cycles which details the effect of contact pressure in tests where the applied displacement amplitude and the frequency remained fixed at 0.4 mm and 2.5 Hz respectively. At the highest contact pressure of 500 MPa, the shortest fretting wear lifetime of 15.6 k cycles is observed. This, however, also exhibits the lowest initial coefficient of friction phase below 0.1. Reducing contact pressure to 350 MPa leads to an increase in the fretting lifetime to 24 k cycles. This test was repeated to demonstrate the repeatability of the fretting tests and failed at a similar fretting lifetime of 22 k cycles. Further reduction to 300 MPa leads to a steady state low friction behaviour being observed for the duration of the test (the test was terminated at 50 k cycles, this being before failure occurred). Thus, the two distinct wear behaviours (steady state low friction with extended lifetime and rising friction to failure) as previously observed for the graphite modified Gr-Mo-DFL system in cylinder-on-flat testing with increasing load (Figure 6.4b) were observed in the flat-on-flat contact configuration for the standard Mo-DFL.

In Figure 6.6b, the effect of applied displacement amplitude on the performance of the Mo-DFL system is examined. With a contact pressure of 350 MPa and a frequency of 2.5 Hz, a change in behaviour from failure with a fretting lifetime of 24 k cycles with a displacement of 0.4 mm to an extended fretting lifetime of > 55.7 k cycles (test had not failed upon its termination) was observed upon reducing the applied displacement amplitude to 0.2 mm.



(a)



(b)

Figure 6.6 Evolution of CoF against number of cycles for fretting tests conducted on flat-on-flat contact configuration where Mo-DFL was deposited on top of a Cu-Ni-In under-layer (a) contact pressures of 500 MPa, 350 MPa and 300 MPa are imposed with an applied displacement amplitude of 0.4 mm; (b) applied displacement amplitudes of 0.4 mm and 0.25 mm are imposed. A frequency of 2.5 Hz is maintained in all tests.

In Figure 6.7, the comparison of the performance of Mo-DFL and the graphite modified Gr-Mo-DFL shows an increase in fretting lifetime from 14.4 k cycles for Mo-DFL to 26 k cycle for Gr-Mo-DFL with a contact pressure of 325 MPa, an applied displacement of 0.5 mm and a frequency of 2.5 Hz.

With further increase of the contact pressure to 350 MPa and a reduction of applied displacement to 0.4 mm, improved performance of the modified Gr-Mo-DFL was still maintained with a lifetime increase from 24 k cycles for Mo-DFL to 29 k cycles for Gr-Mo-DFL. The Gr-Mo-DFL systems also maintain slightly lower friction during the low friction phase of their lifetime before the failure (as defined by a steadily rising CoF) began to occur.

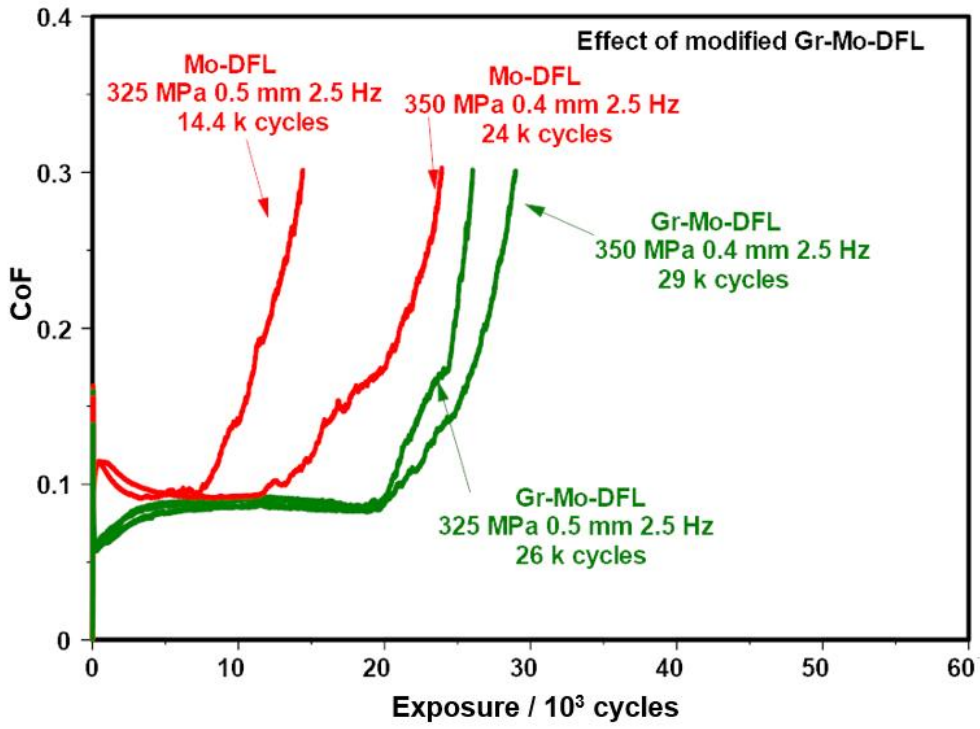
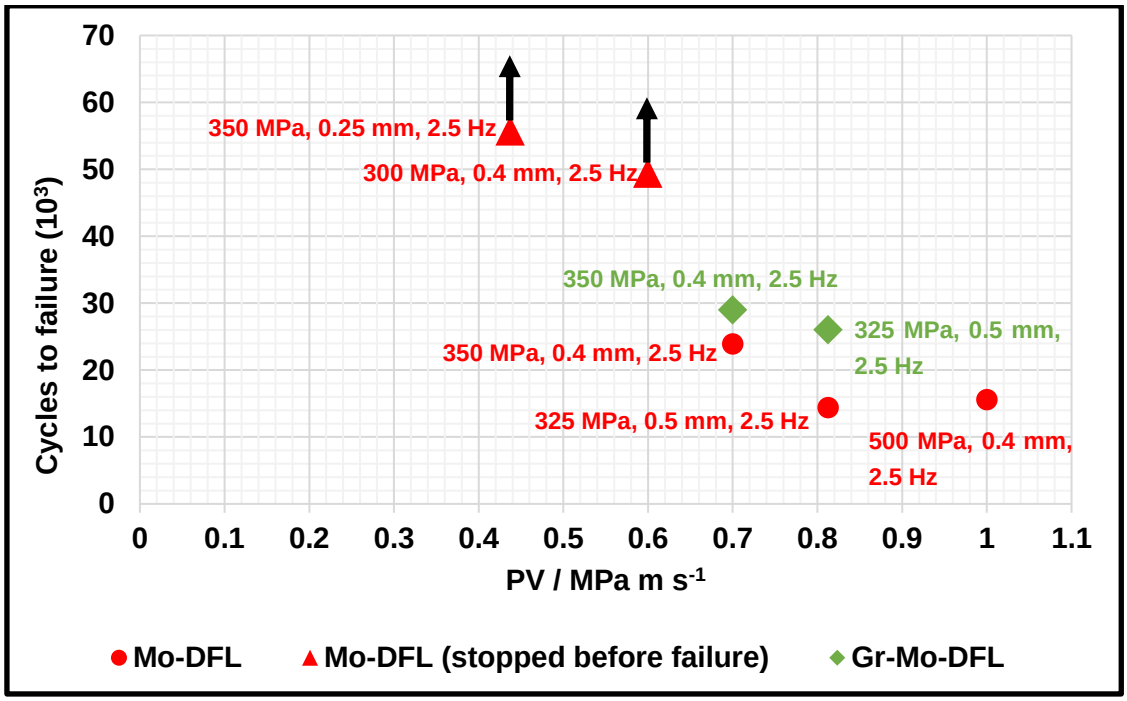


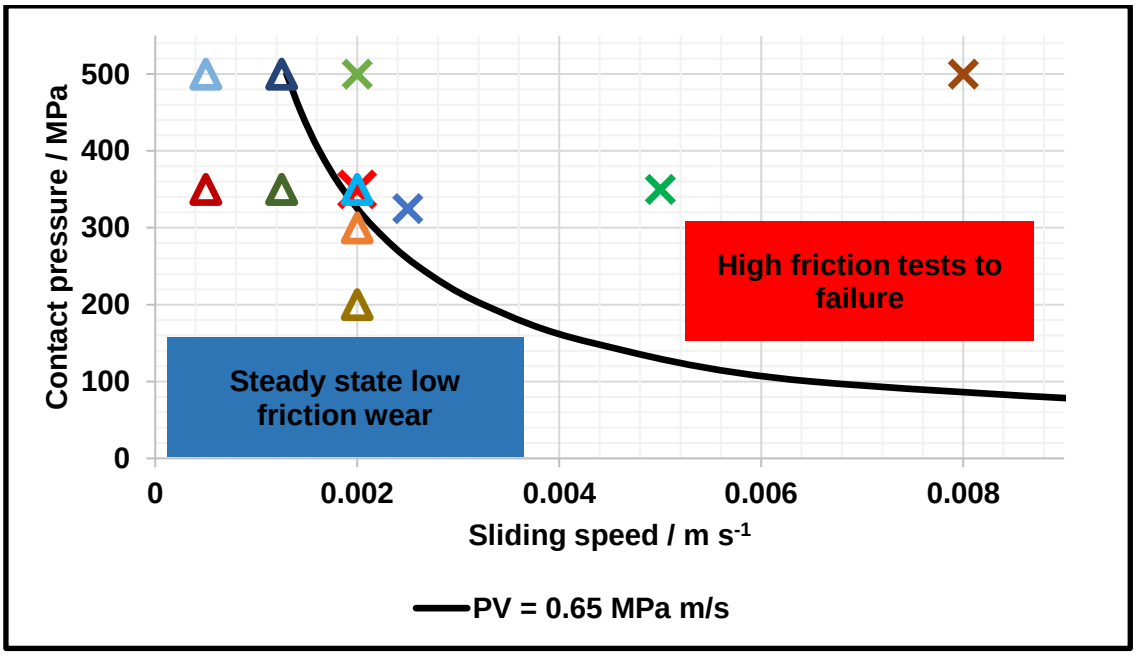
Figure 6.7 Evolution of CoF against number of cycles for fretting tests conducted on flat-on-flat contact configuration for Mo-DFL and Gr-Mo-DFL which were deposited on top of a Cu-Ni-In under-layer. Performance is compared under two different fretting loading conditions.

With a wider range of loading conditions, the PV threshold concept (previously proposed in Section 6.2) is examined on flat contact configuration. Figure 6.8a shows the fretting cycles against the respective PV values of the tests. At PV values of 0.6 MPa m s^{-1} and below, steady state low friction wear is observed, whereas when PV = 0.7 MPa m s^{-1} and above, the behaviour transitions to one where high friction tests to failure are observed. In light of the limited data available, an estimate of a PV limit of ~ 0.65 MPa m s^{-1} is made for the Mo-DFL coating system tested on the flat-on-flat contact configuration.

Figure 6.8b shows the graph with the proposed threshold limit PV value of 0.65 MPa m s^{-1} and highlights combinations of contact pressure and sliding speeds that lead to the observed fretting wear behaviour associated with high friction tests to failure and steady state low friction tests. Fretting tests of varying loading conditions and combinations of normal load and applied displacement amplitudes are plotted on this graph which shows the vast majority of tests, where the test conditions result in a PV value below the proposed threshold limit of 0.65 MPa m s^{-1}, undergo a steady state low friction behaviour, whereas those where PV is above the threshold limit result in high friction tests to failure. This observation adds weight to the concept of the type of failure being associated with the PV of the contact under a specific fretting contact geometry.



(a)



(b)

Figure 6.8 (a) Cycles to failure as a function of the PV value for tests conducted on flat-on-flat contact configuration for both Mo-DFL and Gr-Mo-DFL (b) Map of failure mode for tests as a function of sliding speed and contact pressure for tests with Mo-DFL conducted with the flat-on-flat test setup. The line where PV = 0.65 MPa m s^{-1} is superimposed and is seen to provide a clear boundary between regimes.

In Figure 6.9, BSE SEM images and EDX analysis are presented from a Mo-DFL sample where a steady state low friction wear was observed and where the test was stopped at 50 k cycles before failure had occurred. Bright dotted areas as well as darker regions are observed on the sample surface (Figure 6.9a). EDX mapping of the same surface (Figure 6.9b) shows the surface to be composed of dotted areas of Cu (indicative of removal of the DFL to the point where the Cu-Ni-In is exposed) whilst a large majority of the surface is rich in Mo, indicating that the Mo-DFL coating is still intact in these areas. Figure 6.9c shows the cross-sectional BSE SEM image of the specimen (with higher magnification in the vertical than in the horizontal direction) where a small amount of Mo-DFL can be seen to remain on the top surface of the Cu-Ni-In under-layer, with some exposure of the Cu-Ni-In at the surface but without significant recession into the Cu-Ni-In layer.

The wear specimen of a test which underwent a high friction test to failure was analysed, with results presented in Figure 6.10 where the plan-view BSE SEM images and corresponding EDX mapping images of the surface are presented. A region with a high Mo content is shown to remain in the central region of the test sample; however, BSE imaging indicated that the surrounding area is largely metallic (much higher contrast), with this region being rich in Cu and Ti, which are assumed to be the exposed Cu-Ni-In sub-layer with titanium indicating that the substrate material of one of the samples has been involved in the wearing process. In Figure 6.10c, the cross-sectional BSE SEM image of the sample can be observed which shows the complete wear of Mo-DFL material to have taken place as well as the wear of the Cu-Ni-In under-layer which has been completely worn through in some areas to reveal the titanium alloy substrate.

Figure 6.10d shows a line profile comparison of the steady state low friction wear specimen and the high friction to failure specimens where the low wear depth following steady state wear can be observed at the time the test was stopped at 50 k cycles. A much greater wear depth is observed on the profile for the high friction test to failure. The edges of the profile look to be more worn with higher depths than the central region which gives the profile a ‘W’ shape as reported in [81] for flat-on-flat contacts undergoing adhesive wear behaviour.

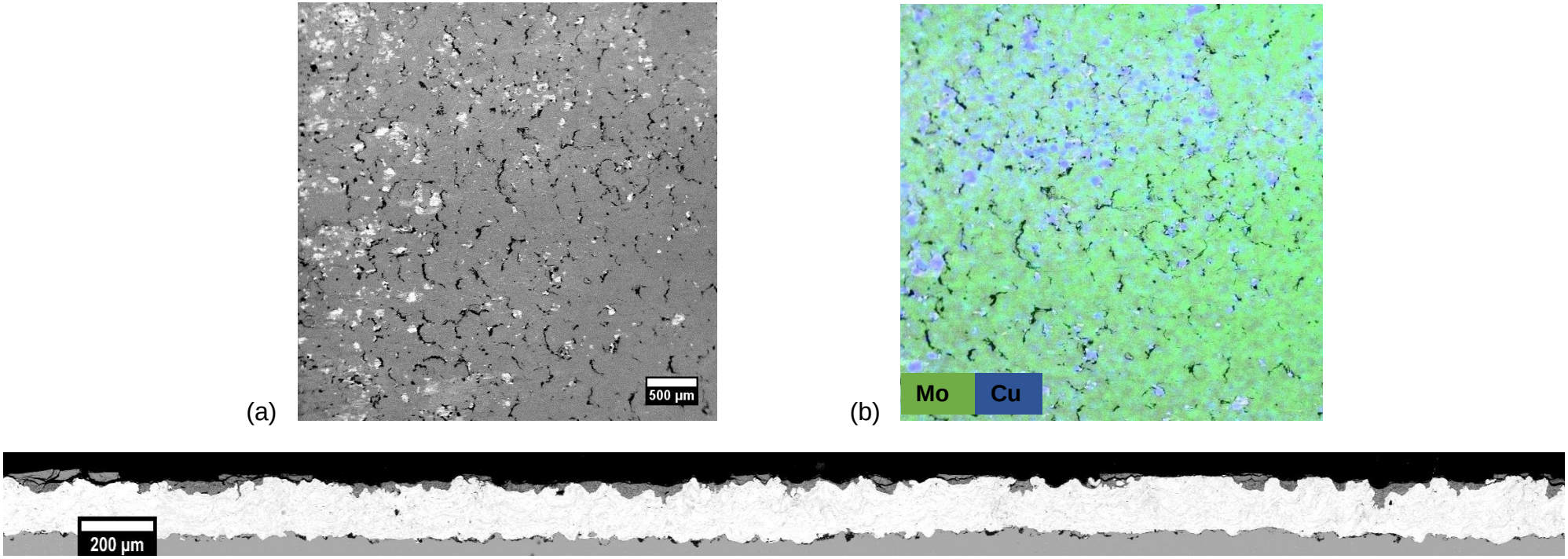
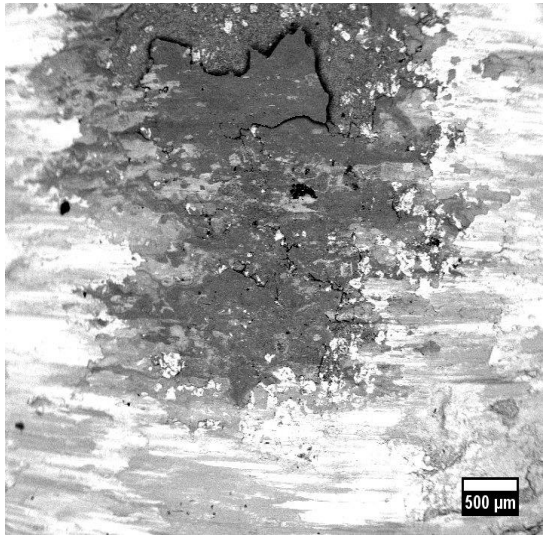
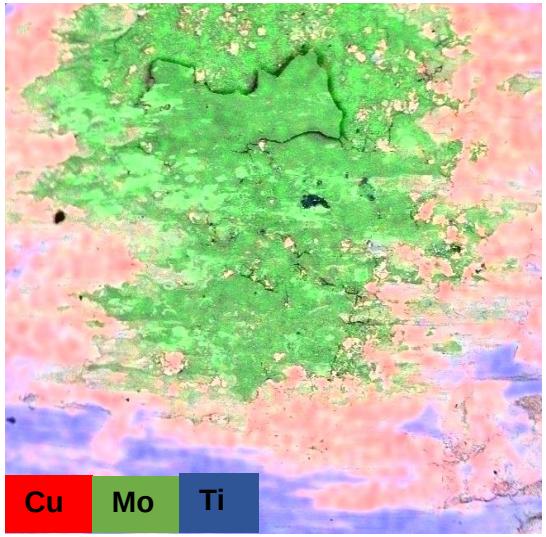


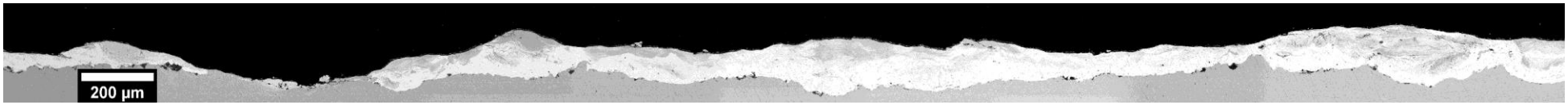
Figure 6.9 BSE SEM images of the wear specimen of the Mo-DFL system tested on flat-on- flat contact undergoing a steady state low friction wear behaviour which was stopped at 50 k cycles (a) plan-view BSE image of the wear sample surface (b) EDX mapping highlighting Mo and Cu contents on the wear sample surface (c) Cross sectional BSE SEM fretting wear scar images of flat samples.

(a)

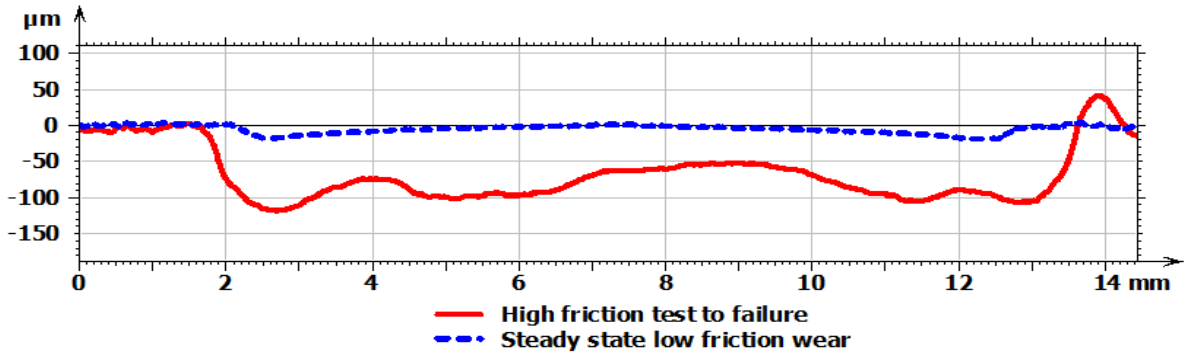


(b)





(c)



(d)

Figure 6.10 BSE SEM images of the wear specimen of the Mo-DFL system tested on flat-on- flat contact undergoing a high friction test to failure wear behaviour (a) plan-view BSE image of the wear sample surface (b) EDX mapping highlighting Mo, Cu, Ti contents on the wear sample surface (c) Cross sectional BSE SEM fretting wear scar images of flat samples, (d) Averaged wear profiles of the steady state low friction wear and high friction test to failure wear.

Accompanying the wear specimen characterisation is associated thermal analysis. Figure 6.11 shows an example of a thermal image captured during a fretting wear test undergoing steady state low friction behaviour that was stopped at 50 k cycles. The thermal camera records the temperature at the edge of the contact interface during the fretting tests and not the temperature of the contact interface (which is obscured during a test).

Figure 6.12 displays the evolution of friction against exposure for tests of Mo-DFL at varying PV values with the maximum temperatures captured by the thermal camera at specific points within the tests presented alongside. When $PV = 0.6$ MPa m s^{-1}, the observed steady state low friction wear shows a stable temperature near the contact interface that ranges between 47 – 52 °C. When $PV \geq 0.7$ MPa m s^{-1}, high friction tests to failure show a rise in temperature near the contact interface which corresponds the increasing coefficient of friction.

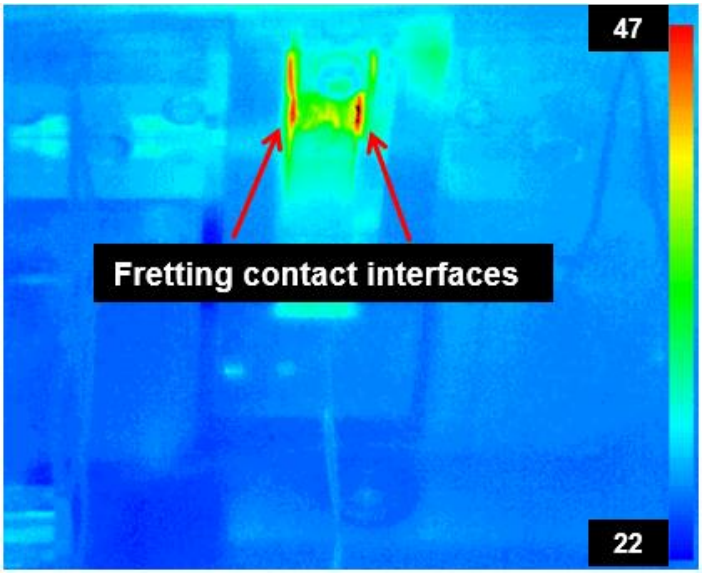


Figure 6.11 An example of the thermal image captured prior to when a steady state low friction wear test was stopped at 50 k cycles. The image captures a side on view of the fretting wear interface and temperatures at the edge of the contacting surface and not the direct contact interface are recorded.

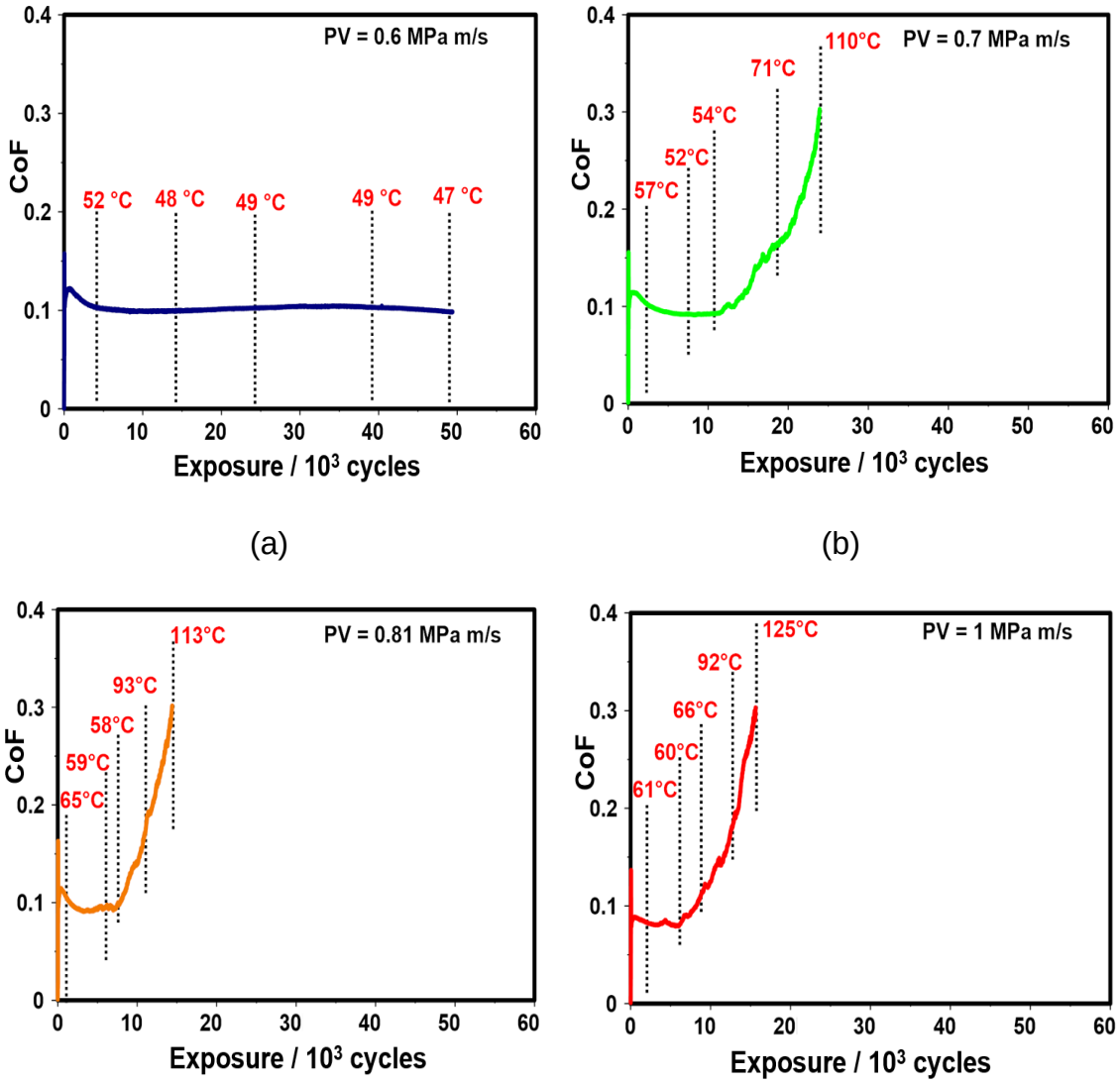


Figure 6.12 Evolution of CoF against number of cycles for fretting tests with the Mo-DFL system deposited on top of a Cu-Ni-In under-layer and conducted on the flat-on-flat contact configuration showing the recorded temperature near the contact interface by a thermal camera at intervening stages of fretting wear lifetimes at different PV values of (a) 0.6, (b) 0.7, (c) 0.81, and (d) 1.

6.4 Discussion

6.4.1 Cylinder-on-flat and flat-on-flat fretting wear behaviour

Initial fretting wear tests on a cylinder-on-flat contact with a normal load of 575 N, an applied displacement amplitude of 0.3 mm and a frequency of 2.5 Hz demonstrated that the durable low friction and low wear features of the Gr-Mo-DFL coating system previously observed on self-mated grit-blasted specimens (Figure 4.3) could also be realised when the DFL was deposited onto a Cu-Ni-In under-layer; it continued to yield significant extension of fretting lifetime and facilitated maintenance of a stable low ECoF ~ 0.25 for the duration of the fretting test which was stopped at 1570 k cycles (before failure occurred) as seen in Figure 6.1. The Mo-DFL however, exhibited system failure at 615 k cycles which suggests that the combination of graphite + MoS_2 is a viable solution to improve the performance of a DFL in accord with the previous work conducted at The University of Nottingham [234].

However, increasing the normal load applied from 575 N to 1000 N in the cylinder-on-flat tests (which increases the initial Hertzian contact pressure 183 MPa to 241 MPa) resulted in the failure of the Gr-Mo-DFL coating system at 905 k cycles (Figure 6.4b). Furthermore, an increase in the applied displacement from 0.3 mm 0.4 mm resulted in an even shorter lifetime of 547 k cycles. With this, two friction-wear behaviours were observed as a function of the imposed loading condition, namely (i) a steady state low friction wear and (ii) high friction tests to failure. A threshold limit is proposed whereby under the threshold limit, a steady state low friction wear is observed with wear characteristic and features similar to those seen in Figure 6.3 where DFL material still occupies the top surface of the Cu-Ni-In coating. The wear behaviour above the threshold leads to high friction and failure is observed to have wear features as seen in Figure 6.2, by which, minimal DFL material remains on the worn surface with a pronounced wear depth into the thermally sprayed Cu-Ni-In under-layer being observed.

It is proposed that a PV limit is useful to describe the threshold limit which can be used as a performance criterion and represents a limiting value for maximum allowable pressure of contact versus sliding speed under normal running conditions of polymer materials [208], [210]. In Figure 6.5, the corresponding PV values of the fretting testing conditions of both the Mo-DFL and Gr-Mo-DFL coating systems on cylinder-on-flat contact can be seen. At a PV value

of 0.274 MPa m s^{-1}, the fretting wear test on Gr-Mo-DFL exhibited a steady state low friction wear behaviour where a low friction phase dominated the evolution of friction for the entire duration of the test which did not reach failure and was therefore stopped at 1570 k cycles as shown in Figure 6.4b. At the same PV value, the Mo-DFL coating system failed at 615 k cycles which shows each DFL coating system (Mo-DFL and Gr-Mo-DFL) to have different PV limits with the graphite modified Gr-Mo-DFL increasing the threshold limit for better fretting wear performance and extended lifetimes. By increasing the loading conditions on the Gr-Mo-DFL system from PV ~ 0.274 to PV ~ 0.361 MPa m s^{-1}, failure occurs which suggests the threshold limit associated with the coating system lay between these two values. Reducing the normal applied load from 575 N to 144 N (which corresponds to approximate initial Hertzian contact pressures of 183 MPa to 91.5 MPa respectfully) and reduced the PV value (from 0.274 to 0.137 MPa m s^{-1}) on the Mo-DFL coating system resulted in the increase of fretting lifetimes from 615 k cycles to 765 k cycle (Figure 6.4a), however a steady state low friction wear behaviour was not observed (Figure 6.5) suggesting a different threshold PV value for the graphite free Mo-DFL on the cylinder-on-flat contact.

Fretting wear tests of the Mo-DFL coating system conducted on a flat-on-flat contact configuration showed that increasing the contact pressure (Figure 6.6a) and applied displacement (Figure 6.6b) leads to a shorter fretting lifetime. The previously observed (on a cylinder-on-flat contact) fretting wear behaviours of steady state low friction wear and high friction tests to failure were also observed with a flat-on-flat contact configuration as a function of the imposed loading condition.

Although lower friction and marginally increased performance was observed for the graphite-modified Gr-Mo-DFL coating system (Figure 6.7) on the flat-on-flat contact, the extended low friction phase was not exhibited which indicates that at the imposed loading conditions, the threshold limit for the Gr-Mo-DFL coating system had already been surpassed.

Figure 6.8 details the corresponding PV values for conducted fretting wear tests. At PV values of ~ 0.6 MPa m s^{-1} and below, a steady state low friction wear behaviour occurs where extended fretting lifetimes are observed. At increased PV values of 0.7 MPa m s^{-1} and above, high friction tests to failure were initiated on the Mo-DFL coating system. A proposed threshold limit for the Mo-DFL coating system on the flat-on-flat contact testing configuration is proposed to exist between the PV values of 0.6 and 0.7 MPa m s^{-1} as shown in Figure 6.8a.

In Figure 6.8b, Mo-DFL fretting wear tests conducted on the flat-on-flat contact configuration over a range of different applied pressures and sliding velocities (i.e. various PV values) are presented as a map with an indication of the failure mode in each case. With a proposed threshold limit of $PV = 0.65$ MPa m s^{-1} as suggested in the previous paragraph, fretting tests where test conditions were such that PV fell below this value displayed a steady state low friction wear behaviour which meant that they ran for extended periods and were typically stopped before failure occurred. Where tests conditions resulted in a PV value above the threshold value of 0.65 MPa m s^{-1}, tests exhibited the wear behaviour which led to high friction and relatively rapid failure. This demonstrates that the proposed threshold limit has merit in separating and classifying the different operational fretting wear behaviours (namely steady state low friction or high friction test to failure) based on the imposed fretting loading condition.

In a previous study by Fouvry and Paulin [114] that investigated fretting wear behaviour of polymer-bonded MoS_2 coating and implemented a PV power factor. Two friction responses were observed which depended on the imposed contact pressure and sliding amplitude conditions which suggested that the intrinsic wear resistance of the bonded MoS_2 coating is mainly controlled by the damage process activated within the interface and therefore depends on dissipated power condition. In lower pressure conditions (under 500 MPa), *Friction Response Type I* displayed an initial low friction period plateau of 0.3 before sharply increasing to 0.8. With higher contact pressure and sliding amplitudes, *Friction Response Type II* was activated which was characterised by a sharp increase of friction (from CoF 0.1 to 0.7) without any low friction plateau. This is in line with current observations with the recognition of two fretting wear behaviours which has been identified as a common behaviour on two different fretting rig systems and contact configurations.

In Figure 6.8b, at PV = 0.7 MPa m s^{-1}, the two proposed fretting wear behaviours were both observed indicating that PV is not a fully sufficient criterion to determine the operative behaviour. A steady state low friction wear occurred from a test conducted with a contact pressure of 350 MPa, an applied displacement of 0.1 mm at a frequency of 10 Hz and a high friction test to failure was initiated with the same contact pressure of 350 MPa, but an applied displacement of 0.4 mm and a frequency of 2.5 Hz. Although the same PV value exists which corresponds to 0.7 MPa m s^{-1} for both tests, different wear behaviours were observed. This suggests that, while the threshold PV concept has been useful in determining the

transitional limits of the DFL fretting wear behaviours from a steady state low friction behaviour (where tests were stopped before failure) to high friction tests to failure, lower contact pressures and applied displacements with higher frequencies can however have less severe effects and maintain the steady state low friction wear whilst; higher contact pressures and applied displacements with lower frequencies could have more severe effects at the contact interface to initiate high friction tests to failure.

As seen in Figure 6.12a, large temperature variations were not observed near the contacting surface of the steady-state low friction wear behaviour when PV = 0.6 MPa m s^{-1} (below the proposed threshold limit when $PV < 0.65$ MPa m s^{-1}). This corresponds with SEM and EDX mapping of steady state low friction wear behaviour as shown in Figure 6.9, whereupon the termination of the fretting test at 50 k cycles, a considerable amount of Mo-DFL material at the contacting surface remained. The Mo-DFL material is shown to still occupy the contacting surface and with this; continue to deliver a stable low friction phase of ~ 0.1 as well as a steady temperature ~ 50 °C (Figure 6.12a) near the contact interface which is maintained before the test is stopped.

Above the proposed threshold limit (when PV > 0.65 MPa m s^{-1}), high friction tests to failure were initiated where the initial low friction plateau had a CoF ~ 0.1 and a stable temperature ~ 60 °C (Figure 6.12b, c & d). As friction rises, the temperature near the contact interface is also shown to increase and upon failure when CoF ~ 0.3, the highest temperature of ~ 115 °C was recorded (Figure 6.12b, c & d). Wear samples from a high friction test to failure test in Figure 6.10 show that significant wear of the Mo-DFL material had occurred on the surface to expose the Cu-Ni-In under-layer along with Ti-6Al-4V substrate upon failure.

The relative surface concentration of the low friction plateau prior to rapid rise of friction is largely made up of MoS_2 material and the increase in friction coefficient was proposed to be related to an asymptotic increase in Cu-Ni-In concentration and symmetrical reduction in MoS_2 component [114]. The rise of temperature near the contact interface is thought to be a result of the ongoing fretting wear process relating to the elimination of the low friction MoS_2-based DFL at the contact interface and the progressive exposure of the Cu-Ni-In sub-layer which leads to a rise in friction.

6.5 Conclusion

Comprehensive experimental fretting wear tests have so far been useful to identify and analyse the influence of fretting loading conditions that alter the wear behaviours of the DFL coated systems. Through this, the following conclusions can be made:

- The durable low friction characteristics of the graphite-modified Gr-Mo-DFL coating system are also observed following its deposition onto Cu-Ni-In surface conditions where it continues to yield significant extension of fretting lifetime. However, under increasingly severe loading conditions, extended low friction and wear capabilities of the Gr-Mo-DFL coating system were not achieved on either the cylinder-on-flat or the flat-on-flat contact configurations.
- Two fretting wear behaviours were identified for the polymer-bonded DFLs on the cylinder-on-flat and flat-on-flat fretting wear systems; a steady state low friction wear and, high friction tests to failure which were observed to exist above a certain PV threshold limit. The fretting wear behaviours have been established as common across two experimental fretting rig contact configurations.
- Under a proposed PV threshold limit, a steady state low friction wear behaviour was observed which is characterised by extended fretting lifetimes, low friction and low wear of the DFL material which was observed to still occupy the wear interface of the testing specimen when the tests are stopped before failure. A stable temperature ~ 50 °C was recorded near the contact interface for the fretting lifetime duration.
- Above the PV threshold, high friction tests to failure were observed which was characterised by severe wear at the contacting surface and complete wear of the DFL upon failure. Increased friction was followed by a rise in temperature near the contacting surface.

Chapter 7. Case Study: Aero-engine fan blade root component wear analysis

Initial analysis of a fan-blade root following normal commercial service was undertaken to observe the damage and wear features which might occur under such conditions. However, as this examination only applies to a single fan blade root, it is recognised that the damage observed may not be typical of all blade types and all service conditions. The service history and loading characteristics for the fan blade root examined were not available. This work, however, does provide an initial analysis of a fan blade root and allows observations of in-service damage to the DFL systems to be compared to the damage observed following laboratory tests (both cylinder-on-flat and flat-on-flat) which have been presented earlier in this thesis. A full blade was provided from which the root section was removed for analysis and two separate sections were analysed on the as removed fan-blade root.

In Figure 7.1, the topographical analysis of *section I* is presented; a front facing optical image of the analysed section is presented in Figure 7.1a where the contacting root wear surface of the section is observed. Two distinct regions are observed on the root, namely a bright region and a darker region. A corresponding surface profile of the entire section is presented in Figure 7.1b where there are again two distinct regions on the surface that correspond to the surface height (shown on the colour scale) which are separated by ~ 50 µm. This was confirmed via a single line profile (Figure 7.1c) taken across the surface from the location as indicated in Figure 7.1b; here, the step change in the surface height can again be observed. This initial analysis of the fan blade root section indicates that a process of DFL delamination is taking place on the fan blade root surface; in some areas, the DFL appears undamaged with a smooth surface, whilst it appears to be entirely absent in others, with a step change between them.

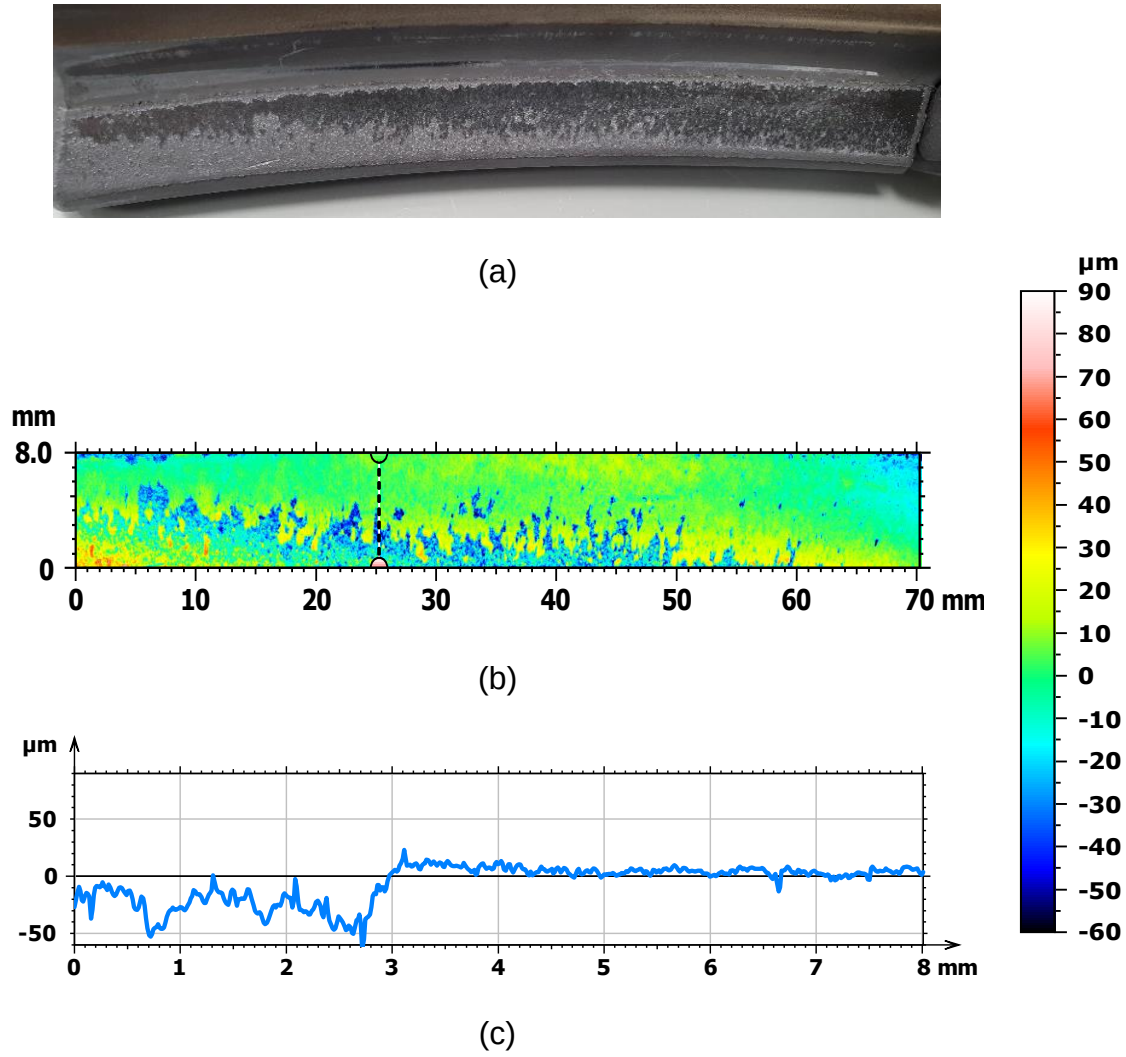


Figure 7.1 Wear surface analysis of the fan blade root section I which features, (a) Image of section I (b) Topographical analysis with a sectioned line profile (c) Corresponding line profile result.

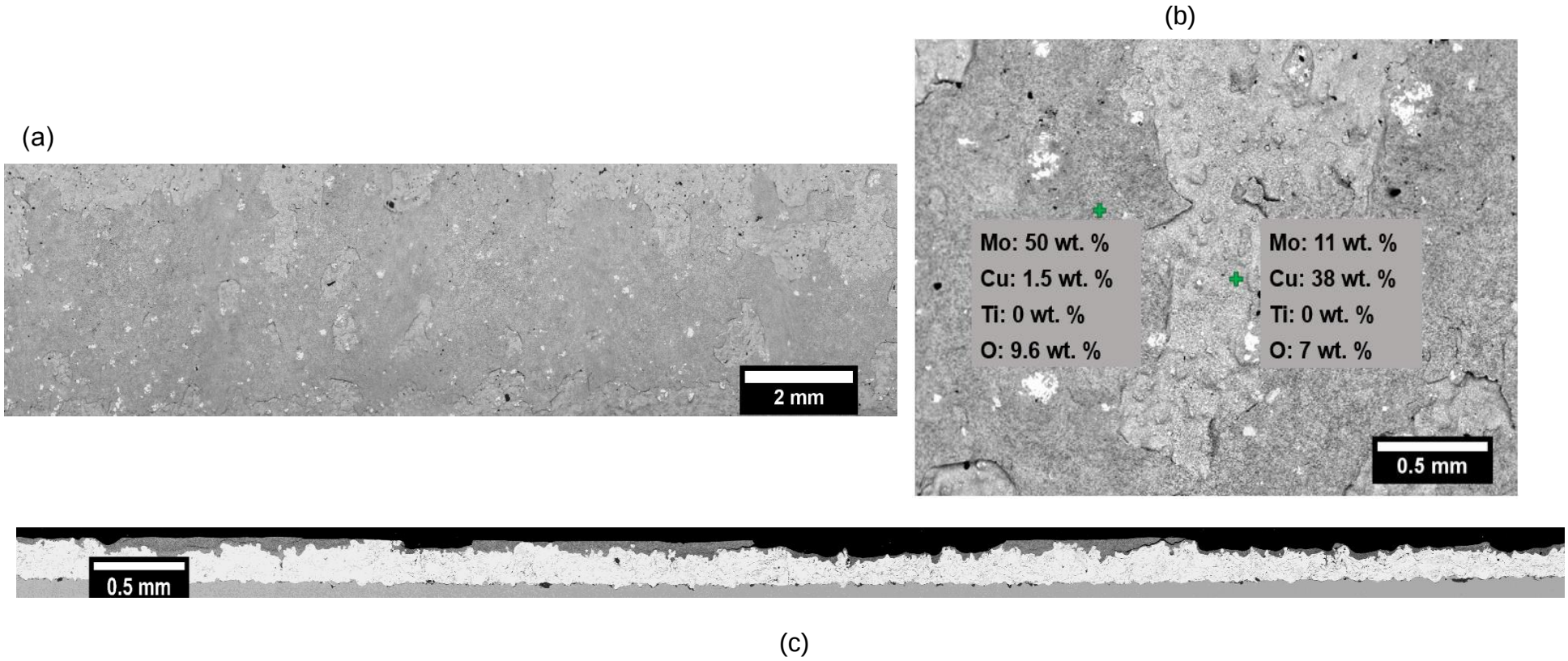


Figure 7.2 BSE SEM images of section I of the fan blade root (a) low magnification plan-view image of the section wear surface (b) high magnification area with EDX point analysis of the wear surface (c) cross-sectional BSE SEM image of fan blade root section I.

Further analysis of the fan blade root required analysis of a smaller metallographically prepared specimen. A low magnification BSE SEM plan-view image of the fan blade root surface is shown in Figure 7.2a. With increased magnification (Figure 7.2b), clear features of the surface can be observed that correlate with the information presented in Figure 7.1. EDX point analysis showed the darker contrast material to have a high Mo content (~ 50 wt. %) along with traces of Cu (1.5 wt. %) and oxygen (~ 9.6 wt. %). The brighter region was shown to have a higher Cu composition (~ 38 wt. %) and lower Mo (~ 11 wt. %) content along with evidence of some oxygen (~ 7 wt. %). No evidence of Ti was found via either of the point analyses.

A BSE SEM image of a metallographic cross-section is presented in Figure 7.2c; from this, it can be inferred that the material making up the higher plateau regions in Figure 7.1c are covered by Mo-DFL of ~ 50 µm thickness, whilst in the lower regions, the bulk of the Mo-DFL has been removed and only a thin layer (~ 10 – 25 µm) of the Mo-DFL coating remains attached to the Cu-Ni-In under-layer. The thin remaining Mo-DFL layer appears to follow the original profile of the rough Cu-Ni-In interface. Furthermore, cracks through the Mo-DFL coating can be made out from the cross-sectional images, which indicate that the removal of the Mo-DFL has taken place by cracking and delamination rather than by attritive wear.

In Figure 7.3, topographical analysis which was undertaken on *section II* of the fan blade root is presented. Noticeably different surface features can be observed in comparison with *section I* with a smooth region making up the bulk of the surface as confirmed by the surface profile and the corresponding line profile (Figure 7.3b & c) where apart from the surface edge, a smooth ‘u’ shaped form exists.

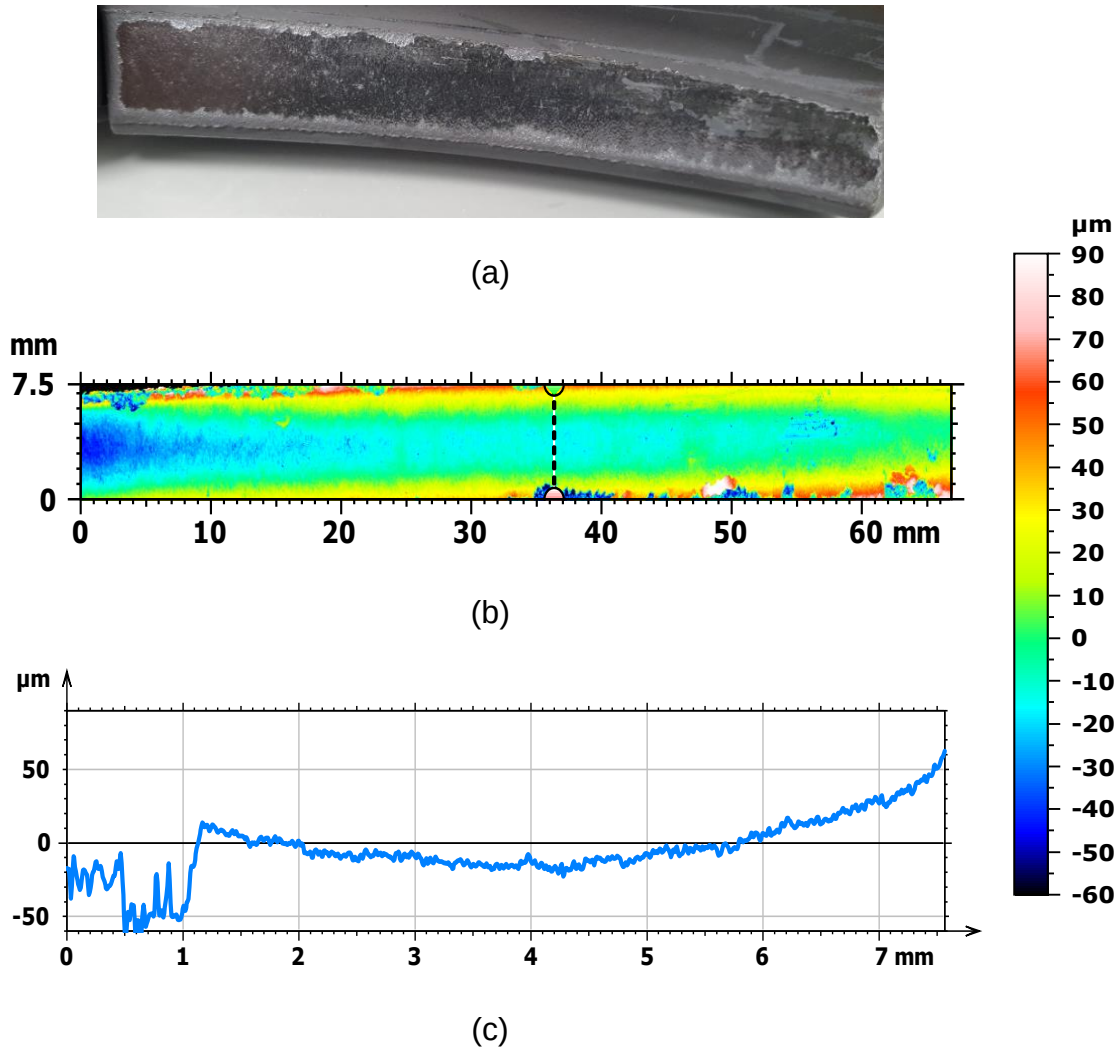


Figure 7.3 Wear surface analysis of the fan blade root section II which features, (a) Image of section II (b) topographical analysis with a sectioned line profile (c) corresponding line profile result.

Figure 7.4a & b displays plan-view BSE SEM images from this section where the large smooth interface is observed with corners and edges of the surface exhibiting a much rougher surface profile. The compositions of these two surfaces were measured by EDX analysis with results as presented in Figure 7.4b. EDX point analysis showed the smooth region to have a high Mo content (~ 45 wt. %) along with traces of Cu (0.65 wt. %) and oxygen (~ 15 wt. %). EDX point analysis on a peak in the rougher region was shown to have slightly lower Mo composition (~ 40 wt. %) and higher Cu (~ 6.25 wt. %) content along with evidence of some oxygen (~ 14 wt. %). EDX point analysis on a bright region in the rough region showed a high Cu (~ 57 wt. %) some oxygen (~ 2.5 wt. %) and no evidence of Mo.

in Figure 7.4c, the cross sectional BSE SEM image of this section can be observed; an area with a full as-deposited (~ 50 µm) thickness of the Mo-DFL material can be seen on top of the Cu-Ni-In layer with the surrounding area only exhibiting the thin layer of DFL which is, again, seen to broadly contour around the original profile of the underlying Cu-Ni-In layer. A notable crack going through the Mo-DFL coating can be observed which appears to propagate within the Mo-DFL coating itself close to the Mo-DFL/Cu-Ni-In interface and broadly following that original Cu-Ni-In topography. A portion of the cracked Mo-DFL coating can be seen which has separated from bulk of the Mo-DFL (i.e. it has delaminated) with a thin layer (~ 10 - 20 µm) of Mo-DFL material remaining below it on the rough Cu-Ni-In interface. In Figure 7.5, high magnification cross-sectional SE SEM images of the cracks within the Mo-DFL coating are presented. Very little plastic deformation of the Mo-DFL on either side of a crack can be observed indicating that these are brittle fractures of the coating, either driven by fast fracture or fatigue.

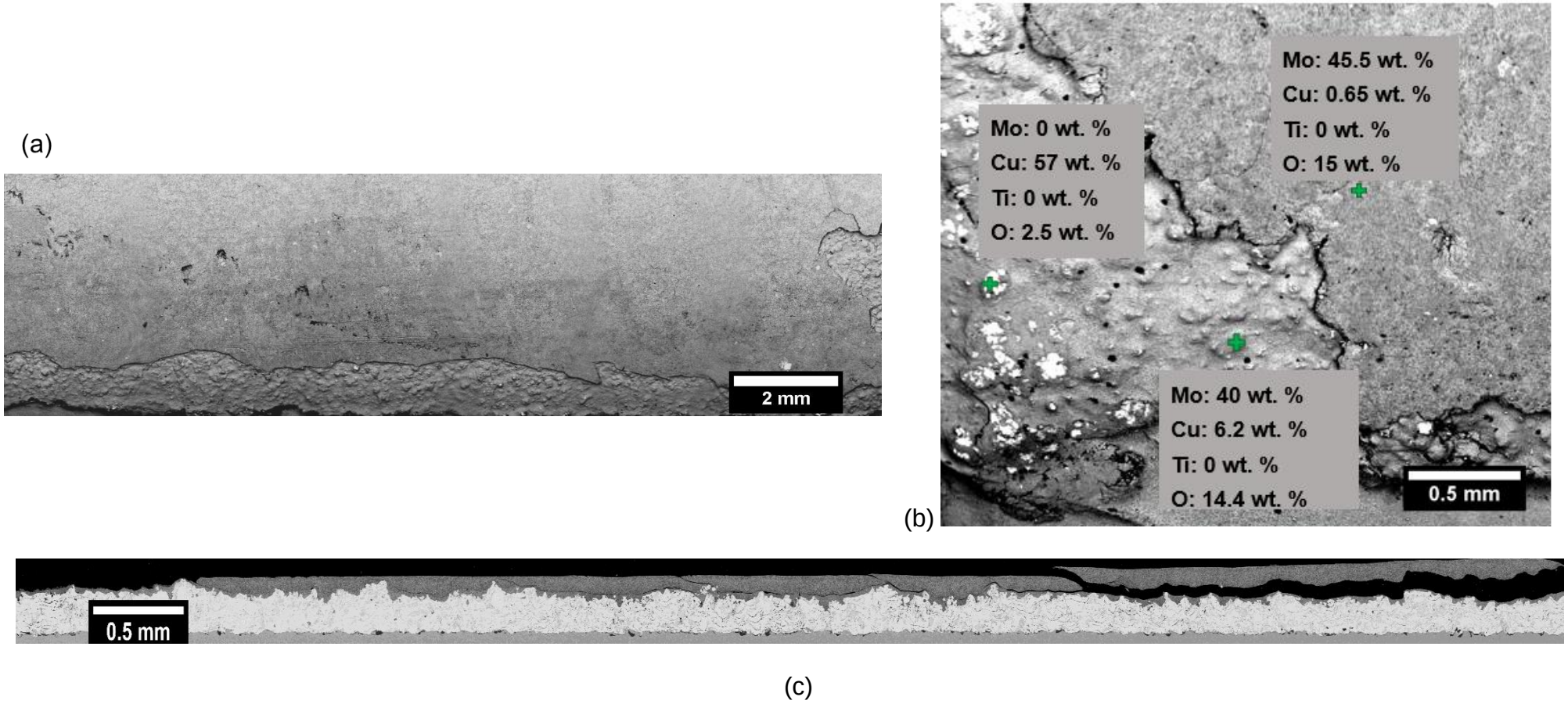


Figure 7.4 BSE SEM images of section II of the fan blade root (a) low magnification plan-view image of the section wear surface (b) high magnification area with EDX point analysis of the wear surface (c) cross-sectional BSE SEM image of fan blade root section II.

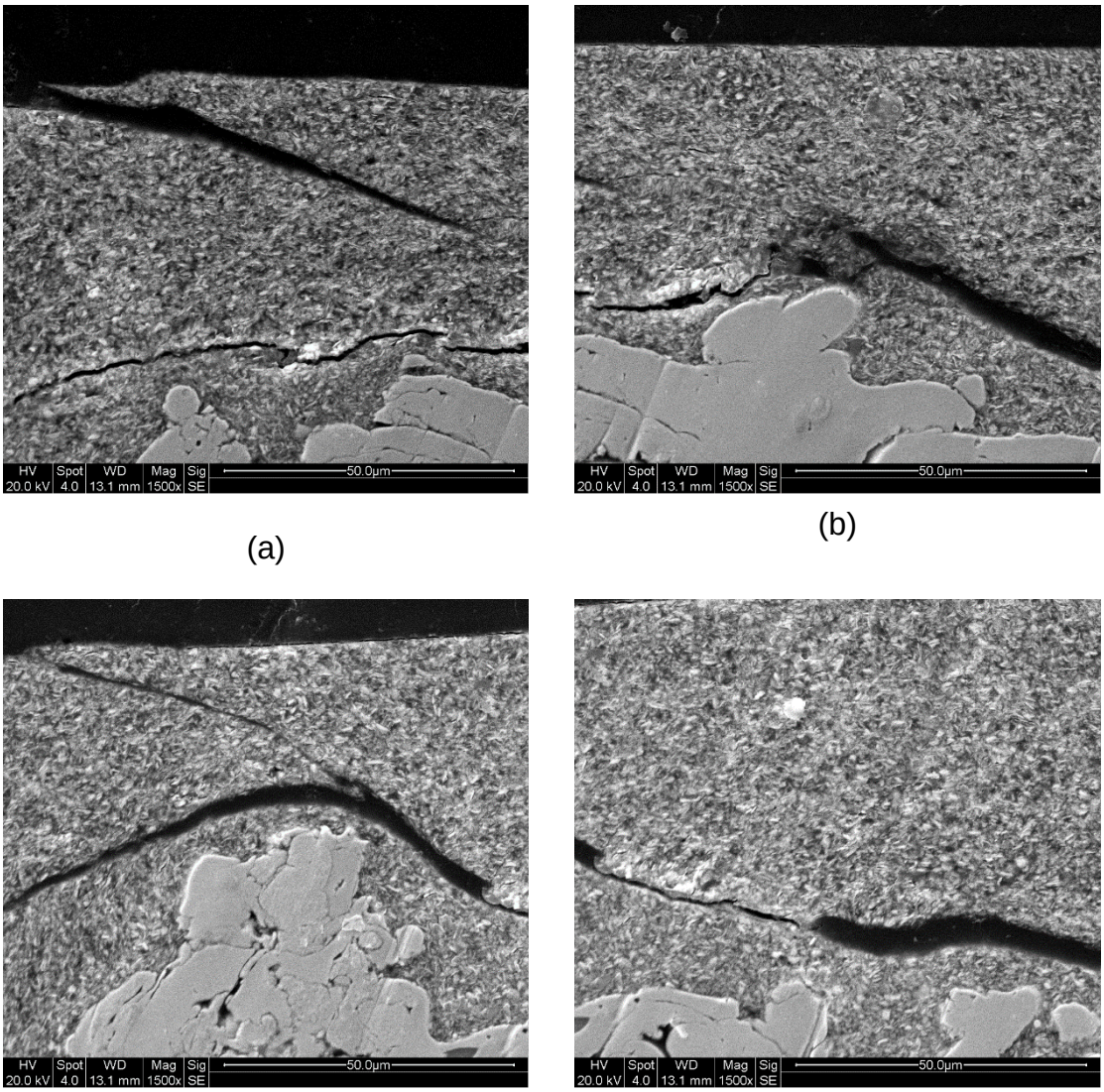


Figure 7.5 High magnification cross-sectional SE SEM images of crack regions on the Mo-DFL coating on fan blade root section II.

7.1 Discussion

Two different sections have been analysed from a single fan blade root. Similar wear features and characteristics have been observed on the surfaces of the individual sections where two regions were identified in the topographical analysis shown in Figure 7.1 and Figure 7.3 for the respective fan blade root sections.

This comprised of a smooth top interface and, with a step height difference ~ 50 µm (Figure 7.1c and Figure 7.3c) an underlying rougher interface was observed. Cross sectional BSE SEM images of the fan blade section as presented in Figure 7.2c and Figure 7.4c, showed regions of thick Mo-DFL coating layer ~ 50 µm and regions where only thin layer of Mo-DFL material is retained which covers the rough Cu-Ni-In interface and follows its topography.

Cracks within the Mo-DFL coating which were observed to propagate along the DFL/Cu-Ni-In interface have also been identified in the examined fan blade root sections and are presented in the cross-sectional BSE SEM images in Figure 7.2c and Figure 7.4c. Complete separation of the DFL coating from the Cu-Ni-In interface is shown in Figure 7.4c where the fractured DFL is separated along the rough interfacial geometry of the underlying Cu-Ni-In interface. In both sections however, no evidence of wear, deformation, or fracture is observed on the underlying Cu-Ni-In layer which looks to remain intact and unaffected by the identified cracks within the Mo-DFL coating. High magnification cross-sectional SE SEM images presented in Figure 7.5 show the propagation and intersection of smaller and larger cracks through the Mo-DFL coating which converge along at the rough Cu-Ni-In interface.

Experimental fretting wear testing samples have been shown to undergo a progressive wear and elimination of the Mo-DFL coating followed by the deformation and wear of the underlying Cu-Ni-In coating as observed in the both cylinder-on-flat (Figure 6.2) and the flat-on-flat contact (Figure 6.10) test geometries. These wear features and failure process have not been observed in the analysed fan blade root sections. Conversely, the nucleation and propagation of cracks within the Mo-DFL coating which was observed to cause DFL separation from the rough Cu-Ni-In interface as shown on fan blade root sections (Figure 7.4c) were not observed in laboratory tests conducted with either the cylinder-on-flat or flat-on-flat test geometries.

The observed cracking identified in the MoS_2 layer on the fan blade root is very different from that of the cracked-paved structure observed at the wear interface of Mo-DFL tests in low-humidity air (Figure 4.5) and at the Gr-Mo-DFL wear interface during an extended low friction phase (Figure 6.3a); no cracked-paved structure was observed on the wear surface of the fan blade root as observed in Figure 7.2a and Figure 7.4a. This suggests that different damage mechanisms of the polymer-bonded MoS_2-based DFL coating are operational in actual service conditions. It should however be noted that the fan blade root analysis had been conducted on a single fan blade root and that to generalise these observations, analysis of further fan blade roots would be useful.

7.2 Conclusion

Fracture and coating delamination has been observed within the Mo-DFL coating on sections from a post-service fan blade root component. Propagation of the cracks followed the rough Cu-Ni-In interface by ~ 20 µm within the Mo-DFL itself; this has shown to enable the separation of the DFL coating from the Cu-Ni-In under-layer. This occurrence has not been observed in the experimental fretting wear samples on either the cylinder-on-flat or the flat-on-flat contact configurations which suggests the possibility of additional damage mechanisms in operational conditions. Moreover, the value of the laboratory tests (cylinder-on-flat or flat-on-flat) as a means to identify the optimum DFL is called into question since different failure mechanisms are operative.

Chapter 8. Summary and Conclusion

The effects of the fretting conditions that influence the wear behaviours and lifetime of aero-engine DFL systems can include the environmental conditions, substrate surface conditions, and fretting loading conditions, all of which have been examined in this work to better understand the mechanisms by which extended fretting lifetimes could be attained. Results from this study have showed that at certain fretting conditions, significant lifetime extension, wear durability and stable low friction wear behaviours of the polymer-bonded DFL coating system can be achieved.

This has been demonstrated in Chapter 4 where the effects of humidity and oxygen on a polymer-bonded MoS_2-based DFL (Mo-DFL) were investigated. It was found that humidity can drastically impact the fretting wear behaviour and have substantial influences on the fretting lifetimes and durability of the Mo-DFL coating system. In low humidity conditions (0.5 – 3 % RH), significant fretting lifetime extension and a sustained low friction phase with reduced wear and minimal surface damage was achieved with and without the presence of oxygen in the environment. As humidity levels was increased, a noticeable correlated rise of the friction and wear was also observed on the Mo-DFL coating system which reduced the overall durability and performance of the coating system.

This work provides a unique contribution to the ongoing discourse in literature regarding the role of humidity on MoS_2-based coatings and the mechanisms that drive their degradation and wear. This has been achieved by investigating the separate effects of water and oxygen on a polymer-bonded MoS_2-based coating in extreme low and high humidity conditions to determine their specific influences on the DFL coating. Previous works that have investigated the effects of humidity on polymer bonded MoS_2 DFL coatings have typically conducted experiments at humidity levels of ~ 10 % RH and above. The current study has implemented and maintained extreme low humidity conditions in the range of 0.5 – 3 % RH which resulted in the observations of unique fretting wear behaviours of the polymer bonded MoS_2-based DFL coating that have revealed a sustained low friction phase and low wear characteristics with minimal damage being incurred on the fretting contact interface. Significant increase of wear and failure of the DFL coating was not observed if the low humidity environment was maintained while increased humidity in the fretting testing environment accelerated the wear depth, increased

the friction and spurred damage at the contact interface which drastically reduced the lifetime of the DFL coating.

This identified low friction characteristics of the polymer-bonded DFL coating system were also observed as a function of the fretting loading conditions in Chapter 6. Various loading conditions were applied to uncover the fretting wear behaviours and performance of the Mo-DFL coating system on both a cylinder-on-flat and an alternate flat-on-flat contact configuration. Two fretting wear behaviours were identified from this experiment; a steady state low friction tests where failure did not occur, and; high friction tests to failure. The identified behaviours were found on the two fretting wear rig systems and contact configurations employed. The combination of nominal contact pressure and the sliding speed at the interface were applied to determine a threshold limit through a PV concept. Below the proposed threshold limit, a continuous steady state low friction wear with extended lifetime existed and above the threshold limit, tests end in a high friction regime linked with coating failure and limited lifetimes.

Traditional wear tests also undergo a steady state low friction phase, this is however usually followed by a wear transition to final failure. In this work, testing conditions which were found to be below the proposed fretting loading threshold limit, a final transition to failure was not observed and instead, a low friction behaviour was sustained for the duration of the tests. Above the proposed threshold limit, the common transition to failure occurs.

Additional fretting conditions that facilitate the extension of fretting lifetimes and durability of the DFL coating systems were also investigated in Chapter 5 with the analysis of the separate effects of the surface material and interfacial geometry upon which the polymer-bonded MoS_2 DFL (Mo-DFL) is deposited. By reducing the roughness of as-sprayed Cu-Ni-In through further surface preparation, the effect of the interfacial geometry was investigated which found that increased Mo-DFL lifetimes and durability of the system was achieved with increased roughness. This indicated that the roughness of as-sprayed Cu-Ni-In is a key factor in extending the lifetime of the DFL which was proposed to provide a mechanical key for the retention of the DFL. The surface of the as-sprayed Cu-Ni-In coating was further modified to be directly comparable to the TI-6Al-4V substrate in a smooth ground and grit-blasted conditions which allowed the effect of the material upon which the DFL is deposited to be isolated. When the DFL was deposited on Cu-Ni-In under-layer, better durability and lifetimes were observed compared to Ti-6Al-4V substrate despite having similar surface topographies.

Although previous studies have also examined and identified the added durability and extension of fretting wear lifetimes provided by the plasma sprayed Cu-Ni-In interlayer in both dry and DFL coated fretting systems. These effects have been attributed to either the interlayer material properties or the high surface roughness that the Cu-Ni-In interlayer provides without directly comparing and testing these parameters. This current work has aimed to resolve this by investigating the specific roles of the interfacial topography and the surface material of the Cu-Ni-In interlayer and understand the wear mechanisms that generate the durability and extension of fretting lifetimes.

As well as identifying the fretting conditions and examining the driving wear mechanisms that enable increased fretting lifetimes of the Mo-DFL coating system, this work has also demonstrated that modifying the bonded MoS_2-based coating with graphite additive can provide better performance and significant extensions of fretting lifetimes in different environmental and loading conditions. This can be observed in Chapter 4 where the graphite modified MoS_2-based coating (Gr-Mo-DFL) exceeded the fretting lifetimes of the graphite-based and MoS_2-based DFL coatings in atmospheric and high humidity environment conditions by a factor of 10 and maintained a stable low friction phase throughout the fretting duration until the test was stopped without the occurrence of failure. In Chapter 6, the graphite modified (Gr-Mo-DFL) coating system was also shown to increase the fretting lifetimes under higher loading conditions when compared to the Mo-DFL coating and; therefore, increased the performance threshold limit.

This result confirmed the observations from previous studies that have reported the increased fretting life and wear performance produced by the mixture of graphite and MoS_2 solid lubricants. However, the expanded fretting conditions that have been implemented in the current work has showed that the increased performance of the graphite modified MoS_2 DFL can be maintained in high humidity environments which have been observed to be highly unfavourable to the MoS_2 DFL. The limits of the graphite modified MoS_2 DFL have also been identified as increased fretting loading parameters resulted in critical wear and failure of the coating.

Typical small scale laboratory fretting tests that have investigated polymer bonded DFL coating systems of the aero-engine fan blade root have mainly focused on the fretting wear mechanisms of the DFL coating. Initial results from the case study conducted in Chapter 7 which analysed the fretting damage incurred on post-

service fan blade roots sections observed the development of cracks within the polymer-bonded MoS_2 DFL coating itself which are shown to have propagated close to the DFL/Cu-Ni-In interface. This observed damage characteristic have not identified on experimental fretting wear samples on either cylinder-on-flat or flat-on-flat contact configurations which suggests the test programmes aren't generating the same mechanism of failure as are observed from post-service fan blade root and additional fatigue-related fretting mechanisms need to be considered for future tests and coating developments for the fan blade root. Further work is required to determine the cause and origins of this mechanism of degradation and to understand if this is a common behaviour that occurs on aero-engine fan blade roots.

The studies presented in this thesis offer an amplified understanding of the fretting wear behaviours of the polymer-bonded DFL in different fretting conditions. This can be useful to further optimise the application of the DFL coating systems for aero-engine operating conditions as well as feed into the design of any future related experimental programmes.

Chapter 9. Future Work

In this thesis, the fretting wear behaviours of a polymer-bonded MoS_2-based (Mo-DFL), graphite-based (Gr-DFL) and a graphite modified MoS_2-based (Gr-Mo-DFL) dry film lubricant systems have been investigated under different conditions. This has highlighted areas where additional studies will be beneficial to gain further insights and understanding of the working mechanism of aero-engine DFL systems.

In Chapter 4, humidity was shown to have a significant effect on the fretting wear behaviour of the Mo-DFL coating. Although experimental tests have been conducted over a wide range of humidity levels; low-humidity (0.5 – 3% RH), ambient atmospheric (25 – 40 % RH) and high-humidity (60 – 75 % RH) conditions, experimental tests focusing on incremental controlled changes in the humidity levels will be useful to better understand and highlight the humidity threshold levels that alters the fretting behaviours of the polymer-bonded MoS_2-based DFL. Further work is also required to determine the mechanisms that facilitate the low friction phase (Stage II) in air and not in argon environments as observed in ambient and high-humidity conditions.

The graphite modified Gr-Mo-DFL was observed to exceed the performance of Mo-DFL and Gr-DFL coatings in ambient atmospheric and high-humidity conditions and maintained a stable friction with extended fretting lifetimes. Further work which investigates whether the specific combination of MoS_2 + graphite is the reason for increased performance or rather simply, the increased total amount of lubricating phases in the DFL paint matrix will be useful.

In Chapter 5, it was shown that increased surface roughness as well as the application of the Cu-Ni-In under-layer was key to the durability and fretting lifetime extension of the Mo-DFL coated fretting system. The rough surface of the as sprayed Cu-Ni-In coating that the DFL was deposited on was proposed to have a significant role as both a mechanical key and a reservoir for the DFL coating maintain low friction and stability at the fretting interface. Further work exploring how controlled surface topographies could be imposed on the Cu-Ni-In interface would be an interesting aspect of the research.

In Chapter 6, the graphite modified Gr-Mo-DFL coating was observed to marginally increase the lifetime of as-received polymer-bonded MoS_2-based DFL (Mo-DFL) when ~ 5 % of graphite powder was added to the paint matrix. Further studies

aiming to understand if incremental increase of the graphite % added as an additive to the Mo-DFL paint can further increase the lifetime of the Mo-DFL coating system under higher loading conditions would be beneficial.

Additional in-depth analysis and characterisation of fan blade roots which have operated across a wide range of in-service conditions are required to understand if the observed cracks are a common behaviour and to shed more light on the damaging mechanism that occur in operating service. This can inform future design and allow optimised experimental testing conditions.

References

[1] G. A. Tomlinson, “The Rusting of Steel Surfaces in Contact,” *Proc. R. Soc. A Math. Phys. Eng. Sci.*, vol. 115, no. 771, pp. 472–483, 1927.

[2] P. L. Hurricks, “The mechanism of fretting — A review,” *Wear*, vol. 15, no. 6, pp. 389–409, Jun. 1970.

[3] D. Cressman, B. Tury, and G. L. Doll, “Effects of surface treatments and coatings on tribological performance of Ti-6Al-4V in the mixed fretting and gross slip regimes,” *Surf. Coatings Technol.*, vol. 290, pp. 110–115, 2016.

[4] J. M. Dobromirski, “Variables of fretting process: Are there 50 of them?,” *Stand. Frett. Fatigue Test Methods Equip.*, vol. 1159, pp. 60–66, 1992.

[5] K. Kim and A. M. Korsunsky, “Dissipated energy and fretting damage in CoCrAlY-MoS2 coatings,” *Tribol. Int.*, vol. 43, no. 3, pp. 676–684, 2010.

[6] S. Fouvry and C. Paulin, “An effective friction energy density approach to predict solid lubricant friction endurance: Application to fretting wear,” *Wear*, vol. 319, no. 1, pp. 211–226, 2014.

[7] S. A. Meguid, “Current Advances in Mechanical Design and Production VII,” in *On the mechanical integrity of aeroengine compressor disc assemblies*, 2000, pp. 161–172.

[8] D. S. Wei and Y. R. Wang, “Analysis of fretting fatigue life of dovetail assemblies based on fracture mechanics method,” *Eng. Fail. Anal.*, vol. 25, pp. 144–155, 2012.

[9] K. Anandavel, R. V. Prakash, and A. Davis, “Effect of preloading on the contact stress distribution of a dovetail interface,” *World Acad. Sci. Eng. Technol.*, vol. 46, no. 10, pp. 879–884, 2010.

[10] R. V. Nandish, S. P. Vizhian, M. Gopinath, and R. Jain, “Elastic Contact Stress Analysis of Dovetail Attachment in Turbine Engines,” *Ijrmet*, vol. 5762, pp. 166–170, 2013.

[11] K. Kim and A. M. Korsunsky, “Effects of imposed displacement and initial coating thickness on fretting behaviour of a thermally sprayed coating,” *Wear*, vol. 271, no. 7–8, pp. 1080–1085, 2011.

[12] S. Fouvry, P. Arnaud, A. Mignot, and P. Neubauer, “Contact size, frequency and cyclic normal force effects on Ti–6Al–4V fretting wear processes: An approach combining friction power and contact oxygenation,” *Tribol. Int.*, vol. 113, no. December 2016, pp. 460–473, 2017.

[13] B. van Peteghem, S. Fouvry, and J. Petit, “Effect of variable normal force and frequency on fretting wear response of Ti–6Al–4V contact,” *Wear*, vol. 271, no. 9–10, pp. 1535–1542, Jul. 2011.

[14] D. B. Luo, V. Fridrici, and P. Kapsa, “Relationships between the fretting wear

behavior and the ball cratering resistance of solid lubricant coatings," *Surf. Coatings Technol.*, vol. 204, no. 8, pp. 1259–1269, 2010.

[15] R. B. Waterhouse and P. H. Shipway, "Fretting Wear," in *Fretting Wear*, 2007.

[16] Q. Yang, W. Zhou, and X. Zhang, "Investigation on the fretting fatigue behaviors of Ti-6Al-4V dovetail joint specimens treated with shot-peening," *Wear*, vol. 372–373, pp. 81–90, 2017.

[17] N. A. Bhatti and M. Abdel Wahab, "Fretting fatigue crack nucleation: A review," *Tribol. Int.*, vol. 121, no. January, pp. 121–138, 2018.

[18] S. Basseville and G. Cailletaud, "An evaluation of the competition between wear and crack initiation in fretting conditions for Ti-6Al-4V alloy," *Wear*, vol. 328–329, pp. 443–455, 2015.

[19] B. W. Lee, J. Suh, H. Lee, and T. G. Kim, "Investigations on fretting fatigue in aircraft engine compressor blade," *Eng. Fail. Anal.*, vol. 18, no. 7, pp. 1900–1908, 2011.

[20] N. S. Xi, P. D. Zhong, H. Q. Huang, H. Yan, and C. H. Tao, "Failure investigation of blade and disk in first stage compressor," *Eng. Fail. Anal.*, vol. 7, no. 6, pp. 385–392, 2000.

[21] S. Fouvry, C. Paulin, and S. Deyber, "Impact of contact size and complex gross–partial slip conditions on Ti–6Al–4V/Ti–6Al–4V fretting wear," *Tribol. Int.*, vol. 42, no. 3, pp. 461–474, Mar. 2009.

[22] L. Shi, D. S. Wei, Y. R. Wang, A. M. Tian, and D. Li, "An investigation of fretting fatigue in a circular arc dovetail assembly," *Int. J. Fatigue*, vol. 82, pp. 226–237, 2016.

[23] A. Kermanpur, H. Sepehri Amin, S. Ziaei-Rad, N. Nourbakhshnia, and M. Mosaddeghfar, "Failure analysis of Ti6Al4V gas turbine compressor blades," *Eng. Fail. Anal.*, vol. 15, no. 8, pp. 1052–1064, Dec. 2008.

[24] I. J. Polmear, "Titanium alloys," in *Light Alloys*, 2005, pp. 299–365.

[25] P. Singh, H. Pungotra, and N. S. Kalsi, "On the characteristics of titanium alloys for the aircraft applications," *Mater. Today Proc.*, vol. 4, no. 8, pp. 8971–8982, 2017.

[26] C. Cui, B. M. Hu, L. Zhao, and S. Liu, "Titanium alloy production technology, market prospects and industry development," *Mater. Des.*, vol. 32, no. 3, pp. 1684–1691, 2011.

[27] J. Mathew J. Donachie, *Titanium: A Technical Guide*, 2nd ed. ASM Internation, 2000.

[28] X. Zhang, Y. Chen, and J. Hu, "Recent advances in the development of aerospace materials," *Prog. Aerosp. Sci.*, vol. 97, no. January, pp. 35–60, 2018.

[29] F. H. Froes, “Mechanical Properties and Testing of Titanium Alloys,” in *Principles of Alloying Titanium*, 2001, pp. 3–17.

[30] R. Pederson, “Microstructure and Phase Transformation of Ti-6Al-4V,” Lulea University of Technology, 2002.

[31] K. Prasad and V. Kumar, “Isothermal and thermomechanical fatigue behaviour of Ti-6Al-4V titanium alloy,” *Mater. Sci. Eng. A*, vol. 528, no. 19–20, pp. 6263–6270, 2011.

[32] R. R. Boyer, “An overview on the use of titanium in the aerospace industry,” *Mater. Sci. Eng. A*, vol. 213, no. 1–2, pp. 103–114, 1996.

[33] H.Dong, “Surface Engineering of Light Alloys,” Woodhead Publishing, 2010, pp. 58–80.

[34] P. C. E. Eden, W. Rose, “The endurance of metals: experiments on rotating beams,” *Univ. Coll. London, Proc. Inst. Mech. Eng.*, vol. 81, pp. 839-974., 1911.

[35] R. B. Waterhouse, “Fretting wear,” *Wear*, vol. 100, no. 1–3, pp. 107–118, Dec. 1984.

[36] G. A. Tomlinson, P. L. Thorpe, and H. J. Gough, “An Investigation of the Fretting Corrosion of Closely Fitting Surfaces,” *Proc. Inst. Mech. Eng.*, vol. 141, no. 1, pp. 223–249, 1939.

[37] C. B. E. I. David, W. Hoeppner, V. Chandrasekaran, Ed., *Fretting Fatigue: Current Technology and Practices.* 2000.

[38] U. S. D. of Transportation, “Literature Review and Preliminary Studies of Fretting and Fretting Fatigue Including Special Application to Aircraft Joints,” 1994.

[39] S. staffan Olof, Vingsbo, “On fretting maps,” *Wear*, no. 126, pp. 131–147, 1988.

[40] S. Fouvry, P. Kapsa, and L. Vincent, “Quantification of fretting damage,” *Wear*, vol. 200, no. 1–2, pp. 186–205, 1996.

[41] C. Mary, S. Fouvry, J. M. Martin, and B. Bonnet, “High temperature fretting wear of a Ti alloy/CuNiIn contact,” *Surf. Coatings Technol.*, vol. 203, no. 5–7, pp. 691–698, 2008.

[42] J. . B. Douglas Godfrey, A. E. Von Doenhoff, and L. S. Stivers, “National advisory committee for aeronautics,” *J. Appl. Phys.*, vol. 14, no. 8, pp. 399–405, 1943.

[43] L. Vincent, Y. Berthier, M. C. Dubourg, and M. Godet, “Mechanics and materials in fretting,” *Wear*, vol. 153, no. 1, pp. 135–148, Mar. 1992.

[44] R. Ramesh and R. Gnanamoorthy, “Effect of hardness on fretting wear behaviour of structural steel, En 24, against bearing steel, En 31,” *Mater. Des.*, vol. 28, no. 5, pp. 1447–1452, Jan. 2007.

[45] H. Lee, S. Mall, J. H. Sanders, S. K. Sharma, and R. S. Magaziner, “Characterization of fretting wear behavior of Cu–Al coating on Ti–6Al–4V substrate,” *Tribol. Int.*, vol. 40, no. 8, pp. 1301–1310, Aug. 2007.

[46] R. B. Waterhouse, “Fretting Corrosion,” *Corrosion*, no. 1929, pp. 8:114-8:123, 1976.

[47] R. B. Waterhouse, “Fretting fatigue,” *Mater. Sci. Eng.*, vol. 25, pp. 201–206, Sep. 1976.

[48] Y. Berthier, L. Vincent, and M. Godet, “Fretting fatigue and fretting wear,” *Tribol. Int.*, vol. 22, no. 4, pp. 235–242, Aug. 1989.

[49] M. Varenberg, G. Halperin, and I. Etsion, “Different aspects of the role of wear debris in fretting wear,” *Wear*, vol. 252, no. 11–12, pp. 902–910, 2002.

[50] G. X. Chen and Z. R. Zhou, “Study on transition between fretting and reciprocating sliding wear,” *Wear*, vol. 250–251, no. PART 1, pp. 665–672, 2001.

[51] M. H. Zhu and Z. R. Zhou, “On the mechanisms of various fretting wear modes,” *Tribol. Int.*, vol. 44, no. 11, pp. 1378–1388, 2011.

[52] Z. R. Zhou, K. Nakazawa, M. H. Zhu, N. Maruyama, P. Kapsa, and L. Vincent, “Progress in fretting maps,” *Tribol. Int.*, vol. 39, no. 10, pp. 1068–1073, 2006.

[53] H. Czichos and D. Dowson, “Tribology: A systems approach to the Science and Technology of friction, lubrication and wear: Amsterdam,” *Tribol. Int.*, vol. 11, no. 4, pp. 259–260, Aug. 1978.

[54] A. Iwabuchi, “The role of oxide particles in the fretting wear of mild steel,” *Wear*, vol. 151, no. 2, pp. 301–311, Dec. 1991.

[55] J. D. Lemm, A. R. Warmuth, S. R. Pearson, and P. H. Shipway, “The influence of surface hardness on the fretting wear of steel pairs-Its role in debris retention in the contact,” *Tribol. Int.*, vol. 81, pp. 258–266, 2014.

[56] T. W. Scharf and S. V. Prasad, “Solid lubricants: A review,” *J. Mater. Sci.*, vol. 48, no. 2, pp. 511–531, 2013.

[57] E. Rabinowicz, *Friction and Wear of Materials*, 2nd ed. New York: Wiley, 1995.

[58] C. H. Hager, J. Sanders, S. Sharma, and A. Voevodin, “Gross slip fretting wear of CrCN, TiAlN, Ni, and CuNiIn coatings on Ti6Al4V interfaces,” *Wear*, vol. 263, no. 1-6 SPEC. ISS., pp. 430–443, 2007.

[59] K. G. Budinski, “Tribological properties of titanium alloys,” *Wear*, vol. 151, pp. 203–217, 1991.

[60] Z. Wu, Y. Xing, P. Huang, and L. Liu, “Tribological properties of dimple-textured titanium alloys under dry sliding contact,” *Surf. Coatings Technol.*, vol. 309, pp. 21–28, 2017.

[61] E. Gemelli and N. H. a. Camargo, “Oxidation kinetics of commercially pure titanium,” *Matéria (Rio Janeiro)*, vol. 12, no. 3, pp. 525–531, 2007.

[62] S. Fayeulle, P. Blanchard, and L. Vincent, “Fretting Behavior of Titanium Alloys,” *Tribol. Trans.*, vol. 36, no. 2, pp. 267–275, 2008.

[63] L. Blades, D. Hills, D. Nowell, K. E. Evans, and C. Smith, “An exploration of debris types and their influence on wear rates in fretting,” *Wear*, vol. 450–451, p. 203252, Jun. 2020.

[64] E. Sauger, S. Fouvry, L. Ponsonnet, P. Kapsa, J. . Martin, and L. Vincent, “Tribologically transformed structure in fretting,” *Wear*, vol. 245, no. 1–2, pp. 39–52, Oct. 2000.

[65] D. A. Rigney, “Transfer, mixing and associated chemical and mechanical processes during the sliding of ductile materials,” *Wear*, vol. 245, no. 1–2, pp. 1–9, Oct. 2000.

[66] C. Mary, S. Fouvry, J. M. Martin, and B. Bonnet, “Pressure and temperature effects on Fretting Wear damage of a Cu–Ni–In plasma coating versus Ti17 titanium alloy contact,” *Wear*, vol. 272, no. 1, pp. 18–37, Oct. 2011.

[67] S. R. Pearson and P. H. Shipway, “Is the wear coefficient dependent upon slip amplitude in fretting? Vingsbo and Söderberg revisited,” *Wear*, vol. 330–331, pp. 93–102, 2015.

[68] H. Mindlin, R.D. and Deresiewicz, “Elastic Spheres in Contact under Varying Oblique Force,” *J. Appl. Mech ASME,* no. 20, pp. 327–344, 1953.

[69] U. Bryggman and S. Söderberg, “Contact conditions in fretting,” *Wear*, vol. 110, no. 1, pp. 1–17, Jul. 1986.

[70] Z. R. Zhou and L. Vincent, “Mixed fretting regime,” *Wear*, vol. 181–183, pp. 531–536, Mar. 1995.

[71] A. R. Warmuth, W. Sun, and P. H. Shipway, “The roles of contact conformity, temperature and displacement amplitude on the lubricated fretting wear of a steel-on-steel contact,” *R. Soc. Open Sci.*, vol. 3, no. 10, 2016.

[72] X. Jin, W. Sun, and P. H. Shipway, “Derivation of a wear scar geometry-independent coefficient of friction from fretting loops exhibiting non-Coulomb frictional behaviour,” *Tribol. Int.*, vol. 102, pp. 561–568, 2016.

[73] S. Fouvry, P. Duó, and P. Perruchaut, “A quantitative approach of Ti-6Al-4V fretting damage: Friction, wear and crack nucleation,” *Wear*, vol. 257, no. 9–10, pp. 916–929, 2004.

[74] S. Fouvry, T. Liskiewicz, P. Kapsa, S. Hannel, and E. Sauger, “An energy description of wear mechanisms and its applications to oscillating sliding contacts,” *Wear*, vol. 255, no. 1–6, pp. 287–298, Aug. 2003.

[75] S. Fouvry and P. Kapsa, “An energy description of hard coating wear mechanisms,” *Surf. Coatings Technol.*, vol. 138, no. 2–3, pp. 141–148, 2001.

[76] J. F. Archard, “Contact and rubbing of flat surfaces,” *J. Appl. Phys.*, vol. 24, no. 8, pp. 981–988, 1953.

[77] A. R. Warmuth, S. R. Pearson, P. H. Shipway, and W. Sun, “The effect of contact geometry on fretting wear rates and mechanisms for a high strength steel,” *Wear*, vol. 301, no. 1–2, pp. 491–500, 2013.

[78] X. Jin, W. Sun, and P. H. Shipway, “The role of geometry changes and debris formation associated with wear on the temperature field in fretting contacts,” *Tribol. Int.*, vol. 102, pp. 392–406, 2016.

[79] S. Fouvry and R. Merhej, “Introduction of a power law formulation to quantify the contact size effects on friction and wear responses of dry oscillating sliding contacts: Application to a chromium steel interface,” *Wear*, vol. 301, no. 1–2, pp. 34–46, Apr. 2013.

[80] A. R. Warmuth, S. R. Pearson, P. H. Shipway, and W. Sun, “The effect of contact geometry on fretting wear rates and mechanisms for a high strength steel,” *Wear*, vol. 301, no. 1–2, pp. 491–500, Apr. 2013.

[81] S. Baydoun, S. Fouvry, S. Descartes, and P. Arnaud, “Fretting wear rate evolution of a flat-on-flat low alloyed steel contact: A weighted friction energy formulation,” *Wear*, vol. 426–427, no. October 2018, pp. 676–693, 2019.

[82] W. Lu, P. Zhang, X. Liu, W. Zhai, J. Luo, and W. Zeng, “Influence of surface topography on torsional fretting wear under flat-on-flat contact,” *Tribol. Int.*, vol. 109, pp. 367–372, May 2017.

[83] R. Merhej and S. Fouvry, “Contact size effect on fretting wear behaviour: Application to an AISI 52100/AISI 52100 interface,” *Lubr. Sci.*, 2009.

[84] P. Arnaud, S. Fouvry, and S. Garcin, “Wear rate impact on Ti-6Al-4V fretting crack risk: Experimental and numerical comparison between cylinder/plane and punch/plane contact geometries,” *Tribol. Int.*, vol. 108, no. July 2016, pp. 32–47, 2017.

[85] L. Ma, K. Eom, J. Geringer, T. S. Jun, and K. Kim, “Literature review on fretting wear and contact mechanics of tribological coatings,” *Coatings*, vol. 9, no. 8, pp. 1–20, 2019.

[86] G. L. Goss and D. W. Hoeppner, “Normal load effects in fretting fatigue of titanium and aluminum alloys,” *Wear*, vol. 27, no. 2, pp. 153–159, Feb. 1974.

[87] S. R. Pearson, “The effect of nitriding on the fretting wear of a high strength steel at ambient and elevated temperatures,” University of Nottingham, 2013.

[88] A. L. M. Tobi, W. Sun, and P. H. Shipway, “Evolution of plasticity-based wear damage in gross sliding fretting of a Ti-6Al-4V non-conforming contact,” *Tribol. Int.*, vol. 113, no. January, pp. 474–486, 2017.

[89] H. P. Soh and H. Ping, “Fretting Wear Studies of Aeroengine Materials,” no. June, 2006.

[90] Q. Wang, Y. Wang, H. Wang, N. Fan, and F. Yan, “Experimental investigation on tribological behavior of several polymer materials under reciprocating sliding and fretting wear conditions,” *Tribol. Int.*, vol. 104, pp. 73–82, Dec. 2016.

[91] J. Li and Y. H. Lu, “Effects of displacement amplitude on fretting wear behaviors and mechanism of Inconel 600 alloy,” *Wear*, vol. 304, no. 1–2, pp. 223–230, Jul. 2013.

[92] N. Fan, “Effect of displacement amplitude on fretting wear of 304 stainless steel in air and sea water,” no. November 2017, pp. 1–10, 2018.

[93] M. Godet, “The third-body approach: A mechanical view of wear,” *Wear*, vol. 100, no. 1–3, pp. 437–452, 1984.

[94] Q. . Liu and Z. . Zhou, “Effect of displacement amplitude in oil-lubricated fretting,” *Wear*, vol. 239, no. 2, pp. 237–243, Apr. 2000.

[95] S. Söderberg, U. Bryggman, and T. McCullough, “Frequency effects in fretting wear,” *Wear*, vol. 110, no. 1, pp. 19–34, Jul. 1986.

[96] A. R. Warmuth, P. H. Shipway, and W. Sun, “Fretting wear mapping: the influence of contact geometry and frequency on debris formation and ejection for a steel-on-steel pair,” *Proc. R. Soc. A Math. Phys. Eng. Sci.*, vol. 471, no. 2178, pp. 20140291–20140291, 2015.

[97] X. Jin, P. H. Shipway, and W. Sun, “The Role of Temperature and Frequency on Fretting Wear of a Like-on-Like Stainless Steel Contact,” *Tribol. Lett.*, vol. 65, no. 3, pp. 1–15, 2017.

[98] M. Kalin and J. Vižintin, “A tentative explanation for the tribochemical effects in fretting wear,” *Wear*, vol. 250, no. 1–12, pp. 681–689, Oct. 2001.

[99] M. H. Wharton and R. B. Waterhouse, “Environmental effects in the fretting fatigue of Ti-6Al-4V,” *Wear*, vol. 62, no. 2, pp. 287–297, Aug. 1980.

[100] H. H. Uhlig and M. Feng, “A Fundamental Investigation of Fretting Corrosion,” 1953.

[101] R. C. Bill, “Fretting Wear of Iron, Nickel and Titanium under Varied Environmental Conditions,” *NASA*, 1979.

[102] Y. Fu, J. Wei, and A. W. Batchelor, “Some considerations on the mitigation of fretting damage by the application of surface-modification technologies,” *J. Mater. Process. Technol.*, vol. 99, no. 1–3, pp. 231–245, Mar. 2000.

[103] S. C. Gordelier and T. C. Chivers, “A literature review of palliatives for fretting fatigue,” *Wear*, vol. 56, no. 1, pp. 177–190, Sep. 1979.

[104] B. V. R. R. Kumar, “A Review on Blisk Technology,” *Int. J. Innov. Res. Sci. Eng. Technol.*, vol. 2, no. 5, pp. 1353–1358, 2013.

[105] J. Aschenbruck, R. Adamczuk, and J. R. Seume, “Recent Progress in Turbine Blade and Compressor Blisk Regeneration,” *Procedia CIRP*, vol. 22,

pp. 256–262, Jan. 2014.

[106] Y. Fu, N. L. Loh, A. W. Batchelor, D. Liu, J. He, and K. Xu, “Improvement in fretting wear and fatigue resistance of Ti–6Al–4V by application of several surface treatments and coatings,” *Surf. Coatings Technol.*, vol. 106, no. 2–3, pp. 193–197, 1998.

[107] Q. Yang, W. Zhou, Y. Zhong, and X. Zhang, “Effect of shot-peening on the fretting wear and crack initiation behavior of Ti-6Al-4V dovetail joint specimens,” *Int. J. Fatigue*, vol. 107, no. September 2017, pp. 83–95, 2018.

[108] C. Bin Tang, D. X. Liu, B. Tang, X. H. Zhang, L. Qin, and C. S. Liu, “Influence of plasma molybdenizing and shot-peening on fretting damage behavior of titanium alloy,” *Appl. Surf. Sci.*, vol. 390, pp. 946–958, 2016.

[109] P. Zhang, W. Lu, X. Liu, W. Zhai, M. Zhou, and W. Zeng, “Torsional fretting and torsional sliding wear behaviors of CuNiAl against 42CrMo4 under dry condition,” *Tribol. Int.*, vol. 118, no. July 2017, pp. 11–19, 2018.

[110] D. B. Luo, V. Fridrici, and P. Kapsa, “Selecting solid lubricant coatings under fretting conditions,” *Wear*, vol. 268, no. 5–6, pp. 816–827, 2010.

[111] J. Xu, M. . Zhu, Z. . Zhou, P. Kapsa, and L. Vincent, “An investigation on fretting wear life of bonded MoS2 solid lubricant coatings in complex conditions,” *Wear*, vol. 255, no. 1–6, pp. 253–258, Aug. 2003.

[112] Y. Ye, J. Chen, and H. Zhou, “An investigation of friction and wear performances of bonded molybdenum disulfide solid film lubricants in fretting conditions,” *Wear*, vol. 266, no. 7–8, pp. 859–864, 2009.

[113] G. R. Y. N. Sabeya, J.-Y. Paris, and J. Denape, “Fretting wear of a coated titanium alloy under free displacement,” *Wear*, vol. 264, no. 3–4, pp. 166–176, Feb. 2008.

[114] S. Fouvry and C. Paulin, “An effective friction energy density approach to predict solid lubricant friction endurance: Application to fretting wear,” *Wear*, vol. 319, no. 1–2, pp. 211–226, Nov. 2014.

[115] A. J. Freimanis, A. E. Segall, J. C. Conway, and E. J. Whitney, “Elevated temperature evaluation of fretting and metal transfer between coated titanium components,” *Tribol. Trans.*, vol. 43, no. 4, pp. 653–658, 2000.

[116] H. Lee, O. Jin, and S. Mall, “Fretting fatigue behaviour of shot-peened Ti-6Al-4V at room and elevated temperatures,” *Fatigue Fract. Eng. Mater. Struct.*, vol. 26, no. 9, pp. 767–778, 2003.

[117] S. Mall, V. K. Jain, and H. A. Fadag, “Effects of shot-peening on fretting fatigue crack growth behavior in Ti-6al-4v,” *Strain*, vol. 47, no. SUPPL. 1, pp. 305–318, 2011.

[118] Q. Yang, W. Zhou, Z. Niu, X. Zheng, Q. Wang, and G. Chen, “Effect of different surface asperities and surface hardness induced by shot-peening on the fretting wear behavior of Ti-6Al-4V,” *Surf. Coatings Technol.*, vol. 349,

pp. 1098–1106, Sep. 2018.

[119] S. Chakravarty, R. G. Andrews, P. Painaik, and A. K. Koul, “The Effect of Surface Modification on Fretting Fatigue in Ti Alloy Turbine Components,” pp. 31–35, 1995.

[120] A. . Hutson, M. Niinomi, T. Nicholas, and D. Eylon, “Effect of various surface conditions on fretting fatigue behavior of Ti–6Al–4V,” *Int. J. Fatigue*, vol. 24, no. 12, pp. 1223–1234, Dec. 2002.

[121] V. Fridrici, S. Fouvry, P. Kapsa, and P. Perruchaut, “Impact of contact size and geometry on the lifetime of a solid lubricant,” *Wear*, vol. 255, no. 7–12, pp. 875–882, Aug. 2003.

[122] V. Fridrici, S. Fouvry, and P. Kapsa, “Fretting wear behavior of a Cu–Ni–In plasma coating,” *Surf. Coatings Technol.*, vol. 163–164, pp. 429–434, Jan. 2003.

[123] M. Marquer, S. Philippon, L. Faure, G. Chassaing, J. Tardelli, and K. Demmou, “Influence of two APS coatings on the high-speed tribological behavior of a contact between titanium alloys,” *Tribol. Int.*, vol. 136, pp. 13–22, Aug. 2019.

[124] Z. Niu, W. Zhou, C. Wang, Z. cao, Q. Yang, and X. Fu, “Fretting wear mechanism of plasma-sprayed CuNiIn coating on Ti-6Al-4V substrate under plane/plane contact,” *Surf. Coatings Technol.*, vol. 408, no. August 2020, p. 126794, 2021.

[125] S. Fouvry, V. Fridrici, C. Langlade, P. Kapsa, and L. Vincent, “Palliatives in fretting: A dynamical approach,” *Tribol. Int.*, vol. 39, no. 10, pp. 1005–1015, 2006.

[126] Z. . Zhou and L. Vincent, “Lubrication in fretting—a review,” *Wear*, vol. 225–229, pp. 962–967, Apr. 1999.

[127] A. Matthews, S. Franklin, and K. Holmberg, “Tribological coatings: Contact mechanisms and selection,” *J. Phys. D. Appl. Phys.*, vol. 40, no. 18, pp. 5463–5475, 2007.

[128] K. Holmberg, A. Matthews, and H. Ronkainen, “Coatings tribology - Contact mechanisms and surface design,” *Tribol. Int.*, vol. 31, no. 1–3, pp. 107–120, 1998.

[129] M. Shima, H. Suetake, I. R. McColl, R. B. Waterhouse, and M. Takeuchi, “On the behaviour of an oil lubricated fretting contact,” *Wear*, vol. 210, no. 1–2, pp. 304–310, Sep. 1997.

[130] P. M. Lugt, “Modern advancements in lubricating grease technology,” *Tribol. Int.*, vol. 97, pp. 467–477, May 2016.

[131] C. Busch, W. Dresel, and R.-P. Heckler, “Lubricants, . Lubricating Greases,” *Ullmann’s Encycl. Ind. Chem.*, vol. 21, pp. 547–571, 2012.

[132] N. R. Whitehouse, “The use of organic and inorganic coatings to reduce

friction, wear and erosion," in *Surface Engineering Casebook*, Elsevier, 1996, pp. 247–253.

[133] C. Donnet, "Advanced solid lubricant coatings for high vacuum environments," *Surf. Coatings Technol.*, vol. 80, no. 1–2, pp. 151–156, Mar. 1996.

[134] C. Donnet and A. Erdemir, "Solid Lubricant Coatings: Recent Developments and Future Trends," *Tribol. Lett.*, vol. 17, no. 3, pp. 389–397, 2004.

[135] C. Donnet and A. Erdemir, "Historical developments and new trends in tribological and solid lubricant coatings," *Surf. Coatings Technol.*, vol. 180–181, pp. 76–84, Mar. 2004.

[136] J. Beard, "The avoidance of fretting," *Mater. Des.*, vol. 9, no. 4, pp. 220–227, Jul. 1988.

[137] A. Matthews, A. Leyland, K. Holmberg, and H. Ronkainen, "Design aspects for advanced tribological surface coatings," *Surf. Coatings Technol.*, vol. 100–101, pp. 1–6, Mar. 1998.

[138] Z. Yang, P. Zhang, Y. L. Di, Z. H. Cai, and Q. Li, "Investigation on Microstructure of CrN-Based Solid Self-Lubricant Composite Coating," *Adv. Mater. Res.*, vol. 538, pp. 406–409, 2012.

[139] F. P. Bowden, D. Tabor, and F. Palmer, "The Friction and Lubrication of Solids," *Am. J. Phys.*, vol. 19, no. 7, pp. 428–429, 1951.

[140] A. Erdemir, "Solid lubricants and self-lubricating films," in *Handbook of Modern Tribology*, 2001, pp. 787–818.

[141] A. W. B. Gwidon Stachowiak, "Solid Lubrication and Surface Treatments," in *Engineering Tribology*, Technology., Butterworth-Heinemann, 2013, pp. 485–526.

[142] W. 0. Winer, "Molybdenum Disulfide as a Lubricant: A Review of The Fundamental Knowledge," *Wear*, vol. 10, pp. 422–452, 1967.

[143] M. R. Vazirisereshk, A. Martini, D. A. Strubbe, and M. Z. Baykara, "Solid Lubrication with MoS2: A Review," pp. 1–31, 2019.

[144] J. M. Martin, C. Donnet, and L. Mogne, "Superlucricity of Molybdenum Disulphide," *Ind. Lubr. Tribol.*, vol. 52, no. 1, pp. 13–18, 1993.

[145] K. Miyoshi, "Solid Lubricants and Coatings for Extreme Environments: State-of-the-Art Survey," *NASA Rep.*, no. January, pp. 1–23, 2007.

[146] X. Li and H. Zhu, "Two-dimensional MoS2: Properties, preparation, and applications," *J. Mater.*, vol. 1, no. 1, pp. 33–44, 2015.

[147] Z. He and W. Que, "Molybdenum disulfide nanomaterials: Structures, properties, synthesis and recent progress on hydrogen evolution reaction," *Appl. Mater. Today*, vol. 3, pp. 23–56, 2016.

[148] R. Holinski and J. Gänsheimer, “A study of the lubricating mechanism of molybdenum disulfide,” *Wear*, vol. 19, no. 3, pp. 329–342, 1972.

[149] K. Miyoshi, *Solid Lubrication Fundamentals and Solid Applications Friction and Wear Properties of Selected Lubricating Films : Case Studies*, no. December 2000. 2000.

[150] A. Savan, E. Pflüger, P. Voumard, A. Schröer, and M. S. Paul, “Modern solid lubrication: Recent developments and applications of MoS2,” *Lubr. Sci.*, vol. 12, no. 2, pp. 185–203, 2000.

[151] M. N. Gardos, “The Synergistic Effects of Graphite on the Friction and Wear of MoS2 Films in Air,” *Tribol. Trans.*, vol. 31, no. 2, pp. 214–227, 1988.

[152] Z. Chen, X. He, C. Xiao, and S. H. Kim, “Effect of humidity on friction and Wear-A critical review,” *Lubricants*, vol. 6, no. 3. 2018.

[153] X. Zhao and S. S. Perry, “The role of water in modifying friction within MoS2 sliding interfaces,” *ACS Appl. Mater. Interfaces*, vol. 2, no. 5, pp. 1444–1448, 2010.

[154] J. K. Lancaster, “A review of the influence of environmental humidity and water on friction, lubrication and wear,” *Tribol. Int.*, vol. 23, no. 6, pp. 371–389, Dec. 1990.

[155] A. J. Haltner and C. S. Oliver, “Effect of water vapor on friction of molybdenum disulfide,” *Ind. Eng. Chem. Fundam.*, vol. 5, no. 3, pp. 348–355, 1966.

[156] J. K. G. Panitz, L. E. Pope, J. E. Lyons, and D. J. Staley, “Tribological properties of MoS2 Coatings in vacuum, low relative humidity and high relative humidity environments.,” vol. 1166, no. June 1998, pp. 2–7, 1987.

[157] T. B. Stewart and P. D. Fleischauer, “Chemistry of Sputtered Molybdenum Disulfide Films,” *Inorg. Chem.*, vol. 21, no. 6, pp. 2426–2431, 1982.

[158] S. Ross and A. Sussman, “Surface oxidation of molybdenum disulfide,” *J. Phys. Chem.*, vol. 59, no. 9, pp. 889–892, 1955.

[159] K. S. Randhawa and A. Patel, “The effect of environmental humidity/water absorption on tribo-mechanical performance of polymers and polymer composites – a review,” *Ind. Lubr. Tribol.*, no. May, 2021.

[160] G. Salomon, A. W. J. De Gee, and J. H. Zaat, “Mechano-chemical factors in MoS2-film lubrication,” *Wear*, vol. 7, no. 1, pp. 87–101, Jan. 1964.

[161] T. Spalvins, “Lubrication with sputtered MoS2 Films: Principles, Operation, Limitations,” *Nasa Tech. Memo.*, 1991.

[162] T. W. Scharf, P. G. Kotula, and S. V. Prasad, “Friction and wear mechanisms in MoS2Sb2O 2Au nanocomposite coatings,” *Acta Mater.*, vol. 58, no. 12, pp. 4100–4109, 2010.

[163] Y. Bai, J. Pu, H. Wang, L. Wang, Q. Xue, and S. Liu, “High humidity and high

vacuum environment performance of MoS2/Sn composite film," *J. Alloys Compd.*, vol. 800, pp. 107–115, 2019.

[164] B. C. Windom, W. G. Sawyer, and D. W. Hahn, "A Raman Spectroscopic Study of MoS2 and MoO3: Applications to Tribological Systems," *Tribol. Lett.*, vol. 42, no. 3, pp. 301–310, 2011.

[165] J. R. Lince, S. H. Loewenthal, and C. S. Clark, "Tribological and chemical effects of long term humid air exposure on sputter-deposited nanocomposite MoS2 coatings," *Wear*, vol. 432–433, no. December 2018, 2019.

[166] J. Luo, M. H. Zhu, Y. D. Wang, J. F. Zheng, and J. L. Mo, "Study on rotational fretting wear of bonded MoS2 solid lubricant coating prepared on medium carbon steel," *Tribol. Int.*, vol. 44, no. 11, pp. 1565–1570, Oct. 2011.

[167] C. Donnet, J. M. Martin, T. Le Mogne, and M. Belin, "The origin of super-low friction coefficient of MoS2 coatings in various environments," *Tribol. Ser.*, vol. 27, no. C, pp. 277–284, 1994.

[168] H. S. Khare and D. L. Burris, "The effects of environmental water and oxygen on the temperature-dependent friction of sputtered molybdenum disulfide," *Tribol. Lett.*, vol. 52, no. 3, pp. 485–493, 2013.

[169] R. L. Fusaro, "Lubrication and failure mechanisms of molybdenum disulfide films. 1: Effect of atmosphere," *NASA Tech. Pap.*, vol. 1343, 1978.

[170] J. M. C. Pritchard, "The effect of humidity on the friction and life of unbonded molybdenum disulphide films," *Wear*, vol. 13, pp. 39–50, 1968.

[171] H. S. Khare and D. L. Burris, "Surface and subsurface contributions of oxidation and moisture to room temperature friction of molybdenum disulfide," *Tribol. Lett.*, vol. 53, no. 1, pp. 329–336, 2014.

[172] F. Meng, C. Yang, and H. Han, "Study on tribological performances of MoS2 coating at high temperature," *Proc. Inst. Mech. Eng. Part J J. Eng. Tribol.*, vol. 232, no. 8, pp. 964–973, 2018.

[173] W. L. Spychalski, M. Pisarek, and R. Szoszkiewicz, "Microscale Insight into Oxidation of Single MoS2 Crystals in Air," *J. Phys. Chem. C*, vol. 121, no. 46, pp. 26027–26033, 2017.

[174] H. Han, Z. Qian, F. Meng, and Z. Cui, "Tribological performances of graphite–MoS2 coating at various high temperatures," *Proc. Inst. Mech. Eng. Part J J. Eng. Tribol.*, vol. 233, no. 12, pp. 1888–1902, 2019.

[175] E. Serpini, A. Rota, A. Ballestrazzi, D. Marchetto, E. Gualtieri, and S. Valeri, "The role of humidity and oxygen on MoS thin films deposited by RF PVD magnetron sputtering," *Surf. Coatings Technol.*, vol. 319, pp. 345–352, Jun. 2017.

[176] R. R. M. Johnston and A. J. W. Moore, "Water adsorption on molybdenum bisulfide containing surface contaminants," *J. Phys. Chem.*, vol. 68, no. 11, pp. 3399–3406, 1964.

[177] G. Volp and V. H. Grassian, “Role(s) of adsorbed water in the surface chemistry of environmental interfaces,” *Chem. Commun.*, vol. 49, no. 30, pp. 3071–3094, 2013.

[178] B. Pilotti, G. Prieto, A. Juan, R. Faccio, and E. Broitman, “Bi2S3 and MoS2 Soft Coatings: A Comparative Study of Their Frictional Behavior Under Different Humidity Levels, Normal Loads, and Sliding Speeds,” *Tribol. Lett.*, vol. 69, no. 3, pp. 1–24, 2021.

[179] X. Zhao, G. Zhang, L. Wang, and Q. Xue, “The Tribological Mechanism of MoS2 Film under Different Humidity,” *Tribol. Lett.*, vol. 65, no. 2, pp. 1–8, 2017.

[180] R. K. Upadhyay and A. Kumar, “Effect of humidity on the synergy of friction and wear properties in ternary epoxy-graphene-MoS2 composites,” *Carbon N. Y.*, vol. 146, pp. 717–727, May 2019.

[181] R. Cox, “Solid Lubricants,” in *Engineered Tribological Composites - The Art of Friction Material Development*, 2012, pp. 351–380.

[182] C. E. Morstein and M. Dienwiebel, “Graphite lubrication mechanisms under high mechanical load,” *Wear*, vol. 477, no. September 2020, p. 203794, 2021.

[183] Y. N. Vasil’ev, I. a. Kolyaev, and V. a. Fugol’, “On the friction mechanism of solid lubricants,” *J. Frict. Wear*, vol. 32, no. 5, pp. 324–332, 2011.

[184] I. Hutchings and P. Shipway, “Friction,” in *Tribology*, 2017, pp. 37–74.

[185] R. H. Savage, “Graphite lubrication,” *J. Appl. Phys.*, vol. 19, no. 1, pp. 1–10, 1948.

[186] R. H. Savage and D. L. Schaefer, “Vapor lubrication of graphite sliding contacts,” *J. Appl. Phys.*, vol. 27, no. 2, pp. 136–138, 1956.

[187] J. K. Lancaster and J. R. Pritchard, “The influence of environment and pressure on the transition to dusting wear of graphite,” *J. Phys. D. Appl. Phys.*, vol. 14, no. 4, pp. 747–762, 1981.

[188] G. W. Rowe, “Some observations on the frictional behaviour of of boron nitride and of graphite,” *Wear*, vol. 3, no. 4, pp. 274–285, 1960.

[189] L. H. T. P.J. Bryant, P.L. Gutshall, “A study of mechanisms of graphite friction and wear,” *Wear*, vol. 7, no. 1, pp. 118–126, 1964.

[190] M. S. Dresselhaus and G. Dresselhaus, “Intercalation compounds of graphite,” *Adv. Phys.*, vol. 51, no. 1, pp. 1–186, 2002.

[191] R. D. Arnell and D. G. Teer, “Lattice parameters of graphite in relation to friction and wear [10],” *Nature*, vol. 218, no. 5147, pp. 1155–1156, 1968.

[192] M. Dienwiebel, G. S. Verhoeven, N. Pradeep, J. W. M. Frenken, J. A. Heimberg, and H. W. Zandbergen, “Superlubricity of graphite,” *Phys. Rev. Lett.*, vol. 92, no. 12, pp. 1–4, 2004.

[193] B. K. Yen, B. E. Schwickert, and M. F. Toney, “Origin of low-friction behavior in graphite investigated by surface x-ray diffraction,” *Appl. Phys. Lett.*, vol. 84, no. 23, pp. 4702–4704, 2004.

[194] F. P. Bowden and J. E. Young, “Friction of Diamond, Graphite, and Carbon and the Influence of Surface Films,” *Proc. R. Soc. A Math. Phys. Eng. Sci.*, vol. 208, no. 1095, pp. 444–455, 1951.

[195] R. F. Deacon and J. F. Goodman, “Lubrication by lamellar solids,” 1957.

[196] X. Li, Y. Gao, J. Xing, Y. Wang, and L. Fang, “Wear reduction mechanism of graphite and MoS2 in epoxy composites,” *Wear*, vol. 257, no. 3–4, pp. 279–283, Aug. 2004.

[197] W. J. Bartz and X. Jinfen, “Wear behaviour and failure mechanism of bonded solid lubricants,” *Wear*, vol. 150, no. 1–2, pp. 231–246, Oct. 1991.

[198] T. Peter and R. Atkinson, “Bonded coatings for the reduction of friction and wear,” *Ind. Lubr. Tribol.*, vol. 50, no. 6, pp. 278–281, 1998.

[199] J. C. Anderson, “Wear of commercially available plastic materials,” *Tribol. Int.*, vol. 15, no. 5, pp. 255–263, 1982.

[200] B. J. Briscoe and S. K. Sinha, “Wear of polymers,” *Proc. Inst. Mech. Eng. Part J J. Eng. Tribol.*, vol. 216, no. 6, pp. 401–413, 2002.

[201] B. J. Briscoe and S. K. Sinha, “Tribological applications of polymers and their composites – past, present and future prospects,” in *Tribology of Polymeric Nanocomposites Friction and Wear of Bulk Materials and Coatings*, 2008, pp. 1–36.

[202] N. K. Myshkin, M. I. Petrokovets, and A. V. Kovalev, “Tribology of polymers: Adhesion, friction, wear, and mass-transfer,” *Tribol. Int.*, vol. 38, no. 11–12, pp. 910–921, Nov. 2005.

[203] Z. Zhang, C. Breidt, L. Chang, F. Haupert, and K. Friedrich, “Enhancement of the wear resistance of epoxy: short carbon fibre, graphite, PTFE and nano-TiO2,” *Compos. Part A Appl. Sci. Manuf.*, vol. 35, no. 12, pp. 1385–1392, Dec. 2004.

[204] K. Friedrich, Z. Zhang, and A. K. Schlarb, “Effects of various fillers on the sliding wear of polymer composites,” *Compos. Sci. Technol.*, vol. 65, no. 15-16 SPEC. ISS., pp. 2329–2343, 2005.

[205] S. Bahadur and D. Gong, “The action of fillers in the modification of the tribological behavior of polymers,” *Wear*, vol. 158, no. 1–2, pp. 41–59, Oct. 1992.

[206] J. Schön, “Coefficient of friction and wear of a carbon fiber epoxy matrix composite,” *Wear*, vol. 257, no. 3–4, pp. 395–407, 2004.

[207] T. P. Yukhno, Y. V. Vvedensky, and L. N. Sentyurikhina, “Low temperature investigations on frictional behaviour and wear resistance of solid lubricant coatings,” *Tribol. Int.*, vol. 34, no. 4, pp. 293–298, 2001.

[208] A. Abdelbary, “Sliding mechanics of polymers,” *Wear Polym. Compos.*, pp. 37–66, Jan. 2014.

[209] S. E. Franklin, “Wear experiments with selected engineering polymers and polymer composites under dry reciprocating sliding conditions,” *Wear*, vol. 250–251, no. PART 2, pp. 1591–1598, 2001.

[210] F. Song, Q. Wang, and T. Wang, “The effects of crystallinity on the mechanical properties and the limiting PV (pressure×velocity) value of PTFE,” *Tribol. Int.*, vol. 93, pp. 1–10, 2016.

[211] J. K. Lancaster, “Estimation of the limiting PV relationships for thermoplastic bearing materials,” *Tribology*, vol. 4, no. 2, pp. 82–86, 1971.

[212] J. K. Lancaster, “Polymer-based bearing materials: The role of fillers and fibre reinforcement,” *Tribology*, vol. 5, no. 6, pp. 249–255, 1972.

[213] P. Samyn and G. Schoukens, “Thermochemical sliding interactions of short carbon fiber polyimide composites at high pv-conditions,” *Mater. Chem. Phys.*, vol. 115, no. 1, pp. 185–195, 2009.

[214] Y. Yamaguchi, “The Limiting Pressure-Velocity (PV) of Plastics Under Unlubricated Sliding,” vol. 22.

[215] R. Bassani, G. Levita, M. Meozzi, and G. Palla, “Friction and wear of epoxy resin on inox steel: Remarks on the influence of velocity, load and induced thermal state,” *Wear*, vol. 247, no. 2, pp. 125–132, 2001.

[216] L. Lin and A. K. Schlarb, “The roles of rigid particles on the friction and wear behavior of short carbon fiber reinforced PBT hybrid materials in the absence of solid lubricants,” *Tribol. Int.*, vol. 119, no. November 2017, pp. 404–410, 2018.

[217] L. Chang, Z. Zhang, C. Breidt, and K. Friedrich, “Tribological properties of epoxy nanocomposites I. Enhancement of the wear resistance by nano-TiO2 particles,” *Wear*, vol. 258, no. 1-4 SPEC. ISS., pp. 141–148, 2005.

[218] N. Myshkin and A. Kovalev, “Adhesion and surface forces in polymer tribology — A review,” *Friction*, vol. 6, no. 2, pp. 143–155, 2018.

[219] S. H. Rhee and K. C. Ludema, “Mechanisms of formation of polymeric transfer films,” *Wear*, vol. 46, no. 1, pp. 231–240, 1978.

[220] R. K. Gunda and S. K. R. Narala, “Tribological studies to analyze the effect of solid lubricant particle size on friction and wear behaviour of Ti-6Al-4V alloy,” *Surf. Coatings Technol.*, vol. 308, pp. 203–212, 2016.

[221] J. Ye, D. Burris, and T. Xie, “A Review of Transfer Films and Their Role in Ultra-Low-Wear Sliding of Polymers,” *Lubricants*, vol. 4, no. 1, p. 4, 2016.

[222] S. M. Yeo and A. A. Polycarpou, “Fretting experiments of advanced polymeric coatings and the effect of transfer films on their tribological behavior,” *Tribol. Int.*, vol. 79, pp. 16–25, Nov. 2014.

[223] A. M. Korsunsky, A. R. Torosyan, and K. Kim, “Development and characterization of low friction coatings for protection against fretting wear in aerospace components,” *Thin Solid Films*, vol. 516, no. 16, pp. 5690–5699, Jun. 2008.

[224] K. Kim and A. M. Korsunsky, “Exponential evolution law of fretting wear damage in low-friction coatings for aerospace components,” *Surf. Coatings Technol.*, vol. 202, no. 24, pp. 5838–5846, 2008.

[225] K. Barman, P. H. Shipway, K. T. Voisey, and G. Pattinson, “Evolution of damage in MoS2-based dry film lubricants (DFLs) in fretting wear—The effect of DFL thickness and contact geometry,” *Prog. Org. Coatings*, vol. 105, pp. 67–80, 2017.

[226] J. Xu, Z. R. Zhou, C. H. Zhang, M. H. Zhu, and J. B. Luo, “An investigation of fretting wear behaviors of bonded solid lubricant coatings,” *J. Mater. Process. Technol.*, vol. 182, no. 1–3, pp. 146–151, 2007.

[227] M. H. Zhu and Z. R. Zhou, “An investigation of molybdenum disulfide bonded solid lubricant coatings in fretting conditions,” *Surf. Coatings Technol.*, vol. 141, no. 2–3, pp. 240–245, Jun. 2001.

[228] D. B. Luo, V. Fridrici, and P. Kapsa, “Evaluating and predicting durability of bonded solid lubricant coatings under fretting conditions,” *Tribol. Int.*, vol. 44, no. 11, pp. 1577–1582, 2011.

[229] G. H. Xu, M. Zhu, J. Liu, Z. Zhou, and H. Liang, “The effect of pre-treatment of substrate on fretting tribological behavior of MoS2 coatings,” *Wear*, vol. 255, no. 1–6, pp. 246–252, Aug. 2003.

[230] K. Barman, P. H. Shipway, K. T. Voisey, and G. Pattinson, “The role of a thermally sprayed CuNiIn underlayer in the durability of a dry-film lubricant system in fretting – A phenomenological model,” *Tribol. Int.*, vol. 123, pp. 307–315, Jul. 2018.

[231] E. Laolu-Balogun, S. P. Owen, S. Read, G. Pattinson, P. H. Shipway, and K. T. Voisey, “Effects of Ti-6Al-4V Surface Condition on the Performance of DFL Lifetimes,” in *Proceedings of the 8th International Conference on Fracture, Fatigue and Wear*, 2021, pp. 657–672.

[232] X. Quan, M. Hu, D. Jiang, F. Yanlong, L. Weng, and D. Jiang, “Friction and wear performance of dual lubrication systems combining WS2–MoS2 composite film and low volatility oils under vacuum condition,” *Tribol. Int.*, vol. 99, pp. 57–66, Jul. 2016.

[233] E. D. Grayfer, M. N. Kozlova, and V. E. Fedorov, “Colloidal 2D nanosheets of MoS2and other transition metal dichalcogenides through liquid-phase exfoliation,” *Adv. Colloid Interface Sci.*, vol. 245, no. April, pp. 40–61, 2017.

[234] K. Barman, “Development of Dry Film Lubricants for Highly Loaded Contacts,” University of Nottingham, 2016.

[235] D. Kirk, “Shot peening,” *Aircr. Eng. Aerosp. Technol. an Int. J.*, vol. 77, no.

4, pp. 349–361, 1999.

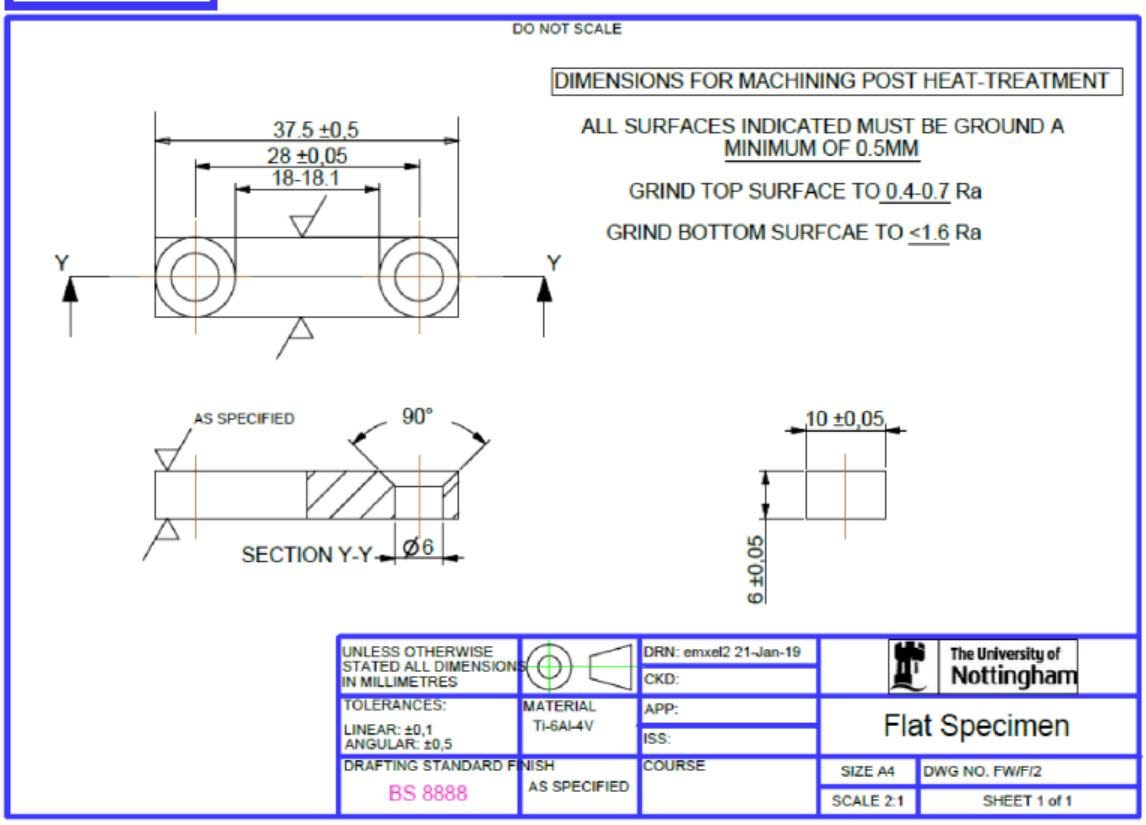
[236] M. Oerilikon, “Material Product Data Sheet Copper Nickel and Copper Nickel Indium Thermal Spray Powders,” pp. 4–7, 2014.

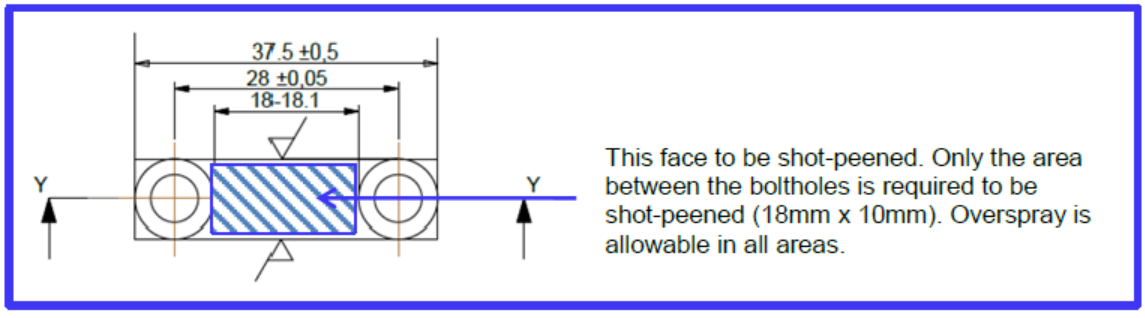
[237] J. S. Zabinski, J. E. Bultman, J. H. Sanders, and J. J. Hu, “Multi-environmental lubrication performance and lubrication mechanism of MoS2/Sb2O3/C composite films,” *Tribol. Lett.*, vol. 23, no. 2, pp. 155–163, 2006.

Appendices

Appendix A: Specimen drawing and shot peening Conditions

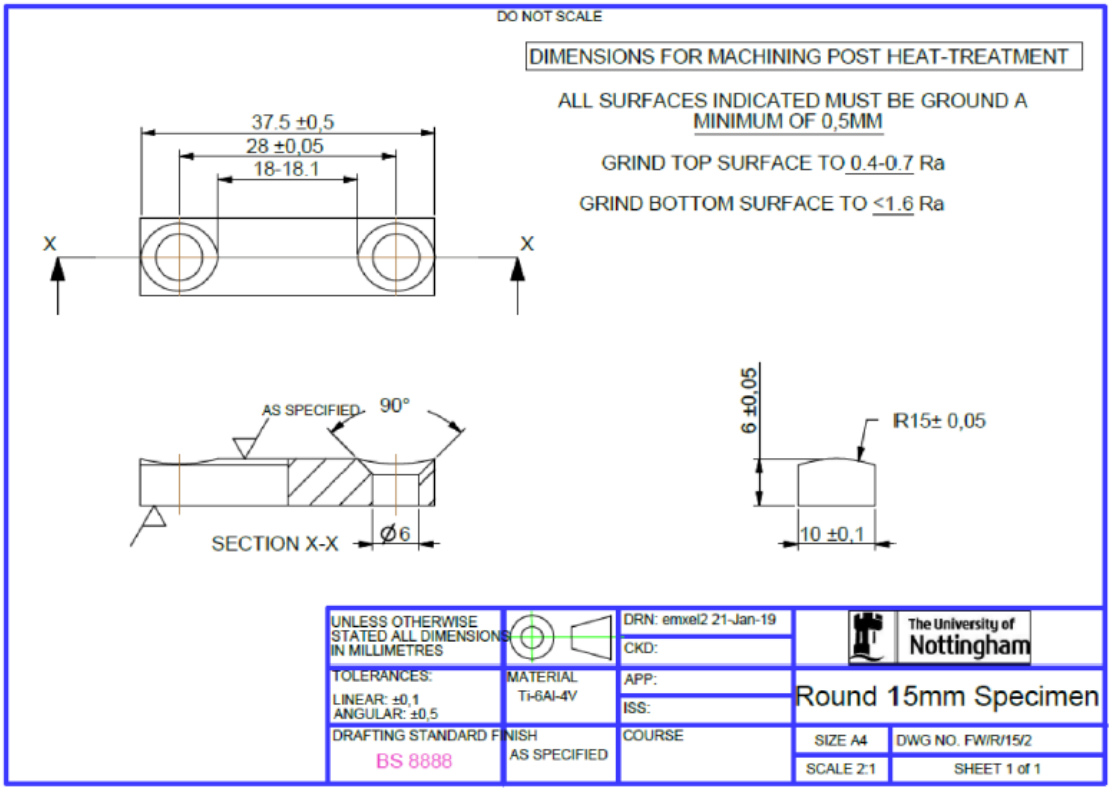
Flat Sample

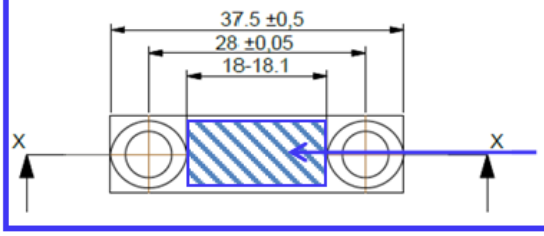




Peening conditions:
6-10A, 230 R 200% coverage
4-8N C glass 100% decontaminate

Round Sample





This face to be shot-peened. Only the area between the boltholes is required to be shot-peened (18mm x 10mm). Overspray is allowable in all areas.

Peening conditions:
6-10A, 230 R 200% coverage
4-8N C glass 100% decontaminate

Appendix B: Technical data sheet for PL237-R2 (as-received MoS2-based DFL)

Technical Data Sheet

Indestructible
® specialist coatings manufacture

Product Name:	Molybdenum Disulphide Dry Film Lubricant
Product Number:	PL237-R2
Product Description:	High temperature resistant Molybdenum disulphide loaded dry film lubricant coating.
Approvals/Specifications:	- MSRR 9274 - RPS661/9 - Rolls Royce Code: 110566 - OMat 4/43 - Kawasaki JMSRR 9276 - NSN: 91-5099-430-9538 - MTU spec MTS-1013A-02 - KHI-JMSRR9274
Performance:	- Resistant to dry heat to 300°C (570°F) - Resistant to Skydrol, Ester lubricants and corrosive engine by products - Designed for operating conditions up to 300°C (570°F) - For use where high wear and pitting occurs and as a protection against fretting, where short service life occurs due to chemical attack, corrosion or high temperature or where lubrication internals are often too short. - Developed at Rolls Royce request to comply with regulations for the environment specified in their collaboration to meet specifications for JSF that makes certain solvents used in the R1 version unusable. - Often used as an alternative to MolyKote 3400A

Appendix C: Technical data sheet for IP9136-R1 (graphite-based DFL)

Technical Data Sheet

Indestructible
® specialist coatings manufacture

Issue 1

Product Name:	Graphite Filled Skydrol Resistant Dry Film Lubricant
Product Number:	IP9136-R1
Product Description:	Spray applied, stoving cured, silicon resin modified dry film lubricant for use where high operating temperatures preclude the use of conventional oils and greases. Suitable for application to steel, aluminium, magnesium and titanium alloys. Used on, for example spherical bearing surfaces to protect against frottage corrosion and on bolts for torque and gives an exceptionally good rubbing wear resistance. When used on bolts, it increases torque end loads. It is also used on turbine blade roots and fir trees where it reduces the likelihood of the disc splitting.
Approvals/Specifications:	- Turbomeca Spec LB 541 - MSRR9276, CPW 27, AMS 3132 (Graphite filled), RR Code 110565, OMAT 4/44C - CoMat #10 – 002, NSN 9150-99-500-0559, Kawasaki – JMSRR 9276, Honeywell Phoenix Arizona PCS 5022, GEC Marconi 1608/0038/001, SNECMA spec P1064, JAEC JCR – 024, MTU – MTS 1173 Alternative to the following: - PL239 (3862X9010) AFS473, which was originally PL239; Superseded PL 94 in about 1984
Performance:	Resistant to dry heat up to 400°C (750°F) in oxidizing atmospheres and 500°C (930°F) where oxygen is excluded, ester lubricants, Skydrol and corrosion. **Tri-n-Butyl-Phosphate**: 3 hours @ 70°C

Appendix D: Material safety data sheet for graphite powder

EU safety data sheet

IMERYS Graphite & Carbon

Trade name: TIMREX® KS, SFG, SLP, SLS, T, T-SLC, MX, MB, KC, MK, F, KL, MAA

Current version : 2.0.4, **issued:** 18.10.2021 **Replaced version:** 2.0.3, **issued:** 04.05.2020 **Region:** GB

SECTION 1: Identification of the substance/mixture and of the company/undertaking

1.1 Product identifier

Trade name

TIMREX® KS, SFG, SLP, SLS, T, T-SLC, MX, MB, KC, MK, F, KL, MAA

C-NERGY™ KS-L, SFG-L

Substance name	Graphite (> 99,5 %)
REACH registration no.	01-2119486977-12

Identification numbers

CAS no.	7782-42-5
EC no.	231-955-3

1.2 Relevant identified uses of the substance or mixture and uses advised against

Relevant identified uses of the substance or mixture
Electrical and thermal conductive additive
Friction modifier
Carbon carrier
Lubricant
Refractories

Uses advised against
None known

1.3 Details of the supplier of the safety data sheet

Address
Imerys Graphite & Carbon Switzerland Ltd.
Strada Industriale 12
6743 Bodio (Switzerland)

Telephone no.	+41 91 873 20 10
Fax no.	+41 91 873 20 19
e-mail	graphiteandcarbon.ch@imerys.com

Information provided by / telephone
Research and Development

Advice on Safety Data Sheet
sdb_info@umco.de

1.4 Emergency telephone number

For Hazardous Materials [or Dangerous Goods] Incident
Spill, Leak, Fire, Exposure, or Accident
Call CHEMTREC Day or Night
International Number: +1 703-741-5970 (collect calls accepted)
Local number: +(44)-870-8200418

SECTION 2: Hazards identification

2.1 Classification of the substance or mixture

Classification information
This product does not meet the classification and labelling criteria given in the Regulation (EC) No 1272/2008 (CLP).

2.2 Label elements

Not relevant

2.3 Other hazards

PBT assessment
The product is not considered to be a PBT.

vPvB assessment
The product is not considered to be a vPvB.

Page 1 of 10

SECTION 3: Composition/information on ingredients

3.1 Substances

Chemical characterization

Substance name	Graphite (> 99,5 %)

Identification numbers

CAS no.	7782-42-5
EC no.	231-955-3

3.2 Mixtures

Not applicable. The product is not a mixture.

SECTION 4: First aid measures

4.1 Description of first aid measures

General information
In case of persisting adverse effects, consult a physician. Change contaminated clothing.

After inhalation
Remove affected person from the immediate area. Ensure supply of fresh air.

After skin contact
When in contact with the skin, clean with soap and water.

After eye contact
Remove contact lenses. Rinse eye thoroughly under running water keeping eyelids wide open and protecting the unaffected eye (at least 10 to 15 minutes).

After ingestion
Rinse out mouth and give plenty of water to drink. Never give anything by mouth to an unconscious person.

4.2 Most important symptoms and effects, both acute and delayed

No data available.

4.3 Indication of any immediate medical attention and special treatment needed

No data available.

SECTION 5: Firefighting measures

5.1 Extinguishing media

Suitable extinguishing media
Foam; Carbon dioxide; Extinguishing powder; Water spray jet; Sand

Unsuitable extinguishing media
High power water jet

5.2 Special hazards arising from the substance or mixture

In the event of fire, the following can be released: Carbon monoxide (CO); Carbon dioxide (CO2)

5.3 Advice for firefighters

Use self-contained breathing apparatus. Wear protective clothing.

SECTION 6: Accidental release measures

6.1 Personal precautions, protective equipment and emergency procedures

For non-emergency personnel
Refer to protective measures listed in sections 7 and 8. Avoid contact with skin, eyes and clothing. Ensure adequate ventilation. Avoid dust formation. High risk of slipping due to leakage/spillage of product.

For emergency responders
Personal protective equipment (PPE) - see section 8. In case of emergency, use of personal protective equipment [DIN EN 469, EN 12021].

6.2 Environmental precautions

Do not discharge into the drains/surface waters/groundwater.

Appendix E: Material safety data sheet for compressed air cylinder

BOC
A Member of The Linde Group

SAFETY DATA SHEET
Air, compressed

Issue Date:	16.10.2013	Version: 1.7	SDS No.: 000010022047
Last revised date:	30.04.2021		1/13

SECTION 1: Identification of the substance/mixture and of the company/undertaking

1.1 Product identifier

Product name: Air, compressed

Other Name: Compressed Air

1.2 Relevant identified uses of the substance or mixture and uses advised against

Identified uses: Industrial and professional. Perform risk assessment prior to use.
Uses advised against: Consumer use.Industrial or technical grade is unsuitable for medical and/or food applications or inhalation.

1.3 Details of the supplier of the safety data sheet

Supplier
BOC
Priestley Road, Worsley
M28 2UT Manchester

Telephone: 0800 111 333

E-mail: ReachSDS@boc.com

1.4 Emergency telephone number: 0800 111 333

SECTION 2: Hazards identification

2.1 Classification of the substance or mixture

Classification according to Regulation (EC) No 1272/2008 as amended.

Physical Hazards

Gases under pressure	Compressed gas	H280: Contains gas under pressure; may explode if heated.

2.2 Label Elements



Signal Word: Warning

Hazard Statement(s): H280: Contains gas under pressure; may explode if heated.

Precautionary Statements
General: None.

Prevention: None.

Response:	None.
Storage:	P403: Store in a well-ventilated place.
Disposal	None.

2.3 Other hazards None.

SECTION 3: Composition/information on ingredients

3.2 Mixtures

Chemical name	Chemical formula	Concentration	CAS-No.	REACH Registration No.	M-Factor:	Notes
Nitrogen	N2	79%	7727-37-9	Listed in Annex IV/V of Regulation (EC) No 1907/2006 (REACH), exempted from registration.	-	
oxygen	O2	21%	7782-44-7	Listed in Annex IV/V of Regulation (EC) No 1907/2006 (REACH), exempted from registration.	-	

The concentrations of the components in the SDS header, product name on page one and in section 3.2 are in mol due to regulatory requirements.
All concentrations are nominal.
This substance has workplace exposure limit(s).
PBT: persistent, bioaccumulative and toxic substance.
vPvB: very persistent and very bioaccumulative substance.

Classification

Chemical name	Classification		Notes
Nitrogen	CLP:	, Press. Gas Compr. Gas;H280	
oxygen	CLP:	Press. Gas Compr. Gas;H280, Oxid. Gas 1;H270	

CLP: Regulation No. 1272/2008.

The full text for all H-statements is displayed in section 16.

Appendix F: Material safety data sheet for compressed argon cylinder

BOC
A Member of The Linde Group

SAFETY DATA SHEET
Argon, compressed

Issue Date:	16.01.2013	Version: 1.5	SDS No.: 000010021700
Last revised date:	19.05.2020		1/13

SECTION 1: Identification of the substance/mixture and of the company/undertaking

1.1 Product identifier

Product name: Argon, compressed

Trade name: Argon Pureshield, Argon Pure, Argon Industrial, Argon Grade N6.0, Argon Research Grade N5.5, Argon Zero Grade N5.0, Argon Food Grade, PYROGON A

Additional identification

Chemical name:	Argon
Chemical formula:	Ar
INDEX No.	-
CAS-No.	7440-37-1
EC No.	231-147-0
REACH Registration No.	Listed in Annex IV/V of Regulation (EC) No 1907/2006 (REACH), exempted from registration.

1.2 Relevant identified uses of the substance or mixture and uses advised against

Identified uses: Industrial and professional. Perform risk assessment prior to use.
Balance gas for mixtures. Blanketing gas. Calibration gas. Carrier gas. Combustion, melting and cutting processes. Fire suppressant gas. Food packaging gas. Inerting gas. Inflation systems. Laboratory use. Laser gas. Pressure head gas, operational assist gas in pressure systems. Process gas. Purge gas. Test gas.
Consumer use.
Shielding gas in gas welding.
It is the responsibility of the end user to ensure that the product as supplied is suitable for its intended use.

Uses advised against Industrial or technical grade is unsuitable for medical and/or food applications or inhalation.

1.3 Details of the supplier of the safety data sheet

Supplier

BOC
Priestley Road, Worsley
M28 2UT Manchester

Telephone: 0800 111 333

E-mail: ReachSDS@boc.com

1.4 Emergency telephone number: 0800 111 333

SECTION 2: Hazards identification

2.1 Classification of the substance or mixture

Classification according to Regulation (EC) No 1272/2008 as amended.

Physical Hazards

Gases under pressure	Compressed gas	H280: Contains gas under pressure; may explode if heated.

2.2 Label Elements



Signal Word: Warning

Hazard Statement(s): H280: Contains gas under pressure; may explode if heated.

Precautionary Statements
General: None.

Prevention: None.

Response: None.

Storage: P403: Store in a well-ventilated place.

Disposal: None.

Supplemental information: EIGA-As: Asphyxiant in high concentrations.

2.3 Other hazards: None.

SECTION 3: Composition/information on ingredients

3.1 Substances

Chemical name Argon
INDEX No.: -
CAS-No.: 7440-37-1
EC No.: 231-147-0
REACH Registration No.: Listed in Annex IV/V of Regulation (EC) No 1907/2006 (REACH), exempted from registration.
Purity: 100%
The purity of the substance in this section is used for classification only, and does not represent the actual purity of the substance as supplied, for which other documentation should be consulted.
Trade name: Argon Pureshield, Argon Pure, Argon Industrial, Argon Grade N6.0, Argon Research Grade N5.5, Argon Zero Grade N5.0, Argon Food Grade, PYROGON A

Chemical name	Chemical formula	Concentration	CAS-No.	REACH Registration No.	M-Factor:	Notes
Argon	Ar	100%	7440-37-1	Listed in Annex IV/V of Regulation (EC) No 1907/2006 (REACH), exempted from registration.	-	

The concentrations of the components in the SDS header, product name on page one and in section 3.2 are in mol due to regulatory requirements. All concentrations are nominal.
This substance has workplace exposure limit(s).
PBT: persistent, bioaccumulative and toxic substance.
vPvB: very persistent and very bioaccumulative substance.

SECTION 4: First Aid Measures

General: In high concentrations may cause asphyxiation. Symptoms may include loss of mobility/consciousness. Victim may not be aware of asphyxiation. Remove victim to uncontaminated area wearing self contained breathing apparatus. Keep victim warm and rested. Call a doctor. Apply artificial respiration if breathing stopped.

4.1 Description of first aid measures

Inhalation: In high concentrations may cause asphyxiation. Symptoms may include loss of mobility/consciousness. Victim may not be aware of asphyxiation. Remove victim to uncontaminated area wearing self contained breathing apparatus. Keep victim warm and rested. Call a doctor. Apply artificial respiration if breathing stopped.

Eye contact: Adverse effects not expected from this product.

Skin Contact: Adverse effects not expected from this product.

Appendix G: Material safety data sheet for thinner (IP9151)



SAFETY DATA SHEET
Thinner

1 IDENTIFICATION OF THE SUBSTANCE/PREPARATION AND OF THE COMPANY/UNDERTAKING

PRODUCT NAME	Thinner
PRODUCT NO.	IP9151
SUPPLIER	INDESTRUCTIBLE PAINT LTD 19-25 Pentos Drive Sparkhill Birmingham England B11 3TA Tel +44(0)121 702 2485 Fax +44(0)121 778 4338 sales@indestructible.co.uk
EMERGENCY TELEPHONE	+44 (0) 121 244 5671

2 HAZARDS IDENTIFICATION

Flammable. Harmful by inhalation, in contact with skin and if swallowed. Irritating to eyes and respiratory system. Limited evidence of a carcinogenic effect.

CLASSIFICATION (1999/45) Xn;R20/21/22. Carc. Cat. 3;R40. Xi;R36/37. R10.

3 COMPOSITION/INFORMATION ON INGREDIENTS

Name	EC No.	CAS-No.	Content	Classification (67/548)
CYCLOHEXANONE		108-94-1	60-100%	Xn;R20. R10.
ISOPHORONE		78-59-1	30-60%	Xn;R21/22. Carc. Cat. 3;R40. Xi;R36/37.

COMPOSITION COMMENTS

The Data Shown is in accordance with the latest EC Directives.

4 FIRST-AID MEASURES

INHALATION

Move the exposed person to fresh air at once. Get medical attention if any discomfort continues.

INGESTION

Immediately rinse mouth and provide fresh air. Do not induce vomiting. If vomiting occurs, the head should be kept low so that stomach vomit doesn't enter the lungs. Get medical attention immediately!

SKIN CONTACT

Immediately remove contaminated clothing. Wash off promptly and flush contaminated skin with water. Promptly remove clothing if soaked through and flush skin with water. Get medical attention if any discomfort continues.

EYE CONTACT

Make sure to remove any contact lenses from the eyes before rinsing. Promptly wash eyes with plenty of water while lifting the eye lids. Get medical attention promptly if symptoms occur after washing.

5 FIRE-FIGHTING MEASURES

EXTINGUISHING MEDIA

Fire can be extinguished using: Foam, carbon dioxide or dry powder. Dry chemicals, sand, dolomite etc.

SPECIAL FIRE FIGHTING PROCEDURES

Use pressurised air mask if product is involved in a fire. Cool containers exposed to flames with water until well after the fire is out.

SPECIFIC HAZARDS

When heated and in case of fire, irritating vapours/gases may be formed. In case of fire, toxic gases may be formed (COx, NOx).

PROTECTIVE MEASURES IN FIRE

Self contained breathing apparatus and full protective clothing must be worn in case of fire.

6 ACCIDENTAL RELEASE MEASURES

PERSONAL PRECAUTIONS

Wear protective clothing as described in Section 8 of this safety data sheet.

ENVIRONMENTAL PRECAUTIONS

Spillages or uncontrolled discharges into watercourses must be IMMEDIATELY alerted to the Environmental Agency or other appropriate regulatory body.

SPILL CLEAN UP METHODS

Keep combustibles away from spilled material. Extinguish all ignition sources. Avoid sparks, flames, heat and smoking. Ventilate. Absorb in vermiculite, dry sand or earth and place into containers.

7 HANDLING AND STORAGE

USAGE PRECAUTIONS

Keep away from heat, sparks and open flame. Avoid spilling, skin and eye contact. Ventilate well, avoid breathing vapours. Use approved respirator if air contamination is above accepted level.

STORAGE PRECAUTIONS

Flammable/combustible - Keep away from oxidisers, heat and flames. Store in tightly closed original container in a dry, cool and well-ventilated place. Keep in original container. Avoid contact with oxidising agents. Store in closed original container at temperatures between 5°C and 25°C.

STORAGE CLASS

Flammable liquid storage.

8 EXPOSURE CONTROLS/PERSONAL PROTECTION

PROTECTIVE EQUIPMENT



PROCESS CONDITIONS

Provide eyewash station.

ENGINEERING MEASURES

Provide adequate ventilation, including appropriate local extraction, to ensure that the defined occupational exposure limit is not exceeded. All handling to take place in well-ventilated area.

RESPIRATORY EQUIPMENT

Wear mask supplied with: Gas cartridge suitable for organic substances.

HAND PROTECTION

Use protective gloves made of: Neoprene. Nitrile. Rubber (natural, latex).

EYE PROTECTION

Wear splash-proof eye goggles to prevent any possibility of eye contact.

OTHER PROTECTION

Wear appropriate clothing to prevent any possibility of skin contact.

HYGIENE MEASURES

DO NOT SMOKE IN WORK AREA! Wash at the end of each work shift and before eating, smoking and using the toilet. Promptly remove any clothing that becomes contaminated. Use appropriate skin cream to prevent drying of skin. When using do not eat, drink or smoke.

9 PHYSICAL AND CHEMICAL PROPERTIES

APPEARANCE	Clear liquid		
COLOUR	Colourless		
ODOUR	Characteristic		
RELATIVE DENSITY	0.94	VOLATILE BY VOL. (%)	100
FLASH POINT (°C)	40-44 CC (Closed cup).	FLAMMABILITY LIMIT - LOWER(%)	0.8

Appendix H: Mechanics of the contact

A cylinder on flat contact geometry is employed and the initial Hertzian contact pressure can be estimated if the existence of the coatings are ignored (i.e. assuming contact of semi-infinite bodies of Ti-6Al-4V or Cu-Ni-In as appropriate). The half-width b of a cylinder-on-flat line contact is given as:

$$b = \sqrt{\frac{4F\left[\frac{1-{\nu_1}^2}{E_1}\right] + \left[\frac{1-{\nu_1}^2}{E_2}\right]}{\pi L\left(\frac{1}{R}\right)}}$$

(Appendix Equation 1)

where E_1, E_2 are the elastic moduli and ν_1, ν_2 are the Poisson's ratios associated with each body respectively. The radii of the cylinder is taken as R, L is the length of the contact and F is the applied normal force.

The maximum contact pressure along the centre line of the contact area is:

$$P_{max} = \frac{2F}{\pi b L}$$

(Appendix Equation 2)

The nominal contact pressure is taken as:

$$P_{mean} = \frac{\pi\, P_{max}}{4}$$

(Appendix Equation 3)

In Appendix Table 1, the initial Hertzian contact pressures of the fretting wear couples are listed dependent on the normal load applied and the constituting materials which make up the contact.

Appendix Table 1 Initial nominal Hertzian contact pressure with a cylinder radius R of 15 mm as a function of applied normal force and material pairing.

Material contact configuration	Applied normal force (F)	Nominal Hertzian contact pressure (MPa)
Ti-6Al-4V – Ti6Al-4V	575	221
Ti-6Al-4V – Ti-6Al-4V	1000	291
Ti-6Al-4V – Cu-Ni-In	144	91.5
Ti-6Al-4V – Cu-Ni-In	575	183
Ti-6Al-4V – Cu-Ni-In	1000	241